UNIVERSITY OF RIJEKA

FACULTY OF BIOTECHNOLOGY AND DRUG DEVELOPMENT

Patrizia Janković

Short catalytic peptides with intrinsic esterase activity

Doctoral thesis

Rijeka, 2024.

UNIVERSITY OF RIJEKA

FACULTY OF BIOTECHNOLOGY AND DRUG DEVELOPMENT

Patrizia Janković

Short catalytic peptides with intrinsic esterase activity

Doctoral thesis

Supervisor: Assist. Prof. Daniela Kalafatović, PhD

Rijeka, 2024.

SVEUČILIŠTE U RIJECI

FAKULTET BIOTEHNOLOGIJE I RAZVOJA LIJEKOVA

Patrizia Janković

Kratki linearni i ciklički katalitički peptidi inspirirani esterazom

Doktorski rad

Mentor: Doc. dr. sc. Daniela Kalafatović

Rijeka, 2024.

Supervisor: Assist. Prof. Daniela Kalafatović, PhD, University of Rijeka, Faculty of Biotechnology and Drug Development

The thesis was defended on the day ———————————————— at the Faculty of Biotechnology and Drug Development, University of Rijeka, in front of the evaluation committee:

1. Assist. Prof. Toni Todorovski, PhD, University of Rijeka, Faculty of Biotechnology and Drug Development
2. Prof. Ruža Frkanec, University of Zagreb, Centre for Research and Knowledge Transfer in Biotechnology
3. Assoc. Prof. Christian W. Gruber, PhD, Medical University of Vienna

Abstract

In this dissertation, two key approaches for the design of catalytic peptides are explored: (i) the incorporation of amino acids from the catalytic triad and (ii) an approach involving metal ions. To identify these main design approaches, a comprehensive dataset based on the collection of published data about purely peptidic catalysts for ester hydrolysis was gathered and analyzed including both active and inactive sequences tested towards the p-NPA and p-NPP substrates providing an insight into the currently developed catalytic mechanisms. Additionally, this open-access dataset also includes the SMILES-based representation of peptides and it can be used for training of machine learning-based models. Moreover, the standard p-NPA method was optimized. This extensively employed assay for determining catalytic activity, initially designed for enzymatic reactions, is not directly applicable to peptides due to variations in reaction parameters, such as the concentrations of catalysts and reaction times, when comparing peptides to enzymes. Consequently, standardizing conditions, including temperature, pH, buffer choice, and concentrations of both substrate and peptide, became essential to ensure accurate and reliable results in peptide reactions. Furthermore, the synthesis of a set of histidine-rich linear and cyclic peptides allowed us to understand the impact of amino acid arrangement, cyclization, and inclusion of D-amino acids on their self-assembly, coordination of Zn^{2+} ions and ability to hydrolyze p-NPA. Investigating structural changes crucial to the functionality of short peptides contributes to the development of a new generation of catalytic peptides and advances our understanding of the potential of self-assembly in improving catalytic efficiency. Additionally, we investigated the feasibility of isolating the active site of an enzyme to develop a minimalist catalyst, with a specific focus on recognizing cysteine as a crucial component within the catalytic triad, essential for the effectiveness of the peptide catalyst. The synthesis of a set of cysteine-rich peptides showing tunable activity resulting from the sensitivity of the thiol groups to the redox environment could open promising opportunities for tailored enzymatic catalysis. The overall goal of this research is to gain a deeper insight into the relationship between the sequence and function of catalytic peptides, leading to the development of innovative peptide catalysts with potential applications in various fields, including biocatalysis, pharmaceutical synthesis, and other industrial processes.

Key words: catalytic, peptides, p-NPA, self-assembly

Sažetak

U ovoj disertaciji predstavljena su dva ključna pristupa za dizajn katalitičkih peptida: (i) peptidne sekvence bazirane na aminokiselinama iz katalitičke trijade i (ii) pristup koji se temelji na interakciji peptida i metalnih iona. U svrhu identifikacije ovih glavnih pristupa, prikupljen je i analiziran sveobuhvatan skup podataka na temelju objavljenih katalitičkih peptida za hidrolizu estera, uključujući aktivne i neaktivne sekvence testirane na supstratima p-NPA i p-NPP, pružajući uvid u trenutno razvijene katalitičke mehanizme. Ovaj skup podataka s otvorenim pristupom uključuje i računalnu reprezentaciju peptida u formatu SMILES koja se može koristiti za treniranje i razvoj modela zasnovanih na strojnom učenju. Nadalje, optimizirana je standardna metoda p-NPA za određivanje katalitičke aktivnosti. Ovaj često korišteni esej, prvotno dizajniran za enzime, nije izravno primjenjiv na peptide zbog varijacija u parametrima katalitičke reakcije, kao što su koncentracija katalizatora i trajanje reakcije u usporedbi peptida s enzimima. Stoga je bilo potrebno standardizirati uvjete, uključujući temperaturu, pH, izbor pufera i koncentracije supstrata i peptida, kako bi se osigurali točni i pouzdani rezultati. Nadalje, sinteza skupa linearnih i cikličkih peptida bogatih histidinima omogućila nam je razumijevanje utjecaja rasporeda aminokiselina, ciklizacije i uključivanja D-aminokiselina na njihovu sposobnost samo-sastavljanja, koordinacije iona Zn^{2+} i sposobnost hidrolize p-NPA. Istraživanje strukturnih promjena ključnih za funkcionalnost kratkih peptida doprinosi razvoju nove generacije katalitičkih peptida i unaprjeđuje naše razumijevanje potencijala samo-sastavljanja u poboljšanju katalitičke učinkovitosti. Dodatno, ispitana je mogućnost izdvajanja aktivnog mjesta enzima radi razvoja minimalističkog katalitičkog peptida, s posebnim naglaskom na cistein kao ključnoj komponenti unutar katalitičke trijade, neophodnoj za učinkovitost takvih peptida. Sinteza seta cisteinom bogatih peptida koji pokazuju prilagodljivu aktivnost kao rezultat osjetljivosti tiolnih skupina na redoks okolinu, otvara nove mogućnosti za prilagodljivu peptidom posredovanu katalizu. Glavni cilj ovog istraživanja je razumjeti odnos između sekvence i funkcije katalitičkih peptida, čime bi se omogućio razvoj inovativnih katalitičkih peptida primjenjivih u različitim područjima, uključujući biokatalizu, sintezu lijekova i industrijske procese.

Ključne riječi: katalitički, peptidi, p-NPA, samo-sastavljanje

Contents

Bibliography   **56**

Appendices   **71**

List of Tables

List of Figures

1 Introduction

1.1 From enzymes to nanozymes

Enzymes, as remarkable biomolecules, exhibit extraordinary catalytic efficiency and display exceptional regio-, stereo-, and substrate specificity, playing a critical role in Earth's evolutionary processes [4]. In-depth investigations into the structure-function relationship have unveiled a sophisticated interplay of multiple chemical interactions, including electrostatic, covalent, and hydrogen bonding (H-bonding), which collectively facilitate catalysis. Enzymes exhibit the ability to recognize specific substrates, forming enzyme-substrate complexes through interactions at their active sites. The induced fit, triggered by substrate binding, results in a conformational change in the enzyme, which brings the reactive groups closer and, thereby, reduces the activation energy necessary for the catalytic reaction (Figure 1). This mechanism enables enzymes to accelerate chemical reactions, efficiently converting substrates into products. Post-reaction, enzymes release the products while remaining unchanged, allowing them to engage in multiple cycles of substrate binding and catalysis [4]. The inherent enzyme specificity proves vital for the regulation of metabolic pathways, underscoring their indispensable role in various cellular processes, including energy production and breakdown of molecules such as proteins, nucleic acids and lipids [1]. Enzymes are classified into seven groups based on their ability to catalyze a wide range of chemical reactions (Table 1).

Hydrolytic enzymes, known as hydrolases (EC3) draw attention for their prevalence in living systems and growing importance in various industrial applications [5]. Within this class, serine proteases have become a central focus in efforts to replicate enzyme functions. The active sites of these enzymes often showcase a hydrophobic binding pocket containing three closely spaced amino acid residues (histidine, aspartate, and serine) collectively referred to as the catalytic triad. This triad is complemented by nearby residues engaged in hydrogen bonding with reaction intermediates and transition states, effectively lowering the activation energy of the catalytic reaction. In many serine proteases, the oxyanion hole, featuring two adjacent peptide N-H moieties, further reinforces this catalytic function [6]. The combination of a hydrophobic pocket, catalytic triad residues, and oxyanion hole in hydrolases collectively facilitates the hydrolysis of specific substrates at rates that approach the diffusion limit [7]. Replicating the unique structural features of hydrolases within a synthetic catalyst remains a persistent challenge for researchers [8].

In the early stages of enzyme biotechnology, the production of enzymes primarily relied on plant tissues and animal organs [9]. Around 1960, roughly 70% of the enzymes were derived from plant tissues or exudates and animal organs. However, within the following two decades, there was a notable transformation in this pattern. By the 1980s,
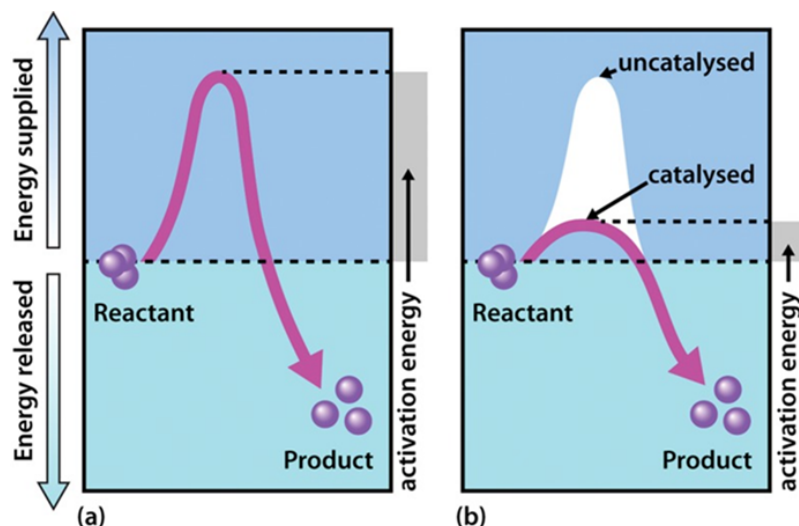
Figure 1: **Schematic representation of energy profiles of a chemical reaction**: (a) without a catalyst and (b) with a catalyst. The y-axis represents the energy level, while the x-axis indicates the reaction progress. The uncatalyzed pathway (a) shows a higher peak, representing a higher activation energy barrier, whereas the catalyzed pathway (b) requires less energy to reach the transition state, as indicated by the lower peak. The overall energy released by the reaction remains unchanged, demonstrating that the catalyst provides an alternative route with a lower activation energy for the reaction to proceed. Reproduced from reference [1]

microbial sources had gained prominence, signifying a substantial shift, and most industrial enzymes were produced from microbial origins [9]. In the enzyme production process, selected microorganisms are grown in controlled fermentation tanks, where optimal conditions are maintained to facilitate enzyme production. During fermentation, microorganisms undergo growth and actively generate the target enzyme as part of their metabolic processes. Critical factors such as temperature, pH, and nutrient availability are carefully regulated to maximize enzyme yield. After fermentation, the culture is harvested, and the enzyme is extracted and purified from the intricate mixture of microbial biomass, fermentation by-products, and media components. Purification employs various techniques such as filtration, chromatography, and precipitation to isolate the enzyme and eliminate impurities. The purified enzyme is then stabilized and concentrated for commercial use [10]. Modern biotechnological methods often incorporate genetic engineering to boost enzyme production by introducing specific genes into microorganisms, creating genetically modified strains optimized for increased enzyme yield [11]. However, the entire process proves to be demanding in terms of resources and time, underscoring the demand for alternative pathways of obtaining catalytically active biomolecules.

Today, different enzymes (proteases, lipases, carbohydrases, isomerases, etc.) have numerous commercial applications due to their high specificity for catalytic reactions [12]. Some applications include the textile, agricultural, cosmetic, pharmaceutical, food,

Table 1: **Classification of enzyme types by Enzyme Commission (EC) numbers and corresponding reactions.** This table outlines seven enzyme categories, reporting their EC number, the general type of reaction they catalyze, and provides examples for each category.

Enzyme Type	EC	Reaction	Examples
Oxidoreductase	EC1	Oxidation reactions involve the transfer from one molecule to another	Lipoxidases Dehydrogenases Glucose oxidase
Transferase	EC2	Transfer of groups of atoms from one molecule to another	Aminotransferase Transaminase
Hydrolase	EC3	Hydrolysis reactions involve the cleavage of substrates by water	Lactase Protease Trypsin
Lyase	EC4	Addition of groups to double bonds or formation of double bonds via the removal of groups	Pectate lysases Decarboxylase Hydratases
Isomerase	EC5	Catalyze the transfer of groups from one position to the other on the same molecule	Topoisomerase Glucose isomerase
Ligase	EC6	Catalyze the joining of two molecules to form a new bond	Glutathione synthase Aminoacyl tRNA synthetase
Translocase	EC7	Catalyze the movement of ions or molecules across membranes or their separation within membranes	ATP synthase Ubiquinone reductase

and processing industries [13]. Enzymes play a crucial role in the production of basic food products (cheese, beer, bread) [14] and are found in detergents [15], and increasingly used in the production of biofuels [16] and biopolymers [17]. In healthcare, they are employed as therapeutic drugs for enzymatic deficiencies and digestive disorders [18], as well as in diagnostic procedures such as ELISA and diabetes testing kits [19]. Enzymes play a pivotal role in the textile industry, where they enable environmentally friendly fiber processing [20]. Their applications have expanded in cosmetics, serving as free radical scavengers in sunscreen, toothpaste, and hair products [21]. Proteases in skin creams aid in exfoliation, contributing to skin health. Additionally, enzymes play a vital role in waste management, breaking down toxic pollutants in industrial and domestic waste for environmental safety [22]. The importance of this topic is further supported by the award of the 2018 Nobel Prize in Chemistry to F.H. Arnold, G.P. Smith, and Sir G.P. Winter for the development of enzymes through directed evolution, now used in the production of biofuels and drugs, as well as for the use of phage display technology to obtain antibodies to combat autoimmune diseases and metastatic carcinoma [23].

Over the past few decades, scientists have increasingly recognized artificial enzymes as cost-effective and exceptionally stable alternatives to natural enzymes in a wide range of applications [24]. Artificial enzymes are synthetic constructs designed to mimic the active sites and reaction environments of natural enzymes. Extensive exploration has been conducted on cyclodextrins [25], metal complexes [26], porphyrins [27], polymers

[28], and biomolecules (including nucleic acids and catalytic antibodies) [29]. However, achieving the intricate substrate specificity exhibited by natural enzymes remains a significant hurdle, affecting the versatility of synthetic counterparts [30]. Additionally, concerns about biocompatibility arise when artificial enzymes are applied in biological systems, as unexpected interactions or immune responses may occur.
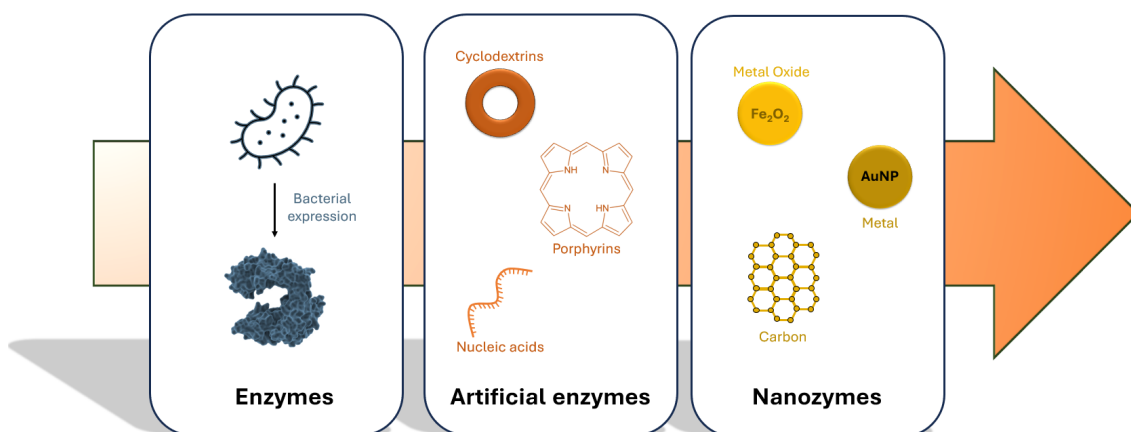
Figure 2: **Schematic representation of catalysts evolution from enyzmes to synthetic analogues.** On the left, enzymes are depicted as complex proteins derived from bacterial expression. In the center, artificial enzymes are illustrated, including cyclodextrins, porphyrins, and nucleic acids that mimic enzymatic activity. On the right, nanozymes are shown, which are nanomaterial-based catalysts, featuring metal oxides like Fe_2O_3, gold nanoparticles (AuNP), and carbon structures, indicating a progressive shift towards engineered catalytic systems with enhanced stability and functionality.

In recent times, inorganic nanomaterials have been found to exhibit enzyme-like activity (Figure 2) [31], mimicking the functionalities observed in natural enzymes [32, 33] for a broad spectrum of applications, ranging from medical biosensing [34] to environmental remediation [35] and treatment of bacterial infections [36]. Composed typically of inorganic, metal or metal oxide nanoparticles, they can replicate catalytic functions such as peroxidase, oxidase, catalase, and others, and offer several advantages over traditional enzymes such as flexibility of design, simplicity in synthesis, and ease of functionalization [37]. However, biocompatibility and toxicity are critical considerations that still need to be addressed for the use of nanozymes, especially in biomedical applications [38].

Despite the described examples of the development of catalytic materials, there is a need to design more biocompatible systems. One option is to focus on peptide-based materials that could offer the advantage of enhanced biocompatibility and specificity, and could be applied to a wide array of biomedical applications such as drug delivery, tissue engineering, and biosensing [39, 40, 41]. Peptide-based materials offer bioactivity, tunable properties, and biodegradability, making them promising candidates for interacting

with biological systems with minimal adverse effects. By exploiting the diverse functionalities of peptides, tailored designs can be achieved to address specific challenges in biomedical fields, thereby paving the way for innovative solutions in healthcare and biotechnology.

1.2   Peptides as minimalistic catalysts

Peptides have gathered attention as a promising group of molecules capable of facilitating biochemical transformations [42, 43, 44, 45]. These short chains of amino acids linked by peptide bonds play critical roles in various biological processes, acting as hormones, neurotransmitters, growth factors, and as key components of the immune response [46]. Unlike proteins, which are complex structures composed of 50 or more amino acids, peptides are smaller, typically containing between 2 and 50 amino acids. These relatively short sequences can be expressed by microorganisms or synthesized in laboratories with solid-phase peptide synthesis (SPPS) which was pioneered by Robert Bruce Merrifield in 1963 [47]. This groundbreaking technique revolutionized the field by simplifying the synthesis of peptides, earning Merrifield the Nobel Prize in Chemistry in 1984. SPPS allows for the stepwise construction of a peptide chain anchored to an insoluble resin [48]. The process begins with the attachment of the C-terminal amino acid of the peptide to a resin, protecting the amino group with a temporary chemical group to prevent unwanted reactions. Subsequent amino acids are then added one at a time, each also protected at the amino group. Between each addition, deprotection and washing steps are carried out to remove the temporary protective groups and any unreacted residues, respectively. This methodology enables the synthesis of complex peptides in a more controlled and efficient manner compared to conventional solution-phase synthesis. Over the years, SPPS has been refined and optimized with improvements in resin materials, protection group strategies, and automation, greatly expanding the accessibility and complexity of synthetic peptides used in research and drug development.

The idea of exploring catalytic peptides as a potential alternative to enzymes originates from the fact that these complex and highly organized enzyme structures had to evolve from simpler precursors [49]. A more profound understanding of their evolutionary journey could yield valuable insights into the fundamental principles governing enzyme catalysis. This understanding, in turn, could pave the way for the development of innovative catalytic sequences and biomimetic systems [50, 51, 52]. Peptide-based catalysts can replicate the active sites of enzymes, enabling the creation of catalytic systems with high specificity and efficiency [53]. They can be modified with diverse functional groups or metals to further boost their catalytic performance [54, 55] and exhibit excellent biocompatibility and low immunogenicity, rendering them well-suited for biomedical ap-

plications [56]. In comparison to enzymes, catalytic peptides offer several advantages, including their simpler structures, smaller size, modularity, and ease of production [57, 58]. Employing peptides as catalysts enables access to a more extensive and diverse chemical space than is possible with traditional small-molecule catalysts, thereby expanding the possibilities within the domain of catalysis and enzyme mimetics. Furthermore, peptides offer flexibility in design through the incorporation of amino acids responsible for diverse catalytic mechanisms in peptidic scaffolds, as well as have the ability to self-assemble into supramolecular architectures, creating nanomaterials with emerging properties [59].

1.3 Exploiting peptide self-assembly for the design of catalytic systems

The top-down and bottom-up approaches are two fundamental strategies used to create nanomaterials [60]. The top-down approach involves starting with a larger, bulk material and then using techniques like etching, milling, or lithography to remove parts of that bulk to achieve the desired smaller structure. This method is prevalent in semiconductor manufacturing where it allows for the precise patterning of microchips. Conversely, the bottom-up approach assembles materials from the molecular or atomic level, allowing components to self-organize into functional structures through chemical or physical interactions.

Peptide self-assembly is the spontaneous organization of peptides into highly ordered structures driven by intermolecular non-covalent interactions such as hydrogen bonding, hydrophobic effects, and electrostatic forces [3]. Sequences can be designed to adopt α-helical structures through inter-chain hydrogen bonding, leading to their self-organization or co-organization into coiled-coil structures facilitated by hydrophobic and electrostatic attractions. This design yields the formation of nanotubes and rigid extended nanofibers [61]. Conversely, inspired by the sequence Ac-AEAEAKAKAEAEAKAK-Am found in zuotin, a Z-DNA-binding yeast peptide, β-sheet forming peptides are usually designed with alternating hydrophobic and hydrophilic residues assembling through interchain hydrogen bonding and backbone amide inter-chain interactions, giving rise to more flexible β-sheet nanofibers that can entangle and form hydrogels at a critical gelation concentration [62]. Additionally, β-hairpin forming peptides, with residues like prolines in the middle facilitating the sequence turn, self-assemble through intra-chain hydrogen bonding into β-sheet-like nanofibrous structures, forming hydrogels [63]. Short aromatic peptides, frequently featuring an Fmoc or other aromatic group at the N-terminus and inspired by amyloid peptides, incorporate diphenylalanine (FF) in the sequence core, drive self-assembly through aromatic π-stacking, resulting in the formation of nanofibers capa-
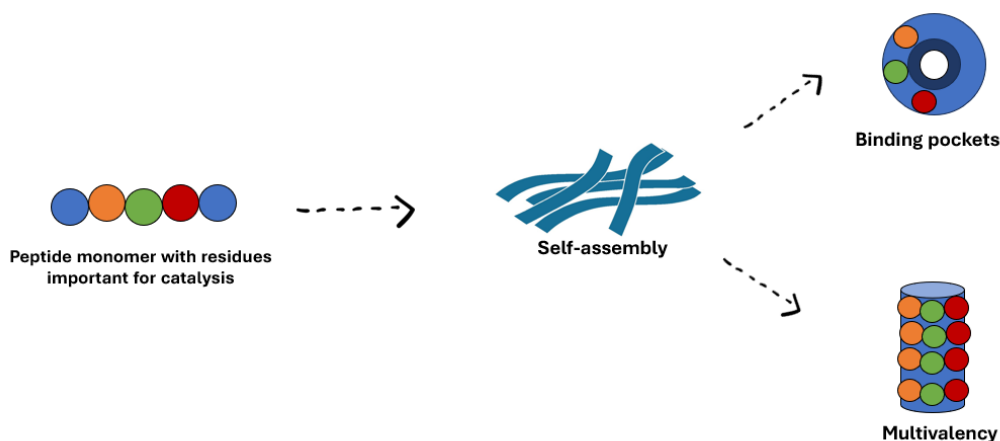
Figure 3: **Diagram illustrating how self-assembly can be exploted for the design of catalytic peptides**. Beginning with the monomeric peptide, leading to self-assembly into structured scaffolds, which facilitate the creation of binding pockets and enable multivalency, ultimately driving efficient catalysis reactions.

ble of hydrogelation [62, 64, 65, 66]. In addition, aliphatic peptide amphiphiles exhibit surfactant-like structures with hydrophilic peptide sequences capped with long hydrophobic hydrocarbon chains, facilitating self-assembly into micellar cylinders or nanofibers in aqueous media [67]. Purely peptidic systems are less explored, however they are particularly appealing due to their inherent biocompatibility [68, 69, 70].

Peptide self-assembly finds its application in pharmaceutical and industrial contexts. In the field of biomedicine, self-assembling peptides are explored for their potential in drug delivery systems, regenerative medicine and tissue engineering [52]. The controlled formation of nanofibers allows for the design of drug carriers with precise release mechanisms, improving therapeutic efficacy and reducing side effects. Additionally, the mimicry of natural extracellular matrices by self-assembling peptides aids in the creation of three-dimensional scaffolds for tissue engineering, promoting cell adhesion and growth. In the domain of materials science, peptide self-assembly contributes to the development of functional nanomaterials that find applications in the fabrication of catalytic systems, sensors, and nanoelectronics [71]. A number of approaches for the design of peptide-based catalytic systems have emerged, taking into account residues responsible for catalysis while exploiting self-assembly for the ordered presentation of catalytic moieties and the reduced dynamics of the system, thereby improving catalytic activity (Figure 3) [72]. By exploiting the potential of peptide self-assembly to form nanostructures with enhanced structural order it is possible to bypass the drawback that monomeric peptides typically lack well-defined three-dimensional structures characteristic for enzymes,

which hinders their catalytic efficiency. Self-assembly facilitates the exploration of multivalency, a concept wherein multiple catalytic residues and binding sites are displayed simultaneously. This increases the likelihood of substrate interaction and catalysis. Additionally, self-assembly allows for the design of specific binding pockets within structured frameworks. For instance, the creation of hydrophobic areas through the self-assembly of amphiphilic peptides can effectively capture a substrate's transition state, enhancing the catalytic process. Moreover, peptide nanostructures formed through self-assembly often demonstrate increased stability and resistance to denaturation. This attribute is particularly valuable for catalytic applications in harsh environments, where stability is crucial for maintaining catalytic activity over time.

However, replicating the intricate environment present in enzymatic active sites continues to be a significant challenge in the field of synthetic catalysis [8]. Enzymatic active sites often feature a complex arrangement of functional groups and a precise three-dimensional structure that are critical for their catalytic activity. Peptide-based catalysts are predominantly modeled after enzymes like aldolases, oxidoreductases, and hydrolases that generally have more flexible requirements regarding the spatial arrangement of functional groups [54]. This flexibility makes it easier to design and construct peptide catalysts that can mimic the function of these enzymes. In the following subsections, design strategies for aldolase, oxidoreductase, and hydrolase mimics that incorporate catalytically active residues into self-assembling scaffolds (Table 2), will be discussed.

1.3.1 Supramolecular aldolase mimics

Aldolases (EC 4) catalyze the formation or cleavage of the C-C bond through an interplay of Lys and phenolic OH of a proximal tyrosine present in the active site [54]. In addition, a Pro is capable of catalyzing an aldol C–C coupling reaction. Examples reported in the literature describe the incorporation of these key residues into self-assembling scaffolds such as the amphiphilic peptide consisting of ^{D}PPE-NH-$C_{12}H_{15}$ that self-assembles and effectively performs stereoselective catalysis for conjugate addition reactions of aldehydes to nitroolefins [73]. The catalytic activity of this peptide was also measured in complex mixtures such as milk and milk substitutes, coffee and tea, fruit and vegetable juices, soft drinks, honey solution, alcoholics, olive oil and vinegar [74]. In another example, a β-sheet forming peptide Ac-KLVFFAL-Am forms nanotubes with Lys residues pointing outwards and catalyzing the retro-aldol reaction of methodol to generate 6-methoxy-2-naphthaldehyde [75]. Similarly, an amphiphilic peptide forming nanotubes consisting of a FFV sequence modified with a decanoic acid at the N-termus and Lys at the C-terminus showed the ability to catalyze retro-aldol reactions of methodol, with increased efficiency upon the co-assembly with Fmoc-Tyr [76]. Finally, an aldolase-mimicking hy-

drogel catalyzing coupling reactions between cyclohexanone and 4-nitro-benzaldehyde was obtained by incorporating a Pro residue at the N-terminus of a β-sheet forming peptide with alternating Phe and Glu residues [77].

1.3.2 Supramolecular oxidoreductase mimics

Oxidoreductases (EC 1) catalyze oxidation–reduction reactions with O_2 or H_2O_2 as electron acceptor, with a flavin group or metal cofactor as part of the active site [54]. Upon self-assembly into nanosheets, the peptide YYACAYY coordinates Cu^{2+} ions and shows catalytic activity for the reaction of pyrrole polymerization [78]. Additionally, examples have been reported where a single Fmoc-amino acid displays catalytic activity upon metal coordination. Fmoc-Phe that is able to coordinate Cu^{2+} ions and self-assemble into nanosheets displaying laccase activity, oxidizing a broad range of widespread environmentally toxic phenolic contaminants [35]. Fmoc-Cys coordinating Fe^{3+} ions and self-assembling into nanovesicles promoting catalase-like reaction with H_2O_2 to generate oxygen with possible application in combating hypoxic tumors [79]. There are also peptides with reported dual activity such as the β-sheet forming Ac-IHIHIQI-Am peptide that assembles into nanofibers which catalyzes the hydrolysis of *para*-nitrophenyl acetate (*p*-NPA) upon Zn^{2+} coordination [80] and oxidation of 2,6-dimethoxyphenol upon Cu^{2+} binding [81]. Similarly, peptides consisting of seven, eight or nine binary alterating His and Tyr residues show both hydrolysis of *p*-NPA and, upon the addition of Cu^{2+}, oxidative polymerization of polypyrrole [82].

1.3.3 Supramolecular hydrolase mimics

Hydrolases (EC 3) typically include esterases, carbonic anhydrases, proteases, phosphatases, and lypases that have at least one histidine residue in the active site and use water to break chemical bonds [5]. Depending on the catalytic mechanism, the active site of the enzyme may include additional histidine residues that coordinate with a metal cofactor, such as Zn^{2+}, or other residues such as aspartate and serine (acting as an acid and a nucleophile, respectively) to form a catalytic triad or dyad. The enzyme carbonic anhydrase exploits the Zn-His mechanism for the rapid conversion of carbon dioxide (CO_2) to bicarbonate (HCO^{3-}) and a proton (H^+) [83]. The active site of carbonic anhydrase contains a zinc ion that is tetrahedrally coordinated by three histidine residues and a water molecule. The zinc ion polarizes the water molecule, significantly lowering its pKa and promoting the release of a proton, thus generating a highly reactive hydroxide ion. This hydroxide ion is perfectly positioned to attack a carbon dioxide molecule that diffuses into the active site, rapidly converting it into bicarbonate. The Zn-His mechanism is a model of efficiency, allowing carbonic anhydrase to process millions of CO_2 molecules

per second. This enzyme's rapid action is crucial for maintaining acid-base balance in blood and tissues [84].

Taking inspiration from the active site of carbonic anhydrase, the heptapeptide with alternating isoleucines and histidines with a glutamine (Ac-IHIHIQI-Am), described in the previous subsection, has been designed to hydrolyze p-NPA upon Zn^{2+} coordination [80]. To explore the impact of sequence composition on self-assembly and catalytic activity, several analogues were proposed, including a tyrosine-glutamine substitution (Ac-IHIHIYI-Am) [85]. This analogue displayed higher binding affinity for Zn^{2+} and demonstrated the potential to form photo-induced crosslinks through dityrosine, thereby expanding their catalytic capabilities. On the other hand, substitutions leading to an increased net charge, such as the glutamine-arginine mutation (Ac-IHIHIRI-Am), resulted in reduced activity. Furthermore, terminal charges of short peptides have shown to influence their activity [86]. Acetylation at the N-terminus and amidation at the C-terminus enhance catalytic activity, while uncapped peptides demonstrate reduced activity [85]. The activity of heptapeptides, such as Ac-IHIHIQI-Am, Ac-IHIHIRI-Am, and Ac-IHIHIYI-Am, that adopting cross β-amyloid fibrillar morphologies, underscores the necessity for a balance between flexibility and rigidity to effectively mimic enzyme active sites. This balance was found to result in higher esterase activity in fibers displaying increased flexibility.

Other metal cofactors can be used to enhance catalytic activity as it is the case with the peptide Ac-NADFDGDQMAVHV-Am inspired by the active site of RNA polymerase that assembles into amyloid fibers upon interaction with Mn^{2+} and catalyzes the hydrolysis of ATP into ADP and AMP [87]. Similarly, the peptide Ac-SDIDVFI-Am, inspired by a DNA polymerase sequence, assembles into amyloids upon Mn^{2+} coordination and catalyzes the hydrolysis of ATP, GTP, CTP and UTP [88]. Moreover, the previously described Ac-IHIHIYI-Am has also been reported to coordinate Cu^{2+} ions and efficiently hydrolyze paraoxon, which is a highly toxic organophosphate pesticide [89]. Metalo-dependent systems are distinguished by their catalytic efficiencies, surpassing those of all other reported designs [90]. Nevertheless, they still do not match the efficiency characteristic for enzymes. Bridging this gap and advancing the field requires a more comprehensive understanding of the delicate balance between sequence composition and function, which is intricately influenced by factors such as self-assembly and metal coordination.

The catalytic triad is a characteristic feature of many enzymes, consisting of three amino acids, typically serine, histidine, and aspartate or glutamate, strategically placed within the enzyme to facilitate the chemical reaction [6]. Each residue plays a critical role in catalysis: Ser acts as a nucleophile, His as a base, and Asp or Glu stabilizes the charge. This cooperative mechanism enables the enzyme to lower the activation energy of the reaction, thereby accelerating the conversion of substrates into products. Incorporating

the catalytic triad in a self-assembling scaffold, is another effective strategy for catalytic peptide design. In a series of three amphiphilic β-sheet peptides, each with a different arrangement of the triadic catalytic amino acids Glu (E), His (H), and Ser (S), and screened for their activities toward the *p*-NPA substrate, Ac-CFEFSFHFP-Am showed the highest catalytic efficiency, underscoring the crucial role of the order of the active residues within the peptide sequence for catalytic activity [91]. Another example is the incorporation of the catalytic triad residues His (H), Ser (S) and Gly (G) at the N-terminus of the QQKFQFQFEQQ scaffold, which has the ability to self-assemble into fibrillar β-sheet nanostructures [92]. This peptide assembly showed catalytic activity without affecting fibril formation. The efficiency of the system was enhanced upon co-assembly with a sequence terminating with an Arg (R) residue in place of a His (RSG). This substitution provided a more effective electrostatic binding site, thereby increasing the overall activity of the system [92]. Similarly, modification of the N-terminus of a pH-responsive self-assembling peptide $[VK]_4V^D PPT[KV]_4$ with HSG catalytic residues led to a catalytic peptide with tunable activity [93]. As the activity of $HSG[VK]_4V^D PPT[KV]_4$ is strictly dependent on self-assembly, in a neutral pH environment, the lysine residues are in a protonated state, leading to repulsive forces that hinder the formation of hydrogen bonds between hairpin strands, resulting in the peptide assuming a random coil structure with no catalytic activity. When the pH is raised to 9, lysine residues deprotonate diminishing these repulsive forces, enabling the peptide to form a β-sheet structure characterized by two strands arranged in an antiparallel fashion displaying catalytic activity. Furthermore, a polyproline scaffold that incorporates catalytic triad or diad residues led to the formation of functional polyproline II (PPII) helices that exhibited efficient *p*-NPA hydrolysis [94]. This approach results in catalysts displaying reduced activity compared to the Zn-His mechanism discussed in subsection 1.4.1. [90], possibly due to an imprecise mimicry of the enzyme's active site structured around the catalytic triad.

The multivalency achieved through self-assembly might not be enough to accurately reproduce the specific geometries inherent to enzyme active sites based on the catalytic triad. In addition to the residues directly involved in catalysis, it would be beneficial to assess the importance of amino acids immediately adjacent to these catalytic residues which can also affect catalytic efficiency by altering microenvironmental conditions, such as local pH or polarity, thereby enhancing interactions with substrates or transition states [72]. Consequently, a more comprehensive approach could be useful to improve the catalytic efficiencies of peptides based on the catalytic triad mechanism.

Table 2: **Overview of peptide-based catalysts**. This table outlines the peptide sequences along with their respective catalyzed reactions, the metal cofactors involved in these reactions (if any), and the enzyme class that each peptide sequence is designed to mimic.

Peptide Sequence [Ref]	Reaction Catalyzed	Metal Cofactor	Enzyme Mimicked
^{D}PPE-NH-C$_{12}$H$_{25}$ [73]	Stereoselective conjugate addition of aldehydes to nitroolefins	None	Aldolase
Ac-KLVFFAL-Am [75]	Retro-aldol reaction of methodol to generate 6-methoxy-2-naphthaldehyde	None	Aldolase
C$_{10}$-FFVK [76]	Retro-aldol reactions of methodol	None	Aldolase
P[FE]$_n$ [77]	Coupling reactions between cyclohexanone and 4-nitro-benzaldehyde	None	Aldolase
YYACAYY [78]	Pyrrole polymerization	Cu^{2+}	Oxidoreductase
Fmoc-F [35]	Oxidizing environmentally toxic phenolic contaminants	Cu^{2+}	Oxidoreductase
Fmoc-C [79]	Catalase-like reaction with H$_2$O$_2$	Fe^{3+}	Oxidoreductase
Ac-IHIHIQI-Am [80] [81]	p-NPA hydrolysis and oxidation of 2,6-dimethoxyphenol	Zn^{2+} or Cu^{2+}	Hydrolase and Oxidoreductase
Ac-[HY]$_n$-Am [82]	p-NPA hydrolysis and oxidative polymerization of polypyrrole	Cu^{2+}	Hydrolase and Oxidoreductase
Ac-IHIHIYI-Am [85] [89]	p-NPA hydrolysis and paraoxon	Zn^{2+} or Cu^{2+}	Hydrolase
Ac-IHIHIRI-Am [86]	p-NPA hydrolysis	Zn^{2+}	Hydrolase
Ac-NADFDGDQMAVHV-Am [87]	Hydrolysis of ATP	Mn^{2+}	Hydrolase
Ac-SDIDVFI-Am[88]	Hydrolysis of ATP, GTP, CTP, UTP	Mn^{2+}	Hydrolase
Ac-CFEFSFHFP-Am [91]	p-NPA hydrolysis	None	Hydrolase
HSGQQKFQFQFEQQ-Am [92]	p-NPA hydrolysis	None	Hydrolase
HSG[VK]$_4$V^{D}PPT[KV]$_4$-Am [93]	p-NPA hydrolysis	None	Hydrolase
Ac-PPWPPHPPPPPGY-Am [94]	p-NPA hydrolysis	None	Hydrolase
Ac-PPHPPHPPPPPGY-Am [94]	p-NPA hydrolysis	None	Hydrolase
Ac-PPSPPHPPPPPGY-Am [94]	p-NPA hydrolysis	None	Hydrolase
Ac-PPSPPHPPDPPGY-Am [94]	p-NPA hydrolysis	None	Hydrolase
Ac-PPCPPHPPDPPGY-Am [94]	p-NPA hydrolysis	None	Hydrolase
Ac-PPPPPHPPPPPGY-Am [94]	p-NPA hydrolysis	None	Hydrolase

1.4 Dynamic covalent chemistry

Unlike supramolecular chemistry, which utilizes weaker non-covalent bonds such as hydrogen bonds and hydrophobic interactions, dynamic covalent chemistry is characterized by the engagement of stronger, more durable covalent bonds [95]. These covalent bonds typically display slower kinetics in both formation and cleavage, highlighting their stability compared to the more transient bonds found in supramolecular structures. These reversible reactions are performed under thermodynamic control, enabling the formation of the most stable product. This principle highlights the importance of thermodynamic stability over kinetic barriers in determining the product distribution. Therefore, the outcome is influenced by reaction conditions, including temperature, pressure, and catalyst presence, allowing precise control over chemical processes [96].

This adaptability makes dynamic covalent chemistry a powerful tool in the development of responsive materials, drug delivery systems, and nanotechnology. The potential of dynamic covalent chemistry in drug delivery lies in its ability to create temporary drug-vector conjugates that form spontaneously and selectively. These conjugates navigate the body effectively and are designed to respond to specific triggers like pH and redox changes, enabling a controlled release of the drug at the targeted site [97]. By harnessing the principles of dynamic covalent chemistry, it is possible to design molecules that exhibit remarkable properties, including the ability to self-heal, adapt, and evolve, opening up new possibilities in materials science and molecular engineering [98].

Dynamic covalent chemistry includes two primary reaction types: firstly, exchange reactions, where one participant is replaced for another, maintaining the same bond type; and secondly, the formation of new dynamic covalent bonds through mechanisms such as condensation (like imine condensation) and addition (such as aldol reactions and cycloadditions) [95]. Bonds identified as dynamic within this context include those between C–C, C–N, C–O, C–S, S–S, and B–O.

1.4.1 Dynamic disulfide bonds

Thiols are a class of organic compounds characterized by the presence of a sulfur-hydrogen (–SH) group attached to a carbon atom [99]. This functional group is analogous to the hydroxyl group (–OH) found in alcohols but is distinguished by sulfur's unique chemical properties, which confer distinct characteristics and reactivity patterns to thiols. In biochemistry, the thiol group of the amino acid cysteine is critical for the structural and functional integrity of proteins [100]. Cysteine residues are capable of forming disulfide bonds (–S–S–), which contribute to the stabilization of protein tertiary and quaternary structures. Additionally, the activity of certain secreted soluble proteins and cell-surface

receptors is controlled through the targeted cleavage of disulfide bonds, highlighting the significant regulatory function of disulfide bridges within these biomolecules [101].

The formation of disulfide bridges is guided by fundamental thermodynamic principles [102]. In systems containing molecules with multiple thiol groups, the initiation of oxidation leads to a dynamic interconversion among dimers, trimers, and more complex oligomeric structures. This process guides the system towards a thermodynamic equilibrium, characterized by equivalent rates of bond formation and dissociation. At equilibrium, the concentrations of both bonded and unbonded species become stabilized, typically favoring the prevalence of a particular species. This equilibrium is sensitive to various external conditions, such as temperature, pH, and the presence of reducing or oxidizing agents, which can shift the balance towards either bonded or unbonded states [103].
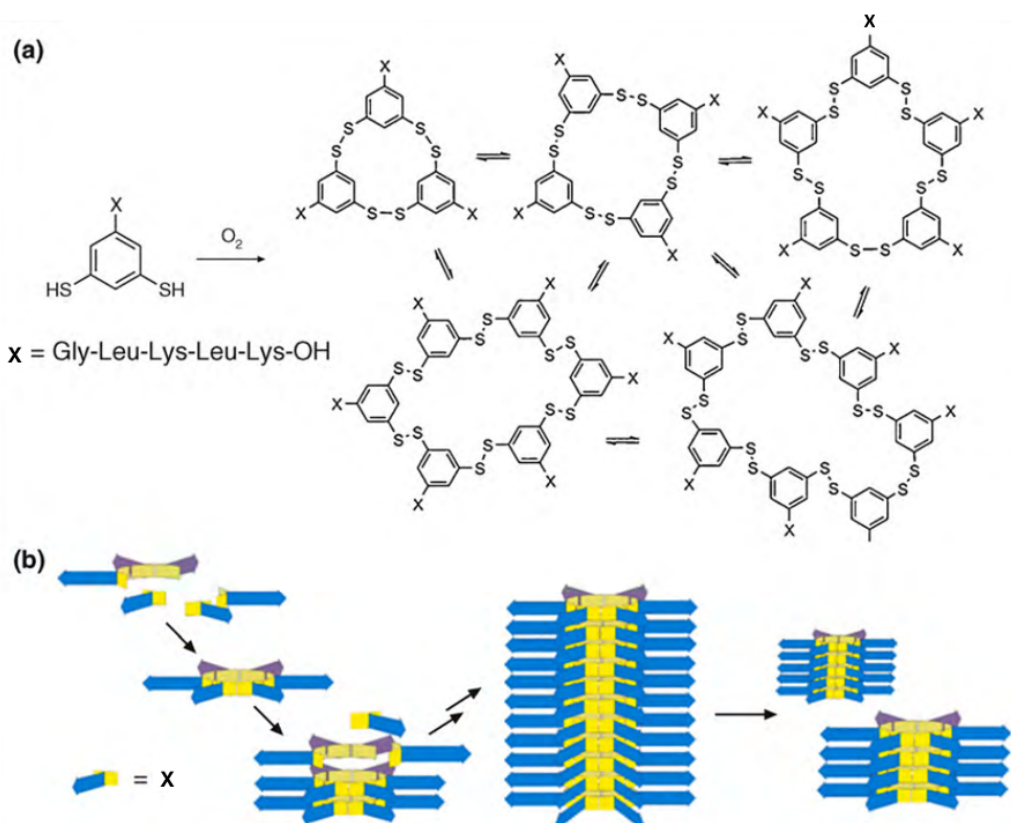
Figure 4: **Schematic illustration of dynamic thiol-disulfide interchange reactions in the presence of oxygen.** (a) The diagram shows the transformation of dithiol benzene derivatives into a network of interchanging disulfide species. (b) The proposed formation of fibers originating from a hexameric macrocycle. It features a core made of benzenedithiol, illustrated in yellow, with the peptide chain represented in blue. The formation of fibers is facilitated by the stacking of these macrocycles, which are stabilized as the peptide chains organize into extended β-sheets. Adapted from [2]

Dynamic disulfide bonds can be used to create a self-replicating system driven by self-organization [2]. In this example, a pseudo-peptide dithiol with a sequence that promotes β-sheet formation undergoes a thiol/disulfide exchange reaction in alkaline water, leading to the formation of various macrocycles, among which, two are capable of self-assembling into fibrous structures (Figure 4). This fibrous formation initiates an auto-templating effect, resulting in the system favoring a single macrocycle. Additionally, the specific macrocycle that is selected varies depending on the type of mechanical agitation applied to the mixture, demonstrating the impact of mechanical forces on the selection process. In another example, disulfide bridges formed between cysteine and penicillamine, an amino acid that closely resembles cysteine but features dimethyl substituents, apart from the thiol group, attached to β-carbon, facilitate the creation of heterodimers characterized by mutual orthogonality [104]. These heterodimers can be used for the labeling of proteins and the assembly of functional hybrid molecules. In addition to the spontaneous formation of disulfide bridges, environment can be used to trigger the oxidation or reduction of thiols that can lead to emerging functions [105]. In the case of the peptide Ac-CFKFEFKFEC-Am, cyclization of the peptide through disulfide bridge formation imposes a conformational limitation, hindering the ability to assume the β-sheet conformation essential for self-assembly [106]. When the disulfide bond is reduced using TCEP, the peptide shifts to the favored β-sheet conformation, leading to rapid self-assembly into fibrillar structures. Similarly, a L-buthionine-sulfoximine-based self-assembled peptide derivative, featuring a disulfide bridge, forms spherical nanoparticles that upon disulfide bridge reduction, triggered by GSH, changes its morphology to nanofibers enabling functions of GSH depletion and biosynthesis inhibition [107].

These examples demonstrate how dynamic covalent chemistry serves as a foundation for innovative applications in bioscience and materials science, enabling the development of novel therapeutic strategies and biomaterials with tunable properties.

1.5 Optimization of peptide sequences for biomedical applications

The studies of natural hormones including vasopressin, oxytocin, insulin and gonadotropin-releasing hormone (GnRH) and their phisiological activities lead to the development of the first therapeutic peptide, insulin, in 1921 [56]. Since then, the field of therapeutic peptides has expanded, and nowdays there are more than 80 peptide drugs approved worldwide [108]. Therapeutic peptides can act as neurotransmitters, hormones, growth factors, anti-infective agents or ion channel ligands [109]. Similarly to biological therapeutics, they trigger intracellular effects by binding to cell surface receptors while offering the advantages of lower immunogenicity and reduced production cost compared to biological therapeutics. However, only 6 % of FDA-approved therapeutics are peptide-based

drugs [110]. One of the main limitations in therapeutic use is their poor metabolic stability, which hampers their oral administration. The trial-and-error-based synthesis and profile tests are a huge barrier for concise and rapid lead optimization. Having a peptide molecule that combines high potency and selectivity with metabolic stability and membrane permeability would be highly advantageous. Recent advances in peptide synthesis, site-specific modifications and functionalization strategies have played a crucial role in addressing these limitations [111, 112]. For example, strategies including N-terminal acetylation, cyclization and incorporation of D-amino acids have proven effective in enhancing the stability and structural diversity of peptides [113]. This, in turn, results in improved peptide bioactivity and pharmacokinetics. In the following subsections, I will explore the most common strategies for peptide modifications, categorized by whether the modifications include chemical alterations to the sequence or changes to the peptide's configuration.

1.5.1 Modifications at the sequence level

Serum stability refers to the resilience of a substance, such as a peptide, protein, or drug, when exposed to the conditions found in blood serum and it can be easily assessed in the laboratory by incubating the peptide in human serum at $37°C$, taking samples at specific time intervals to analyze peptide concentration and assess degradation over time [114]. Peptides typically exhibit a stability ranging from 2 to 30 minutes [115], which can be enhanced through various modifications at the sequence level that include chemical modifications of the sequence or the introduction of unnatural amino acids (Figure 5) [113].
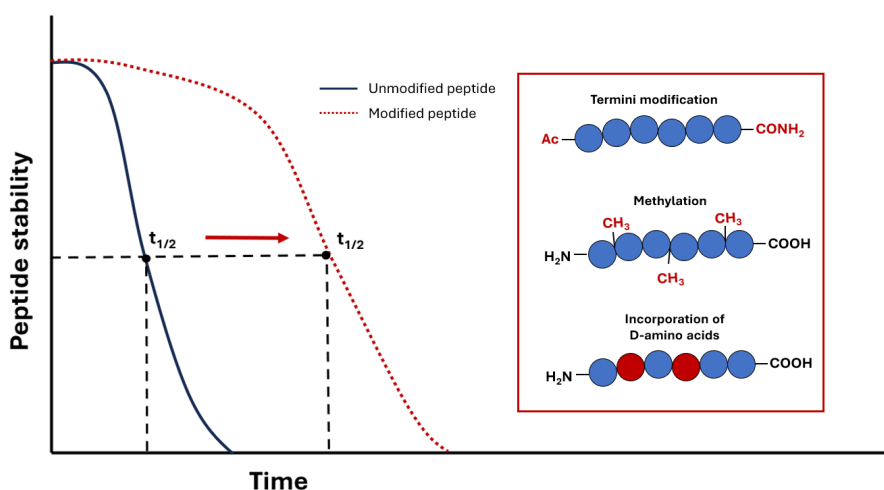
Figure 5: **Modifications at the sequence level.** Graphical representation comparing the stability over time of an unmodified peptide versus a modified peptide. The modified peptide shows an extended half-life ($t_{1/2}$) due to modifications including termini protection, methylation, and the introduction of D-amino acids, all of which contribute to increased stability against enzymatic degradation.

N-methylation, a process extensively employed in nature for DNA and histone modifications, can be applied in peptide synthesis to alter the stability of peptides by protecting them from proteases [116]. Methylation at the N-backbone of peptides has shown to introduce steric hindrance, effectively obstructing enzymatic cleavage [42]. Moreover, it reduces the polar surface area, particularly in cyclic peptides, thus improving their membrane permeability and oral bioavailability [117]. N-terminal acetylation, a cotranslational modification, affects approximately 85% of human proteins and 50% of yeast proteins influencing their stability, activity, folding, and localization [118, 119]. N-terminal acetylation of peptides can be performed as the final step in solid-phase peptide synthesis (SPPS) by treating the unprotected N-terminus with acetic anhydride. This modification has been shown to protect peptides from aminopeptidases, thereby enhancing their stability in serum. [120]. C-terminal amidated peptides can be synthesized using Rink amide resin during solid-phase peptide synthesis (SPPS). This resin features a linker that, upon cleavage, releases the peptide with an amidated C-terminus. This modification enhances the peptide's resistance to degradation by carboxypeptidases, which typically target free carboxyl termini [121]. While C-terminal amidation alone offers negligible stability improvements alone, its combination with N-terminal acetylation significantly elevates peptide stability, indicating a synergistic effect that extends beyond the additive contributions of each modification.

The incorporation of D-amino acids represents a well-established strategy to enhance the serum stability of peptides [113]. Given that D-amino acids are not naturally found in proteins within the human body, proteolytic enzymes, which are tailored to recognize and cleave peptide sequences made of proteinogenic L-amino acids, fail to identify peptides containing D-amino acids as targets for degradation. The substitution of L-amino acids with D-amino acids in peptides can be performed by replacing them fully or partially. Full substitution, known as the enantio approach, involves replacing all the L-amino acids with their D- counterparts. On the other hand, the retro-enantio approach entails the introduction of D-amino acids together with reversing the peptide sequence. Research indicates that the enantio strategy enhances serum stability, while the retro-enantio method improves both serum stability and membrane permeability [122, 123]. Partial substitution of L-amino acids with D-amino acids is strategically employed when certain residues should remain in the L-form, such as in peptides involved in epitope recognition, while still aiming to enhance serum stability. Studies have shown that the efficacy of partial substitution in improving serum stability is influenced by the position of the substituted amino acids [124]. In particular, substitutions positioned near both the N- and C- termini have been associated with the greatest improvement in serum stability.

1.5.2 Cyclization

Peptide cyclization is a strategic modification of the sequence that involves the formation of a covalent bond within an initially linear peptide sequence, leading to improved serum stability, binding affinity and cell-membrane permeability [121, 125, 126]. One of the primary benefits of peptide cyclization is its ability to confer protection against prote-olytic enzymes. The closed-loop ring structure can restrict access to susceptible cleavage sites, reducing the peptide's vulnerability to enzymatic hydrolysis. This enhanced stability extends the peptide's half-life in biological environments, improving its efficacy as a potential therapeutic agent [126]. Moreover, peptide cyclization can contribute to structural rigidity, promoting specific conformations essential for biological activity. The constrained topology imposed by cyclization can limit conformational changes resulting in improved binding affinity and enhanced biological activity [127]. The impact of cyclization on the stability of peptides is highly context-dependent and can vary based on the specific peptide sequence, the type of cyclization strategy employed and the intended application.

Peptide cyclization can be broadly classified into five main categories (Figure 6) [128]:

- side chain-to-side chain

- disulfide bridge formation

- head-to-tail (also known as backbone cyclization)

- head-to-side chain

- tail-to-side chain

Given the directional nature of polypeptides, where the first residue possesses amino functionality (N-terminus) and the last residue has carboxylate functionality (C-terminus), cyclization can be achieved by connecting the N- and C-termini through an amide bond, also known as head-to-tail cyclization. Another type of cyclization is the formation of intramolecular disulfide bonds between the thiol functionalities of two cysteine residues, resulting in a cyclic conformation commonly found in peptides and proteins, including insulin and antibodies. It should be noted that approximately 50% of the cysteine residues in polypeptides exist in the form of disulfide bonds [129]. Hormones such as oxytocin, vasopressin, and somatostatin are examples of natural cyclic peptides, cyclized through the formation of disulfide bridges [126]. Moreover, tail-to-side chain cyclization in peptide synthesis involves synthesizing a linear peptide with a reactive side chain, then promoting the formation of an amide bond between this side chain and the C-terminus in solution
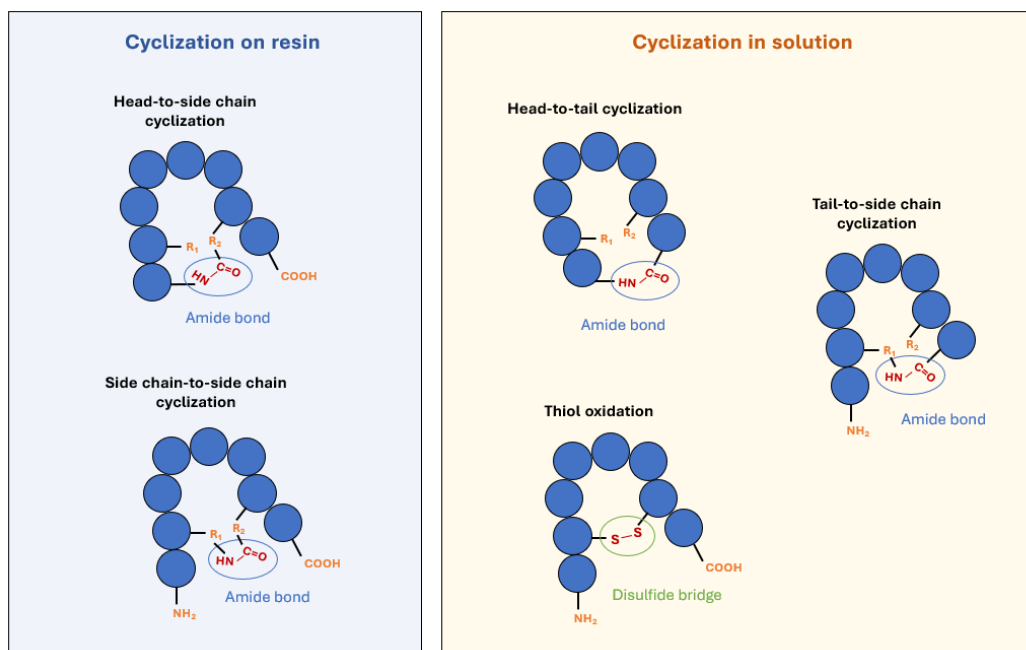
Figure 6: **Overview of Peptide Cyclization Methods.** On the left side, the image illustrates cyclization processes performed while the peptide is still on the resin, highlighting head-to-side chain and side chain-to-side chain cyclization, each of which yields an amide bond in different configurations. The right side of the image shows peptide cyclization reactions conducted in solution featuring head-to-tail and tail-to-side chain cyclizations that result in the formation of an amide bond, as well as thiol oxidation leading to the formation of a disulfide bridge.

[130]. The primary limitation of these cyclizations is the requirement to conduct them in solution. This often leads to a lack of precise control over the reaction, resulting in unwanted side reactions due to insufficient selectivity and a complex purification process, ultimately yielding low amounts of the desired pure peptide [131].

Alternatively, cyclization techniques that involve the formation of amide bonds between two side chains or a side chain and the N-terminus, after selective removal of side chain protecting groups such as Mmt or 0-2-PhiPr, can be effectively performed on resin [132]. The formation of such amide bonds employs more reactive coupling agents such as phosphonium salt (PyBOP), making it less straightforward than standard amide bond formation between amino acids, but ultimately leading to a substantial yield of pure cyclic peptides following resin cleavage and application of standard purification methods. Recent advances in the field of cyclic peptides combine thiol chemistry and non-native linkage, creating extensive cyclic libraries, wherein linear dithiol peptides are cyclized through interactions with bis-electrophiles. These cyclization methods yield highly pure peptides that can be screened for serum stability and biological activity and accelerate the detection of therapeutic peptides [133].

2 Discussion

Despite significant advances in the field of catalytic peptides, a comprehensive understanding of the fundamental factors influencing their performance and the intricate sequence-activity relationship remains challenging. This challenge arises from the complex interplay between the intrinsic structure of peptides and their extrinsic environment.

In our research, we conducted a thorough review of the existing literature to delineate the primary trends in peptide self-assembly that are applicable as frameworks for integrating catalytic residues described in section 2.1. Subsequently, we created a detailed dataset comprising sequences identified as active or inactive towards specific substrates, namely *para*-nitrophenyl acetate (*p*-NPA) and *para*-nitrophenyl phosphate (*p*-NPP), as cited in the literature described in Section 2.2. This process aimed to collect and analyze the accumulated knowledge within this field using it as a starting point for the design of novel catalytic systems. Our research identified two primary design strategies prevalent in the literature: the integration of His residues capable of coordinating with zinc (Zn) ions, and the embedding of a catalytic triad within self-assembling scaffolds. Based on these findings, we developed two novel systems consisting of histidine-rich peptides (Section 2.3) and cysteine-rich peptides (Section 2.5), each adopting one of the strategies outlined.

During the compilation of our dataset, we focused on the *p*-NPA assay as a standardized method for assessing the catalytic activity of enzymes and peptides due to its widespread application. This assay offers a rapid and straightforward means for the preliminary screening of potential catalytic sequences. Nevertheless, it is a sensitive technique that necessitates careful consideration of several variables, including temperature, pH, and peptide concentration, to guarantee consistent and reproducible outcomes. We documented our experiences and findings related to this assay in the context of peptide research and synthesized our insights into a published article, described in Section 2.5. Additionally, our analysis highlighted a noticeable absence of cyclic peptides in the designs reported to date. The conformational heterogeneity exhibited by linear peptides may contribute to their lower catalytic performance compared to enzymes. To address this issue, we proposed the introduction of rigidity through cyclization in both of our designed systems as a means to evaluate whether the reduced flexibility of short peptides can impact their catalytic activity.

Our research on the effect of amino acid disposition, cyclization, and incorporation of D-amino acids on the ability of peptides to self-assemble, coordinate Zn^{2+} ions, and show intrinsic hydrolase-like activity sheds light on the relationship between peptide structure and activity, further advancing our understanding of the principles governing the catalytic activity of short peptides. Additionally, by utilizing the dynamic covalent chemistry of the thiol group of Cys as part of the catalytic triad, we have created a catalytic

peptide that features tunable activity, responsive to changes in its environment.

In the sections that follow, we will provide an in-depth exploration of the major contributions of this work, complemented by a critical examination of the results derived from the doctoral thesis situating the research within the broader framework of existing scientific knowledge. Sections 2.1, 2.2, 2.3 and 2.5 delve into research that has been peer-reviewed and published in journals. Section 2.4 highlights our most recent results, released as a preprint and in the process of being finalized for submission to a journal.

2.1 Exploiting peptide self-assembly for the development of minimalistic viral mimetics

Peptide self-assembly is a natural phenomenon in which peptides spontaneously organize into well-defined supramolecular structures driven by non-covalent interactions such as hydrogen bonding, hydrophobic effects, and electrostatic forces [60]. Biomedical applications of peptide self-assembly can be found in drug delivery, where peptides can form carriers capable of encapsulating therapeutic agents, targeting specific cells, and releasing drugs in response to environmental stimuli [52]. Moreover, peptide materials can be used in tissue engineering, where peptide scaffolds provide a framework for cell attachment and growth, aiding in tissue regeneration [134]. In the wake of the COVID-19 pandemic, there was an urgent demand to develop new viral mimetics to boost our defenses against viral infections, offering innovative approaches to vaccine development or targeted therapeutic delivery [135]. In this sudden change in every aspect of life (social, economical, etc.) driven by the pandemic, we envisioned that peptide self-assembly could offer a potential solution in building biocompatible nanoamterilas with potential application in therapy and diagnosis by exploiting the existing knowledge on supramolecular materials.

In this manuscript, an overview of the morphological control of nanostructures, achieved through sequence design, is presented, that is exemplified by three main self-assembly patterns: (i) peptides with high content of aromaticity, (ii) binary alternating sequences of hydrophobic-hydrophilic residues that generally lead to fibrillar morphology, and (iii) surfactant-like peptides that can form fibrillar or sperical morphologies depending on the peptide sequence (Figure 7) [3]. Moreover, the review focuses on the possibility to obtain dimensional control and enhance structural complexity through co-assembly. Finally, we highlight the importance of peptide self-assembly in the design of virus-like materials by dividing them into two main categories, namely capsid-like nanomaterials and multicomponent peptide-DNA complexes, where we describe the use of peptides as structural and functional components, respectively.

It is important to highlight the significance of peptide self-assembly for the design and creation of synthetic models that closely mimic the structural attributes of specific viruses. By leveraging the process of peptide self-assembly, it is possible to engineer cost-effective viral mimetics that are capable of selectively binding to cellular receptors, enabling precise drug delivery directly into the cells. Furthermore, they can serve as an invaluable research platform, allowing for in-depth study of viral mechanisms and
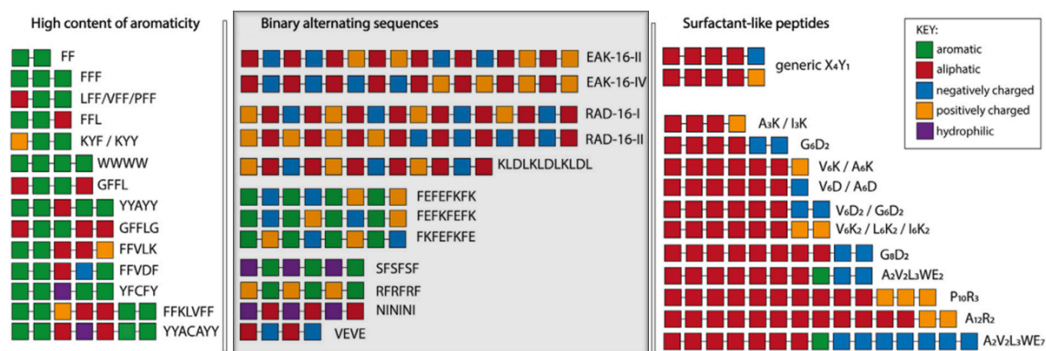
Figure 7: **Schematic representation of the main sequence patterns found in self-assembling peptides**. They can be divided in three categories, namely high content of aromaticity, binary alternating patterns of hydrophobic-hydrophilic residues and surfactant-like, highlighting the pattern chosen for the design of out first catalytic system. Adapted and reproduced in part from [3].

interactions without the inherent risks associated with handling live, potentially hazardous viruses. In addition to the advantages described above, this work is important beyond the design of viral mimetics offering an overview of the main principles that drive self-assembly in purely peptidic systems to a wider community interested in other peptide materials' applications . The relevance of this field can be seen from the large number of high-impact publications on the topic that describe various new avenues of using peptide materials in biomedicine and other fields [52, 70, 136, 137].

With this knowledge in mind, it is possible to navigate the vast peptide chemical space of sequences that self-assemble and direct the choice of amino acids for the peptide design favourable for a specific application (Figure 8). In drug delivery applications, spherical nanostructures are favored for their proficiency in encapsulating drugs, guiding the selection towards peptides with surfactant-like properties [138]. In contrast, the engineering of tissue scaffolds requires fibrous structures capable of supporting a three-dimensional cellular architecture [139]. This structural requirement promotes the use of peptides with either a significant presence of aromatic amino acids or peptides that feature binary alternating patterns of hydrophobic and hydrophilic residues, which are inclined to form fibrous β-sheet-like assemblies.

In the context of this dissertation, peptide self-assembly is exploited as a means of enhancing the catalytic activity of peptides. Incorporating catalytically active residues into self-assembling peptide scaffolds leads to a multivalency effect upon peptide self-assembly, thereby achieving better activity than with individual peptide monomers (Figure 9A). An alternative strategy involves the integration of catalytic residues and binding site residues into multiple sequences, which show self-assembly propensity [92]. Through the co-assembly process, these peptides collaboratively form active sites that mimic those observed in enzymes, thereby replicating their catalytic functions. Furthermore, self-
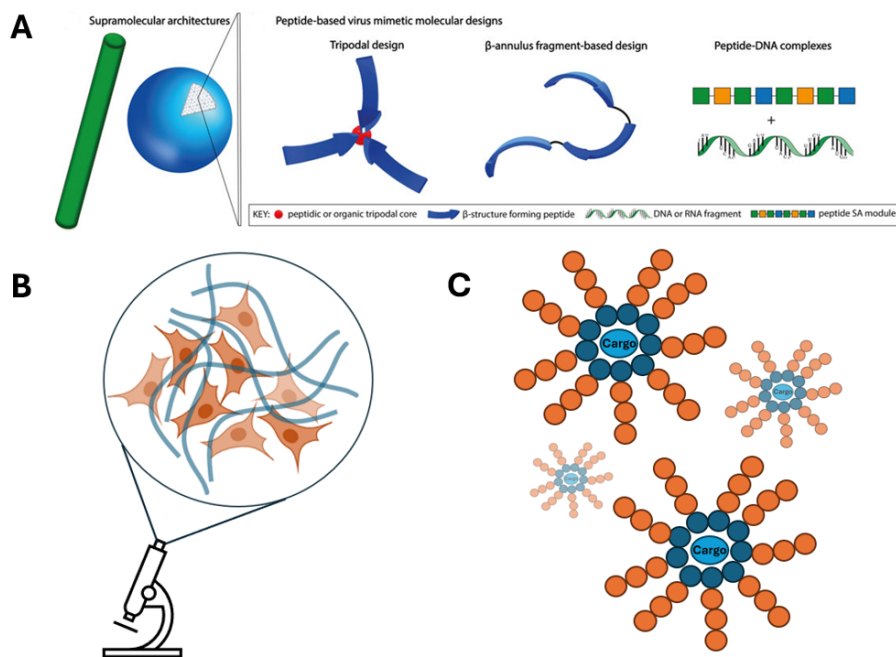
Figure 8: **Strategically directed peptide self-assembly for targeted applications.** (A) The most common supramolecular morphologies of self-assembling peptides and molecular designs used for peptide-based virus mimetics based on capsid-like materials (tripodal and β-annulus designs) and peptide-DNA/RNA complexes. Other applications include (B) tissue scaffolds based on fibrillar morphology or (C) entrapping cargo into spherical assemblies.

assembly can also be exploited to regulate the activity of catalytic peptides (Figure 9B). The integration of catalytically indispensable residues into a scaffold, whose assembly is dependant upon pH variations, enables precise control over the peptides' reactivity [93]. This sensitivity arises from amino acids within the sequence possessing charged side chains (Lys), which promote assembly only when the side chains attain a neutral charge, thereby eliminating electrostatic repulsions. Consequently, this leads to the creation of tunable catalysts, which are activated in specific pH conditions upon peptide self-assembly. Notably, alterations in pH facilitate reversible 'on' and 'off' catalytic activity, enabling the peptide to undergo multiple cycles of activation and deactivation.

This literature review was the basis for the design of our first catalytic system described in the section 2.3 of the thesis. The peptide design was based on the binary alternating sequences of hydrophobic-hydrophilic residues being histidine and isoleucine. The choice of this design was driven by the objective to exploit the His-Zn catalytic mechanism, which relies on the interaction between histidine residues and a metal cofactor for the hydrolysis of esters. To incorporate histidine effectively, it was critical to have two such residues to be in close proximity for metal cofactor coordination, without being adjacent to avoid potential interference caused by their bulky imidazole side chains and charge. Therefore, inspired by Rufo et al. [80] we adopted a binary alternating pattern
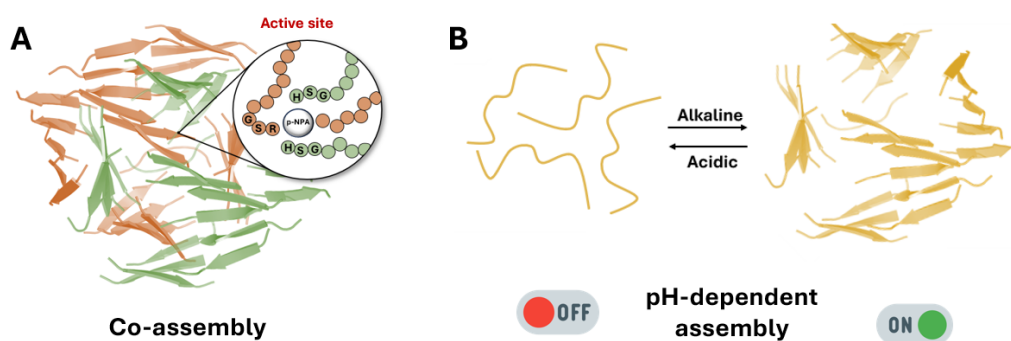
Figure 9: **Self-assembly has an influence on catalytic activity of peptides.** (A) The co-assembly contributes to the creation of active sites that mimic those in enzymes, enhancing the catalytic efficiency. (B) The dependence of self-assembly on solution pH enables the use of pH variations as a regulatory switch for catalysis, allowing for controlled activation or deactivation of the catalytic process.

of histidine and isoleucine, balancing the need for a hydrophobic amino acid to facilitate peptide self-assembly with the requirement for a hydrophilic amino acid to engage in metal cofactor coordination, ultimately leading to improved self-assembly propensity and enhanced catalytic activity. This topic, pointing out the main advantages and disadvantages of the described design strategy, will be described more in detail in section 2.3.

2.2 Manually curated dataset of catalytic peptides for ester hydrolysis

Publication: Janković, P., Otović, E., Mausa, G., and Kalafatovic, D. (2023). *Data in Brief*, 109290.

With the increasing demand for enzymes as a solution for various biological and industrial problems, combined with their difficult and expensive production and inherent instability in organic solvents or under harsh temperature and pH conditions, peptides have emerged as a valuable alternative [58]. Catalytic peptides are simple, tunable, and low-cost biomolecules able to catalyze a variety of chemical reactions, including ester hydrolysis [43, 44]. However, due to the lack of well-defined three-dimensional structures they often present lower catalytic efficiencies when compared to enzymes. Various mechanisms of action and sequence designs have been developed so far in order to bridge this gap between catalytic peptides and enzymes [57]. One of the first successful purely peptidic catalyst was Ac-IHIHIQI-Am based on the active site of carbonic anhydrase featuring two histidines that coordinate the metal coofactor, alongside isoleucines and a glutamine promoting self-assembly into fibrillar nanostructures, thereby enhancing the catalytic efficiency [80]. Over the past decade, majority of the studies investigating the His-Zn^{2+} catalytic mechanism in short peptide catalysts have focused on modifications of the Ac-IHIHIQI-Am sequence yielding peptides with comparable activities [85, 86]. Other mechanisms explored in the literature include the incorporation of catalytic triad residues or just histidine as functional moieties into self-assembling scaffolds mimicking enzymatic active sites, however such approaches often lead to less effective catalysts than those utilizing metal coordination to drive their catalytic activity [91, 93]. To effectively address and improve the field, it was essential to collect and analyze all existing publications on the topic of purely peptidic catalysts. This comprehensive comparison of research efforts was crucial to identify current gaps in the field, making it easier to pinpoint weaknesses of existing designs with the intention of advancing the field.

In this paper, we present the first extensive, manually collected dataset consisting of published catalytic sequences active towards the *para*-nitrophenyl acetate (*p*-NPA) and the *para*-nitrophenyl phosphate (*p*-NPP) substrates. Along with the positive instances with experimentally confirmed esterase activity, we also annotated negative entries with experimentally confirmed lack of activity, which are of great importance in advancing the knowledge on sequence-to-function relationship, specifically in data-based approaches such as machine learning. Often, negative results remain unpublished resulting in imbal-

anced datasets with mostly positive instances.

As catalytic reactions and mechanisms are heterogeneous and substrate-dependent, data collection was based on the standard colorimetric assays used for the experimental validation of ester and phosphoester hydrolysis. These reactions were selected with the intention of standardizing the reported catalytic parameters and allow easier comparison of reported catalytic peptides. The hydrolysis of *p*-NPA serves as a widely accepted benchmark for assessing catalytic activity, primarily because it is a straightforward reaction that can be monitored via UV/Vis spectroscopy. This method facilitates a rapid screening process, allowing for the swift identification of peptides that exhibit potential catalytic activity.

p-NPA $R_1 = CH_3$

p-NPB $R_2 = (CH_2)_2CH_3$

p-NPO $R_3 = (CH_2)_6CH_3$
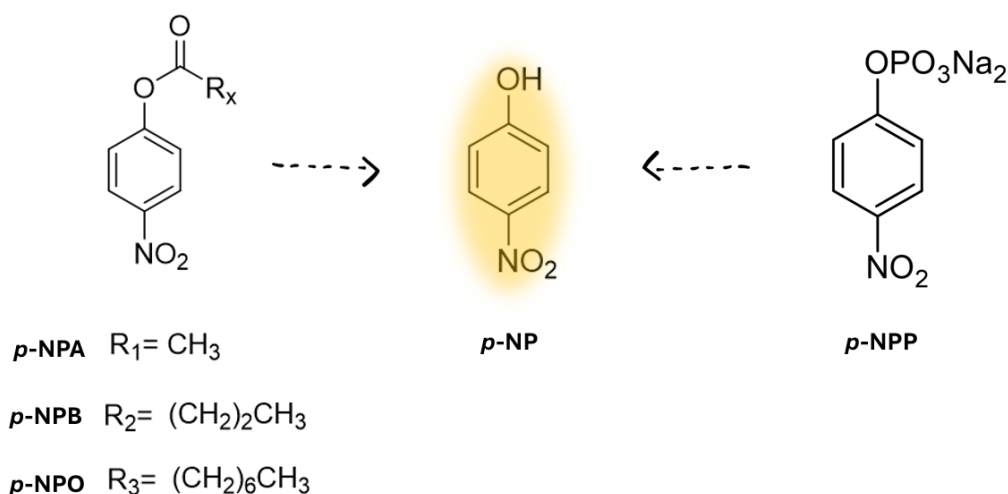
Figure 10: **Benchmark substrates used to obtain a standardized dataset.** This schematic represents the chemical conversion of esterase substrates: para-nitrophenyl acetate (*p*-NPA), para-nitrophenyl butyrate (*p*-NPB), and para-nitrophenyl octanoate (*p*-NPO), along with the phosphatase substrate *para*-nitrophenyl phosphate (*p*-NPP) into *para*-nitrophenol (*p*-NP). These compounds were chosen as standard benchmarks to uniformize the reported results, as their hydrolysis produces a common product, which can be detected through UV/vis absorption at 405 nm.

In addition to data on *p*-NPA hydrolysis, our dataset incorporates available information about other alkyl-based substrates efficiently catalyzed by peptides, such as *para*-nitrophenyl butyrate (*p*-NPB) and *para*-nitrophenyl octanoate (*p*-NPO). These substrates are utilized for peptides that exhibit activity toward *p*-NPA, aiming to determine if their activity persists when confronted with substrates of greater complexity. Our study incorporates also peptides that hydrolyse *para*-nitrophenyl phosphate (*p*-NPP), a substrate that not only presents a more complex reaction, but also holds biological relevance because the processes of phosphorylation and dephosphorylation are fundamental to numerous signaling pathways, thereby underlining the critical role these reactions play in cellular

27

communication and function [140]. Moreover, we specifically selected these reactions because they uniformly yield *para*-nitrophenol (*p*-NP) as the final product (Figure 10). This consistency allows for direct comparison of catalytic efficiencies across different peptides and substrates, as the product formation is monitored using the same analytical technique.
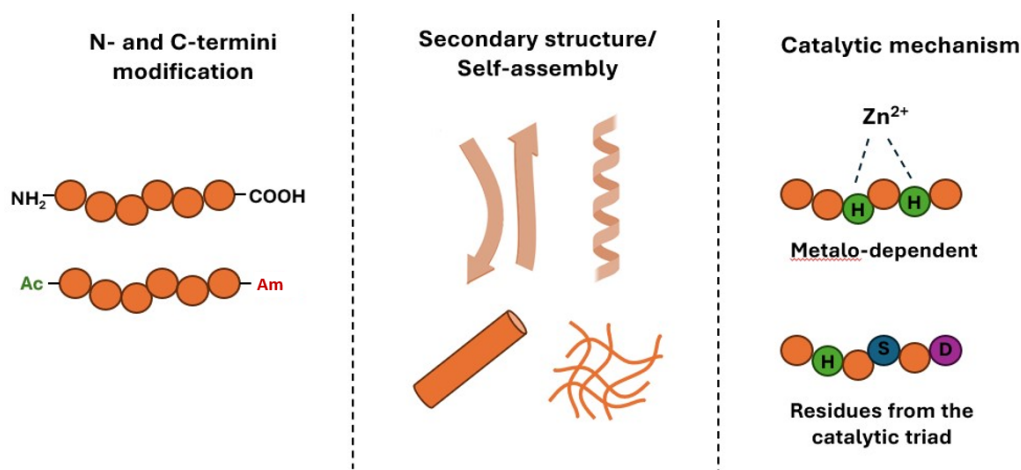
Figure 11: **Sequence characteristics included in the catalytic peptide dataset.** The first panel shows N- and C- termini modifications, with examples of both free amino (-NH$_2$) and carboxyl (-COOH) termini, as well as acetylated (Ac) and amidated (Am) termini. The second panel represents the observed secondary and supramolecular structures of catalytic peptides, including helices and β-sheets organizing into nanofibers. The final panel displays the identified catalytic mechanisms within the dataset: the metallo-dependent approach with histidines coordinating zinc ions and the approach exploiting residues from the catalytic triad.

Other important features included in the dataset are N- and C- termini modifications, self-assembly propensity and mechanism of action (Figure 11). Acetylation of the N-terminus and amidation of the C-terminus have been shown to improve catalytic activity by eliminating terminal charges that can affect the interaction of the substrate with the peptide. Thus, 75 % of the peptides in our dataset have both termini modified. The self-assembly propensity was included to determine the extent of designs that rely on self-assembly for the improvement of catalytic efficiency, along with the morphology of the supramolecular structures. We classified the collected peptides according to the active residues present in their sequences. Our analysis showed that over half of the designs (53%) utilize a metallo-dependent approach, whereas the rest exploits histidines or a combination of residues from the catalytic triad (Figure 12). Furthermore, we provide a descriptive statistical analysis of the dataset as well as the SMILES (Simplified Molecular-Input Line-Entry System) annotation which can be useful for machine learning-based predictive modeling because it encodes important information about the molecular structure of the peptides.

This dataset provides a comprehensive overview of the latest advances in the field of
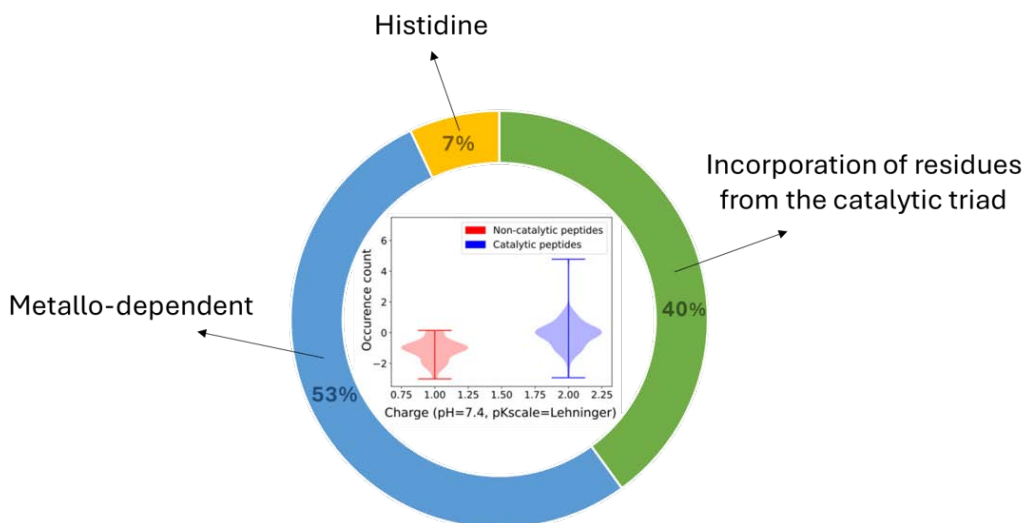
Figure 12: **Catalytic mechanism distribution in the peptide dataset.** The pie chart categorizes the peptides by their catalytic mechanisms as reported in the dataset: 53 % utilize a metallo-dependent mechanism, 7% rely on histidine, and 40 % involve residues from the catalytic triad. The inset violin plot contrasts the charge distribution of catalytic versus non-catalytic peptides, suggesting a correlation between charge at physiological pH and catalytic activity.

catalytic peptides, providing valuable insights into strategies employed for their design. It serves as a crucial resource for researchers, laying the groundwork for the creation of innovative next-generation peptide-based catalysts. By analyzing this dataset, it is possible to identify trends, challenges, and opportunities within current catalytic approaches, thereby informing the development of more efficient, effective, and sustainable catalytic solutions.

Based on this dataset, combined with the knowledge derived from the exploration of self-assembly mechanisms detailed in Section 2.1, we developed a catalytic system described in Section 2.3. When the catalytic efficiencies across the entire dataset were compared, we observed that Ac-IHIHIQI-Am peptide remains to date one of the most efficient catalysts reported in literature. Interestingly, most of its modifications and analogues involved linear peptides with substitutions that incorporated bulky or charged amino acids. These substitutions significantly alter the peptide's characteristics, impacting the catalytic efficiency. Therefore, we implemented a subtle modification, substituting glutamine with asparagine, which differs only by a carbon atom in the side chain. This seemingly minor change influenced both the catalytic activity and the self-assembly propensity. In addition, we observed that the existing designs lacked cyclic peptides. To address this gap, we cyclized our peptide through head-to-side chain cyclization. This process introduced structural rigidity, which allowed us to explore its effects on metal coordination, catalytic activity, and self-assembly properties. Through these modifications, we aimed to deepen

our understanding of the intricate relationship between the peptide sequence, the corresponding supramolecular structure and functional performance.

2.3 Factors influencing the catalytic activity of metal-dependent histidine-rich peptides: sequence, conformation, stereochemistry, self-assembly or their interplay?

Publication: Janković, P., Babić, M., Perčić, M., Pina, A. S., and Kalafatović, D. (2023). *Molecular Systems Design and Engineering*, 8(11), 1371-1380.

Over the past decade, peptides have been increasingly recognized for their versatility as catalysts across a spectrum of chemical reactions, such as ester hydrolysis, leading to the exploration and development of various design strategies aimed at optimizing peptide-based catalysts [58, 72]. Specifically, as highlighted in Section 2.2, the most prominent approach present in the literature combines peptide self-assembly with the integration of histidine residues to enable a metal-dependent catalytic function. As illustrated in Figure 12 of Section 2.2, this approach accounts for over half of the strategies reported. Inspired by the mechanism of carbonic anhydrase, with three histidine residues coordinating a metal cofactor, the fist reported metal-dependent peptide Ac-IHIHIQI-Am [80] forms β-sheet-like assemblies and is capable of catalyzing the hydrolysis of *p*-NPA, highlighting the potential of peptides as versatile and efficient catalysts in biochemical reactions. Since then, a variety of analogues utilizing the Zn-His mechanism have been developed and reported, showcasing the widespread adoption and exploration of this catalytic strategy [85, 86]. However, understanding the sequence-to-function correlation in peptide-based catalysts remains a formidable task, as even subtle alterations at the sequence level can alternate their catalytic activity.

The purpose of this paper is to elucidate the intricate relationship between peptide sequences, their self-assembly propensity and catalytic activity [141]. To address this challenge, based on the described self-assembly patterns together with the manually curated dataset with examples of catalytic peptides reported in the literature, we propose a set of linear and cyclic histidine-rich peptides inspired by ac-IHIHIQI-Am [80], evaluating the influence of amino acid disposition, cyclization, and incorporation of D-amino acids on their self-assembly behavior, zinc coordination ability and catalytic activity (Figure 13. Current studies on catalytic peptides have shown that positioning two histidine residues within the peptide sequence with a single amino acid gap creates an optimal arrangement for metal coordination [142]. This configuration allows the histidines to be close enough to cooperatively coordinate a single zinc ion while being adequately spaced to avoid interference from bulky side chains or electrostatic repulsions. Upon self-assembly, multiple histidine residues come into closer spatial proximity, allowing for simultaneous coordi-

nation of histidines from multiple sequences with the same zinc ion, improving catalytic efficiency.
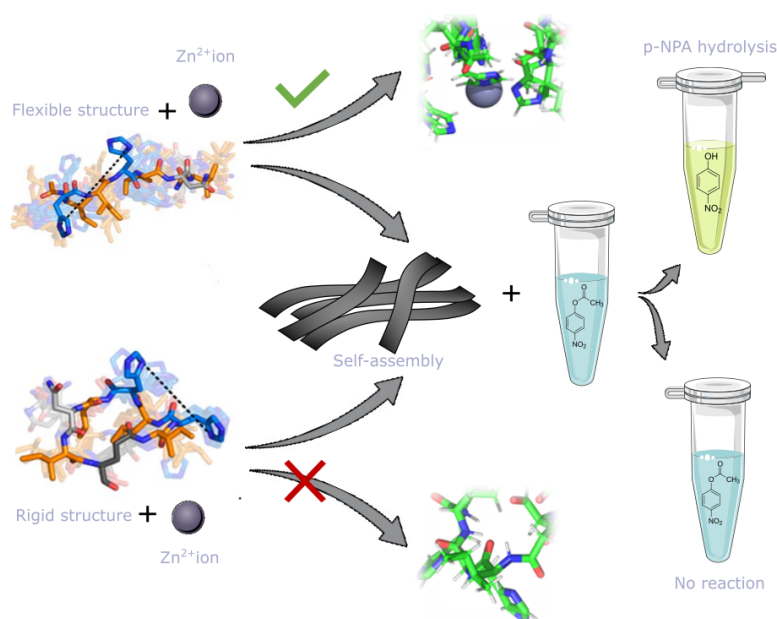
Figure 13: **Influence of peptide conformation on zinc-induced catalytic activity of short peptides.** The upper part of the figure shows a linear, flexible peptide that, effectively coordinates a Zn^{2+} ion and self-assembles, successfully catalyzing the hydrolysis of p-NPA into the yellow-colored p-NP. The lower section illustrates that peptide cyclization enhances rigidity without impeding self-assembly. However, this conformation fails to effectively coordinate Zn^{2+} ions, thus preventing the hydrolysis of p-NPA.

Our aim was to determine the impact of the mutation of glutamine from the previously reported Ac-IHIHIQI-Am sequence [80] into asparagine (Ac-IHIHINI-Am) on the efficiency to hydrolyze p-NPA and self-assemble into a fibrillar morphology. Both glutamine and asparargine are recognized for their role in promoting self-assembly, but asparagine exhibits the unique feature of forming asparagine ladders, which enhance the stability of amyloid fibrils [143]. Therefore, we aimed to investigate whether this subtle substitution could enhance self-assembly, potentially resulting in improved catalytic activity. Furthermore, we explored how positioning asparagine, either closer to the C-terminus with two histidine residues separated by a single isoleucine (Ac-IHIHINI-Am) or towards the peptide's center, leaving the two histidines separated by two isoleucines and asparagine (Ac-IHINIHI-Am), affects both self-assembly propensity and catalytic activity. However, we made sure that the hydrophobic-hydrophilic pattern remains intact upon shifting the asparagine within the sequence. This approach was adopted to minimize the modification's disruption on self-assembly processes relying on the specific sequence pattern.

As mentioned in section 2.2, we pinpointed a notable shortcoming in the design of metallo-dependent catalytic peptides, as no attention was paid to the design of cyclic

catalytic peptides. To bridge this gap, we explored the advantages of cyclic peptides in metallo-catalysis and their potential to improve stability, specificity, and catalytic efficiency. Linear peptides are characterized by their flexible and heterogeneous structures, which undergo constant conformational changes. Although catalytic systems require a degree of flexibility to facilitate interactions with both the metal cofactor and the substrate, excessive flexibility may be counterproductive. Systems that are too flexible can rapidly shift between conformations, failing to maintain the optimal conformation long enough for catalysis to occur. Therefore, we investigated the use of cyclization as a strategy to introduce constraints within the peptide sequence, potentially enhancing the catalytic activity. By limiting the conformational flexibility of the peptide, cyclization aims to stabilize the structure in a configuration that is more conducive to catalysis. This approach seeks to optimize the balance between the necessary flexibility and structural rigidity, potentially improving the efficiency and specificity of the catalytic reaction.

We employed head-to-side chain cyclization to obtain histidine-rich cyclic peptides (Figure 14). This type of cyclization, described in the introduction (1.5 section) relies on the incorporation of a C-terminal glutamic acid, where the carboxyl group of the side chain is protected with a γ-2-phenylisopropyl ester (O-2-PhiPr). This protective group can be selectively removed while the peptide remains attached to the resin, enabling its coupling with the peptide's N-terminus to form an amide bond. The cyclization reaction needed to be optimized, as we discovered that the standard uronium salt (HBTU) used as coupling agent for amide bond formation in SPPS synthesis was not effective for the ring formation. Therefore, we replaced it with a phosphonium salt (PyBOP) that exhibited extraordinary reactivity and enabled the *in situ* activation and coupling reaction of the N-termini and the carboxyl group of the glutamate side chain. This cyclization method resulted in a significant yield of the cyclic peptide of interest, indicating its effectiveness in synthesizing cyclic peptides. We opted for this cyclization method instead of the conventional head-to-tail approach performed in solution, which involves forming an amide bond between the peptide's N-terminus and C-terminus, because solution-based cyclizations typically yield fewer products due to the formation of additional side products, unlike those conducted on resin.

Our findings demonstrate that, while both linear peptides and one cyclic analogue exhibited self-assembly behavior, only Ac-IHIHINI-Am displayed efficient catalytic activity on multiple ester substrates (*p*-NPA, *p*-NPB, *p*-NPO) (Figure 13). Both linear (Ac-IHIHINI-Am and Ac-IHINIHI-Am) and one cyclic peptide ([IhIhINIE-Am]) show self-assembly info β-sheet-like structures, characterized by a peak at 1623 cm^{-1} in the attenuated total reflectance-Fourier-transform infrared (ATR-FTIR) spectrum, an increase in the Thioflavine T (ThT) fluorescence intensity and a circular dichroism (CD) spectra
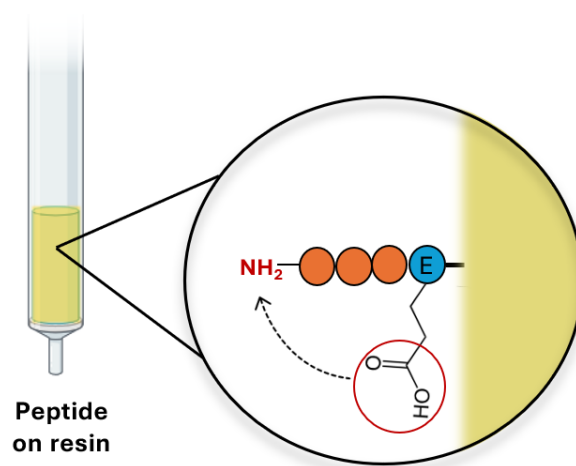
Figure 14: **Overview of peptide cyclization performed on resin.** Visual representation of the head-to-side chain cyclization process performed on resin highlighting the C-terminal glutamic acid residue in blue and the free N-terminus indicated in red available for reaction.

with a minimum at 212 nm and a maximum at 197 nm, with AFM showing a visiual confirmation of fibrilar nanostructures.

Various studies have drawn a connection between a peptide's capacity to self-assemble and its catalytic activity [80, 86]. However, our findings indicate that this correlation does not universally apply. This discrepancy highlights the complexity of the relationship between self-assembly propensity and catalytic efficiency, suggesting that other factors, including metal coordination, may significantly influence the catalytic performance of peptide-based systems. We employed CD analysis to explore the peptides' interactions with the metal cofactor. This technique provided a detailed examination of the structural alterations and binding interactions that occur upon metal association, shedding light on the relationship between the peptide-metal interaction and catalytic function. The Ac-IHIHINI-Am peptide, which demonstrated catalytic activity, underwent a notable transition to a more ordered β-sheet conformation in the presence of zinc. This change was clearly indicated by a shift in the CD spectrum's minima towards 220 nm. Conversely, adding Zn^{2+} to Ac-IHINIHI-Am led to a shift towards a less organized structure. These findings underline the distinct manner in which each peptide interacts with the metal cofactor which is determined by the disposition of amino acids within the sequence. In addition, zinc titration analyses monitored using CD revealed that Ac-IHIHINI-Am successfully binds the metal cofactor, a key element for its catalytic activity. In contrast, Ac-IHINIHI-Am showed no binding affinity for Zn^{2+}, suggesting that the addition of metal ions could potentially induce structural destabilization by promoting unfavorable electrostatic interactions.

This research demonstrates that two linear peptide sequences, while consisting of
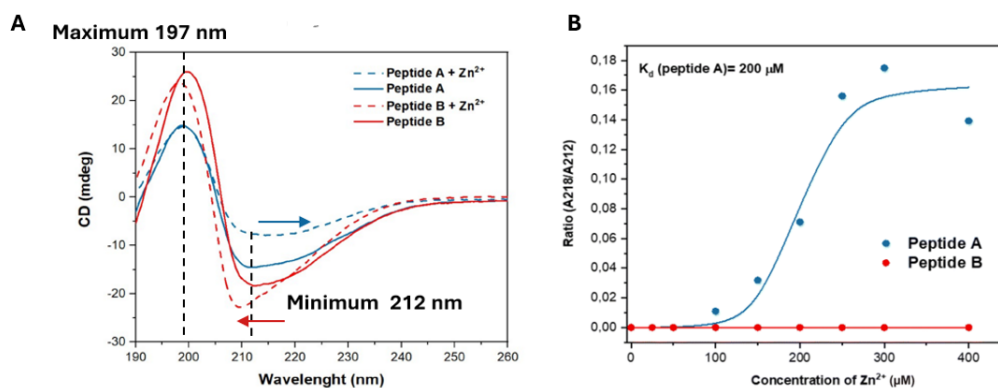
Figure 15: **The positioning of amino acids within the sequence influences the peptide's interaction with the metal cofactor.** (A) CD spectra of Ac-IHIHINI-Am named Peptide A and Ac-IHINIHI-Am named peptide B with and without Zn^{2+}, indicating the presence of β-sheet assemblies in both peptides, (B) Zn^{2+} titration curve of Ac-IHIHINI-Am (blue) and Ac-IHINIHI-Am (red), demonstrating that Ac-IHIHINI-Am exhibits strong metal binding, while Ac-IHINIHI-Am shows no affinity.

identical amino acids arranged differently within the sequence and able to self-assemble into supramolecular nanostructures, exhibit distinct interactions with the metal cofactor essential for catalytic activity (Figure 15). This finding significantly contributes to our understanding of the peptide design principles utilizing the His-Zn interaction mechanism, as it uncovers a level of complexity in the catalytic functions of short peptides that surpasses previous assumptions that only sequence mutations affecting self-assembly propensity influence the overall catalytic activity. The critical role of amino acid positioning within peptide sequences is emphasized, showing that even subtle modifications can significantly affect their functional capabilities, without necessarily impacting their self-assembly properties.

Another significant contribution presented in this paper shows how we can modulate the self-assembly of cyclic peptides through chirality. Previous research have shown that an alternating D- and L- arrangement in cyclic peptides promotes self-assembly [144] and that chirality can affect the morphology of the supramolecular structures of cyclic peptides [145]. Our research reveals that the cyclization of a fiber-forming linear peptide Ac-IHIHINI-Am results in a highly soluble cyclic analog ([IHIHINIE]-Am), or alternatively, by introducing an alternating D- and L-amino acid sequence ([IhIhINIE]-Am), it can be converted into a cyclic analog that assembles into β-sheets and fibrillar nanostructures. This finding highlights the potential to fine-tune the self-assembly of cyclic peptides by making stereochemical modifications, which has implications that extend beyond the field of self-assembling catalytic peptides. It enables us to selectively determine whether a cyclic peptide should self-assemble or remain highly soluble, depending on its intended

application. For instance, self-assembly could be advantageous for drug delivery systems, where the formation of stable nanostructures is beneficial for transporting therapeutic agents. On the other hand, enhanced solubility is particularly valuable in scenarios such as receptor binding, where it is crucial for all interactive residues to be readily accessible.

Finally, the question of catalytic activity in cyclic peptides remains unresolved. Our findings indicate that the cyclic peptide showing self-assembly does not effectively coordinate with the metal cofactor, as indicated by the CD spectra that shows no difference upon metal addition. This observation suggests the need to explore alternative cyclization techniques or reconsider the size of the cyclic peptide, since it is plausible that the cavity created by our current cyclic design is insufficient to accommodate zinc. This limitation could be attributed to the bulkiness of histidines and isoleucines or steric hindrances arising from an unsuitable ring size. Nevertheless, this research paves the way for innovative approaches in the design of histidine-rich peptides, by uncovering the complexities involved in metal coordination and self-assembly in both linear and cyclic histidine-rich peptides. This work not only contributes to a deeper understanding of the functionality of short catalytic peptides but also opens avenues for the creation of more effective and efficient next-generation histidine-rich peptide catalysts.

2.4 Short catalytic peptides with tunable activity: Cys confers functionality and adaptability

The second widely exploited sequence-based approach for the design of catalytic peptides, following closely the previously described His-Zn mechanism, is the incorporation of residues from the catalytic triad into a previously known self-assembling peptide such as MAX1 [146]. Self-assembly initiates the catalytic function of the system by inducing multivalency, wherein multiple peptide molecules interact simultaneously. However, the catalytic triad approach involves a sophisticated interaction among several residues, which typically necessitates precise geometric alignment following enzyme folding to function effectively, raising questions about the reliability of this design strategy in accurately mimicking the active sites of enzymes. In the article published in the Journal of Chemical Information and Modeling, where I contributed as co-author, we focused on enzyme class EC 3.1, specifically hydrolyses targeting ester bonds with established catalytic mechanisms, excluding those lacking the catalytic triad for their activity, and performed a statistical analysis of the 22 selected enzymes [147]. The most common catalytic triad residues in hydrolases are serine as the nucleophile, histidine as the base, and aspartate as the acid. It was confirmed that the critical residues for catalysis are mostly far apart in the sequence, however they come close in space as the enzyme folds. Consequently, to replicate the active site with a peptide containing the primary sequence that incorporates all the amino acids found between the catalytic triad residues, the extraction of more than 50 amino acids would be required. This necessity pushes beyond the boundaries of the minimalistic approach of catalytic peptide design, extending into the domain of protein engineering. However, we recognized that the microenvironment surrounding the active residues is largely conserved, suggesting its importance in catalysis, underscoring the necessity for a design strategy that addresses this consideration and incorporates other residues from the primary sequence, beyond the catalytic triad.

Based on these observations, in our manuscript, currently available as a preprint and nearing submission, we focused on replicating the active site microenvironment and selected the enzyme protein-glutamate methylesterases (CheD) that had the active site residues closest in the sequence. We selected a specific portion of the active site, extending from threonine (Thr21), that stabilizes His44 and Cys27 acting as the catalytic acid, to
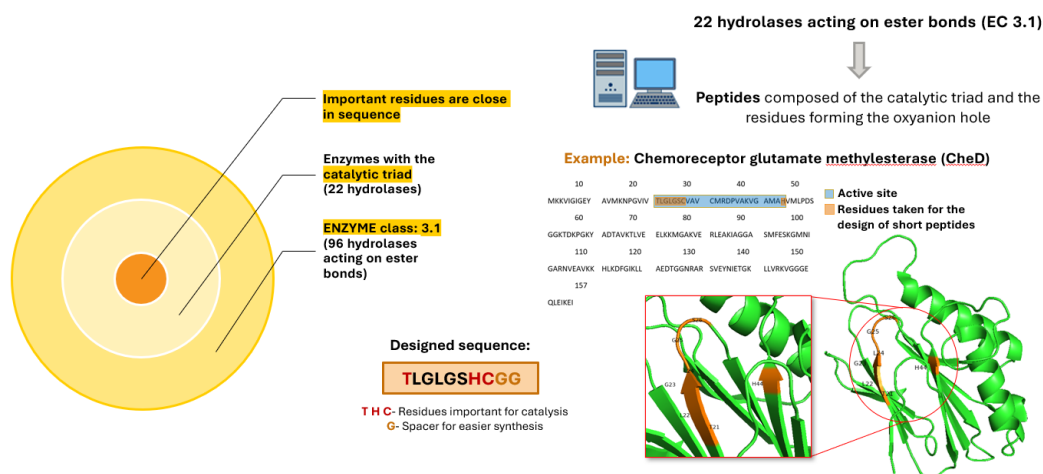
Figure 16: **Overview for the design process of the CG10 peptide.** By evaluating the enzyme class 3.1 (Hydrolases cleaving ester bonds) and filtering out those lacking the catalytic triad, we identified 22 enzymes and performed a statistical analysis of their composition. The enzyme Chemoreceptor glutamate methylesterase (CheD) was highlighted for its closely situated residues important for catalysis, guiding the design of our catalytic peptide Ac-TLGLGLSHCGG-Am (CG10). The peptide incorporates a targeted sequence with histidine, serine, and cysteine residues essential for catalysis with glycine linkers to facilitate synthesis.

cysteine (Cys27), acting as the nucleophile, including the LGLGS spacer found in the primary sequence of the enzyme between threonine and cysteine. To complete the catalytic triad essential for enzymatic activity, we incorporated histidine (His44), acting as base, which was not originally part of this segment. Recognizing its position more towards the C-terminus in the enzyme sequence, as illustrated in Figure 16, we added histidine to the C-terminus of the peptide. The proposed sequence (CG10) was modified with two additional glycines for easier synthesis to avoid racemization. Moreover, to better understand the sequence-to-function relationship of short linear and cyclic catalytic peptides, we synthesized:

- the CG11 analogue by adding a cysteine at the N-terminal of CG10 with a dual purpose of assessing the impact of an additional nucleophile on activity, as well as to perform a disulfide bridge cyclization (cy-CG11)

- the cy-TE10 peptide by modifing the CG10 sequence with an C-terminal glutamic acid to allow for the head-to-side chain cyclization, as previously described in Section 2.3.

- the TSH10 analogue by replacing the cysteine in CG10 with a serine to understand how a nucleophile mutation affects activity; serine is frequently chosen as the preferred nucleophile in the design of peptides featuring a catalytic triad, due to its more controllable reactivity, attributed to its -OH group, which is less reactive com-

pared to the highly reactive -SH group found in cysteine
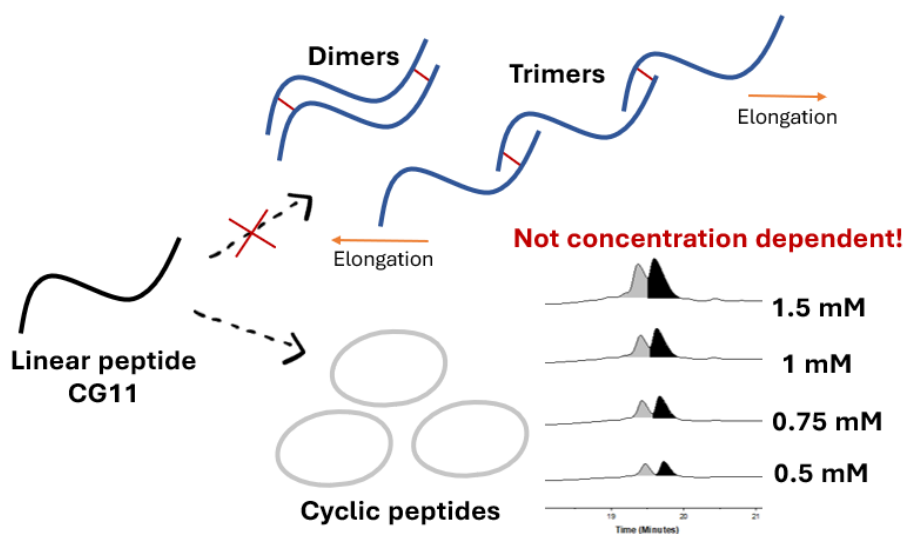
Figure 17: **The CG11 peptide shows preferential cyclization over dimerization or oligomerization.** The diagram depicts the linear peptide CG11 undergoing cyclization rather than dimerizing or forming higher-order oligomers. The process is shown to be not concentration dependent, as indicated by the chromatograms at varying concentrations (0.5 mM to 1.5 mM), which consistently demonstrate the predominance of cyclization over elongation into dimers or trimers.

Cyclization of CG11 by disulfide bridge formation into cy-CG11 was performed through a controlled oxidation process at low peptide concentrations (10^{-5} M) to prevent unwanted dimerizations and oligomerizations. This involved dissolving less than 10 mg of peptide in 500 mL of MilliQ water, complicating the subsequent HPLC purification due to the high volume of the solution requiring multiple HPLC injections. Consequently, we implemented a solid-phase extraction step before HPLC, using a C18 column to reduce the volume of the solution. This additional purification step reduced the yield, making the disulfide bridge formation method less attractive compared to the more efficient head-to-side chain cyclization that yields higher product quantities. Given that this process proved to be both time-consuming and resource-intensive, we tested varying concentrations of CG11 to identify the highest concentration that allows for spontaneous oxidation into the cyclic version cy-CG11 rather than a dimer or oligomer, thereby optimizing the cyclization process. Surprisingly, we discovered that our peptide undergoes spontaneous cyclization at concentrations up to 1.5 mM when dissolved in MilliQ water and left at room temperature for over 24 hours. However, the peptide remained in its linear form when it was dissolved in PBS buffer. This phenomenon may be attributed to trace metals inevitably present in water, which could catalyze the oxidation process, whereas the salts in PBS buffer may inhibit this process by quenching the metals and preventing their

effect on CG11 oxidation [148]. The findings suggest that under the conditions tested, the CG11 peptide does not form dimers, and any oxidation that occurs leads solely to its cyclic form (Figure 17). For this reason, we performed the following cyclizations by dissolving the CG11 peptide at the desired concentration in MiliQ water and allowing it to spontaneously oxidize for 24 to 48 hours, monitoring the progress of the cyclization using HPLC. This method greatly facilitated a more efficient cyclization process through disulfide bridge formation.
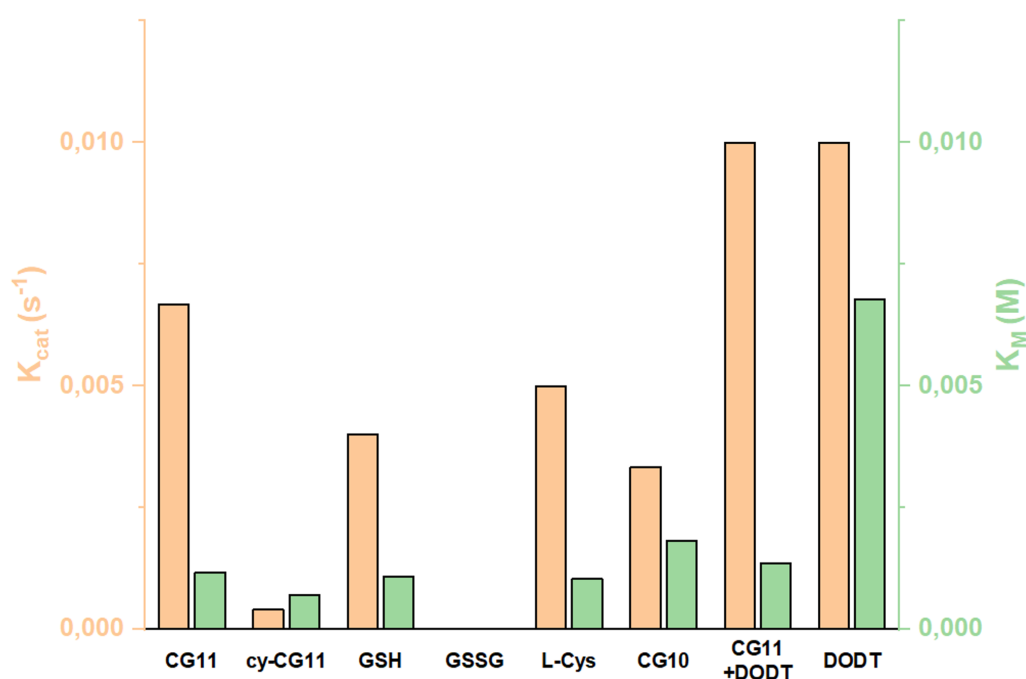
Figure 18: **Comparative analysis of thiol-containing molecules in catalytic activity**. The bar chart presents a side-by-side comparison of various thiol group-containing molecules, including peptides CG11 and cy-CG11, along with small molecules GSH, GSSG, L-Cys, and DODT, evaluated for their catalytic efficiency. The dual-axis chart compares the turnover number (k_{cat}) on the left vertical axis and the substrate affinity (K_M) on the right vertical axis, providing insights into the catalytic potential and substrate binding affinity of each molecule tested. These metrics collectively suggest that CG11 in combination with DODT represents the most effective catalyst among the tested entities, due to its high catalytic turnover and strong substrate binding.

The catalytic activity of all the synthesized analogues was assessed and the results showed an interesting correlation between the number of available thiol groups within the sequence and catalytic activity (Figure 18). The linear peptide CG11, designed for cyclization via disulfide bridge formation with two cysteine residues, was evaluated for its ability to hydrolyze p-NPA prior to cyclization and it demonstrated greater activity compared to the CG10 peptide, which contains only one cysteine residue. Alternatively, the activity was lost when free thiol groups were removed from the sequence, either through
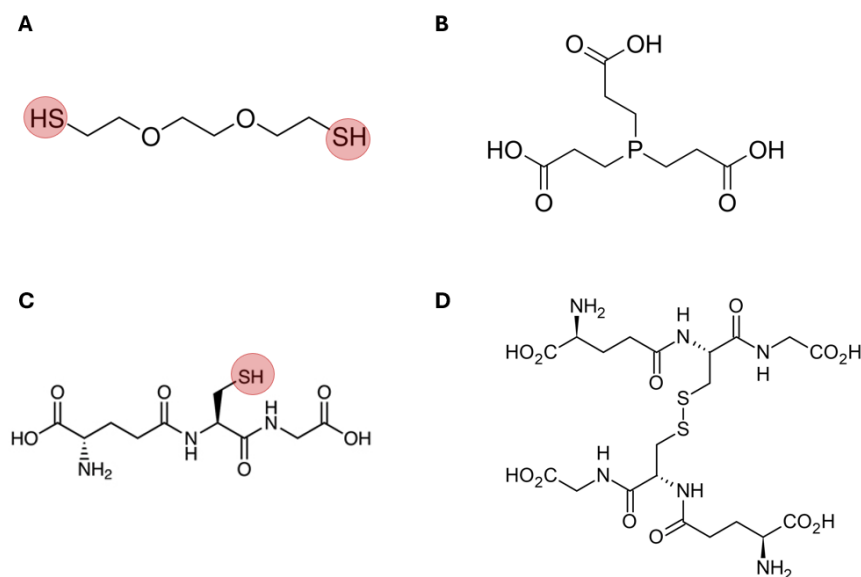
Figure 19: **Chemical structures of reducing agents and thiol-containing molecules.** The structures highlight (A) DODT, (B) TCEP, (C) GSH and (D) GSSG utilized in confirming the correlation between catalytic activity and the presence of thiol groups. The free thiol groups are indicated in red.

mutating cysteine to serine in the TSH10 analogue or by cyclizing CG11 through oxidation of its thiol groups to create the cy-CG11 analogue.

To prevent the oxidation of cysteines and retain catalytic activity, a variety of reducing agents such as 2,2 -(Ethylenedioxy)diethanethiol (DODT) or tris(2-carboxyethyl)phosphine (TCEP) can be used. Therefore, we conducted *p*-NPA hydrolysis experiments using CG11, employing both DODT and TCEP as reducing agents to compare their effects on activity. However, DODT contains two thiol groups that could potentially interfere with the hydrolysis of *p*-NPA, as our findings indicate a correlation between the hydrolysis rate and the number of free thiol groups (Figure 19). We discovered synergistic interactions between CG11 and DODT in the hydrolysis of *p*-NPA as the combination of CG11 and DODT exhibited an enhanced activity compared to CG11 incubated with TCEP, a non-thiol containing reducing agent. Moreover, we tested DODT alone which hydrolysed *p*-NPA with a turnover number identical to that of the CG11+DODT combination. However, DODT's overall efficacy was lower due to its weak substrate affinity, as indicated by a high K_M value. Therefore, reducing agents with thiol groups should be either avoided or their presence and potential synergistic effects carefully considered and clearly disclosed in the results.

To further investigate the effect of other thiol-containing molecules on the hydrolysis of *p*-NPA, we assessed the catalytic activity of the tripeptide glutathione (GSH), which consists of glycine, cysteine and glutamic acid (Figure 19), and the single amino acid

41

L-Cysteine. The catalytic activity assays showed similar efficiency in the hydrolysis of *p*-NPA for GSH and L-Cys, both relying solely on the thiol group for activity. Furthermore, after observing that CG11 has a reduced activity upon oxidation into cy-CG11, we compared the hydrolytic activities of glutathione (GSH) and its oxidized form (GSSG) wherein the thiol group is part of a disulfide bridge therefore not available for reaction, similarly to the cy-CG11 peptide. This comparison aimed to confirm that the loss of catalytic activity is correlated with thiol oxidation. We found that GSH shows no activity upon oxidation into GSSG. These results suggest a bias towards thiol groups in *p*-NPA hydrolysis and stress the importance of substrate choice in catalytic activity evaluation, especially with *p*-NPA, a commonly used benchmark. Given its reactivity with cysteine, alternative more stable substrates such as *p*-NPP should be considered for more reliable assessments.

These insights into assessing the catalytic activity of cysteine-rich peptides, along with the factors affecting the hydrolysis rate of *p*-NPA detailed in Section 2.5, represent a significant contribution to the field of catalytic peptides. They underscore critical shortcomings of this widely used assay, highlighting the need to carefully address the experimental setups and guide the community towards achieving more accurate and reproducible results in peptide catalysis research. These observations led us to transition from using *p*-NPA to investigating more complex and biologically relevant substrates. Consequently, we evaluated CG11's ability to hydrolyze *p*-NPP and ATP, revealing its phosphatase activity as it effectively catalyzed both substrates. This discovery holds significant relevance because the majority of signaling pathways in human cells depend on phosphorylation and dephosphorylation processes [100]. The phosphatase activity of our peptide offers promising avenues for application in biological contexts.

Considering that CG11 was identified as the best catalyst and that its activity can be tuned based on the dynamic covalent chemistry of its thiol groups, the next aim was to investigate whether the oxidation of the linear peptide could be controlled through environmental factors, thus directly influencing its catalytic activity. For this purpose, HPLC oxidation kinetic analyses were performed to examine how the presence of reducing or oxidizing agents influence peptide's cyclization. We demonstrate that with the addition of 0.1 eq of TCEP we are able to inhibit the oxidation of CG11 to its cyclic form, cy-CG11, and by adding 1 eq of TCEP we are able to cleave the preformed disulfide bond, converting it from cyclic to linear CG11 form. Conversely, with the addition of H_2O_2, the peptide rapidly oxidizes to its cyclic form, requiring only 5 minutes to complete the transformation. This environmental adaptability provided by cysteine was exploited for tunable catalysis. By manipulating cysteine reduction from cy-CG11 into CG11 with TCEP, we effectively controlled the peptide's activity, transitioning from inactive to active states. In

addition to modifying catalytic activity, we observed a structural transformation upon oxidation using circular dichroism (CD) spectroscopy, with cy-CG11 adopting a β-hairpin conformation, whereas CG11 exhibited a helical structure. A comparable approach has been documented in the literature for regulating the self-assembly of the amphipathic Ac-(FKFE)$_2$-Am sequence [106]. The introduction of two cysteines at both the N- and C-termini, followed by cyclization, resulted in the loss of the peptide's self-assembly propensity. Treating this cyclic peptide, in a random coil configuration, with TCEP effectively reduced the restrictive disulfide bond allowing the peptide to relax into a stable β-strand conformation, consequently triggering self-assembly. However, this approach primarily addresses conformational changes resulting from thiol oxidation and does not investigate changes in functionality.

TCEP, being a potent reducing agent, does not mimic the conditions typically present in the human body. Therefore, we wanted to explore whether we could employ a trigger that reflects an irregularity characteristic of diseased or tumor tissues, aiming for a more physiologically relevant approach. We identified glutatione (GSH) as a potential target. GSH is typically found in all body cells and it is crucial for the removal and detoxification of carcinogens through the regulation of reactive oxygen species (ROS), however elevated GSH levels are characteristic for tumor cells and are associated with tumor progression and increased resistance to chemotherapeutic drugs [149]. Therefore, we investigated whether elevated GSH levels could be leveraged to reduce our cyclic peptide, thereby activating it, while simultaneously decreasing GSH levels, as GSH converts to GSSG upon reducing another molecule. This approach offers the dual benefit of hydrolysis by exposing the thiol groups in our CG11 peptide and decreasing GSH levels. We demonstrated that the reduction of the peptide is influenced by the concentration of GSH, with the quantity of linear peptide produced being proportional to the amount of GSH added to the solution. Specifically, concentrations of GSH at 1 mM had no impact on ring opening, whereas concentrations exceeding 10 mM resulted in the formation of the linear counterpart. This finding underscores the peptide's potential for selectively targeting tumor cells, staying inert in healthy tissues, thereby paving the way for targeted cancer therapies (Figure 20). Moreover, the ability to hydrolyze ATP introduces a new avenue for selectively exhausting ATP in cancer cells, which could lead to targeted cell death [150]. Thus, the dual strategy of decreasing GSH levels and hydrolyzing ATP in cancer cells presents a novel and potentially effective method for tumor suppression.

Finally, to evaluate the enhancement of stability through cyclization, we compared the serum stability of the cyclic peptides cy-CG11 and cy-TE10 against the linear CG11. Notably, only cy-TE10, which was synthesized via an unnatural cyclization method, exhibited increased resistance to protease degradation, maintaining stability throughout the

24-hour testing period. The formation of a disulfide bridge in cy-CG11 did not enhance stability, potentially because such linkages are common in enzymes and may be readily recognized and targeted by proteases. Conversely, the amide bond formed between the side chain of glutamic acid and the N-terminus in cy-TE10 represents a linkage not typically found in enzymes, possibly allowing it to elude proteolytic attack. While peptides generally have a stability window ranging from 2 to 30 minutes minutes [115], our data indicate that the half-lives of CG11 and its cyclic analogue, cy-CG11, could be extended to roughly 3.5 hours. This improvement in stability, likely due to the amidation of the C-terminus and acetylation of the N-terminus, might retain its suitability for medical use. Alternatively, employing strategies like the retro-enantio approach may achieve the targeted stability while preserving the adjustable catalytic activity.
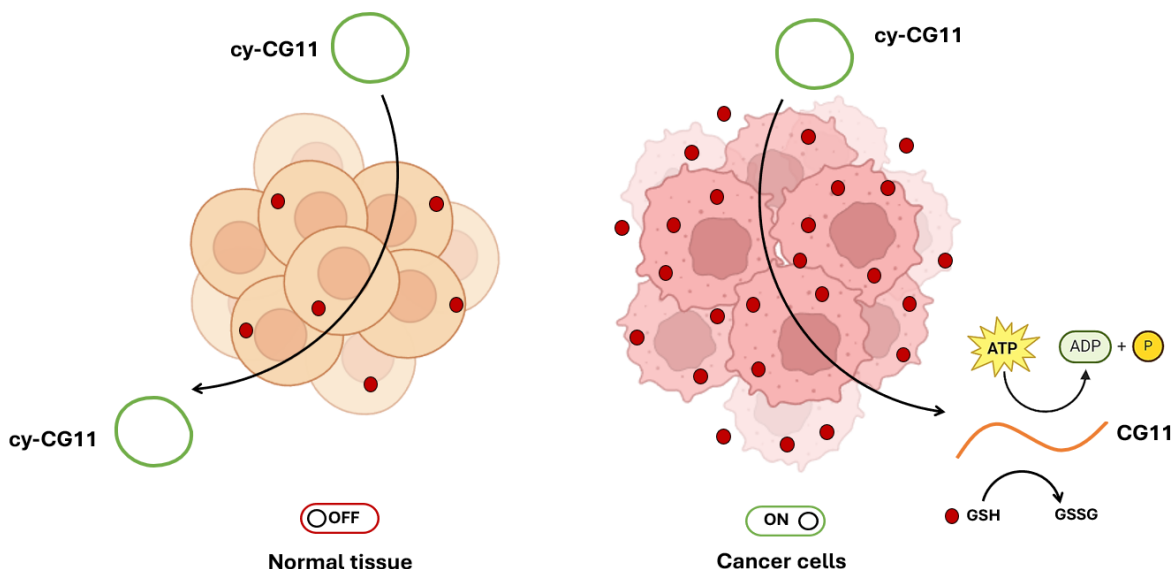
Figure 20: **Selective activation of cy-CG11 in different tissue types for targeted cancer therapy.** The hypothesis is that the cyclic peptide cy-CG11 remains non-reactive in normal tissues, whereas in cancer cells, the increased GSH levels typical of such cells trigger its reduction to the active linear form, CG11. This activated CG11 can then participate in the hydrolysis of ATP in tumor environments, potentially leading to cancer cell death. This illustrates cy-CG11's capacity for targeted therapeutic action within the altered redox conditions of cancerous tissues. Created with BioRender.

The overall importance of this work stems from the fact that hydrolases are vital enzymes that carry out all important degradative reactions in the human body such as the hydrolysis of proteins, nucleosides and lipids [5]. Additionally, hydrolases play a crucial role in industrial processes, such as biofuel production and plastic degradation, with nearly 75% of all industrial enzymes being hydrolases. Thus, mimicking the activity of enzymes in small catalytic peptides holds immense promise for both healthcare and industrial applications. Their development and optimization could lead to more sustainable

industrial processes, reduce the environmental impact of various sectors, and also open up new avenues in medical treatment. Apart from the design of novel chemoterapeutics as being explored in this section, hydrolytic peptides can also be designed as an alternative to conventional enzyme replacement therapy, which requires intravenous administration due to potential protein degradation in the stomach. In contrast, peptides are resistant to low pH levels and therefore could be administered in tablet form, providing simpler therapy application and reducing treatment costs. Moreover, many enzyme replacement therapies for lysosomal storage disorders elicit an anti-drug antibody response, which may diminish their effectiveness or cause hypersensitivity reactions [18]. Peptides are generally less immunogenic than larger proteins due to their smaller size, which might not present sufficient structural elements for the immune system to identify them as foreign entities. This characteristic can enhance the efficacy of enzyme replacement therapies by reducing the likelihood of immune responses that compromise treatment effectiveness [151].

2.5 Determining the esterase activity of peptides and peptide assemblies

In previous sections, I have shown several successful examples of peptide sequences and supramolecular peptide assemblies with catalytic activity toward various substrates. However, while performing the *p*-NPA assay optimization, I noticed the importance of factors including pH, temperature and concentration of the catalyst to ensure the reproducibility of the catalytic activity results.
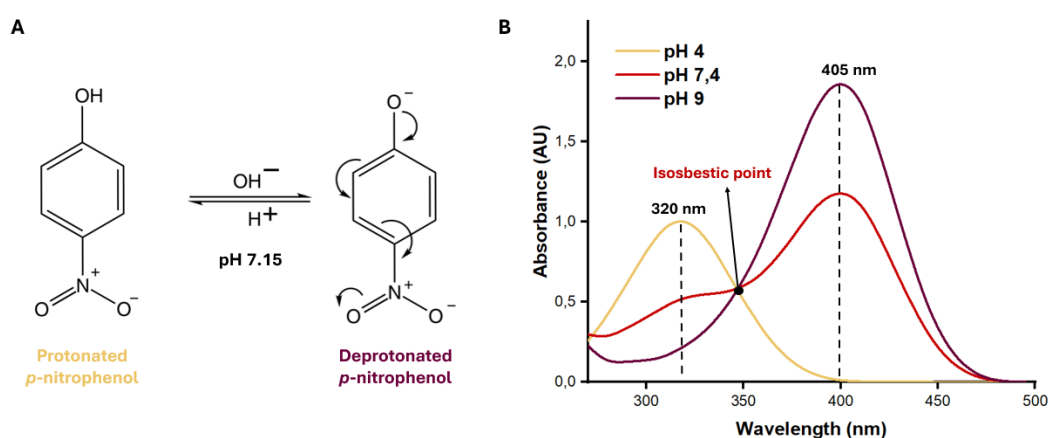
Figure 21: **pH-dependent protonation states of *p*-nitrophenol and corresponding absorption spectra.** (A) The protonated form of *p*-nitrophenol at acidic pH on the left and its deprotonated form at alkaline pH on the right, illustrating the pH-dependent shift in protonation at 7.15. (B) The UV-Vis absorption spectra for p-nitrophenol across different pH values, with a peak at 320 nm characteristic of the protonated form, and a peak at 405 nm indicative of the deprotonated form, which is commonly utilized in analytical measurements. The isosbestic point at 347 nm indicates the unique wavelength where the absorbance of both protonated and deprotonated forms remains the same, regardless of the pH.

The hydrolysis of *p*-NPA leads to the formation of *para*-nitrophenol (*p*-NP) which behaves as a pH indicator, changing color with pH variations [152]. Below its pKa of 7.15, *p*-NP remains in its protonated, colorless form with a maximum absorbance at 320 nm (Figure 21). Conversely, above this pH, *p*-NP adopts a yellow color that intensifies with increasing pH, reaching maximum intensity around pH 9 with a maximum absorbance at 405 nm. This presents a significant challenge in accurately reporting catalytic activities of peptides, as the assay quantifies only the non-ionized (yellow) portion of *p*-NP visible at 405 nm. Variations in pH due to factors like minor temperature changes or the aging of buffers can lead to discrepancies in results. Therefore, when presenting findings from this assay, it is essential to specify the exact pH at which the assay was conducted. The reason why the assay is performed in alkaline pH and only the production of non-ionized (yel-

46

low) portion of *p*-NP is monitored is due to obstacles with monitoring the formation of the protonated form in the the UV spectrum such as the absorption characteristics of the 96-well plate material utilized in these assays, often being polystyrene, which significantly absorbs in this spectral range. Even if a suitable plate material were found, another complication arises from *p*-NPA interference. To meet the requirements of Michaelis-Menten kinetics, a high concentration of the substrate is necessary, resulting in the concentration of *p*-NPA significantly exceeding that of the product, *p*-NP. The dominant absorption peak of the benzyl group of *p*-NPA at 300 nm masks the peak at 320 nm corresponding to the protonated portion of *p*-NP, making accurate detection of *p*-NP at lower pH values challenging. Another possibility to bypass the obstacle of pH affecting accurate detection of *p*-NP formation is to monitor the reaction at the isosbestic point [153]. This is a specific wavelength in the absorbance spectrum where two (or more) species have the same absorbance. At this wavelength, the absorbance remains constant, regardless of changes in the concentration of these species. The isosbestic point of *p*-NP is at 347 nm. This method is useful for analyzing the catalytic activity of proteins that rapidly hydrolyse *p*-NPA as the absorbance peak at 300 nm quickly diminishes, thereby avoiding interference at this wavelength. However, when we analyze peptides with lower catalytic activities we noticed that the problem of *p*-NPA supressing the *p*-NP peaks is present even in this spectral range, thus providing inacurate results (Figure 22).
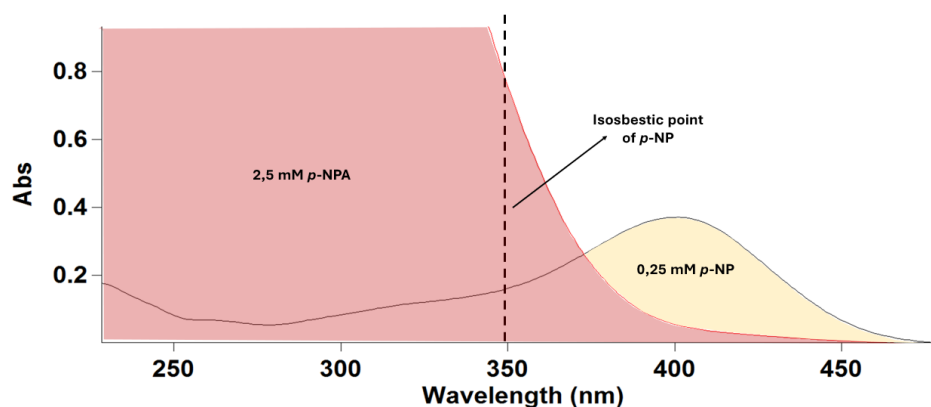
Figure 22: **UV-Vis spectral overlap of *p*-NPA and *p*-NP at the isosbestic point due to high *p*-NPA concentration.** This absorption spectrum delineates the distinct peaks of *p*-NPA and *p*-NP, with an observed isosbestic point where we can detect the concentration of *p*-NP regardless of pH. However, at high concentrations, *p*-NPA's peak surpasses the isosbestic point, potentially affecting accurate catalytic activity measurements by overshadowing the *p*-NP signal at 347 nm.

Moreover, we observed variations attributed to the temperature at which the assay was performed. Temperature is a well-recognized factor used to modulate reaction rates as higher temperatures contribute to increased kinetic energy among molecules, enhancing the likelihood of reactions. This effect typically requires temperatures of 50°C or higher

to manifest significantly. However, we found that even minor temperature fluctuations, common in laboratory environments during summer or winter, can impact the results of p-NPA hydrolysis. To validate this, we assessed p-NPA autohydrolysis at 25°C and 37°C in PBS, TRIS, and TRIS with $ZnCl_2$ buffers, commonly used in our p-NPA assays. At 37°C, all three buffers showed an increased rate of autohydrolysis, with the most pronounced difference observed in the PBS buffer, where over 50% more p-NPA was hydrolyzed.

A significant challenge while working with peptide assemblies, described in Section 2.3, was identifying the appropriate concentration ratio of peptide to p-NPA to adhere to Michaelis-Menten kinetics accurately. A fundamental aspect of this kinetics is the presumption that the substrate's concentration surpasses that of the peptide by at least an order of magnitude. This ensures that the substrate concentration change is minimal and can be considered negligible for the calculations. When dealing with enzymes, nanomolar concentrations are used, aligning with Michaelis-Menten kinetics. Peptide monomers can be analyzed within the micromolar range, allowing for adherence to Michaelis-Menten kinetics, yet the process of peptide self-assembly occurs only in concentrated peptide solutions, thus the study of the catalytic activity of peptide assemblies demands millimolar concentrations. This requirement poses a significant challenge due to the resulting need for p-NPA concentrations up to 10 mM, far exceeding its typical solubility limit of 1 mM in aqueous buffers. Consequently, these elevated concentrations frequently result in p-NPA precipitation, compromising the reliability of the results. It is crucial to account for this limitation when working with peptide assemblies, acknowledging that only changes in color can be observed and reported, while deriving accurate kinetic constants and parameters proves to be challenging with p-NPA as a substrate. For precise quantification of catalytic activity, p-NPP can be used as an alternative substrate, maintaining solubility at high millimolar concentrations.

Beyond the quantification issues of the product at different pH, temperature and substrate concentrations, p-NPA presents a challenge due to its inherent instability, leading to autohydrolysis. At physiological pH, autohydrolysis does not significantly impact the overall hydrolysis rate. However, at elevated pH levels, the substrate becomes more unstable, experiencing not only an increased rate of autohydrolysis but also elevated susceptibility to hydrolysis by catalytic peptides. This phenomenon can create a misleading perception of a peptide's activity, suggesting enhanced effectiveness at higher pH due to supposed intrinsic properties, when in reality, it is attributable to the substrate's increased instability. Furthermore, as discussed in Section 2.4, the inherent instability of p-NPA biases the reaction towards strong nucleophiles such as cysteine, as we demonstrate that even small molecules containing a thiol group can hydrolyze p-NPA, potentially leading to misleading conclusions about the catalytic activity of cysteine-rich peptides.
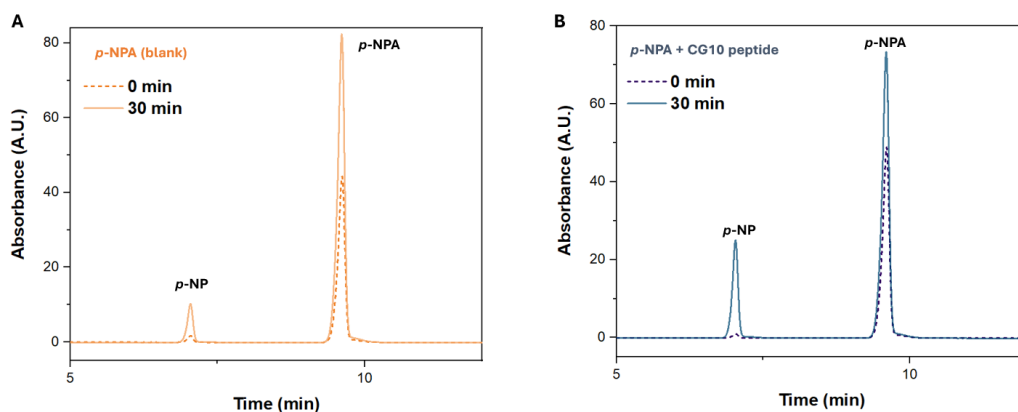
Figure 23: **High-Performance Liquid Chromatography (HPLC) analysis of *p*-NPA hydrolysis.** (A) The control reaction without the catalyst, showing a negligible *p*-NP formation due to auto-hydrolysis after 30 minutes. (B) The reaction with the CG10 peptide, showing an increase in *p*-NP concentration over 30 minutes, demonstrating the peptide's catalytic effect on *p*-NPA hydrolysis. For both reactions, a heightened peak for p-NPA is noticeable after 30 minutes, likely due to its increased solubility in the reaction buffer over time, rendering the p-NPA peak an unreliable metric for evaluating the peptide's catalytic activity.

To address the issue of inaccurate detection of *p*-NP formation at varying pH levels, we employed HPLC, a highly precise method, to monitor *p*-NPA hydrolysis. We used a C18 column and measured the absorbance at 320 nm to detect the benzyl group present in *p*-NPA and the protonated form of *p*-NP due to the acidic conditions of the mobile phase containing 0.1% TFA. However, given that HPLC methods typically take 20-30 minutes per run, achieving precise time points proved challenging, unlike UV/Vis analysis where product formation is monitored every minute. This limitation allowed us to observe only the start and end of the reaction, reducing the accuracy of our analysis. However, we successfully monitored product formation and, by establishing a calibration curve with *p*-NP, it would be possible to calculate the kinetic parameters (Figure 23). However, analyzing a single concentration of *p*-NPA requires a total of four HPLC runs: *p*-NPA (blank) at time zero and after 30 minutes and *p*-NPA with the peptide at time zero and after 30 minutes. Given a 20-minute method duration, the analysis of just one *p*-NPA concentration takes at least 1 hour and 30 minutes. To determine the kinetic parameters it is necessary to analyze at least four concentrations of *p*-NPA, stretching the analysis time for a single peptide to around 6 hours. In contrast, the UV/Vis method in a 96-well plate enables the simultaneous analysis of multiple peptides within 30 minutes, clearly highlighting the time-consuming nature of HPLC as a significant limitation. Thus, HPLC is both costly and time-intensive, rendering it impractical for an assay such as *p*-NPA hydrolysis intended as quick, high-throughput screening method to identify catalytic peptides.

The significance of this research originates from the absence of standardized pro-

tocols for studying catalytic peptides and peptide assemblies, a procedure typically implemented from enzymatic studies which does not entirely translate to peptides. This oversight has led to inaccuracies and inconsistently reported results. Therefore, it was crucial to evaluate factors such as temperature, pH, and substrate concentration to identify potential issues in catalytic peptide research that might otherwise go unnoticed. Future research should take these factors into account and report them alongside kinetic parameters to enable effective comparison of multiple catalytic systems. Moreover, advancing the field of peptide catalysts necessitates the development of novel substrates beyond the traditional *p*-NPA assay and the creation of new analytical techniques for more detailed reaction monitoring. As the field of catalytic peptides is still emerging, establishing precise methods to assess catalytic activity is essential for its continued development and progress.

3 Conclusion

3.1 Main contributions

This thesis outlines valuable achievements in peptide research, a field gaining importance due to the escalating interest in peptide therapeutics. We have successfully established a method for the synthesis, analysis, and purification of linear peptides. We demonstrate the effective synthesis of cyclic peptides on and off resin, enhancing our capability in peptide manipulation. Moreover, this thesis offers a comprehensive characterization of peptide-based supramolecular structures, employing a variety of techniques including FTIR, ThT binding, and AFM. Additional studies were conducted using instruments such as circular dichroism (CD), accessed during professional development under the Erasmus program. The synthesized peptides and peptide nanostructures have also shown to be functional, exhibiting catalytic activity on various substrates, including those of biological relevance. Within this work the method for measuring catalytic activity of peptides and peptide assemblies was refined, ensuring reproducibility of results in future research. Lastly, it was determined that the activity of short cyclic and linear peptides is influenced by a variety of factors, including metal cofactors, the arrangement of amino acids within the sequence, and the choice of nucleophile, highlighting the complexity and potential of peptide-based systems. The significance of this research is underscored by the fact that the results have led to multiple presentations (two oral presentations and eight posters, with two poster awards) at prestigious international conferences and the publication of five scientific papers, with the lead authorship on four of them.

Following the sections, the main contributions of this research can be summarized in five main points:

- **Description of three key sequence patterns found in self-assembling peptides**: high aromatic content peptides, binary alternating hydrophobic-hydrophilic sequences, and surfactant-like peptides, which allow us to rationalize the available knowledge on sequence-to-assemble correlation and enable the knowledge-instructed design of peptide sequences. Moreover, the possibility of directing the supramolecular morphology through sequence design is addressed, thereby navigating the intricate and not fully elucidated relationship between peptide sequences and their self-assembly. Additionally, we describe peptide co-assembly mechanisms (cooperative, orthogonal, disruptive, random) and their use to fine-tune nanostructure morphology and properties by adjusting peptide mixing ratios. Finally, our work addresses the use of peptide-based building blocks to design supramolecular structures that mimic

viruses. Distinguishing the role of peptidic components used for the fabrication of virus mimetics into structural and functional modules we categorize peptide-based design into: capsid-like nanomaterials and multicomponent peptide-DNA complexes, showcasing their potential for biomimetic applications.

- **A comprehensive dataset consisting of all the published catalytic sequences active towards the *p*-NPA, *p*-NPP substrate and other alkyl-based substrates.** Along with the positive instances, we also present negative entries (reported sequences that do not show catalytic activity) that are of great importance in research, but often remain unpublished. Negative results are crucial for providing a comprehensive understanding of the topic, preventing redundant efforts, refining research methods, enhancing credibility, and are essential for training robust and accurate machine learning models for the prediction of catalytic peptides. As catalytic reactions and mechanisms are heterogeneous and substrate-dependent, herein we focus only on a small set of similar substrates enabling activity comparison between sequences. Furthermore, we provide a descriptive statistical analysis of the dataset including features such as N- and C- termini modifications, self-assembly propensity and mechanism of action, as well as the SMILES (Simplified Molecular-Input Line-Entry System) annotations, which can be useful for machine learning-based predictions because they encode important information about the molecular structure. This dataset offers an insight into the currently developed catalytic mechanisms and can be used for the development of next-generation peptide-based catalysts.

- **A set of linear and cyclic histidine-rich peptides** demonstrating how amino acid arrangement, cyclization, and D-amino acid incorporation influence the peptides' ability to self-assemble, bind Zn^{2+} ions, and exhibit hydrolase-like activity. We employed a range of characterization techniques, including FTIR, ThT binding, CD, and AFM, to elucidate the structural changes related to the functional properties of the peptides. Among the four peptides designed, two linear peptides and one cyclic show self-assembly, with one linear peptide also displaying catalytic activity. This study demonstrates that the presence of essential catalytic amino acids alone does not guarantee effective metal cofactor coordination through self-assembly. It underscores the importance of the specific sequence arrangement of amino acids, which influences the peptide's interaction with the metal cofactor and thereby its catalytic activity. Additionally, the study shows that it is possible to control the self-assembly of cyclic peptides through chirality, however coordinating metals within these peptides present challenges, possibly due to inadequate ring sizes. To achieve

effective metal binding, it is essential to explore various cyclization techniques to precisely adjust the ring size. Overall, the results of our study have implications for the design and optimization of metal-dependent peptide catalysts with improved efficiency and specificity.

- **A set of cysteine-rich peptides** consisting of residues from the catalytic triad and having cysteine as nucleophile s**howing both esterase and phosphatase activities demonstrated by successful hydrolysis of *p*-NPA, *p*-NPP, and ATP**. The catalytic activity of our cysteine-rich peptides is positively associated with the number of thiol groups within their sequence. Furthermore, employing head-to-side chain cyclization we improved the serum stability of the suggested sequence without compromising its catalytic efficiency. Alternatively, cyclization through disulfide bridge formation enabled tunable activity resulting from the sensitivity of the thiol groups to the redox environment. Finally, our findings reveal that high concentrations of GSH can break down the disulfide bridge in cyclic peptides, triggering catalysis through ring opening. This reaction converts GSH into GSSG, reducing GSH levels and undermining its role in promoting tumor growth and resistance to chemotherapy. This novel approach could open promising opportunities for tailored peptide catalysts and therapeutic applications.

- **A refined, reproducible and reliable protocol for assessing the catalytic activity of peptides and peptide assemblies.** We highlight the need to maintain standardized conditions, specifically regarding pH and temperature, to ensure the reproducibility of results. This necessity arises from the unique properties of the *p*-NPA substrate as its hydrolysis rate increases with temperature, and it can exist in a protonated and deprotonated form, with absorbance peaks at 320 nm and 405 nm, respectively. Commonly, the *p*-NPA assay is performed by measuring the absorbance at 405 nm. Slight pH shifts can affect the concentration of the deprotonated form and lead to inaccurate interpretations of the peptide's true catalytic performance. Given that peptides typically exhibit slower reaction rates compared to enzymes, minor environmental fluctuations can lead to notable discrepancies in *p*-NPA hydrolysis rates which affect the reproducibility of the results, a concern that is less pronounced with fast-reacting enzymes. Furthermore, when the catalytic activity of peptide assemblies is assessed, it is imperative to take into account the principles of the Michaelis-Menten kinetics and assure one order of magnitude difference between the substrate and the peptide.

3.2 Future directions

Peptides offer several advantages over enzymes, such as resilience to external factors like pH fluctuations and temperature changes. Furthermore, peptides are versatile and modular, making them an invaluable tool for addressing a wide array of challenges. One potential application involves using peptides to address the global issue of plastic pollution. Certain catalytic peptides have hydrolytic activity capable of breaking down chemical bonds in polymeric materials [154]. For example, PET, commonly used in plastic bottles, contains ester bonds that peptides could effectively hydrolyze. As plastic pollution becomes an increasingly pressing environmental problem, progress in this area and additional research are more urgent than ever. Catalytic peptides could also find biological applications, such as selectively inhibiting signaling pathways in tumor cells, potentially halting tumor growth or inducing cell death. By developing adaptable systems like the cysteine-rich peptide-based one we are studying, which responds to the environment and activates only under conditions present in tumors, it is possible to selectively target only tumor cells, enabling targeted therapy with minimal side effects. Furthermore, peptides can be engineered as alternatives to conventional enzyme replacement therapies, which require intravenous administration due to the potential degradation of proteins in the stomach. In contrast, peptides are resistant to low pH and could therefore be administered orally in pill form, simplifying treatment and reducing healthcare costs. This research paves the way for the development of peptide-based smart systems that can change properties in response to external stimuli like temperature, pH, light, or chemical environment. Such systems might be used for targeted drug delivery, responding to the specific biochemical environment of a tumor to release therapeutic agents directly where needed. Additionally, peptide-based smart systems could lead to innovations in self-healing materials or biosensors, opening novel pathways for incorporating peptides into a wide range of biomedical applications.

Possible immediate future work include:

- Circular Dichroism (CD) and *p*-NPP hydrolysis analyses could be conducted on analogues of Cys-rich peptides featuring various LGLG linker lengths to investigate the correlation between secondary structure and efficient *p*-NPP hydrolysis, and to determine whether *p*-NPA hydrolysis based on the catalytic triad mechanism is predominantly sequence-dependent, while hydrolysis of more complex substrates may also be influenced by conformation.

- Prior to evaluating the *in vitro* activity of the CG11 peptide, it would be beneficial to assess its potential cytotoxicity with the MTT assay, which measures cell metabolic

activity as a proxy for viability. This assay would enable us to determine to what extent our peptides affect the health and survival of treated cells. In addition, to investigate the ability of peptides to enter cells, we could label them with a small fluorescent dye. This approach would allow direct visualization and quantification of peptide uptake by cells using fluorescence microscopy.

- Should the CG11 peptide exhibit favorable biocompatibility in cell culture experiments, we could proceed to evaluate its capacity to hydrolyze ATP intracellularly. Furthermore, we could investigate the activation of our cyclic peptide (cy-CG11) across a range of GSH concentrations in tumor cell cultures to determine whether reduction of cy-CG11 to its active form, CG11, can be induced by GSH levels typically found in different tumor cells [149].

Bibliography

[1] P. K. Robinson, "Enzymes: principles and biotechnological applications," *Essays in biochemistry*, vol. 59, p. 1, 2015.

[2] J. M. Carnall, C. A. Waudby, A. M. Belenguer, M. C. Stuart, J. J.-P. Peyralans, and S. Otto, "Mechanosensitive self-replication driven by self-organization," *Science*, vol. 327, no. 5972, pp. 1502–1506, 2010.

[3] P. Janković, I. Santek, A. S. Pina, and D. Kalafatovic, "Exploiting peptide self-assembly for the development of minimalistic viral mimetics," *Frontiers in chemistry*, vol. 9, p. 723473, 2021.

[4] J. Peretó, R. Fani, J. I. Leguina, A. Lazcano, *et al.*, "Enzyme evolution and the development of metabolic pathways," *New Beer in an Old Bottle: Eduard Buchner and the Growth of Biochemical Knowledge*, pp. 173–98, 1997.

[5] E. Shukla, A. D. Bendre, and S. M. Gaikwad, "Hydrolases: the most diverse class of enzymes," in *Hydrolases*, IntechOpen London, 2022.

[6] P. Carter and J. A. Wells, "Dissecting the catalytic triad of a serine protease," *Nature*, vol. 332, no. 6164, pp. 564–568, 1988.

[7] M. E. Davis, J. D. Madura, J. Sines, B. A. Luty, S. A. Allison, J. Andrew, *et al.*, "[22] diffusion-controlled enzymatic reactions," in *Methods in Enzymology*, vol. 202, pp. 473–497, Elsevier, 1991.

[8] M. D. Nothling, Z. Xiao, A. Bhaskaran, M. T. Blyth, C. W. Bennett, M. L. Coote, and L. A. Connal, "Synthetic catalysts inspired by hydrolytic enzymes," *ACS Catalysis*, vol. 9, no. 1, pp. 168–187, 2018.

[9] A. Illanes, "Enzyme production," in *Enzyme biocatalysis: Principles and applications*, pp. 57–106, Springer, 2008.

[10] J. B. van Beilen and Z. Li, "Enzyme technology: an overview," *Current Opinion in biotechnology*, vol. 13, no. 4, pp. 338–344, 2002.

[11] R. J. Whitehurst and M. Van Oort, *Enzymes in food technology*, vol. 388. Wiley Online Library, 2010.

[12] O. Kirk, T. V. Borchert, and C. C. Fuglsang, "Industrial enzyme applications," *Current opinion in biotechnology*, vol. 13, no. 4, pp. 345–351, 2002.

[13] J. Chapman, A. E. Ismail, and C. Z. Dinu, "Industrial applications of enzymes: Recent advances, techniques, and outlooks," *Catalysts*, vol. 8, no. 6, p. 238, 2018.

[14] Y. Zhang, S. He, and B. K. Simpson, "Enzymes in food bioprocessing—novel food enzymes, applications, and related techniques," *Current opinion in food science*, vol. 19, pp. 30–35, 2018.

[15] F. Hasan, A. A. Shah, S. Javed, and A. Hameed, "Enzymes used in detergents: lipases," *African journal of biotechnology*, vol. 9, no. 31, pp. 4836–4844, 2010.

[16] S. V. Ranganathan, S. L. Narasimhan, and K. Muthukumar, "An overview of enzymatic production of biodiesel," *Bioresource technology*, vol. 99, no. 10, pp. 3975–3981, 2008.

[17] K. Matsumoto and S. Taguchi, "Enzyme and metabolic engineering for the production of novel biopolymers: crossover of biological and chemical processes," *Current opinion in biotechnology*, vol. 24, no. 6, pp. 1054–1060, 2013.

[18] D. Concolino, F. Deodato, and R. Parini, "Enzyme replacement therapy: efficacy and limitations," *Italian journal of pediatrics*, vol. 44, pp. 117–126, 2018.

[19] M. Raja, A. Raja, M. Imran, A. Santha, and K. Devasena, "Enzymes application in diagnostic prospects," *Biotechnology*, vol. 10, no. 1, pp. 51–59, 2011.

[20] K. Mojsov, "Application of enzymes in the textile industry: a review," 2011.

[21] K. Sunar, U. Kumar, and S. Deshmukh, "Recent applications of enzymes in personal care products," in *Agro-Industrial Wastes as Feedstock for Enzyme Production*, pp. 279–298, Elsevier, 2016.

[22] R. Singh, M. Kumar, A. Mittal, and P. K. Mehta, "Microbial enzymes: industrial progress in 21st century," *3 Biotech*, vol. 6, pp. 1–15, 2016.

[23] D. Paria and P. L. Venugopalan, "Controlling evolution: The nobel prize in chemistry 2018," *IEEE pulse*, vol. 10, no. 4, pp. 12–16, 2019.

[24] R. Breslow, "Artificial enzymes," *Science*, vol. 218, no. 4572, pp. 532–537, 1982.

[25] B. Zhang and R. Breslow, "Ester hydrolysis by a catalytic cyclodextrin dimer enzyme mimic with a metallobipyridyl linking group," *Journal of the American Chemical Society*, vol. 119, no. 7, pp. 1676–1681, 1997.

[26] M. T. Reetz, G. Lohmer, and R. Schwickardi, "Systhesis and catalytic activity of dendritic diphosphane metal complexes," *Angewandte Chemie International Edition in English*, vol. 36, no. 13-14, pp. 1526–1529, 1997.

[27] B. Mondal, P. Sen, A. Rana, D. Saha, P. Das, and A. Dey, "Reduction of co2 to co by an iron porphyrin catalyst in the presence of oxygen," *ACS Catalysis*, vol. 9, no. 5, pp. 3895–3899, 2019.

[28] D. Alonso and A. Mondragón, "Mechanisms of catalytic rna molecules," *Biochemical Society Transactions*, vol. 49, no. 4, pp. 1529–1535, 2021.

[29] D. Hilvert, "Critical analysis of antibody catalysis," *Annual review of biochemistry*, vol. 69, no. 1, pp. 751–793, 2000.

[30] M. Wittwer, U. Markel, J. Schiffels, J. Okuda, D. F. Sauer, and U. Schwaneberg, "Engineering and emerging applications of artificial metalloenzymes with whole cells," *Nature Catalysis*, vol. 4, no. 10, pp. 814–827, 2021.

[31] B. Liu and J. Liu, "Surface modification of nanozymes," *Nano Research*, vol. 10, pp. 1125–1148, 2017.

[32] X. Ren, D. Chen, Y. Wang, H. Li, Y. Zhang, H. Chen, X. Li, and M. Huo, "Nanozymes-recent development and biomedical applications," *Journal of Nanobiotechnology*, vol. 20, no. 1, p. 92, 2022.

[33] R. Mandal, A. Ghosh, N. K. Rout, M. Prasad, B. Hazra, S. Sar, S. Das, A. Datta, and P. K. Tarafdar, "Self-assembled prebiotic amphiphile-mixture exhibit tunable catalytic properties," *Organic & Biomolecular Chemistry*, 2023.

[34] A. Shamsabadi, T. Haghighi, S. Carvalho, L. C. Frenette, and M. M. Stevens, "The nanozyme revolution: Enhancing the performance of medical biosensing platforms," *Advanced Materials*, p. 2300184, 2023.

[35] P. Makam, S. S. Yamijala, V. S. Bhadram, L. J. Shimon, B. M. Wong, and E. Gazit, "Single amino acid bionanozyme for environmental remediation," *Nature communications*, vol. 13, no. 1, p. 1505, 2022.

[36] J. Yi, Q. Deng, Z. Liu, H. Wang, X. Liu, J. Ren, and X. Qu, "Nanozyme-based supramolecular self-assembly as an artificial host defense system for treatment of bacterial infections," *Small*, p. 2301096, 2023.

[37] H. Wei and E. Wang, "Nanomaterials with enzyme-like characteristics (nanozymes): next-generation artificial enzymes," *Chemical Society Reviews*, vol. 42, no. 14, pp. 6060–6093, 2013.

[38] Y. Ai, Z.-N. Hu, X. Liang, H.-b. Sun, H. Xin, and Q. Liang, "Recent advances in nanozymes: from matters to bioapplications," *Advanced Functional Materials*, vol. 32, no. 14, p. 2110432, 2022.

[39] D. Berillo, A. Yeskendir, Z. Zharkinbekov, K. Raziyeva, and A. Saparov, "Peptide-based drug delivery systems," *Medicina*, vol. 57, no. 11, p. 1209, 2021.

[40] A. Altunbas and D. J. Pochan, "Peptide-based and polypeptide-based hydrogels for drug delivery and tissue engineering," *Peptide-based materials*, pp. 135–167, 2012.

[41] Q. Liu, J. Wang, and B. J. Boyd, "Peptide-based biosensors," *Talanta*, vol. 136, pp. 114–127, 2015.

[42] J. Chatterjee, F. Rechenmacher, and H. Kessler, "N-methylation of peptides and proteins: an important element for modulating biological functions," *Angewandte Chemie International Edition*, vol. 52, no. 1, pp. 254–269, 2013.

[43] A. S. Pina, L. Morgado, K. L. Duncan, S. Carvalho, H. F. Carvalho, A. J. Barbosa, B. d. P. Mariz, I. P. Moreira, D. Kalafatovic, B. M. M. Faustino, *et al.*, "Discovery of phosphotyrosine-binding oligopeptides with supramolecular target selectivity," *Chemical science*, vol. 13, no. 1, pp. 210–217, 2022.

[44] X. Liu, R. Waters, H. E. Gilbert, G. T. Barroso, K. M. Boyle, and L. S. Witus, "The role of β-hairpin conformation in ester hydrolysis peptide catalysts based on a trpzip scaffold," *RSC advances*, vol. 11, no. 38, pp. 23714–23718, 2021.

[45] M. A. Beasley, A. D. Dunkelberger, M. D. Thum, E. S. Ryland, K. P. Fears, A. B. Grafton, J. C. Owrutsky, J. G. Lundin, and C. R. So, "Extremophilic behavior of catalytic amyloids sustained by backbone structuring," *Journal of Materials Chemistry B*, vol. 10, no. 45, pp. 9400–9412, 2022.

[46] N. Sewald and H.-D. Jakubke, *Peptides: chemistry and biology*. John Wiley & Sons, 2015.

[47] A. R. Mitchell, "Bruce merrifield and solid-phase peptide synthesis: A historical assessment," *Peptide Science*, vol. 90, no. 3, pp. 175–184, 2008.

[48] M. Stawikowski and G. B. Fields, "Introduction to peptide synthesis," *Current protocols in protein science*, vol. 69, no. 1, pp. 18–1, 2012.

[49] S. Studer, D. A. Hansen, Z. L. Pianowski, P. R. Mittl, A. Debon, S. L. Guffy, B. S. Der, B. Kuhlman, and D. Hilvert, "Evolution of a highly active and enantiospecific metalloenzyme from short peptides," *Science*, vol. 362, no. 6420, pp. 1285–1288, 2018.

[50] M. Frenkel-Pinter, M. Samanta, G. Ashkenasy, and L. J. Leman, "Prebiotic peptides: Molecular hubs in the origin of life," *Chemical reviews*, vol. 120, no. 11, pp. 4707–4765, 2020.

[51] V. Alva and A. N. Lupas, "From ancestral peptides to designed proteins," *Current opinion in structural biology*, vol. 48, pp. 103–109, 2018.

[52] A. Levin, T. A. Hakala, L. Schnaider, G. J. Bernardes, E. Gazit, and T. P. Knowles, "Biomimetic peptide self-assembly for functional materials," *Nature Reviews Chemistry*, vol. 4, no. 11, pp. 615–634, 2020.

[53] J. Han, H. Gong, X. Ren, and X. Yan, "Supramolecular nanozymes based on peptide self-assembly for biomimetic catalysis," *Nano Today*, vol. 41, p. 101295, 2021.

[54] Y. Lou, B. Zhang, X. Ye, and Z.-G. Wang, "Self-assembly of the de novo designed peptides to produce supramolecular catalysts with built-in enzyme-like active sites: A review of structure-activity relationship," *Materials Today Nano*, p. 100302, 2023.

[55] P. Dowari, M. K. Baroi, T. Das, B. K. Das, S. Das, S. Chowdhuri, A. Garg, A. Debnath, and D. Das, "Development of a hydrolase mimicking peptide amphiphile and its immobilization on silica surface for stereoselective and enhanced catalysis," *Journal of Colloid and Interface Science*, vol. 618, pp. 98–110, 2022.

[56] L. Wang, N. Wang, W. Zhang, X. Cheng, Z. Yan, G. Shao, X. Wang, R. Wang, and C. Fu, "Therapeutic peptides: Current applications and future directions," *Signal Transduction and Targeted Therapy*, vol. 7, no. 1, p. 48, 2022.

[57] O. Zozulia, M. Dolan, and I. Korendovych, "Catalytic peptide assemblies," *Chemical Society Reviews*, vol. 47, no. 10, pp. 3621–3639, 2018.

[58] S. Carvalho, D. Q. Peralta Reis, S. V. Pereira, D. Kalafatovic, and A. S. Pina, "Catalytic peptides: The challenge between simplicity and functionality," *Israel Journal of Chemistry*, vol. 62, no. 9-10, p. e202200029, 2022.

[59] S. Zhang, "Emerging biological materials through molecular self-assembly," *Biotechnology advances*, vol. 20, no. 5-6, pp. 321–339, 2002.

[60] E. Gazit, "Self-assembled peptide nanostructures: the design of molecular building blocks and their technological utilization," *Chemical Society Reviews*, vol. 36, no. 8, pp. 1263–1269, 2007.

[61] E. De Santis, H. Alkassem, B. Lamarre, N. Faruqui, A. Bella, J. E. Noble, N. Micale, S. Ray, J. R. Burns, A. R. Yon, *et al.*, "Antimicrobial peptide capsids of de novo design," *Nature communications*, vol. 8, no. 1, p. 2263, 2017.

[62] Y. Gao, L. Wang, X. Zhang, Z. Zhou, X. Shen, H. Hu, R. Sun, and J. Tang, "Advances in self-assembled peptides as drug carriers," *Pharmaceutics*, vol. 15, no. 2, p. 482, 2023.

[63] L. A. Castillo-Díaz, J. A. Ruiz-Pacheco, M. A. Elsawy, J. E. Reyes-Martínez, and A. I. Enríquez-Rodríguez, "Self-assembling peptides as an emerging platform for the treatment of metabolic syndrome," *International Journal of Nanomedicine*, pp. 10349–10370, 2020.

[64] C. Diaferia, E. Rosa, G. Morelli, and A. Accardo, "Fmoc-diphenylalanine hydrogels: Optimization of preparation methods and structural insights," *Pharmaceuticals*, vol. 15, no. 9, p. 1048, 2022.

[65] S. Fleming and R. V. Ulijn, "Design of nanostructures based on aromatic peptide amphiphiles," *Chemical Society Reviews*, vol. 43, no. 23, pp. 8150–8177, 2014.

[66] J. Raeburn and D. J. Adams, "Multicomponent low molecular weight gelators," *Chemical Communications*, vol. 51, no. 25, pp. 5170–5180, 2015.

[67] M. P. Hendricks, K. Sato, L. C. Palmer, and S. I. Stupp, "Supramolecular assembly of peptide amphiphiles," *Accounts of chemical research*, vol. 50, no. 10, pp. 2440–2448, 2017.

[68] D. Kalafatovic, M. Nobis, J. Son, K. I. Anderson, and R. V. Ulijn, "Mmp-9 triggered self-assembly of doxorubicin nanofiber depots halts tumor growth," *Biomaterials*, vol. 98, pp. 192–202, 2016.

[69] A. Lampel, S. A. McPhee, S. Kassem, D. Sementa, T. Massarano, J. M. Aramini, Y. He, and R. V. Ulijn, "Melanin-inspired chromophoric microparticles composed of polymeric peptide pigments," *Angewandte Chemie*, vol. 133, no. 14, pp. 7642–7647, 2021.

[70] P. W. Frederix, G. G. Scott, Y. M. Abul-Haija, D. Kalafatovic, C. G. Pappas, N. Javid, N. T. Hunt, R. V. Ulijn, and T. Tuttle, "Exploring the sequence space for (tri-) peptide self-assembly to design and discover new hydrogels," *Nature chemistry*, vol. 7, no. 1, pp. 30–37, 2015.

[71] T. Li, X.-M. Lu, M.-R. Zhang, K. Hu, and Z. Li, "Peptide-based nanomaterials: Self-assembly, properties and applications," *Bioactive Materials*, vol. 11, pp. 268–282, 2022.

[72] K. L. Duncan and R. V. Ulijn, "Short peptides in minimalistic biocatalyst design," *Biocatalysis*, vol. 1, no. 1, pp. 67–81, 2015.

[73] J. Duschmalé, S. Kohrt, and H. Wennemers, "Peptide catalysis in aqueous emulsions," *Chemical communications*, vol. 50, no. 60, pp. 8109–8112, 2014.

[74] T. Schnitzer, J. W. Rackl, and H. Wennemers, "Stereoselective peptide catalysis in complex environments–from river water to cell lysates," *Chemical Science*, vol. 13, no. 31, pp. 8963–8967, 2022.

[75] T. O. Omosun, M.-C. Hsieh, W. S. Childers, D. Das, A. K. Mehta, N. R. Anthony, T. Pan, M. A. Grover, K. M. Berland, and D. G. Lynn, "Catalytic diversity in self-propagating peptide assemblies," *Nature chemistry*, vol. 9, no. 8, pp. 805–809, 2017.

[76] A. Reja, S. P. Afrose, and D. Das, "Aldolase cascade facilitated by self-assembled nanotubes from short peptide amphiphiles," *Angewandte Chemie International Edition*, vol. 59, no. 11, pp. 4329–4334, 2020.

[77] M. Tena-Solsona, J. Nanda, S. Díaz-Oltra, A. Chotera, G. Ashkenasy, and B. Escuder, "Emergent catalytic behavior of self-assembled low molecular weight peptide-based aggregates and hydrogels," *Chemistry–A European Journal*, vol. 22, no. 19, pp. 6687–6694, 2016.

[78] H.-S. Jang, J.-H. Lee, Y.-S. Park, Y.-O. Kim, J. Park, T.-Y. Yang, K. Jin, J. Lee, S. Park, J. M. You, *et al.*, "Tyrosine-mediated two-dimensional peptide assembly and its role as a bio-inspired catalytic scaffold," *Nature communications*, vol. 5, no. 1, p. 3665, 2014.

[79] Y. Li, P. Sun, L. Zhao, X. Yan, D. K. Ng, and P.-C. Lo, "Ferric ion driven assembly of catalase-like supramolecular photosensitizing nanozymes for combating hypoxic tumors," *Angewandte Chemie International Edition*, vol. 59, no. 51, pp. 23228–23238, 2020.

[80] C. M. Rufo, Y. S. Moroz, O. V. Moroz, J. Stöhr, T. A. Smith, X. Hu, W. F. De-Grado, and I. V. Korendovych, "Short peptides self-assemble to produce catalytic amyloids," *Nature chemistry*, vol. 6, no. 4, pp. 303–309, 2014.

[81] O. V. Makhlynets, P. M. Gosavi, and I. V. Korendovych, "Short self-assembling peptides are able to bind to copper and activate oxygen," *Angewandte Chemie International Edition*, vol. 55, no. 31, pp. 9017–9020, 2016.

[82] M. Díaz-Caballero, S. Navarro, M. Nuez-Martínez, F. Peccati, L. Rodríguez-Santiago, M. Sodupe, F. Teixidor, and S. Ventura, "ph-responsive self-assembly of amyloid fibrils for dual hydrolase-oxidase reactions," *ACS catalysis*, vol. 11, no. 2, pp. 595–607, 2020.

[83] S. Lindskog, "Structure and mechanism of carbonic anhydrase," *Pharmacology & therapeutics*, vol. 74, no. 1, pp. 1–20, 1997.

[84] C. T. Supuran, "Carbonic anhydrases-an overview," *Current pharmaceutical design*, vol. 14, no. 7, pp. 603–614, 2008.

[85] R. Song, X. Wu, B. Xue, Y. Yang, W. Huang, G. Zeng, J. Wang, W. Li, Y. Cao, W. Wang, *et al.*, "Principles governing catalytic activity of self-assembled short peptides," *Journal of the American Chemical Society*, vol. 141, no. 1, pp. 223–231, 2018.

[86] Z. Al-Garawi, B. McIntosh, D. Neill-Hall, A. Hatimy, S. Sweet, M. Bagley, and L. Serpell, "The amyloid architecture provides a scaffold for enzyme-like catalysts," *Nanoscale*, vol. 9, no. 30, pp. 10773–10783, 2017.

[87] O. Monasterio, E. Nova, and R. Diaz-Espinoza, "Development of a novel catalytic amyloid displaying a metal-dependent atpase-like activity," *Biochemical and biophysical research communications*, vol. 482, no. 4, pp. 1194–1200, 2017.

[88] C. Castillo-Caceres, E. Duran-Meza, E. Nova, R. Araya-Secchi, O. Monasterio, and R. Diaz-Espinoza, "Functional characterization of the atpase-like activity displayed by a catalytic amyloid," *Biochimica et Biophysica Acta (BBA)-General Subjects*, vol. 1865, no. 1, p. 129729, 2021.

[89] Z. Lengyel, C. M. Rufo, Y. S. Moroz, O. V. Makhlynets, and I. V. Korendovych, "Copper-containing catalytic amyloids promote phosphoester hydrolysis and tandem reactions," *ACS catalysis*, vol. 8, no. 1, pp. 59–62, 2018.

[90] P. Janković, E. Otović, G. Mausa, and D. Kalafatovic, "Manually curated dataset of catalytic peptides for ester hydrolysis," *Data in brief*, vol. 48, p. 109290, 2023.

[91] A. Baruch-Leshem, C. Chevallard, F. Gobeaux, P. Guenoun, J. Daillant, P. Fontaine, M. Goldmann, A. Kushmaro, and H. Rapaport, "Catalytically active peptides affected by self-assembly and residues order," *Colloids and Surfaces B: Biointerfaces*, vol. 203, p. 111751, 2021.

[92] C. Zhang, X. Xue, Q. Luo, Y. Li, K. Yang, X. Zhuang, Y. Jiang, J. Zhang, J. Liu, G. Zou, *et al.*, "Self-assembled peptide nanofibers designed as biological enzymes for catalyzing ester hydrolysis," *Acs Nano*, vol. 8, no. 11, pp. 11715–11723, 2014.

[93] C. Zhang, R. Shafi, A. Lampel, D. MacPherson, C. G. Pappas, V. Narang, T. Wang, C. Maldarelli, and R. V. Ulijn, "Switchable hydrolase based on reversible formation of supramolecular catalytic site using a self-assembling peptide," *Angewandte Chemie International Edition*, vol. 56, no. 46, pp. 14511–14515, 2017.

[94] P.-Y. Hung, Y.-H. Chen, K.-Y. Huang, C.-C. Yu, and J.-C. Horng, "Design of polyproline-based catalysts for ester hydrolysis," *Acs Omega*, vol. 2, no. 9, pp. 5574–5581, 2017.

[95] Y. Jin, C. Yu, R. J. Denman, and W. Zhang, "Recent advances in dynamic covalent chemistry," *Chemical Society Reviews*, vol. 42, no. 16, pp. 6634–6654, 2013.

[96] J. Hu, S. K. Gupta, J. Ozdemir, and H. Beyzavi, "Applications of dynamic covalent chemistry concept toward tailored covalent organic framework nanomaterials: A review," *ACS applied nano materials*, vol. 3, no. 7, pp. 6239–6269, 2020.

[97] S. Ulrich, "Growing prospects of dynamic covalent chemistry in delivery applications," *Accounts of chemical research*, vol. 52, no. 2, pp. 510–519, 2019.

[98] L. Yang, L. Sun, H. Huang, W. Zhu, Y. Wang, Z. Wu, R. E. Neisiany, S. Gu, and Z. You, "Mechanically robust and room temperature self-healing ionogel based on ionic liquid inhibited reversible reaction of disulfide bonds," *Advanced Science*, vol. 10, no. 20, p. 2207527, 2023.

[99] P. Nagy and C. C. Winterbourn, "Redox chemistry of biological thiols," in *Advances in molecular toxicology*, vol. 4, pp. 183–222, Elsevier, 2010.

[100] L. B. Poole, "The basics of thiols and cysteines in redox biology and chemistry," *Free Radical Biology and Medicine*, vol. 80, pp. 148–157, 2015.

[101] P. J. Hogg, "Disulfide bonds as switches for protein function," *Trends in biochemical sciences*, vol. 28, no. 4, pp. 210–214, 2003.

[102] J. Li, P. Nowak, and S. Otto, "Dynamic combinatorial libraries: from exploring molecular recognition to systems chemistry," *Journal of the American Chemical Society*, vol. 135, no. 25, pp. 9222–9239, 2013.

[103] P. Nagy, "Kinetics and mechanisms of thiol–disulfide exchange covering direct substitution and thiol oxidation-mediated pathways," *Antioxidants & redox signaling*, vol. 18, no. 13, pp. 1623–1641, 2013.

[104] S. Yao, A. Moyer, Y. Zheng, Y. Shen, X. Meng, C. Yuan, Y. Zhao, H. Yao, D. Baker, and C. Wu, "De novo design and directed folding of disulfide-bridged peptide heterodimers," *Nature communications*, vol. 13, no. 1, p. 1539, 2022.

[105] M. A. Wouters, S. W. Fan, and N. L. Haworth, "Disulfides as redox switches: from molecular mechanisms to functional significance," *Antioxidants & redox signaling*, vol. 12, no. 1, pp. 53–91, 2010.

[106] C. J. Bowerman and B. L. Nilsson, "A reductive trigger for peptide self-assembly and hydrogelation," *Journal of the American Chemical Society*, vol. 132, no. 28, pp. 9526–9527, 2010.

[107] Y. Gao, Y. Li, H. Cao, H. Jia, D. Wang, C. Ren, Z. Wang, C. Yang, and J. Liu, "Hypertoxic self-assembled peptide with dual functions of glutathione depletion and biosynthesis inhibition for selective tumor ferroptosis and pyroptosis," *Journal of Nanobiotechnology*, vol. 20, no. 1, p. 390, 2022.

[108] K. Fosgerau and T. Hoffmann, "Peptide therapeutics: current status and future directions," *Drug discovery today*, vol. 20, no. 1, pp. 122–128, 2015.

[109] I. W. Hamley, "Small bioactive peptides for biomaterials design and therapeutics," *Chemical reviews*, vol. 117, no. 24, pp. 14015–14041, 2017.

[110] K. Sharma, K. K. Sharma, A. Sharma, and R. Jain, "Peptide-based drug discovery: Current status and recent advances," *Drug Discovery Today*, vol. 28, no. 2, p. 103464, 2023.

[111] J. Fetse, S. Kandel, U.-F. Mamani, and K. Cheng, "Recent advances in the development of therapeutic peptides," *Trends in Pharmacological Sciences*, 2023.

[112] A. P. Davenport, C. C. Scully, C. de Graaf, A. J. Brown, and J. J. Maguire, "Advances in therapeutic peptides targeting g protein-coupled receptors," *Nature Reviews Drug Discovery*, vol. 19, no. 6, pp. 389–413, 2020.

[113] M. C. Lucana, Y. Arruga, E. Petrachi, A. Roig, R. Lucchi, and B. Oller-Salvia, "Protease-resistant peptides for targeting and intracellular delivery of therapeutics," *Pharmaceutics*, vol. 13, no. 12, p. 2065, 2021.

[114] H. Jenssen and S. I. Aspmo, "Serum stability of peptides," *Peptide-based drug design*, pp. 177–186, 2008.

[115] S. C. Penchala, M. R. Miller, A. Pal, J. Dong, N. R. Madadi, J. Xie, H. Joo, J. Tsai, P. Batoon, V. Samoshin, *et al.*, "A biomimetic approach for enhancing the in vivo half-life of peptides," *Nature chemical biology*, vol. 11, no. 10, pp. 793–798, 2015.

[116] J. Chatterjee, B. Laufer, and H. Kessler, "Synthesis of n-methylated cyclic peptides," *Nature protocols*, vol. 7, no. 3, pp. 432–444, 2012.

[117] T. R. White, C. M. Renzelman, A. C. Rand, T. Rezai, C. M. McEwen, V. M. Gelev, R. A. Turner, R. G. Linington, S. S. Leung, A. S. Kalgutkar, *et al.*, "On-resin n-methylation of cyclic peptides for discovery of orally bioavailable scaffolds," *Nature chemical biology*, vol. 7, no. 11, pp. 810–817, 2011.

[118] G. Liszczak, J. M. Goldberg, H. Foyn, E. J. Petersson, T. Arnesen, and R. Marmorstein, "Molecular basis for n-terminal acetylation by the heterodimeric nata complex," *Nature structural & molecular biology*, vol. 20, no. 9, pp. 1098–1105, 2013.

[119] K. T. Nguyen, S.-H. Mun, C.-S. Lee, and C.-S. Hwang, "Control of protein degradation by n-terminal acetylation and the n-end rule pathway," *Experimental & molecular medicine*, vol. 50, no. 7, pp. 1–8, 2018.

[120] Y. Marciano, N. Nayeem, D. Dave, R. V. Ulijn, and M. Contel, "N-acetylation of biodegradable supramolecular peptide nanofilaments selectively enhances their proteolytic stability for targeted delivery of gold-based anticancer agents," *ACS Biomaterials Science & Engineering*, vol. 9, no. 6, pp. 3379–3389, 2023.

[121] L. T. Nguyen, J. K. Chau, N. A. Perry, L. de Boer, S. A. Zaat, and H. J. Vogel, "Serum stabilities of short tryptophan-and arginine-rich antimicrobial peptide analogs," *PloS one*, vol. 5, no. 9, p. e12684, 2010.

[122] R. Prades, B. Oller-Salvia, S. M. Schwarzmaier, J. Selva, M. Moros, M. Balbi, V. Grazú, J. M. de La Fuente, G. Egea, N. Plesnila, *et al.*, "Applying the retro-enantio approach to obtain a peptide capable of overcoming the blood–brain barrier," *Angewandte Chemie International Edition*, vol. 54, no. 13, pp. 3967–3972, 2015.

[123] A. Carrera-Aubesart, S. Defaus, C. Pérez-Peinado, D. Sandín, M. Torrent, M. Á. Jiménez, and D. Andreu, "Examining topoisomers of a snake-venom-derived peptide for improved antimicrobial and antitumoral properties," *Biomedicines*, vol. 10, no. 9, p. 2110, 2022.

[124] R. Tugyi, K. Uray, D. Iván, E. Fellinger, A. Perkins, and F. Hudecz, "Partial d-amino acid substitution: Improved enzymatic stability and preserved ab recognition of a muc2 epitope peptide," *Proceedings of the National Academy of Sciences*, vol. 102, no. 2, pp. 413–418, 2005.

[125] C. Ngambenjawong, H. H. Gustafson, J. M. Pineda, N. A. Kacherovsky, M. Cieslewicz, and S. H. Pun, "Serum stability and affinity optimization of an m2 macrophage-targeting peptide (m2pep)," *Theranostics*, vol. 6, no. 9, p. 1403, 2016.

[126] X. Ji, A. L. Nielsen, and C. Heinis, "Cyclic peptides for drug development," *Angewandte Chemie International Edition*, vol. 63, no. 3, p. e202308251, 2024.

[127] T. A. Hill, N. E. Shepherd, F. Diness, and D. P. Fairlie, "Constraining cyclic peptides to mimic protein structure motifs," *Angewandte Chemie International Edition*, vol. 53, no. 48, pp. 13020–13041, 2014.

[128] H. C. Hayes, L. Y. Luk, and Y.-H. Tsai, "Approaches for peptide and protein cyclisation," *Organic & biomolecular chemistry*, vol. 19, no. 18, pp. 3983–4001, 2021.

[129] I. Bosnjak, V. Bojović, T. Segvić-Bubić, and A. Bielen, "Occurrence of protein disulfide bonds in different domains of life: a comparison of proteins from the protein data bank," *Protein Engineering, Design & Selection*, vol. 27, no. 3, pp. 65–72, 2014.

[130] J. R. Frost, Z. Wu, Y. C. Lam, A. E. Owens, and R. Fasan, "Side-chain-to-tail cyclization of ribosomally derived peptides promoted by aryl and alkyl amino-functionalized unnatural amino acids," *Organic & biomolecular chemistry*, vol. 14, no. 24, pp. 5803–5812, 2016.

[131] C. Bechtler and C. Lamers, "Macrocyclization strategies for cyclic peptides and peptidomimetics," *RSC Medicinal Chemistry*, vol. 12, no. 8, pp. 1325–1351, 2021.

[132] R.-Y. Zhang, P. Thapa, M. J. Espiritu, V. Menon, and J.-P. Bingham, "From nature to creation: Going around in circles, the art of peptide cyclization," *Bioorganic & Medicinal Chemistry*, vol. 26, no. 6, pp. 1135–1150, 2018.

[133] M. L. Merz, S. Habeshian, B. Li, J.-A. G. David, A. L. Nielsen, X. Ji, K. Il Khwildy, M. M. Duany Benitez, P. Phothirath, and C. Heinis, "De novo development of small cyclic peptides that are orally bioavailable," *Nature Chemical Biology*, pp. 1–10, 2023.

[134] J. Chen and X. Zou, "Self-assemble peptide biomaterials and their biomedical applications," *Bioactive materials*, vol. 4, pp. 120–131, 2019.

[135] T. Abdullah, K. Bhatt, L. J. Eggermont, N. O'Hare, A. Memic, and S. A. Bencherif, "Supramolecular self-assembled peptide-based vaccines: current state and future perspectives," *Frontiers in Chemistry*, vol. 8, p. 598160, 2020.

[136] K. Tao, P. Makam, R. Aizen, and E. Gazit, "Self-assembling peptide semiconductors," *Science*, vol. 358, no. 6365, p. eaam9756, 2017.

[137] N. J. Sinha, M. G. Langenstein, D. J. Pochan, C. J. Kloxin, and J. G. Saven, "Peptide design and self-assembly into targeted nanostructure and functional materials," *Chemical Reviews*, vol. 121, no. 22, pp. 13915–13935, 2021.

[138] J. Yang, H.-W. An, and H. Wang, "Self-assembled peptide drug delivery systems," *ACS Applied Bio Materials*, vol. 4, no. 1, pp. 24–46, 2020.

[139] B. He, X. Yuan, J. Wu, Y. Bai, and D. Jiang, "Self-assembling peptide nanofiber scaffolds for bone tissue engineering," *Science of Advanced Materials*, vol. 7, no. 7, pp. 1221–1232, 2015.

[140] F. Ardito, M. Giuliani, D. Perrone, G. Troiano, and L. Lo Muzio, "The crucial role of protein phosphorylation in cell signaling and its use as targeted therapy," *International journal of molecular medicine*, vol. 40, no. 2, pp. 271–280, 2017.

[141] P. Jankovic, M. Babic, M. Percic, A. S. Pina, and D. Kalafatovic, "Factors influencing the catalytic activity of metal-dependent histidine-rich peptides: sequence, conformation, stereochemistry, self-assembly or their interplay?," *Molecular Systems Design & Engineering*, vol. 8, no. 11, pp. 1371–1380, 2023.

[142] A. Matera, J. Brasun, M. Cebrat, and J. Swiatek-Kozowska, "The role of the histidine residue in the coordination abilities of peptides with a multi-histidine sequence towards copper (ii) ions," *Polyhedron*, vol. 27, no. 6, pp. 1539–1555, 2008.

[143] S. A. Klein, A. Majumdar, and D. Barrick, "A second backbone: the contribution of a buried asparagine ladder to the global and local stability of a leucine-rich repeat protein," *Biochemistry*, vol. 58, no. 33, pp. 3480–3493, 2019.

[144] I. Insua and J. Montenegro, "1d to 2d self assembly of cyclic peptides," *Journal of the American Chemical Society*, vol. 142, no. 1, pp. 300–307, 2019.

[145] A. Jeziorna, K. Stopczyk, E. Skorupska, K. Luberda-Durnas, M. Oszajca, W. Lasocha, M. Górecki, J. Frelek, and M. J. Potrzebowski, "Cyclic dipeptides as building units of nano-and microdevices: Synthesis, properties, and structural studies," *Crystal Growth & Design*, vol. 15, no. 10, pp. 5138–5148, 2015.

[146] K.-Y. Huang, C.-C. Yu, and J.-C. Horng, "Conjugating catalytic polyproline fragments with a self-assembling peptide produces efficient artificial hydrolases," *Biomacromolecules*, vol. 21, no. 3, pp. 1195–1201, 2020.

[147] M. Babic, P. Jankovic, S. Marchesan, G. Mausa, and D. Kalafatovic, "Esterase sequence composition patterns for the identification of catalytic triad microenvironment motifs," *Journal of chemical information and modeling*, vol. 62, no. 24, pp. 6398–6410, 2022.

[148] G. Bagiyan, I. Koroleva, N. Soroka, and A. Ufimtsev, "Oxidation of thiol compounds by molecular oxygen in aqueous solutions," *Russian chemical bulletin*, vol. 52, pp. 1135–1141, 2003.

[149] L. Kennedy, J. K. Sandhu, M.-E. Harper, and M. Cuperlovic-Culf, "Role of glutathione in cancer: From mechanisms to therapies," *Biomolecules*, vol. 10, no. 10, p. 1429, 2020.

[150] W. Lieberthal, S. A. Menza, and J. S. Levine, "Graded atp depletion can cause necrosis or apoptosis of cultured mouse proximal tubular cells," *American Journal of Physiology-Renal Physiology*, vol. 274, no. 2, pp. F315–F327, 1998.

[151] J. Suhorutsenko, N. Oskolkov, P. Arukuusk, K. Kurrikoff, E. Eriste, D.-M. Copolovici, and U. Langel, "Cell-penetrating peptides, pepfects, show no evidence of toxicity and immunogenicity in vitro and in vivo," *Bioconjugate chemistry*, vol. 22, no. 11, pp. 2255–2262, 2011.

[152] R. Syedd-León, M. Sandoval-Barrantes, H. Trimiño-Vásquez, L. R. Villegas-Peñaranda, and G. Rodríguez-Rodríguez, "Revisiting the fundamentals of p-nitrophenol analysis for its application in the quantification of lipases activity. a graphical update.," *Uniciencia*, vol. 34, no. 2, pp. 31–43, 2020.

[153] P. Y. Peng YangYang, F. S. Fu ShiYu, L. H. Liu Hao, and L. Lucia, "Accurately determining esterase activity via the isosbestic point of p-nitrophenol.," vol. 11, p. 10099–10111, 2016.

[154] X. Li, Y. Zhou, Z. Lu, R. Shan, D. Sun, J. Li, and P. Li, "Switchable enzyme mimics based on self-assembled peptides for polyethylene terephthalate degradation," *Journal of Colloid and Interface Science*, vol. 646, pp. 198–208, 2023.

Appendices

The following section includes scientific papers in the final published version:

- Jankovic, P., Santek, I., Pina, A. S., & Kalafatovic, D. (2021). Exploiting peptide self-assembly for the development of minimalistic viral mimetics. *Frontiers in chemistry*, 9, 723473.

- Jankovic, P., Otovic, E., Mausa, G., & Kalafatovic, D. (2023). Manually curated dataset of catalytic peptides for ester hydrolysis. *Data in brief*, 48, 109290.

- Jankovic, P., Babić, M., Percic, M., Pina, A. S., & Kalafatovic, D. (2023). Factors influencing the catalytic activity of metal-dependent histidine-rich peptides: sequence, conformation, stereochemistry, self-assembly or their interplay?. *Molecular Systems Design & Engineering*, 8(11), 1371-1380.

- Janković, P., & Kalafatovic, D. (2024). Short catalytic peptides with tunable activity: Cys confers functionality and adaptability. *Available as preprint.*

- Janković, P., & Kalafatovic, D. (2024). Determining the esterase activity of peptides and peptide assemblies. *Methods in Enzymology.* In press.

frontiers
in Chemistry

Exploiting Peptide Self-Assembly for the Development of Minimalistic Viral Mimetics

Patrizia Janković[1], Iva Šantek[1], Ana Sofia Pina[2,3] and Daniela Kalafatovic[1]*

[1]Department of Biotechnology, University of Rijeka, Rijeka, Croatia, [2]Associate Laboratory i4HB - Institute for Health and Bioeconomy, NOVA School of Science and Technology, NOVA University Lisbon, Caparica, Portugal, [3]UCIBIO – Applied Molecular Biosciences Unit, Department of Chemistry, NOVA School of Science and Technology, NOVA University Lisbon, Caparica, Portugal

Viruses are natural supramolecular nanostructures that form spontaneously by molecular self-assembly of complex biomolecules. Peptide self-assembly is a versatile tool that allows mimicking viruses by creating their simplified versions through the design of functional, supramolecular materials with modularity, tunability, and responsiveness to chemical and physical stimuli. The main challenge in the design and fabrication of peptide materials is related to the precise control between the peptide sequence and its resulting supramolecular morphology. We provide an overview of existing sequence patterns employed for the development of spherical and fibrillar peptide assemblies that can act as viral mimetics, offering the opportunity to tackle the challenges of viral infections.

Keywords: self-assembly, viral mimetics, peptides, minimalistic, co-assembly

INTRODUCTION

Designed bio-nanomaterials are often inspired by basic processes found in nature such as molecular recognition and self-assembly (Lehn, 2002; Whitesides and Grzybowski, 2002; Yang et al., 2020a). Viruses present a great source of inspiration for the design of life-like materials (Whitesides, 2015; Maslanka Figueroa et al., 2021) as they constitute simple, yet sophisticated supramolecular assemblies that contain genetic code and present well-defined rod-like or spherical morphologies. In addition, they show the ability to self-replicate, respond to physical and chemical stimuli, adapt to the environment, and evade the immune system which makes them ideal candidates to be manipulated and repurposed.

A variety of virus-mimetic materials have been developed for biological and chemical sensing (Mao et al., 2009), drug delivery (Li et al., 2016), cancer immunotherapy (Mohsen et al., 2020) and vaccine design (Abudula et al., 2020). Virus-like particles (VLPs), formed by the multimeric self-assembly of expressed viral structural proteins in absence of genetic material, are the most studied ones (Ludwig and Wagner, 2007; Ferreira and Martins, 2017; Roldão et al., 2019). The complexity of their fabrication, that requires fully folded proteins and efficient upstream and downstream strategies, impacts the production yields, and is associated to high costs. Other examples include polymer peptide nanogels (Lee et al., 2008), dendritic lipopeptides (Liang et al., 2019), iron oxide-lactoferrin magneto-responsive nanocapsules (Fang et al., 2015), peptide-DNA condensates (Cao et al., 2018), rabies-inspired gold nanorods (Lee et al., 2017) or metal–organic frameworks (Qiao et al., 2020). However, the potential of minimalistic, purely peptidic, supramolecular nanostructures to resemble the morphology and/or functionality of viruses has not been fully exploited yet.
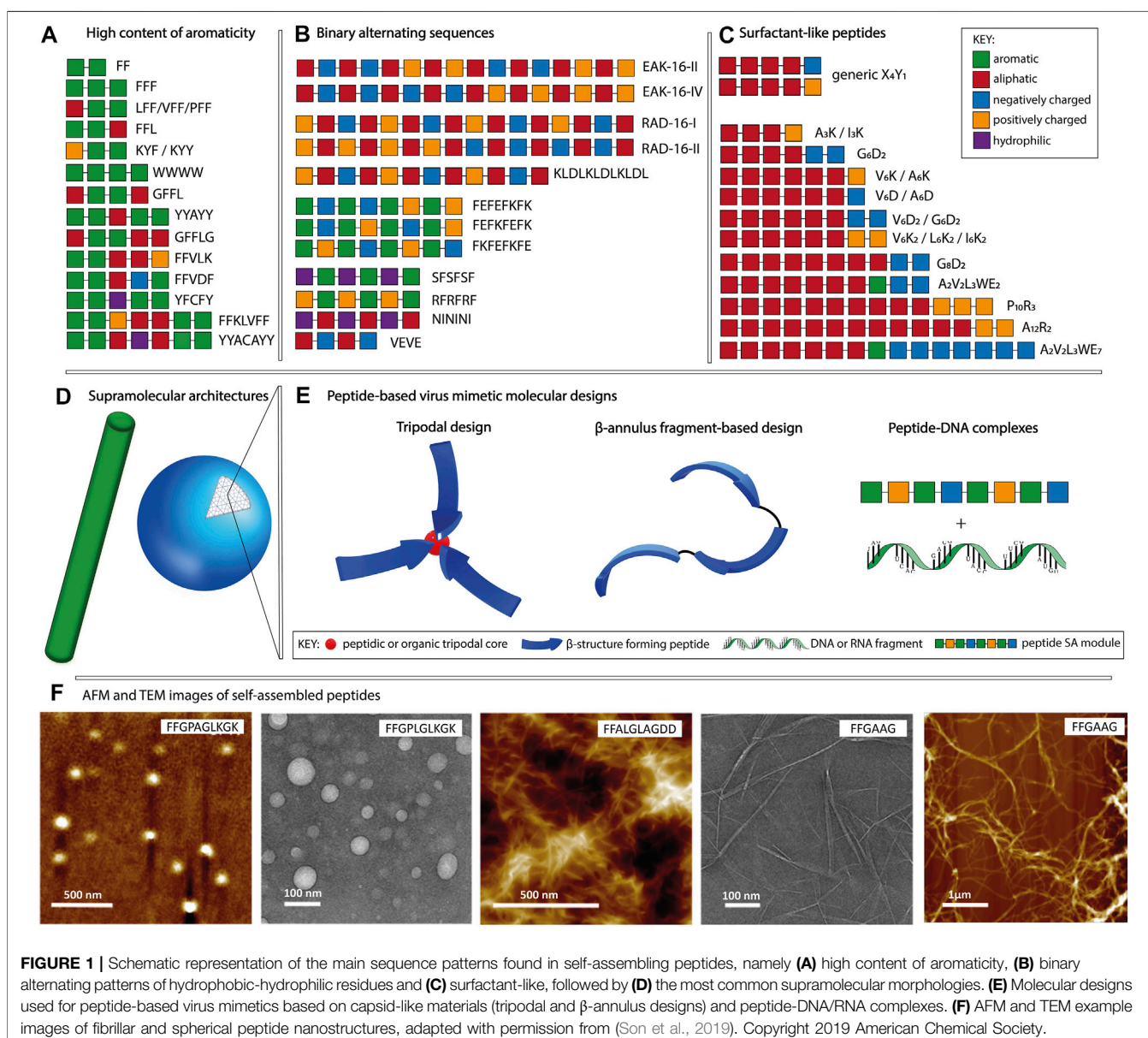
FIGURE 1 | Schematic representation of the main sequence patterns found in self-assembling peptides, namely **(A)** high content of aromaticity, **(B)** binary alternating patterns of hydrophobic-hydrophilic residues and **(C)** surfactant-like, followed by **(D)** the most common supramolecular morphologies. **(E)** Molecular designs used for peptide-based virus mimetics based on capsid-like materials (tripodal and β-annulus designs) and peptide-DNA/RNA complexes. **(F)** AFM and TEM example images of fibrillar and spherical peptide nanostructures, adapted with permission from (Son et al., 2019). Copyright 2019 American Chemical Society.

Several peptide-based therapeutics have reached the market while others are in various phases of clinical development for the treatment of cancer and metabolic disorders (Vlieghe et al., 2010; Craik et al., 2013). Compared to their protein counterparts, peptides are easier to synthesize and more stable under harsh conditions (Fosgerau and Hoffmann, 2015). Furthermore, peptides can be exploited as building blocks for the fabrication of highly ordered nanostructures with varying morphologies and surface functionalities, developed for drug delivery, tissue engineering, and regenerative medicine due to their inherent biocompatibility and biodegradability (Zhang, 2003; Collier et al., 2010; Woolfson and Mahmoud, 2010; Frederix et al., 2015; Smith et al., 2015; Slocik and Naik, 2017; Lampel et al., 2018; Sharma et al., 2021).

Peptide-based nanomaterials offer simple and low costs alternatives to VLPs (Matsuura, 2012; Hendricks et al., 2017; Singh et al., 2017; Cai et al., 2020). When designing peptide-based virus mimetics, the main

strategy is capsid reconstruction through the formation of supramolecular assemblies based on peptide segments with the goal of mimicking the viral architecture and functionality of efficient cell entry, immune evasion, and targeted cargo delivery. In here, we provide an overview of sequence patterns that drive peptide self-assembly, followed by the potential to achieve dimensional control through co-assembly. Finally, examples of peptide-based building blocks used in the design of supramolecular virus mimetics are discussed.

MORPHOLOGICAL CONTROL THROUGH SEQUENCE DESIGN

In the context of molecular self-assembly, the composition and the physico-chemical properties of amino acid side chains dictate

their behavior in different environments. In a hydrophilic environment, aromatic amino acids tend to aggregate due to hydrophobic interactions and π-π stacking, whereas polar and charged amino acids promote nanostructure formation through hydrogen bonds and electrostatic interactions, respectively. In addition, the position of a particular amino acid within the sequence, as well as the type of neighboring residues, affect the formation of supramolecular assemblies and their morphologies. Although it is possible to identify distinct sequence patterns with the tendency to form a particular nanostructure, it is challenging to attribute a supramolecular morphology based solely on the amino acid composition. Peptide sequences can self-assemble into a variety of shapes, including spheres, fibers, vesicles and tubes, with diameters in the 10–100 nm range and in the case of nanofibers, reaching micrometers in length (Gazit, 2007a; Zhao et al., 2008). In this section, we will focus on three main patterns used in the design of purely peptidic materials (**Figures 1A–C**): (i) high content of aromaticity, (ii) binary alternating hydrophobic-hydrophilic and (iii) surfactant-like.

Peptides With High Content of Aromaticity

Peptides composed of aromatic amino acids preferentially self-assemble into nanofibers with high intermolecular β-sheet content. Short motifs such as FF, YY, and WW constitute fundamental building blocks for self-assembly, with diphenylalanine being the most widely studied one (Gazit, 2007b; Frederix et al., 2015; Tao et al., 2017). Depending on the combination of amino acids adjacent to the FF motif and its position within the sequence, various morphologies such as fibrous and plate-like assemblies for FFF, nanospheres for CFF, helical fibrils for PFF and heterogeneous nanostructures for FFV, VFF, and LFF, are observed (Reches and Gazit, 2004; Tamamis et al., 2009; Marchesan et al., 2012; Frederix et al., 2015; Bera et al., 2019). Examples of fiber forming peptides (**Figure 1A**) having longer sequences include FFKLVFF, GFFLG, GFFL, FFAGL, FFVLK, FFVDF, and WWWW (Kalafatovic et al., 2016; Diaferia et al., 2018; Son et al., 2019; Yang et al., 2020b). Moreover, tyrosine-rich sequences including YYAYY, YYACAYY, YFCFY, KYF, and KYY were found to assemble into nanosheets, nanocapsules or nanofibers (Frederix et al., 2015; Lee et al., 2019; Sloan-Dennison et al., 2021). Amyloid-like peptides find applications in plaque-associated neurodegenerative diseases research or as biosensors and nanocarriers (Gazit, 2007b; Al-Halifa et al., 2019).

Binary Alternating Sequences of Hydrophobic-Hydrophilic Residues

Peptides with the binary-alternating patters rely on hydrogen bonds and/or electrostatic interactions for the formation of supramolecular assemblies. The first reported self-assembling peptide, EAK16-II (AEAEAKAKAEAEAKAK) is a repetitive segment derived from a natural yeast protein consisting of alternating hydrophobic and hydrophilic, positively, and

negatively charged amino acids (Zhang et al., 1993; Zhang, 2017). It was shown that the disposition of amino acids within the sequence and the pH of the environment influence the supramolecular morphology of EAK16 (Hong et al., 2003). At neutral pH, EAK16-II formed fibrils and its analogue EAK16-IV (AEAEAEAEAKAKAKAK) formed globular assemblies, whereas both peptides showed fibrillar assemblies at conditions above or below the neutral. Other examples (**Figure 1B**) including RAD16-I (RADARADARADARADA), RAD16-II (RARADADARARADADA), KLDLKLDLKLDL, FKFEFKFE, FEFKFEFK, FEFEFKFK, VEVE, SFSFSF, RFRFRF, and NININI have been reported to self-assemble into fibers (Kisiday et al., 2002; Marini et al., 2002; Yokoi et al., 2005; Cui et al., 2009; Guilbaud et al., 2010; Mandal et al., 2014; Do et al., 2016; Gao et al., 2017; Pelin et al., 2020). In addition to linear sequences, cyclic peptides have been used as building blocks allowing for manipulation of the supramolecular morphology through monomer design (Mandal et al., 2013). Cyclic peptides having the $[WR]_n$ structure, where $n \in \{3,4,5\}$, favor the formation of vesicle-type assemblies, unlike the linear designs with the binary alternating pattern, that preferentially assemble into fibrillar morphologies. The main applications of peptides classified in this category are related to their ability to form hydrogels. Such biomaterials can serve as scaffolds for tissue engineering, bioprinting, cell proliferation, regenerative medicine and drug delivery (Liu and Zhao, 2011; Levin et al., 2020; Gelain et al., 2021).

Surfactant-Like Peptides

Surfactant-like peptides formed by combining aliphatic and charged segments have been also reported as self-assembly units. Their design is based on a hydrophobic tail composed of V, I, L, G, A or P followed by a charged head group containing K, D, R or E (**Figure 1C**). Examples include V_6K, V_6K_2, V_6D, V_6D_2, I_3K, I_6K_2, A_3K, A_6K, A_6D, G_4D_2, G_6D_2, G_8D_2, $A_{12}R_2$, $A_2V_2L_3WE_{2/7}$, $P_{10}R_3$, etc. (Vauthey et al., 2002; van Hell et al., 2007; Yoon et al., 2008; Wang et al., 2009; Zhao, 2009; Xu et al., 2010; Hamley et al., 2013). These sequences can assemble into various morphologies comprising micelles, fibers, vesicles and tubes. The size and shape of the formed supramolecular assemblies depend on the type of amino acids used to constitute the amphiphile as well as the number of aliphatic and charged residues. In addition, factors such as temperature, solution pH and ionic strength affect the self-assembly process. The ability to form lipid bilayer-like assemblies makes them ideal for applications in immunotherapy, gene and drug delivery. Moreover, they can be used as protective envelopes for the delivery of enzymes and other biomolecules (Dasgupta and Das, 2019).

DIMENSIONAL CONTROL THROUGH CO-ASSEMBLY

Compared to the unimolecular assemblies described above, supramolecular co-assemblies lead to the formation of

TABLE 1 | Examples of peptide-based viral mimetic design strategies.

Strategy	Peptidic component / sequence	Role (structural (s) / functional (f))	Supramolecular Morphology	Development Stage	Ref.
Capsid mimicking nanomaterials with C$_3$ symmetry (trigonal or based on α-helical or β-sheet forming peptides)					
Trigonal (trimesoyl) peptide conjugate	C[i]-FKFEFKFE[ii] Ci-KTWTWTE[iii] (γE-C[i]-G)[iv]	i) Conjugation to core molecule (s) ii) β-sheet self-assembly unit (s) iii) Tryptophane zipper based β-sheet self-assembly (s) iv) self-assembly unit (s)	Nanospheres	Biophysical data	Matsuura et al. (2005) Matsuura et al. (2011) Matsuura et al. (2009)
Wheel (trimesoyl) peptide conjugate	(FKFE-C[i]-KFE)[ii]	i) Conjugation to core molecule (s) ii) β-sheet self-assembly unit (s)	Nanofibers	Biophysical data	Murasato et al. (2008)
Trigonal (tertiary amine) dipeptide conjugate	WW FF	β-sheet self-assembly unit (s)	Nanospheres Nanotubes	Biophysical data	Ghosh et al., (2007)
Trigonal (ethyl benzene)-peptide conjugate	(γE-C[i]-G)[ii]	i) Conjugation to core molecule (s) ii) Self-assembly unit (s)	Nanospheres	Biophysical data	Matsuura et al., (2010a)
Peptide triskelion (trilateral honeycomb symmetry)	βAKK[i]-(RRWTWE)3[ii, iii]	i) Trigonal core (s) ii) Tryptophane zipper based β-sheet self-assembly (s) iii) Antimicrobial activity (f)	Nanocapsules	Cell assays (RNA delivery, antimicrobial activity)	Castelletto et al. (2016)
Trigonal peptidic coiled coil heterodimers	K$_β$AK$_β$AK[i]-(KIAKLKQKIQKLKAKIAKLKQ)$_3$[ii] C$_β$AEISALEQEIASLEQEISALEQ[iii]	i) Trigonal core (s) ii) Cationic, covalently bound antimicrobial component (s) iii) Anionic component for heterodimer formation (s)	Nanospheres	Cell assays (RNA delivery, antimicrobial activity)	De Santis et al., (2017)
β-annulus fragment from TBSV capsid	INHVGGTGGAIMAPVAVTRQLVGS[i] INHVGGTGGAIMAPVAVTRQLVGG[i-] CGGGKIAALKKKNAALKQKIAALKQ[ii] EIAALEKENAALEQEIAALEQ[iii]	i) β-annulus segment (s) ii) Cationic component covalently bound to β-annulus (s) iii) Anionic component for heterodimer formation (s)	Hollow nanocapsules Nanospheres	Biophysical data	Matsuura et al. (2010b); Fujita and Matsuura (2017)
β-annulus fragment from SMV	GISMAPSAQGAM[i]-FKFE[ii]	i) β-annulus segment (s) ii) β-sheet self-assembly unit (s)	Nanospheres	Biophysical data	Matsuura et al., (2016)
Tecto-dendrimeric design	C[i]-GG[ii]-EIARLEQEIARLEQEIARLEYEIARLE[iii]	i) Disulfide crosslinking (s) ii) Glycine linker (s) iii) α-helical conformation promoting sequence (s)	Spherical particles	Cell assays (gene transfection)	Noble et al., (2016)
Multicomponent peptide-DNA complexes					
Surfactant-like sequences	I$_3$V$_3$A$_3$G$_3$-K3[ii]	i) β-sheet self-assembly unit (s) ii) DNA condensing (f)	Nanosheets for peptidic component Heterogeneous morphologies *via* condensation with DNA	Cell assays (gene transfection)	Cao et al., (2018)
Multicomponent, glucose-peptide conjugate	GSGSGS[i]-K$_8$[ii]-GGSGGS[iii]-(WKWE)$_3$WG[iv]	i) linker (s) ii) siRNA binding site (f) iii) linker (s) iv) β-sheet self-assembly unit (s)	β-nanoribbons for peptidic component and for complexes with siRNA and dsDNA	Cells assays (siRNA transfection)	Lim et al., (2008)

TABLE 1 | (*Continued*) Examples of peptide-based viral mimetic design strategies.

Strategy	Peptidic component / sequence	Role (structural (s) / functional (f))	Supramolecular Morphology	Development Stage	Ref.
Cocoon-like viral mimics based on β-sheet forming sequences (C6 = alkyl linker)	K_3^i-C_6-WLVFFAQQ[ii]-G[iii]-SPD[iv]	i) cationic, DNA binding region (f) ii) amyloid / β-sheet segment (s) iii) glycine linker (s) iv) hydrophilic segment (s)	Nanoribbons for peptidic component Nanococoons *via* condensation with DNA	Biophysical data	Ni and Chau, (2014)
	K_3^i-C_6-X[ii]-G[iii]-SPD[iv] where X ∈ $\{L_8, L_6, L_4, A_8, A_6, (L_2A_2)_2\}$		Nanofibers for peptidic component Nanococoons *via* condensation with DNA for $L_8, L_6, L_4, (L_2A_2)_2$	Cell assays (gene transfection)	Ni and Chau, (2017)
Tat–LK15 conjugate	(RKKRRQRRRGGG[i]-KLLKLLLKLLLKLLK[ii])[iii]	i) Cell penetrating (f) ii) Membrane lytic, amphipathic (f) iii) DNA binding (f)	Peptide-DNA complex (morphology not determined)	Cells assays (gene transfection)	Saleh et al. (2010)
Multicomponent	K_6^i-GGFLG[ii]- FWRGENGRKTRSAYERMCNILKGK[iii]	i) DNA binding (f) ii) Enzyme cleavable (s/f) iii) Influenza-derived epitope (f)	Dimer formation through disulphide linkage for peptide component Spherical aggregates in presence of DNA	Cells assays (gene transfection)	Haines et al. (2001)
Multicomponent, bola-amphiphile	RGD[i]-GPLGLAG[ii]-I_3[iii]-G-R_8[iv]	i) Integrin binding (f) ii) enzyme cleavable (hydrophobic) (s/f) iii) structural (hydrophobic) (s) iv) Cell penetrating, DNA binding (f)	Nanospheres for peptidic component only Rod-like or spherical shapes in presence of DNA	Cells assays (gene transfection)	Wang et al. (2020)
Bi-functional bola-amphiphile with hydrocarbon (C_{12}) core	RGD[i]-C_{12}-R_8[ii]	i) Integrin binding (f) ii) Cell penetrating, DNA binding (f)	Spherical nanoparticles *via* condensation with DNA	Cells assays (gene transfection)	Chen et al., (2013)

nanostructures with increased chemical diversity and structural complexity that can resemble natural systems. Peptides can co-assemble in cooperative, orthogonal, disruptive or random manner (Makam and Gazit, 2018). It is possible to fine-tune the morphology and dimension of nanostructures, and consequently their chemical, mechanical and physical properties, by controlling the mixing ratio of the individual building blocks. For example, the co-assembly of FF and FFF can be tuned to obtain nanorods, spherical nanovesicles, hollow nanotubes and toroid-like nanostructures (Guo et al., 2016). The disruptive co-assembly of the FF motif with its capped version Boc-FF allowed for the precise control of the nanotube length from 12 to 8 μm by changing the mixing ratio from 20:1 to 5:1, respectively (Adler-Abramovich et al., 2016). The cooperative co-assembly of dendrimeric poly (lysine) hydrophilic heads with linear poly (leucine) hydrophobic tails allowed the morphology control of the formed peptidosomes by alternating the ratio of dendrimeric to linear component. When the ratio changed from 10:1 to 1:5, the size of the nanoparticles increased from 300 to 800 nm and their morphology changed from spherical to fusiform (Xu et al., 2012). The ability to achieve dimensional control constitutes a promising tool for the design of peptide supramolecular materials where specific morphologies or dimensions are required. However, the co-assembly of peptide-based nanomaterials has not been researched extensively and constitutes an opportunity to improve the future design of peptide materials (Sasselli et al., 2017).

VIRAL MIMETICS

Recently, the concept of mimicking viral capsids by creating their simplified versions through molecular self-assembly following the bottom-up strategy has emerged. Peptide self-assembly is a powerful tool to create biocompatible, tunable, low-cost supramolecular materials. It allows the conversion of chemically simple building blocks into a wide range of supramolecular architectures featuring modularity, functional diversity, adaptability and responsiveness to stimuli (Lampel, 2020). Peptides are versatile molecules for the design of virus mimetics as they can act as structural components as well as functional domains that favor selective binding, cell entry, endosomal escape or possess a specific activity (e.g., antimicrobial or catalytic). Short

peptides offer the possibility to use minimal recognition modules for the design of functional materials and offer unique platforms for mimicking complex systems (Levin et al., 2020).

In this review, we distinguish the role of peptidic components used for the fabrication of virus mimetics into structural and functional modules (**table 1**). The structural modules are based on patterns that drive the formation of ordered supramolecular nanostructures having spherical or fibrillar morphologies (**Figure 1D, F**), dictated by the sequence, as described in **section 2**. In addition, trigonal cores (peptidic or organic), linkers (glycine or alkyl), cysteine residues serving as conjugation points, coiled coil, α-helical or β-annulus segments contribute to the design of structural modules. On the other hand, functional modules, related to the inherent biological signaling typical for peptides, are based on sequences with known activities such as cell penetration, integrin binding, DNA condensation and antimicrobial activity. Accordingly, peptide-based viral mimetic designs are divided into: i) capsid reconstruction strategies where structural modules contribute to the final supramolecular morphology and ii) simplified virus-like complexes where structural and functional peptidic modules are complexed with DNA or RNA fragments.

Capsid-Like Nanomaterials

Viral capsids with icosahedral symmetry formed through the assembly of multiple protein subunits have inspired the design of artificial, peptide-based nanostructures for applications in gene delivery and cancer immunotherapy (Matsuura, 2018; Cai et al., 2020). In capsid reconstruction, it is important to maintain the n-fold rotational symmetry with n ∈ {3,5}. The C_3 assembly can be achieved at the molecular level by designing trigonal conjugates or through folding-assembly pathways of peptides with helical conformations or β-annulus segments found on capsid-forming proteins (**Figure 1E**).

Trigonal designs induce the symmetry through the manipulation of the tripodal core (organic or peptidic) conjugated to peptidic structural modules that favor β-sheet-like self-assembly including the WTW tryptophane zipper and the FKFE-based binary alternating pattern. Examples are trymesoyl conjugates bearing three β-sheet-forming sequences (CFKFEFKFE or CKTWTWTE) attached through the C-terminal cysteine, that assemble into spherical morphologies (Matsuura et al., 2005, 2011). Similarly, a wheel-like trigonal design where the same core is conjugated to FKFECKFE through the central cysteine residue, self-assembled into fibers (Murasato et al., 2008). A clathrin triskelion-inspired conjugate, having a tris(2-aminoethyl) amine core linked to three aromatic di-tryptophan modules, self-assembled into nanospheres. In contrast, the conjugate containing the FF motif linked to the same core resulted in the formation of nanotubes, indicating that the morphology of the assemblies could be tuned through the dipeptide sequence (Ghosh et al., 2007). Furthermore, the choice of the core molecule can influence the properties of the obtained assemblies. For glutathione ($_\gamma$ECG) attached to two different cores, the 1,3,5-tris(aminomethyl)-2,4,6-triethyl benzene

showed improved conformational rigidity compared to the trimesoyl, giving rise to nanospheres with narrow size distribution (Matsuura et al., 2009; Matsuura et al., 2010a).

A purely peptidic triskelion, designed by conjugating each amino acid of the core sequence $_\beta$AKK to the antimicrobial RRWTWE peptide containing the virus-derived tryptophane zipper, self-assembled into nanocapsules with dual function consisting of siRNA delivery and intrinsic antimicrobial activity (Castelletto et al., 2016). In this case, the RRWTWE sequence contains both the structural (β-sheet-forming) and functional (antimicrobial) modules. In another example, the core $K_\beta AK_\beta AK$ sequence was conjugated to a positively charged antimicrobial (KIAKLKQKIQKLKAKIAKLKQ) peptide to form a trigonal conjugate, that upon addition of a complementary anionic sequence (C_βAEISALEQEIASLEQEISALEQ), assembled in a coiled-coil hetero dimer. The resulting C_3 subunit gave rise to capsid-like nanomaterials with antimicrobial activity (De Santis et al., 2017).

The reconstruction of capsid morphology based on the assembly of β-annulus peptide segments from Tomato bushy stunt virus (INHVGGTGGAIMAPVAVTRQLVG) and *Sesbania* mosaic virus (GISMAPSAQGAM) is able to maintain the C_3 symmetry while allowing for introduction of surface modifications (Matsuura et al., 2010b; Matsuura et al., 2016). Among others, these include coating with gold nanoparticles to enhance the imaging efficiency (Matsuura et al., 2015) or with albumin to confer greater serum stability without eliciting immune response or toxicity (Matsuura and Honjo, 2019).

At the sequence level, the β-annulus segments can be modified with β-sheet promoting sequences (FKFE) to improve their assembly propensity into spherical morphologies (Matsuura et al., 2016). Moreover, with the intention of mimicking spike-bearing viruses such as Influenza and SARS-CoV-2, the β-annulus segment covalently linked to a cationic, coiled-coil-forming sequence at the C-terminus (CGGGKIAALKKKNAALKQKIAALKQ) gives rise to nanospheres. In the presence of a complementary anionic peptide (EIAALEKENAALEQEIAALEQ) and depending on the ratio of the cationic to anionic component, spherical (4:1) or fibrillar (1:1) assemblies with surface-exposed dimeric coiled coils are obtained (Fujita and Matsuura, 2017).

Another strategy is the use of a tecto-dendrimeric architecture as template to achieve C_3 assembly into spherical particles for gene delivery. The design is based on structural coiled-coil subunits (CGG-EIARLEQEIARLEQEIARLEYEIARLE) configured into helical wheels, containing a GG spacer motif adjacent to a cysteine residue allowing for disulfide crosslinking (Noble et al., 2016).

Multicomponent Peptide-DNA Complexes

Virus-mimicking nanostructures can be formed through the complexation of peptides with DNA or RNA (**Figure 1E**), simulating the co-assembly of capsid proteins with viral genomes. Predominantly positively charged peptides have the tendency to condense negatively charged gene fragments making the resulting virus mimicking nanostructures ideal candidates for gene delivery (Miyata et al., 2012). Compared to conventional, cytotoxic DNA condensation agents such as polyelectrolytes and lipidic surfactants,

short peptides have higher biocompatibility and consequently lower toxicity. Moreover, their structure can easily be modified to obtain high affinity DNA binders (Wang et al., 2020). Furthermore, the condensation with the peptidic vector confers protection from DNases. Several peptide-DNA/RNA co-assemblies have been reported containing structural or functional modules or their combination resulting in multicomponent designs.

Peptide-DNA condensates composed of lysine modified surfactant-like, binary alternating or amyloid-like structural modules, have been reported. While the cationic region drives the binding to DNA or RNA through electrostatic attraction, peptide self-assembly and β-sheet formation takes place via hydrogen bonds and hydrophobic interactions. Surfactant-like sequences, obtained by varying the position of aliphatic amino acids (A, G, I, and L) as well as the position of the cationic (K_3) region from N- to C- terminus, including cone-like ($G_3A_3V_3I_3K_3$, $K_3I_3V_3A_3G_3$), dumbbell-like ($I_3V_3A_3G_3K_3$, $K_3G_3A_3V_3I_3$) and irregular shaped sequences ($V_3G_3I_3A_3K_3$, $K_3A_3I_3G_3V_3$) gave rise to nanorods, nanosheets and nanofibrils, respectively. The $I_3V_3A_3G_3K_3$ was the most efficient one in inducing DNA condensation showing high content of ordered domains (Cao et al., 2018). This example shows that the supramolecular morphology and content of ordered domains could be fine-tuned through sequence engineering. Furthermore, a glucose-peptide conjugate [Glucose-GSGSGS-K_8-GGSGGS-(WKWE)$_3$WG] containing a functional, cationic segment (K_8) for siRNA binding positioned between two linkers (GSGSGS and GGSGGS) and a binary alternating structural motif (WKWE)$_3$, assembled into bilayered β-nanoribbons. The carbohydrate ligand exhibited the dual function of maintaining the β-nanoribbons neutrally charged while enhancing the cell binding through glucose transporters (Lim et al., 2008). Therefore, this design offers the formation of a controllable filamentous morphology able to bind RNA while presenting surface functionalization that yields high transfection efficiency.

Another example is the design of the cocoon-like virus mimetics based on a sequence (K_3-C_6-WLVFFAQQGSPD) containing the cationic, DNA binding region (K_3) at the N-terminus, followed by the alkyl linker (C_6) and three structural components, namely, the amyloid-like motif (LVFFA), the glycine linker and the hydrophilic (SPD) region (Ni and Chau, 2014). The β-sheet forming segment can be modified from amyloid to aliphatic (L_8, L_6, L_4, and $L_2A_2L_2A_2$) while maintaining the self-assembly propensity of the whole sequence. The peptides alone self-assemble into fibrillar aggregates, while their interaction with DNA in various ratios induces condensation into nanococoons (Ni and Chau, 2017).

Cell penetrating peptides including the arginine-rich, R_8 and the HIV-1 derived, Tat (RKKRRQRRRGGG) constitute the main functional modules used for the design of DNA condensates (Kalafatovic and Giralt, 2017). The covalent conjugation of Tat to the amphipathic LK15 sequence (KLLKLLLKLLLKLLK) resulted in improved cellular uptake and transfection efficiency, compared to Tat or LK15 alone (Saleh et al., 2010). CL22 (K_6-GGFLG-FWRGENGRKTRSAYERMCNILKGK) is an example of purely

peptidic design containing an enzyme cleavable segment adjacent to the DNA binding region at the N-terminus and the Influenza nucleoprotein-derived sequence at the C-terminus. It assembles into spherical aggregates in the presence of DNA and attains maximum gene transfection efficiency upon spontaneous dimerization through the disulfide bond between cysteines at the C-terminus (Haines et al., 2001). Bola amphiphiles, composed of a central hydrophobic segment flanked by two hydrophilic ones, have the ability to self-assemble into fibrillar or spherical nanostructures depending on the sequence design (Chen et al., 2013). Examples are the purely peptidic RGD-GPLGLAG-I_3-G-R_8 (Wang et al. 2020) and the fatty acid containing RGD-C_{12}-R_8 (Chen et al., 2013) that accommodate both functional and structural motifs, where RGD is crucial for integrin-binding and R_8 for cell penetration. Additionally, the PLGLA sequence serves as an enzyme-cleavable segment, while I_3 confers hydrophobicity. The main drawback of peptide-DNA/RNA co-assemblies, mainly based on functional modules, is that oppositely charged polyions often form heterogeneous aggregates. The challenges resulting from the lack of control over their morphology, degree of order and size, often hamper the efficiency of gene transfection or delivery.

The DNA fragment length and composition can affect the formation of peptide-DNA complexes but also their morphology. The mechanism of formation depends on the peptides' intrinsic ability to self-assemble. Self-assembling peptide sequences condense the DNA by reorganizing to a final morphology that is often different from the one formed by the peptide alone. On the other hand, predominantly cationic and/or cell-penetrating peptides, unable to self-assemble, tend to form irregular aggregates in the presence of DNA. Moreover, the size of the complex can be controlled by varying the length of the DNA fragment. For example, the $I_3V_3A_3G_3K_3$–DNA complex size decreased from 122 to 85 nm by shortening the DNA fragment from 2000 to 300 bp (base pairs). Even though most examples use λ-DNA (~4.8 kbp), shorter DNA fragments (2000—300 bp) were explored with the intention to improve the DNA delivery efficiency (Cao et al., 2018).

However, the key factor influencing the morphology of peptide-DNA complexes is the R + / − ratio of the positively charged peptide residues to the negatively charged DNA fragments. A stable peptide-DNA complex is formed when all the negative charges are successfully neutralized. For example, RGD-GPLGLAG-I_3-G-R_8 that self-assembles into spheres, upon the interaction with DNA and depending on the R + / - values forms thread-like (R + / - = 0.5) complexes or highly condensed rod-like or spherical (R + / - = 3) nanostructures (Wang et al., 2020). In another example, the R + / - of 10 is the minimum requirement for DNA condensation with K_3C_6SPD, where the peptide alone self-assembles into nanoribbons. However, upon DNA addition, the electrostatic interactions drive the self-assembly into amorphous aggregates (R + / - = 5), or agglomerations with small striped nanococoons (R + / - = 10). The R + / - = 20 presents the optimal ratio for nanococoon formation, while at R + / - of 25 and 50 both nanococoons and filamentous nanoribbons are formed (Ni and Chau, 2014).

FUTURE PERSPECTIVES

The idea of exploiting known principles of peptide self-assembly to obtain spherical or fibrillar nanostructures by including important features such as cell penetration, antimicrobial activity or viral transfection is conceptually attractive. Such systems are promising as they can be easily engineered and modified to include specific sequences found on the receptor binding domains of spike proteins. In addition, they can be designed as vehicles able to deliver cargo into cells. So far, morphology rather than functionality has been mimicked and it constitutes an advantage from the point of view of easy production compared to VLPs. A step towards functionality of peptide materials is their ability to enhance viral transfection by increasing the β-sheet content of supramolecular nanostructures (Sieste et al., 2021). However, efforts are needed to achieve controllable and complex functions such as self-replication and catalysis in the future. Although largely unexplored for clinical use, because of the multiscale and multiparameter optimization challenges of supramolecular nanostructures (Sieste et al., 2021), we envision that peptides have great potential in becoming future nanotechnological solutions in covid-19 therapy and diagnostics.

The intention of this review is to emphasize the increasing importance of peptide self-assembly in the design and fabrication of minimalistic, synthetic models applicable to a variety of viral infections. We expect that future research in this field will deliver simple and cost-effective viral mimetics composed of peptide modules found on the surface of specific viruses, rationally designed to assemble into multivalent and multifunctional nanostructures able to selectively bind receptors of interest, penetrate cells and carry cargos. In addition to mimicking the viral morphology, such systems would partly resemble basic functionality through the display of known functional modules and their combinations aiming for possible synergistic effects. Such an approach could lead to the development of efficient and safe platforms to study viral infections without the need of complicated genetic manipulations. Moreover, the developed models will provide screening platforms that can be rationally designed, allowing for rapid discovery of potential inhibitors or surface protein binders. Therefore, they could be used as safe alternatives for antiviral drug discovery or as vehicles for mRNA vaccines.

AUTHOR CONTRIBUTION

PJ and DK conceived and designed the review, PJ, IŠ, AP, and DK analysed the literature and wrote the manuscript. All authors have read and approved the final version of the manuscript.

FUNDING

ACKNOWLEDGMENTS

REFERENCES

Abudula, T., Bhatt, K., Eggermont, L. J., O'Hare, N., Memic, A., and Bencherif, S. A. (2020). Supramolecular Self-Assembled Peptide-Based Vaccines: Current State and Future Perspectives. *Front. Chem.* 8, 1–11. doi:10.3389/fchem.2020.598160

Adler-Abramovich, L., Marco, P., Arnon, Z. A., Creasey, R. C. G., Michaels, T. C. T., Levin, A., et al. (2016). Controlling the Physical Dimensions of Peptide Nanotubes by Supramolecular Polymer Coassembly. *ACS Nano.* 10, 7436–7442. doi:10.1021/acsnano.6b01587

Al-Halifa, S., Babych, M., Zottig, X., Archambault, D., and Bourgault, S. (2019). Amyloid Self-Assembling Peptides: Potential Applications in Nanovaccine Engineering and Biosensing. *Pept. Sci.* 111, e24095–12. doi:10.1002/pep2.24095

Bera, S., Mondal, S., Xue, B., Shimon, L. J. W., Cao, Y., and Gazit, E. (2019). Rigid Helical-like Assemblies from a Self-Aggregating Tripeptide. *Nat. Mater.* 18, 503–509. doi:10.1038/s41563-019-0343-2

Cai, Y., Ran, W., Zhai, Y., Wang, J., Zheng, C., Li, Y., et al. (2020). Recent Progress in Supramolecular Peptide Assemblies as Virus Mimics for Cancer Immunotherapy. *Biomater. Sci.* 8, 1045–1057. doi:10.1039/c9bm01380f

Cao, M., Wang, Y., Zhao, W., Qi, R., Han, Y., Wu, R., et al. (2018). Peptide-Induced DNA Condensation into Virus-Mimicking Nanostructures. *ACS Appl. Mater. Inter.* 10, 24349–24360. doi:10.1021/acsami.8b00246

Castelletto, V., De Santis, E., Alkassem, H., Lamarre, B., Noble, J. E., Ray, S., et al. (2016). Structurally Plastic Peptide Capsules for Synthetic Antimicrobial Viruses. *Chem. Sci.* 7, 1707–1711. doi:10.1039/c5sc03260a

Chen, J.-X., Xu, X.-D., Yang, S., Yang, J., Zhuo, R.-X., and Zhang, X.-Z. (2013). Self-Assembled BolA-like Amphiphilic Peptides as Viral-Mimetic Gene Vectors for Cancer Cell Targeted Gene Delivery. *Macromol. Biosci.* 13, 84–92. doi:10.1002/mabi.201200283

Collier, J. H., Rudra, J. S., Gasiorowski, J. Z., and Jung, J. P. (2010). Multi-component Extracellular Matrices Based on Peptide Self-Assembly. *Chem. Soc. Rev.* 39, 3413–3424. doi:10.1039/b914337h

Craik, D. J., Fairlie, D. P., Liras, S., and Price, D. (2013). The Future of Peptide-Based Drugs. *Chem. Biol. Drug Des.* 81, 136–147. doi:10.1111/cbdd.12055

Cui, H., Muraoka, T., Cheetham, A. G., and Stupp, S. I. (2009). Self-assembly of Giant Peptide Nanobelts. *Nano Lett.* 9, 945–951. doi:10.1021/nl802813f

Dasgupta, A., and Das, D. (2019). Designer Peptide Amphiphiles: Self-Assembly to Applications. *Langmuir* 35, 10704–10724. doi:10.1021/acs.langmuir.9b01837

De Santis, E., Alkassem, H., Lamarre, B., Faruqui, N., Bella, A., Noble, J. E., et al. (2017). Antimicrobial Peptide Capsids of De Novo Design. *Nat. Commun.* 8, 1–11. doi:10.1038/s41467-017-02475-3

Diaferia, C., Balasco, N., Sibillano, T., Giannini, C., Vitagliano, L., Morelli, G., et al. (2018). Structural Characterization of Self-Assembled Tetra-Tryptophan Based Nanostructures: Variations on a Common Theme. *ChemPhysChem* 19, 1635–1642. doi:10.1002/cphc.201800026

Do, T. D., De Almeida, N. E. C., Lapointe, N. E., Chamas, A., Feinstein, S. C., and Bowers, M. T. (2016). Amino Acid Metaclusters: Implications of Growth

Trends on Peptide Self-Assembly and Structure. *Anal. Chem.* 88, 868–876. doi:10.1021/acs.analchem.5b03454

Fang, J.-H., Lee, Y.-T., Chiang, W.-H., and Hu, S.-H. (2015). Magnetoresponsive Virus-Mimetic Nanocapsules with Dual Heat-Triggered Sequential-Infected Multiple Drug-Delivery Approach for Combinatorial Tumor Therapy. *Small* 11, 2417–2428. doi:10.1002/smll.201402969

Ferreira, D., and Martins, I. M. (2017). "Artificial Virus Particles," in *Bioinspired Materials for Medical Applications* (Elsevier), 427–450. doi:10.1016/B978-0-08-100741-9.00015-2

Fosgerau, K., and Hoffmann, T. (2015). Peptide Therapeutics: Current Status and Future Directions. *Drug Discov. Today.* 20, 122–128. doi:10.1016/j.drudis.2014.10.003

Frederix, P. W. J. M., Scott, G. G., Abul-Haija, Y. M., Kalafatovic, D., Pappas, C. G., Javid, N., et al. (2015). Exploring the Sequence Space for (Tri-)peptide Self-Assembly to Design and Discover New Hydrogels. *Nat. Chem.* 7, 30–37. doi:10.1038/nchem.2122

Fujita, S., and Matsuura, K. (2017). Self-Assembled Artificial Viral Capsids Bearing Coiled-Coils at the Surface. *Org. Biomol. Chem.* 15, 5070–5077. doi:10.1039/c7ob00998d

Gao, J., Tang, C., Elsawy, M. A., Smith, A. M., Miller, A. F., and Saiani, A. (2017). Controlling Self-Assembling Peptide Hydrogel Properties through Network Topology. *Biomacromolecules* 18, 826–834. doi:10.1021/acs.biomac.6b01693

Gazit, E. (2007b). Self Assembly of Short Aromatic Peptides into Amyloid Fibrils and Related Nanostructures. *Prion* 1, 32–35. doi:10.4161/pri.1.1.4095

Gazit, E. (2007a). Self-assembled Peptide Nanostructures: The Design of Molecular Building Blocks and Their Technological Utilization. *Chem. Soc. Rev.* 36, 1263–1269. doi:10.1039/b605536m

Gelain, F., Luo, Z., Rioult, M., and Zhang, S. (2021). Self-assembling Peptide Scaffolds in the Clinic. *Npj Regen. Medmed.* 6, 1–8. doi:10.1038/s41536-020-00116-w

Ghosh, S., Reches, M., Gazit, E., and Verma, S. (2007). Bioinspired Design of Nanocages by Self-Assembling Triskelion Peptide Elements. *Angew. Chem. Int. Ed.* 46, 2002–2004. doi:10.1002/anie.200604383

Guilbaud, J.-B., Vey, E., Boothroyd, S., Smith, A. M., Ulijn, R. V., Saiani, A., et al. (2010). Enzymatic Catalyzed Synthesis and Triggered Gelation of Ionic Peptides. *Langmuir* 26, 11297–11303. doi:10.1021/la100623y

Guo, C., Arnon, Z. A., Qi, R., Zhang, Q., Adler-Abramovich, L., Gazit, E., et al. (2016). Expanding the Nanoarchitectural Diversity through Aromatic Di- and Tri-peptide Coassembly: Nanostructures and Molecular Mechanisms. *ACS Nano.* 10, 8316–8324. doi:10.1021/acsnano.6b02739

Haines, A., Irvine, A., Mountain, A., Charlesworth, J., Farrow, N., Husain, R., et al. (2001). CL22 - A Novel Cationic Peptide for Efficient Transfection of Mammalian Cells. *Gene Ther.* 8, 99–110. doi:10.1038/sj.gt.3301314

Hamley, I. W., Dehsorkhi, A., Castelletto, V., Seitsonen, J., Ruokolainen, J., and Iatrou, H. (2013). Self-assembly of a Model Amphiphilic Oligopeptide Incorporating an Arginine Headgroup. *Soft Matter* 9, 4794–4801. doi:10.1039/c3sm50303h

Hendricks, M. P., Sato, K., Palmer, L. C., and Stupp, S. I. (2017). Supramolecular Assembly of Peptide Amphiphiles. *Acc. Chem. Res.* 50, 2440–2448. doi:10.1021/acs.accounts.7b00297

Hong, Y., Legge, R. L., Zhang, S., and Chen, P. (2003). Effect of Amino Acid Sequence and pH on Nanofiber Formation of Self-Assembling Peptides EAK16-II and EAK16-IV. *Biomacromolecules* 4, 1433–1442. doi:10.1021/bm0341374

Kalafatovic, D., and Giralt, E. (2017). Cell-penetrating Peptides: Design Strategies beyond Primary Structure and Amphipathicity. *Molecules* 22, 1929–1938. doi:10.3390/molecules22111929

Kalafatovic, D., Nobis, M., Son, J., Anderson, K. I., and Ulijn, R. V. (2016). MMP-9 Triggered Self-Assembly of Doxorubicin Nanofiber Depots Halts Tumor Growth. *Biomaterials* 98, 192–202. doi:10.1016/j.biomaterials.2016.04.039

Kisiday, J., Jin, M., Kurz, B., Hung, H., Semino, C., Zhang, S., et al. (2002). Self-assembling Peptide Hydrogel Fosters Chondrocyte Extracellular Matrix Production and Cell Division: Implications for Cartilage Tissue Repair. *Proc. Natl. Acad. Sci.* 99, 9996–10001. doi:10.1073/pnas.142309999

Lampel, A. (2020). Biology-Inspired Supramolecular Peptide Systems. *Chem* 6, 1222–1236. doi:10.1016/j.chempr.2020.03.005

Lampel, A., Ulijn, R. V., and Tuttle, T. (2018). Guiding Principles for Peptide Nanotechnology through Directed Discovery. *Chem. Soc. Rev.* 47, 3737–3758. doi:10.1039/c8cs00177d

Lee, C., Hwang, H. S., Lee, S., Kim, B., Kim, J. O., Oh, K. T., et al. (2017). Rabies Virus-Inspired Silica-Coated Gold Nanorods as a Photothermal Therapeutic Platform for Treating Brain Tumors. *Adv. Mater.* 29, 1605563–1605568. doi:10.1002/adma.201605563

Lee, E. S., Kim, D., Youn, Y. S., Oh, K. T., and Bae, Y. H. (2008). A Virus-Mimetic Nanogel Vehicle. *Angew. Chem. Int. Ed.* 47, 2418–2421. doi:10.1002/anie.200704121

Lee, J., Ju, M., Cho, O. H., Kim, Y., and Nam, K. T. (2019). Tyrosine-Rich Peptides as a Platform for Assembly and Material Synthesis. *Adv. Sci.* 6, 1801255. doi:10.1002/advs.201801255

Lehn, J.-M. (2002). Toward Self-Organization and Complex Matter. *Science* 295, 2400–2403. doi:10.1126/science.1071063

Levin, A., Hakala, T. A., Schnaider, L., Bernardes, G. J. L., Gazit, E., and Knowles, T. P. J. (2020). Biomimetic Peptide Self-Assembly for Functional Materials. *Nat. Rev. Chem.* 4, 615–634. doi:10.1038/s41570-020-0215-y

Li, Y., Lai, Y., Xu, X., Zhang, X., Wu, Y., Hu, C., et al. (2016). Capsid-like Supramolecular Dendritic Systems as pH-Responsive Nanocarriers for Drug Penetration and Site-specific Delivery. *Nanomedicine: Nanotechnology, Biol. Med.* 12, 355–364. doi:10.1016/j.nano.2015.09.015

Liang, H., Hu, A., Chen, X., Jin, R., Wang, K., Ke, B., et al. (2019). Structure Optimization of Dendritic Lipopeptide Based Gene Vectors with the Assistance from Molecular Dynamic Simulation. *J. Mater. Chem. B.* 7, 915–926. doi:10.1039/c8tb02650e

Lim, Y.-b., Lee, E., Yoon, Y.-R., Lee, M. S., and Lee, M. (2008). Filamentous Artificial Virus from a Self-Assembled Discrete Nanoribbon. *Angew. Chem.* 120, 4601–4604. doi:10.1002/ange.200800266

Liu, J., and Zhao, X. (2011). Design of Self-Assembling Peptides and Their Biomedical Applications. *Nanomedicine* 6, 1621–1643. doi:10.2217/nnm.11.142

Ludwig, C., and Wagner, R. (2007). Virus-like Particles-Universal Molecular Toolboxes. *Curr. Opin. Biotechnol.* 18, 537–545. doi:10.1016/j.copbio.2007.10.013

Makam, P., and Gazit, E. (2018). Minimalistic Peptide Supramolecular Co-assembly: Expanding the Conformational Space for Nanotechnology. *Chem. Soc. Rev.* 47, 3406–3420. doi:10.1039/c7cs00827a

Mandal, D., Nasrolahi Shirazi, A., and Parang, K. (2014). Self-assembly of Peptides to Nanostructures. *Org. Biomol. Chem.* 12, 3544–3561. doi:10.1039/c4ob00447g

Mandal, D., Tiwari, R. K., Nasrolahi Shirazi, A., Oh, D., Ye, G., Banerjee, A., et al. (2013). Self-assembled Surfactant Cyclic Peptide Nanostructures as Stabilizing Agents. *Soft Matter.* 9, 9465–9475. doi:10.1039/c3sm50764e

Mao, C., Liu, A., and Cao, B. (2009). Virus-based Chemical and Biological Sensing. *Angew. Chem. Int. Ed.* 48, 6790–6810. doi:10.1002/anie.200900231

Marchesan, S., Easton, C. D., Kushkaki, F., Waddington, L., and Hartley, P. G. (2012). Tripeptide Self-Assembled Hydrogels: Unexpected Twists of Chirality. *Chem. Commun.* 48, 2195–2197. doi:10.1039/c2cc16609g

Marini, D. M., Hwang, W., Lauffenburger, D. A., Zhang, S., and Kamm, R. D. (2002). Left-Handed Helical Ribbon Intermediates in the Self-Assembly of a β-Sheet Peptide. *Nano Lett.* 2, 295–299. doi:10.1021/nl015697g

Maslanka Figueroa, S., Fleischmann, D., and Goepferich, A. (2021). Biomedical Nanoparticle Design: What We Can Learn from Viruses. *J. Controlled Release.* 329, 552–569. doi:10.1016/j.jconrel.2020.09.045

Matsuura, K. (2012). Construction of Spherical Virus-Inspired Peptide Nanoassemblies. *Polym. J.* 44, 469–474. doi:10.1038/pj.2012.16

Matsuura, K., Fujino, K., Teramoto, T., Murasato, K., and Kimizuka, N. (2010a). Glutathione Nanosphere: Self-Assembly of Conformation-Regulated Trigonal-Glutathiones in Water. *Bcsj* 83, 880–886. doi:10.1246/bcsj.20100048

Matsuura, K., Hayashi, H., Murasato, K., and Kimizuka, N. (2011). Trigonal Tryptophane Zipper as a Novel Building Block for pH-Responsive Peptide Nano-Assemblies. *Chem. Commun.* 47, 265–267. doi:10.1039/c0cc01324b

Matsuura, K., and Honjo, T. (2019). Artificial Viral Capsid Dressed up with Human Serum Albumin. *Bioconjug. Chem.* 30, 1636–1641. doi:10.1021/acs.bioconjchem.9b00327

Matsuura, K., Matsuyama, H., Fukuda, T., Teramoto, T., Watanabe, K., Murasato, K., et al. (2009). Spontaneous Self-Assembly of Nanospheres from Trigonal Conjugate of Glutathione in Water. *Soft Matter.* 5, 2463–2470. doi:10.1039/b819472f

Matsuura, K., Mizuguchi, Y., and Kimizuka, N. (2016). Peptide Nanospheres Self-Assembled from a Modified β -annulus Peptide of Sesbania Mosaic Virus. *Biopolymers* 106, 470–475. doi:10.1002/bip.22774

Matsuura, K., Murasato, K., and Kimizuka, N. (2005). Artificial Peptide-Nanospheres Self-Assembled from Three-Way Junctions of β-Sheet-Forming Peptides. *J. Am. Chem. Soc.* 127, 10148–10149. doi:10.1021/ja052644i

Matsuura, K. (2018). Synthetic Approaches to Construct Viral Capsid-like Spherical Nanomaterials. *Chem. Commun.* 54, 8944–8959. doi:10.1039/C8CC03844A

Matsuura, K., Ueno, G., and Fujita, S. (2015). Self-assembled Artificial Viral Capsid Decorated with Gold Nanoparticles. *Polym. J.* 47, 146–151. doi:10.1038/pj.2014.99

Matsuura, K., Watanabe, K., Matsuzaki, T., Sakurai, K., and Kimizuka, N. (2010b). Self-Assembled Synthetic Viral Capsids from a 24-mer Viral Peptide Fragment. *Angew. Chem. Int. Ed.* 49, 9662–9665. doi:10.1002/anie.201004606

Miyata, K., Nishiyama, N., and Kataoka, K. (2012). Rational Design of Smart Supramolecular Assemblies for Gene Delivery: Chemical Challenges in the Creation of Artificial Viruses. *Chem. Soc. Rev.* 41, 2562–2574. doi:10.1039/c1cs15258k

Mohsen, M. O., Speiser, D. E., Knuth, A., and Bachmann, M. F. (2020). Virus-like Particles for Vaccination against Cancer. *WIREs Nanomed Nanobiotechnol.* 12, 1–17. doi:10.1002/wnan.1579

Murasato, K., Matsuura, K., and Kimizuka, N. (2008). Self-Assembly of Nanofiber with Uniform Width from Wheel-type Trigonal-β-Sheet-Forming Peptide. *Biomacromolecules* 9, 913–918. doi:10.1021/bm701302p

Ni, R., and Chau, Y. (2014). Structural Mimics of Viruses through Peptide/DNA Co-assembly. *J. Am. Chem. Soc.* 136, 17902–17905. doi:10.1021/ja507833x

Ni, R., and Chau, Y. (2017). Tuning the Inter-nanofibril Interaction to Regulate the Morphology and Function of Peptide/DNA Co-assembled Viral Mimics. *Angew. Chem.* 129, 9484–9488. doi:10.1002/ange.201703596

Noble, J. E., De Santis, E., Ravi, J., Lamarre, B., Castelletto, V., Mantell, J., et al. (2016). A De Novo Virus-like Topology for Synthetic Virions. *J. Am. Chem. Soc.* 138, 12202–12210. doi:10.1021/jacs.6b05751

Pelin, J. N. B. D., Gerbelli, B. B., Edwards-Gayle, C. J. C., Aguilar, A. M., Castelletto, V., Hamley, I. W., et al. (2020). Amyloid Peptide Mixtures: Self-Assembly, Hydrogelation, Nematic Ordering, and Catalysts in Aldol Reactions. *Langmuir* 36, 2767–2774. doi:10.1021/acs.langmuir.0c00198

Qiao, C., Zhang, R., Wang, Y., Jia, Q., Wang, X., Yang, Z., et al. (2020). Rabies Virus-Inspired Metal-Organic Frameworks (MOFs) for Targeted Imaging and Chemotherapy of Glioma. *Angew. Chem. Int. Ed.* 59, 16982–16988. doi:10.1002/anie.202007474

Reches, M., and Gazit, E. (2004). Formation of Closed-Cage Nanostructures by Self-Assembly of Aromatic Dipeptides. *Nano Lett.* 4, 581–585. doi:10.1021/nl035159z

Roldão, A., Silva, A. C., Mellado, M. C. M., Alves, P. M., and Carrondo, M. J. T. (2017). Viruses and Virus-like Particles in Biotechnology: Fundamentals and Applications. *Compr. Biotechnol.*, 633–656. doi:10.1016/B978-0-12-809633-8.09046-4

Saleh, A. F., Aojula, H., Arthanari, Y., Offerman, S., Alkotaji, M., and Pluen, A. (2010). Improved Tat-Mediated Plasmid DNA Transfer by Fusion to LK15 Peptide. *J. Controlled Release.* 143, 233–242. doi:10.1016/j.jconrel.2009.12.025

Sasselli, I. R., Moreira, I. P., Ulijn, R. V., and Tuttle, T. (2017). Molecular Dynamics Simulations Reveal Disruptive Self-Assembly in Dynamic Peptide Libraries. *Org. Biomol. Chem.* 15, 6541–6547. doi:10.1039/c7ob01268c

Sharma, P., Pal, V. K., and Roy, S. (2021). An Overview of Latest Advances in Exploring Bioactive Peptide Hydrogels for Neural Tissue Engineering. *Biomater. Sci.* 9, 3911–3938. doi:10.1039/D0BM02049D

Sieste, S., Mack, T., Lump, E., Hayn, M., Schütz, D., Röcker, A., et al. (2021). Supramolecular Peptide Nanofibrils with Optimized Sequences and Molecular Structures for Efficient Retroviral Transduction. *Adv. Funct. Mater.* 31, 2009382. doi:10.1002/adfm.202009382

Singh, N., Kumar, M., Miravet, J. F., Ulijn, R. V., and Escuder, B. (2017). Peptide-Based Molecular Hydrogels as Supramolecular Protein Mimics. *Chem. Eur. J.* 23, 981–993. doi:10.1002/chem.201602624

Sloan-Dennison, S., Lampel, A., Raßlenberg, E., Ulijn, R. V., Smith, E., Faulds, K., et al. (2021). Elucidation of the Structure of Supramolecular Polymorphs in Peptide Nanofibres Using Raman Spectroscopy. *J. Raman Spectrosc.*, 1–7. doi:10.1002/jrs.6121

Slocik, J. M., and Naik, R. R. (2017). Sequenced Defined Biomolecules for Nanomaterial Synthesis, Functionalization, and Assembly. *Curr. Opin. Biotechnol.* 46, 7–13. doi:10.1016/j.copbio.2016.11.025

Smith, D. J., Brat, G. A., Medina, S. H., Tong, D., Huang, Y., Grahammer, J., et al. (2015). A Multiphase Transitioning Peptide Hydrogel for Suturing Ultrasmall Vessels. *Nat. Nanotech.* 11, 95–102. doi:10.1038/nnano.2015.238

Son, J., Kalafatovic, D., Kumar, M., Yoo, B., Cornejo, M. A., Contel, M., et al. (2019). Customizing Morphology, Size, and Response Kinetics of Matrix Metalloproteinase-Responsive Nanostructures by Systematic Peptide Design. *ACS Nano.* 13, 1555–1562. doi:10.1021/acsnano.8b07401

Tamamis, P., Adler-Abramovich, L., Reches, M., Marshall, K., Sikorski, P., Serpell, L., et al. (2009). Self-assembly of Phenylalanine Oligopeptides: Insights from Experiments and Simulations. *Biophysical J.* 96, 5020–5029. doi:10.1016/j.bpj.2009.03.026

Tao, K., Makam, P., Aizen, R., and Gazit, E. (2017). Self-assembling Peptide Semiconductors. *Science* 358, eaam9756. doi:10.1126/science.aam9756

van Hell, A. J., Costa, C. I. C. A., Flesch, F. M., Sutter, M., Jiskoot, W., Crommelin, D. J. A., et al. (2007). Self-Assembly of Recombinant Amphiphilic Oligopeptides into Vesicles. *Biomacromolecules* 8, 2753–2761. doi:10.1021/bm0704267

Vauthey, S., Santoso, S., Gong, H., Watson, N., and Zhang, S. (2002). Molecular Self-Assembly of Surfactant-like Peptides to Form Nanotubes and Nanovesicles. *Proc. Natl. Acad. Sci.* 99, 5355–5360. doi:10.1073/pnas.072089599

Vlieghe, P., Lisowski, V., Martinez, J., and Khrestchatisky, M. (2010). Synthetic Therapeutic Peptides: Science and Market. *Drug Discov. Today.* 15, 40–56. doi:10.1016/j.drudis.2009.10.009

Wang, J., Han, S., Meng, G., Xu, H., Xia, D., Zhao, X., et al. (2009). Dynamic Self-Assembly of Surfactant-like Peptides A6K and A9K. *Soft Matter.* 5, 3870–3878. doi:10.1039/b901653h

Wang, Y., Nie, Y., Ding, Z., Yao, M., Du, R., Zhang, L., et al. (2020). An Amphiphilic Peptide with Cell Penetrating Sequence for Highly Efficient Gene Transfection. *Colloids Surf. A: Physicochemical Eng. Aspects.* 590, 124529. doi:10.1016/j.colsurfa.2020.124529

Whitesides, G. M. (2015). Bioinspiration: Something for Everyone. *Interf. Focus.* 5, 20150031. doi:10.1098/rsfs.2015.0031

Whitesides, G. M., and Grzybowski, B. (2002). Self-assembly at All Scales. *Science* 295, 2418–2421. doi:10.1126/science.1070821

Woolfson, D. N., and Mahmoud, Z. N. (2010). More Than Just Bare Scaffolds: Towards Multi-Component and Decorated Fibrous Biomaterials. *Chem. Soc. Rev.* 39, 3464–3479. doi:10.1039/c0cs00032a

Xu, H., Wang, Y., Ge, X., Han, S., Wang, S., Zhou, P., et al. (2010). Twisted Nanotubes Formed from Ultrashort Amphiphilic Peptide I3K and Their Templating for the Fabrication of Silica Nanotubes. *Chem. Mater.* 22, 5165–5173. doi:10.1021/cm101019p

Xu, X., Yuan, H., Chang, J., He, B., and Gu, Z. (2012). Cooperative Hierarchical Self-Assembly of Peptide Dendrimers and Linear Polypeptides into Nanoarchitectures Mimicking Viral Capsids. *Angew. Chem. Int. Ed.* 51, 3130–3133. doi:10.1002/anie.201106080

Yang, J., Zhang, X., Liu, C., Wang, Z., Deng, L., Feng, C., et al. (2021a). Biologically Modified Nanoparticles as Theranostic Bionanomaterials. *Prog. Mater. Sci.* 118, 100768. doi:10.1016/j.pmatsci.2020.100768

Yang, P., Li, Y.-J., Cao, Y., Zhang, L., Wang, J.-Q., Lai, Z.-W., et al. (2020b). Rapid Discovery of Self-Assembling Peptides with One-Bead One-Compound Peptide Libraries. *Res. Sq.*, 1–15. doi:10.21203/rs.3.rs-109949/v1

Yokoi, H., Kinoshita, T., and Zhang, S. (2005). Dynamic Reassembly of Peptide RADA16 Nanofiber Scaffold. *Proc. Natl. Acad. Sci.* 102, 8414–8419. doi:10.1073/pnas.0407843102

Yoon, Y.-R., Lim, Y.-b., Lee, E., and Lee, M. (2008). Self-assembly of a Peptide Rod-Coil: A Polyproline Rod and a Cell-Penetrating Peptide Tat Coil. *Chem. Commun.*, 1892–1894. doi:10.1039/b719868j

Zhang, S. (2017). Discovery and Design of Self-Assembling Peptides. *Interf. Focus.* 7, 20170028. doi:10.1098/rsfs.2017.0028

Zhang, S. (2003). Fabrication of Novel Biomaterials through Molecular Self-Assembly. *Nat. Biotechnol.* 21, 1171–1178. doi:10.1038/nbt874

Zhang, S., Holmes, T., Lockshin, C., and Rich, A. (1993). Spontaneous Assembly of a Self-Complementary Oligopeptide to Form a Stable Macroscopic Membrane. *Proc. Natl. Acad. Sci.* 90, 3334–3338. doi:10.1073/pnas.90.8.3334

Zhao, X. (2009). Design of Self-Assembling Surfactant-like Peptides and Their Applications. *Curr. Opin. Colloid Interf. Sci.* 14, 340–348. doi:10.1016/j.cocis.2009.07.002

Zhao, X., Pan, F., and Lu, J. R. (2008). Recent Development of Peptide Self-Assembly. *Prog. Nat. Sci.* 18, 653–660. doi:10.1016/j.pnsc.2008.01.012

Conflict of Interest: The authors declare that the research was conducted in the absence of any commercial or financial relationships that could be construed as a potential conflict of interest.

Data Article

Manually curated dataset of catalytic peptides for ester hydrolysis

Patrizia Janković [a], Erik Otović [b,c], Goran Mauša [b,c,**],
Daniela Kalafatovic [a,c,*]

[a] *University of Rijeka, Department of Biotechnology, Rijeka 51000, Croatia*
[b] *University of Rijeka, Faculty of Engineering, Rijeka 51000, Croatia*
[c] *University of Rijeka, Center for Artificial Intelligence and Cybersecurity, Rijeka 51000, Croatia*

ARTICLE INFO

ABSTRACT

Catalytic peptides are low cost biomolecules able to catalyse chemical reactions such as ester hydrolysis. This dataset provides a list of catalytic peptides currently reported in literature. Several parameters were evaluated, including sequence length, composition, net charge, isoelectric point, hydrophobicity, self-assembly propensity and mechanism of catalysis. Along with the analysis of physico-chemical properties, the SMILES representation for each sequence was generated to provide an easy-to-use means of training machine learning models. This offers a unique opportunity for the development and validation of proof-of-concept predictive models. Being a reliable manually curated dataset, it also enables the benchmark for comparison of new models or models trained on automatically gathered peptide-oriented datasets. Moreover, the dataset provides an insight in the currently developed catalytic mechanisms and can be used as the foundation for the development of next-generation peptide-based catalysts.

© 2023 The Author(s). Published by Elsevier Inc.
This is an open access article under the CC BY license
(http://creativecommons.org/licenses/by/4.0/)

---

* Corresponding author at: University of Rijeka, Department of Biotechnology, Rijeka 51000, Croatia.
** Co-corresponding author.
E-mail addresses: gmausa@riteh.hr (G. Mauša), daniela.kalafatovic@uniri.hr (D. Kalafatovic).
Social media: @Jankovic_Pat (P. Janković), @ErikOtovic (E. Otović), @danikalafatovic (D. Kalafatovic)

Specifications Table

Subject	Chemistry
Specific subject area	Catalytic peptides: a compilation of experimentally validated catalytic peptides alongside selected physico-chemical properties and SMILES annotations.
Type of data	Tables in CSV format containing sequences composed of (i) proteinogenic and (ii) non-proteinogenic amino acids as separate lists.
	Figures depicting the distribution of length, composition and properties for catalytic and non-catalytic peptides (for p-NPA hydrolysis)
How the data were acquired	A literature search was conducted to identify all the reported peptide sequences with ester hydrolysis activity, experimentally determined through the para-nitrophenyl acetate (p-NPA) and para-nitrphenyl phosphate (p-NPP) assays.
	Charge, hydrophobicity and isoelectric point were computed with peptides.py library. Sequence similarities were computed in Python programming language and peptide alignment was performed with Needleman-Wunsch alignment algorithm from sckit-bio library. SMILES representation of peptides was generated with RDKit library.
Data format	Raw Analyzed
Description of data collection	Data collection was based on the standard colorimetric assays used for the experimental validation of ester and phosphoester hydrolysis. This reaction was selected to standardize the reported catalytic parameters. Other important features included in the dataset are N- and C- termini modifications, self-assembly propensity and mechanism of action.
Data source location	The data was sourced from publicly available articles [1–22] found through academic search engines.
Data accessibility	Repository name: Mendeley Data
	Data identification number: 10.17632/6s9kxj2ndr.2
	Direct URL to data: https://data.mendeley.com/datasets/6s9kxj2ndr

Value of the Data

- The analyzed physico-chemical properties for proteinogenic instances offer insight into existing design strategies important for the development of new catalytic sequences.
- The dataset is based on the catalytic activity towards the same type of reaction (ester hydrolysis) which opens up the opportunity for analysis of sequence-activity relationship and their straightforward comparison.
- The provided SMILES (Simplified molecular-input line-entry system) annotations encode important information about the molecular structure (atoms types, bond, chirality, etc.) which can be useful for machine learning-based predictive modelling.
- The presented manually curated dataset can be used to develop and test proof-of-concept models, but also for the comparison and validation of models trained on automatically gathered peptide datasets.

1. Objective

The objective of this dataset is to provide the first comprehensive collection of purely peptidic catalysts including both active and inactive sequences serving as a platform for the design of novel catalytic sequences. Creating comprehensive datasets of peptide catalysts is challenging as their catalytic activities may encompass a wide range of chemical transformations and mechanisms. This dataset focuses on peptide sequences that catalyze ester and phosphoester hydrolysis, two widely-studied and important reactions in biological systems. In order to maintain consistency and comparability among the included peptides, we selected only those that follow Michaelis–Menten kinetics, which provides a reliable framework for determining kinetic parameters such as the catalytic efficiency (k_{cat}/K_M).

2. Data Description

We provided a list in CSV format (raw data reposited in Mendeley data), containing 101 positive and negative entries of catalytic peptides active towards the p-NPA and p-NPP substrates [1–22]. In addition, activities towards other alkyl-based substrates including p-NPB (p-nitrophenyl butyrate), p-NPO (p-nitrophenyl octanoate), p-NPMA (p-nitrophenyl methoxyacetate), p-NPH (p-nitrophenyl hexanoate), p-NPS (p-nitrophenyl salicylate), p-NPProp (p-nitrophenyl propionate), p-NPPalm (p-nitrophenyl palmitate), indoxyl acetate, HPNPP (2-hydroxypropyl-4-nitrophenylphosphate) and BNPP (Bis(4-nitrophenyl)phosphate), were added when available. Peptides were categorized into two tables based on whether they contained proteinogenic or non-proteinogenic amino acids. The tables are comprised of nine columns containing one-letter amino acid codes, N- and C- termini modifications, SMILES (Simplified molecular-input line-entry system) annotations, the substrates tested along with the corresponding catalytic parameter (k_{cat}/K_M), mechanisms of action, ability to form secondary structures and/or self-assemble. The SMILES annotations of peptides without termini modifications are provided for sequences containing only proteinogenic amino acids.

Alongside the tables we performed a descriptive statistical analysis of peptides active on p-NPA, that represent the majority of entries. The violin plot representation was used to visualize the distribution of physico-chemical properties important for catalytic activity: charge at pH = 7.4 on the Lehninger scale (Fig. 1(c)), hydrophobicity on Eisenberg scale (Fig. 1(d)) and isoelectric point (Fig. 1(e)). Moreover, a table showing sequence termini modification combinations (Fig. 1(a)) and a histogram indicating the percentage of peptides depending on three main catalysis mechanisms (Fig. 1(b)) were presented for the catalytic peptides. Finally, the histogram of peptide lengths (Fig. 2(a)), the frequency analysis of proteinogenic amino acids reflecting the composition of peptides (Fig. 2(b)) and the similarity analysis of sequences (Fig. 2(c)–(e)) were provided for the active and inactive peptides.

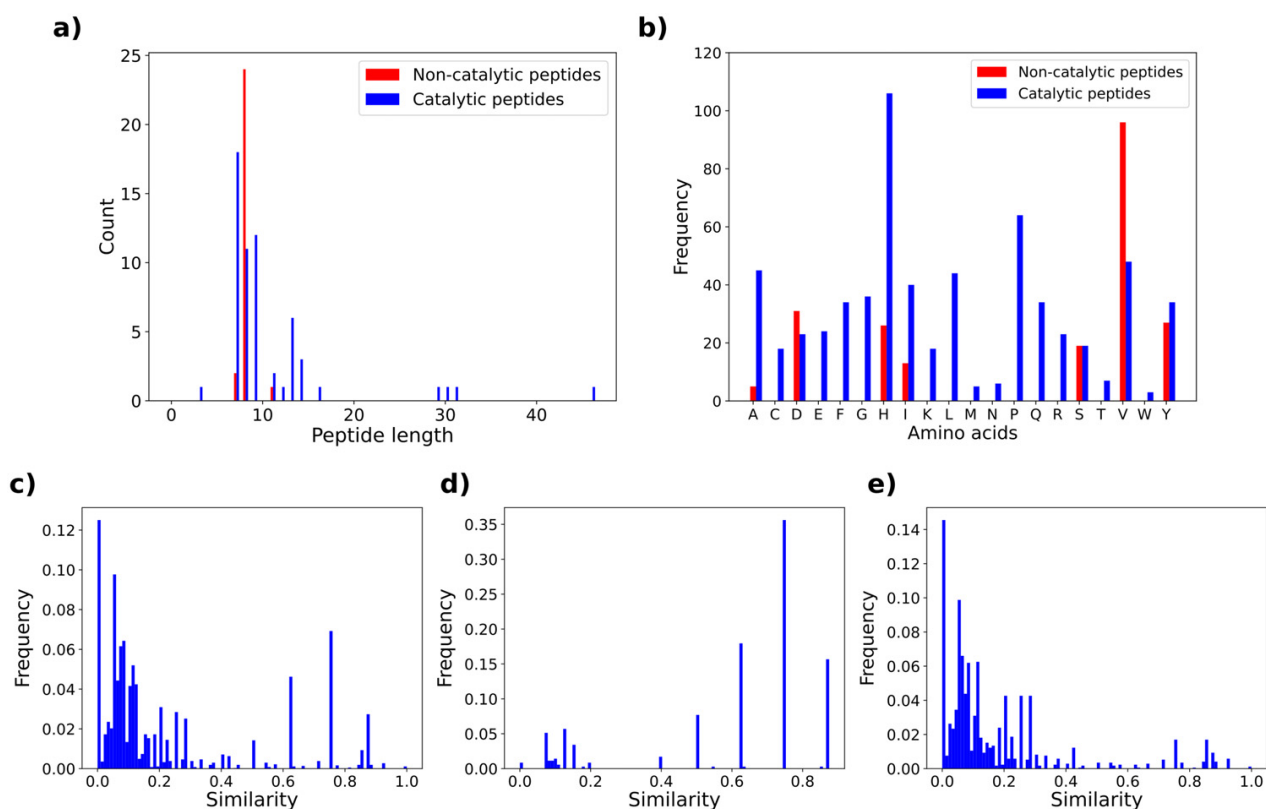**Fig. 1.** Statistical and physico-chemical properties computed for sequences active on p-NPA: (a) number of peptides with a specific combination of N- and C- termini and (b) distribution of peptides by catalysis mechanism. Distributions of examined physico-chemical properties: (c) charge on Lehninger scale at pH = 7.4, (d) hydrophobicity on Eisenberg scale and (e) isoelectric point on Lehninger scale.
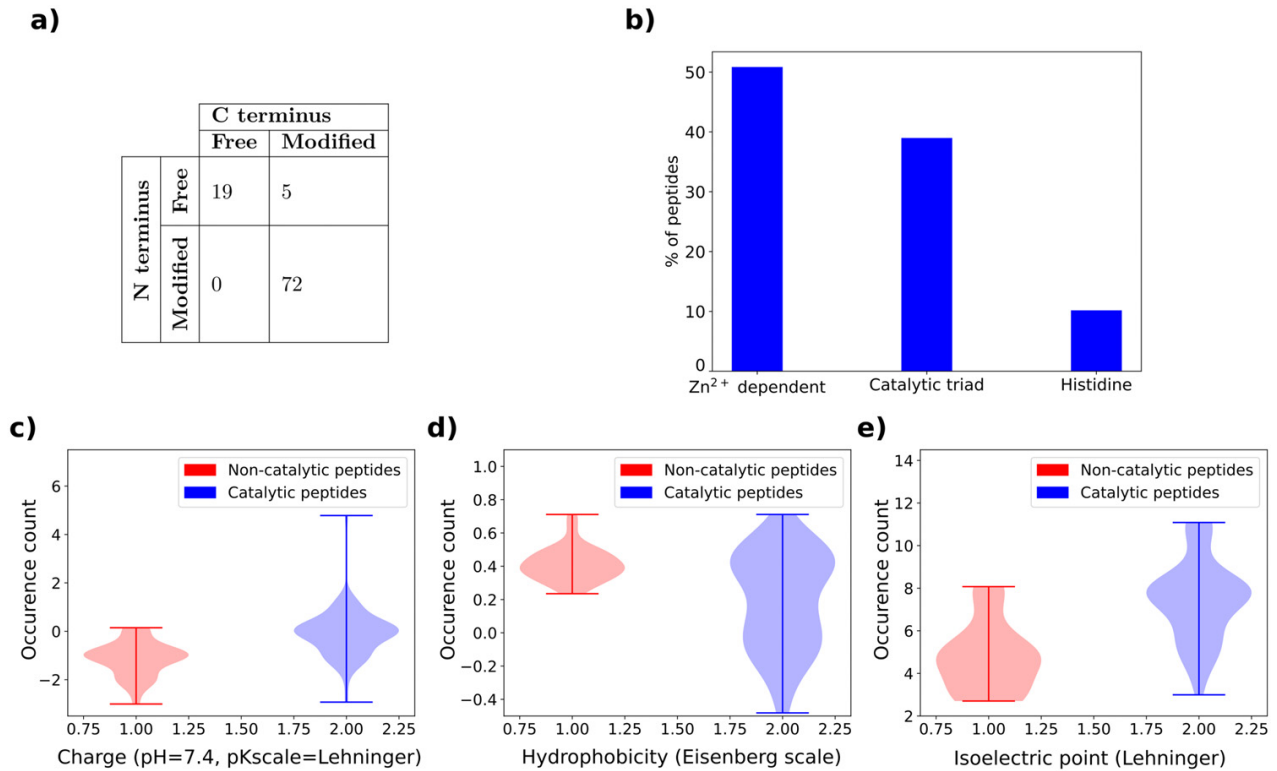
Fig. 2. Statistical properties of sequences that catalyze the p-NPA substrate: (a) distribution of sequence lengths, (b) distribution of 20 proteinogenic amino acids. Similarity computed for pairs of peptides among: (c) all sequences, (d) inactive peptides and (e) active peptides.

3. Experimental Design, Materials and Methods

Data regarding catalytic peptides were collected from published articles up to the year 2023. Articles were searched in the academic search engine Google Scholar for the keywords catalytic peptides, p-NPA, p-NPP and self-assembly. The provided statistical analyses were performed only for peptides active on the p-NPA substrate with Python 3.8 programming language. All properties were separately analyzed for active and inactive sequences containing only proteinogenic amino acids. Distribution of amino acid residues (e.g. peptide length) was obtained by counting the number of peptides that are of specific length. Furthermore, we provide the overview of peptide compositions that was computed by counting how many times each amino acid occurs in the dataset. We also computed and analyzed the distributions of theoretical physico-chemical properties relevant to the catalytic activity with peptides.py 0.3.1 Python library. GRAVY hydrophobicity index of an amino acids sequence was computed using Eisenberg scale, by summing the hydrophobicity of individual amino acids and dividing this value by the length of the sequence. The net charge of the peptide sequence is computed by the Henderson–Hasselbalch equation at pH = 7.4 using Lehninger pKa scale. Isoelectric point, representing the pH level at which peptide carries no net charge, was computed for a Lehninger pKa scale. The peptide similarity was separately computed for the whole dataset, only for negative entries and only for positive entries. All pairs of peptides are aligned with the Needleman–Wunsch method from scikit-bio 0.5.8 Python library. The relative similarity representing the percentage of corresponding residues is computed for each pair of peptides in the dataset with respect to the longer peptide and thus achieves a value from a range [0, 1].

Ethics Statement

Not applicable.

Declaration of Competing Interest

The authors declare that they have no known competing financial interests or personal relationships that could have appeared to influence the work reported in this paper.

Data Availability

Catalytic Peptides Dataset (Reference data) (Mendeley Data).

CRediT Author Statement

Patrizia Janković: Conceptualization, Methodology, Investigation, Writing – original draft; **Erik Otović:** Data curation, Visualization, Writing – original draft, Formal analysis; **Goran Mauša:** Visualization, Investigation, Supervision, Writing – review & editing; **Daniela Kalafatovic:** Conceptualization, Investigation, Supervision, Funding acquisition, Writing – review & editing.

Acknowledgments

References

[1] C.M. Rufo, Y.S. Moroz, O.V. Moroz, J. Stöhr, T.A. Smith, X. Hu, W.F. DeGrado, I.V. Korendovych, Short peptides self-assemble to produce catalytic amyloids, Nat. Chem. 6 (4) (2014) 303–309.
[2] C. Zhang, R. Shafi, A. Lampel, D. MacPherson, C.G. Pappas, V. Narang, T. Wang, C. Maldarelli, R.V. Ulijn, Switchable hydrolase based on reversible formation of supramolecular catalytic site using a self-assembling peptide, Angew. Chem. Int. Ed. 56 (46) (2017) 14511–14515.
[3] K.-Y. Huang, C.-C. Yu, J.-C. Horng, Conjugating catalytic polyproline fragments with a self-assembling peptide produces efficient artificial hydrolases, Biomacromolecules 21 (3) (2020) 1195–1201.
[4] P.-Y. Hung, Y.-H. Chen, K.-Y. Huang, C.-C. Yu, J.-C. Horng, Design of polyproline-based catalysts for ester hydrolysis, ACS Omega 2 (9) (2017) 5574–5581.
[5] A. Garcia, M. Kurbasic, S. Kralj, M. Melchionna, S. Marchesan, A biocatalytic and thermoreversible hydrogel from a histidine-containing tripeptide, Chem. Commun. 53 (58) (2017) 8110–8113.
[6] T. Carlomagno, M.C. Cringoli, S. Kralj, M. Kurbasic, P. Fornasiero, P. Pengo, S. Marchesan, Biocatalysis of d, l-peptide nanofibrillar hydrogel, Molecules 25 (13) (2020) 2995.
[7] Y. Wang, L. Yang, M. Wang, J. Zhang, W. Qi, R. Su, Z. He, Bioinspired phosphatase-like mimic built from the self-assembly of de novo designed helical short peptides, ACS Catal. 11 (9) (2021) 5839–5849.
[8] S. Liang, X.-L. Wu, M.-H. Zong, W.-Y. Lou, Construction of Zn-heptapeptide bionanozymes with intrinsic hydrolase–like activity for degradation of di (2-ethylhexyl) phthalate, J. Colloid Interface Sci. 622 (2022) 860–870.
[9] B.S. Der, D.R. Edwards, B. Kuhlman, Catalysis by a de novo zinc-mediated protein interface: implications for natural enzyme evolution and rational enzyme engineering, Biochemistry 51 (18) (2012) 3933–3940.
[10] J.P. Casey Jr, R.J. Barbero, N. Heldman, A.M. Belcher, Versatile de novo enzyme activity in capsid proteins from an engineered M13 bacteriophage library, J. Am. Chem. Soc. 136 (47) (2014) 16508–16514.
[11] C. Zhang, X. Xue, Q. Luo, Y. Li, K. Yang, X. Zhuang, Y. Jiang, J. Zhang, J. Liu, G. Zou, et al., Self-assembled peptide nanofibers designed as biological enzymes for catalyzing ester hydrolysis, ACS Nano 8 (11) (2014) 11715–11723.
[12] M.L. Zastrow, A.F. Peacock, J.A. Stuckey, V.L. Pecoraro, Hydrolytic catalysis and structural stabilization in a designed metalloprotein, Nat. Chem. 4 (2) (2012) 118–123.
[13] A.J. Nicoll, R.K. Allemann, Nucleophilic and general acid catalysis at physiological pH by a designed miniature esterase, Org. Biomol. Chem. 2 (15) (2004) 2175–2180.
[14] Z. Al-Garawi, B. McIntosh, D. Neill-Hall, A. Hatimy, S. Sweet, M. Bagley, L. Serpell, The amyloid architecture provides a scaffold for enzyme-like catalysts, Nanoscale 9 (30) (2017) 10773–10783.

[15] M.P. Friedmann, V. Torbeev, V. Zelenay, A. Sobol, J. Greenwald, R. Riek, Towards prebiotic catalytic amyloids using high throughput screening, PLoS One 10 (12) (2015) e0143948.

[16] T. Takahashi, M. Cheung, T. Butterweck, S. Schankweiler, M.J. Heller, Quest for a turnover mechanism in peptide-based enzyme mimics, Catal. Commun. 59 (2015) 206–210.

[17] H.F. Carvatho, R.J. Branco, F.A. Leite, M. Matzapetakis, A.C.A. Roque, O. Iranzo, Hydrolytic zinc metallopeptides using a computational multi-state design approach, Catal. Sci. Technol. 9 (23) (2019) 6723–6736.

[18] A. Baruch-Leshem, C. Chevallard, F. Gobeaux, P. Guenoun, J. Daillant, P. Fontaine, M. Goldmann, A. Kushmaro, H. Rapaport, Catalytically active peptides affected by self-assembly and residues order, Colloids Surf., B 203 (2021) 111751.

[19] M. Díaz-Caballero, S. Navarro, M. Nuez-Martínez, F. Peccati, L. Rodríguez-Santiago, M. Sodupe, F. Teixidor, S. Ventura, pH-responsive self-assembly of amyloid fibrils for dual hydrolase-oxidase reactions, ACS Catal. 11 (2) (2020) 595–607.

[20] Y. Maeda, N. Javid, K. Duncan, L. Birchall, K.F. Gibson, D. Cannon, Y. Kanetsuki, C. Knapp, T. Tuttle, R.V. Ulijn, et al., Discovery of catalytic phages by biocatalytic self-assembly, J. Am. Chem. Soc. 136 (45) (2014) 15893–15896.

[21] C. Mahato, S. Menon, A. Singh, S.P. Afrose, J. Mondal, D. Das, Short peptide-based cross-β amyloids exploit dual residues for phosphoesterase like activity, Chem. Sci. 13 (32) (2022) 9225–9231.

[22] A.S. Pina, L. Morgado, K.L. Duncan, S. Carvalho, H.F. Carvalho, A.J. Barbosa, B.d.P. Mariz, I.P. Moreira, D. Kalafatovic, B.M.M. Faustino, et al., Discovery of phosphotyrosine-binding oligopeptides with supramolecular target selectivity, Chem. Sci. 13 (1) (2022) 210–217.

MSDE

Molecular Systems Design & Engineering

rsc.li/molecular-engineering

ROYAL SOCIETY
OF CHEMISTRY

PAPER
Daniela Kalafatovic *et al.*
Factors influencing the catalytic activity of
metal-dependent histidine-rich peptides: sequence,
conformation, stereochemistry, self-assembly or
their interplay?

IChemE ADVANCING
CHEMICAL
ENGINEERING
WORLDWIDE

Check for updates

Factors influencing the catalytic activity of metal-dependent histidine-rich peptides: sequence, conformation, stereochemistry, self-assembly or their interplay?†

Patrizia Janković, [iD][a] Marko Babić,[a] Marko Perčić,[bcd] Ana S. Pina [iD][e] and Daniela Kalafatovic [iD] *[ad]

The sequence-to-function relationship of peptide-based catalysts remains a challenge, as even subtle modifications at the sequence level can alternate their catalytic activity. A set of linear and cyclic histidine-rich peptides was synthesized to assess the impact of amino acid disposition, cyclization, and incorporation of D-amino acids on their ability to self-assemble, coordinate Zn^{2+} ions, and show intrinsic hydrolase-like activity. Self-assembly into β-sheets was confirmed for both linear peptides and one cyclic analogue (cy-hh) by FTIR, ThT binding, CD, and AFM. Interestingly, only peptide A demonstrated efficient ester hydrolysis of *p*-NPA, *p*-NPB and *p*-NPO substrates, indicative of its effective Zn^{2+} coordination. Our findings highlight that increased rigidity of the peptide can hinder metal ion coordination by limiting the necessary conformational adjustments for optimal Zn^{2+} binding. These insights into the structural changes underlying the function of short peptides offer valuable knowledge for the design of metal-dependent peptide-based catalysts.

Design, System, Application

We investigated the impact of modifications at the sequence level, including amino acid disposition, cyclization and chirality of key residues involved in catalysis on the functionality and self-assembly propensity of Ac-IHIHINI-Am and its analogues. Our research sought to uncover the molecular principles governing catalytic activity in metal-dependent peptides. While the introduction of rigidity in cyclic peptides hindered the coordination of metal ions due to strict geometric requirements, the conformationally heterogeneous linear analogue exhibited more favorable metal coordination, proving to be the critical factor for achieving catalytic activity, surpassing the importance of self-assembly propensity. This work contributes to a deeper comprehension of catalytic activity in histidine-rich peptides and holds great promise for the future exploration of novel metal-dependent catalytic peptides. Understanding the intricate relationship between peptide sequence and function allows for the optimization of their catalytic performance and opens up diverse possibilities for their application in various industrial processes and therapeutic settings.

1 Introduction

Nanozymes are a class of nanoscale materials that exhibit intrinsic catalytic activity, mimicking the functions of natural enzymes.[1,2] They show unique properties that make them attractive for applications ranging from medical biosensing,[3] treatment of bacterial infections,[4] to environmental remediation.[5] Nanozymes are typically composed of inorganic, metal, or metal oxide nanoparticles that resemble catalytic functions, including peroxidase, oxidase, catalase, and other activities.[3] They offer several advantages over traditional enzymes, including versatility of design, ease of synthesis and functionalization.[6]

Peptides have gained attention as a promising class of molecules able to catalyze biochemical transformations.[7–11] Their significance comes from the fact that amino acids responsible for various catalytic mechanisms can be incorporated into a variety of designs and also from their ability to self-assemble in supramolecular architectures with

[a] *University of Rijeka, Department of Biotechnology, Radmile Matejčić 2, 51000 Rijeka, Croatia. E-mail: daniela.kalafatovic@uniri.hr*
[b] *University of Rijeka, Faculty of Engineering, Vukovarska 58, 51000 Rijeka, Croatia*
[c] *University of Rijeka, Centre for Micro- and Nanosciences and Technologies, 51000 Rijeka, Croatia*
[d] *University of Rijeka, Center for Artificial Intelligence and Cybersecurity, 51000 Rijeka, Croatia*
[e] *Instituto de Tecnologia Química e Biológica António Xavier (ITQB), Universidade Nova de Lisboa, Av. da República, 2780-157, Oeiras, Portugal*

This journal is © The Royal Society of Chemistry and IChemE 2023

Mol. Syst. Des. Eng., 2023, **8**, 1371–1380 | **1371**

emerging properties. In addition, peptides have a plausible evolutionary role as promiscuous precursors to complex and well-organized enzyme structures with extraordinary levels of substrate specificity and catalytic efficiency.[12] A deeper understanding of their evolutionary journey could provide valuable insights into the fundamental principles underlying enzyme catalysis and pave the way for the design of novel catalytic sequences and biomimetic systems.[8,12–14]

Peptide-based catalysts can be designed and engineered precisely to mimic the active sites of enzymes, allowing the development of highly specific and efficient catalytic systems.[15] Peptides can be modified with various functional groups or metals to further enhance their catalytic performance.[16,17] Furthermore, they offer excellent biocompatibility and low immunogenicity, making them suitable for biomedical applications.[18,19] Compared to enzymes, catalytic peptides offer several advantages, such as their smaller size, simpler structures, modularity, and ease of production.[20,21] Using peptides as catalysts may enable access to a chemical space larger than that of traditional small-molecule catalysts, leading to new possibilities for synthetic chemistry and biotechnology.

Catalytic peptides often display lower efficiencies compared to enzymes because of the lack of complex three-dimensional structures present in enzymes. To bridge this gap between simplicity and functionality, self-assembly has emerged as a promising approach.[15,19] Peptide self-assembly is the spontaneous organization of peptides into well-defined structures that display unique physical and chemical properties, different from those of their individual constituent monomers.[22,23] By organizing peptides into specific architectures, it is possible to create catalytic sites with enhanced activity and selectivity.[20,21,24] In addition, peptides are susceptible to proteolytic degradation, have reduced stability in plasma, and limited oral bioavailability.[18] Nevertheless, recent advances in peptide synthesis and modification techniques have helped overcome some of these limitations. For example, N-acetylation[25,26] or cyclization[27,28] are effective strategies for increasing the stability and structural diversity of peptides, leading to improved bioactivity and pharmacokinetics.[29]

Several design strategies have been developed to identify effective catalytic peptides, including mimicking natural enzymes, incorporating catalytic motifs or cofactors, and using directed evolution or combinatorial chemistry.[21,30,31] The most prominent strategies to mimic natural enzymes include metal coordination and incorporation of catalytic triad residues into short peptide sequences with self-assembly propensity.[32] The coordination of metal ions within peptides is often accomplished through specific amino acid residues, such as histidine, cysteine, aspartic acid, and glutamic acid, that can act as ligands for metal ions and consequently stabilize them within the peptide structure. Such stable and active metal–peptide complexes have been used to catalyze oxidation, reduction, hydrolysis, and isomerization.[16,33] One of the designs studied most

extensively involves alternating hydrophobic amino acids with histidines, which can coordinate Zn^{2+} ions.[34] The optimal amino acid combination consists of an interplay of isoleucines, histidines, and a single glutamine. To evaluate the effect of sequence composition on self-assembly and catalytic activity, multiple analogs, including substitution of tyrosine–glutamine, were proposed that showed increased binding affinity to Zn^{2+} and the potential to form photo-induced cross-links via dityrosine.[35] In general, short peptides capped through acetylation at the N-terminus and amidated at the C-terminus exhibit higher activity, whereas uncapped peptides and substitutions leading to increased net charge such as isoleucine-aspartic acid mutation lead to a reduction in activity. The sequence-dependent activity of the Ac-IHIHIQI-Am, Ac-IHIHIRI-Am, and Ac-IHIHIYI-Am heptapeptides assuming cross-β amyloid fibrillar morphologies showed that a flexibility–rigidity balance is required to efficiently mimic the active sites of the enzyme and resulted in higher esterase activity in fibers with increased flexibility.[36]

Despite the development of numerous catalytic peptides, fundamental understanding of the key factors that influence their performance and the sequence–activity relationship remains challenging. This is due to the complex interplay between their intrinsic structure and the extrinsic environment. The conformational heterogeneity of peptides could be one of the reasons why the catalytic performance of peptides is lower than that of enzymes. To address this issue, we propose the introduction of rigidity through cyclization to assess whether the reduced flexibility of short peptides can have an impact on their catalytic activity. The present study involved the design and synthesis of two linear and two cyclic histidine-rich peptides that shared the same set of amino acids, isoleucine, histidine, and asparagine. The impact of amino acid disposition within the sequence, cyclization, and incorporation of D-amino acids in cyclic analogues was evaluated to determine their effect on peptide self-assembly propensity, ability to coordinate zinc ions and the intrinsic hydrolase-like activity (Fig. 1). Our findings demonstrate that in addition to the well-established design principles of catalytic peptides, such as sequence motifs for metal coordination and self-assembly propensity, the flexibility of the peptide sequence plays a crucial role in metal coordination, which ultimately impacts the catalytic activity.

2 Results and discussion

A set of two linear and two cyclic histidine-rich peptides was evaluated in terms of their aggregation propensity and catalytic activity toward ester hydrolysis in the presence of Zn^{2+} ions (Table 1). Peptides were prepared using Fmoc-solid phase peptide synthesis on Rink amide resin, whereby head-to-side chain cyclization was performed on-resin through the formation of an amide bond between the N-terminus and the glutamic acid (E) side chain, after deprotection of the 2-phenylisopropyl (O-2-PhiPr) group. The linear peptides, Ac-
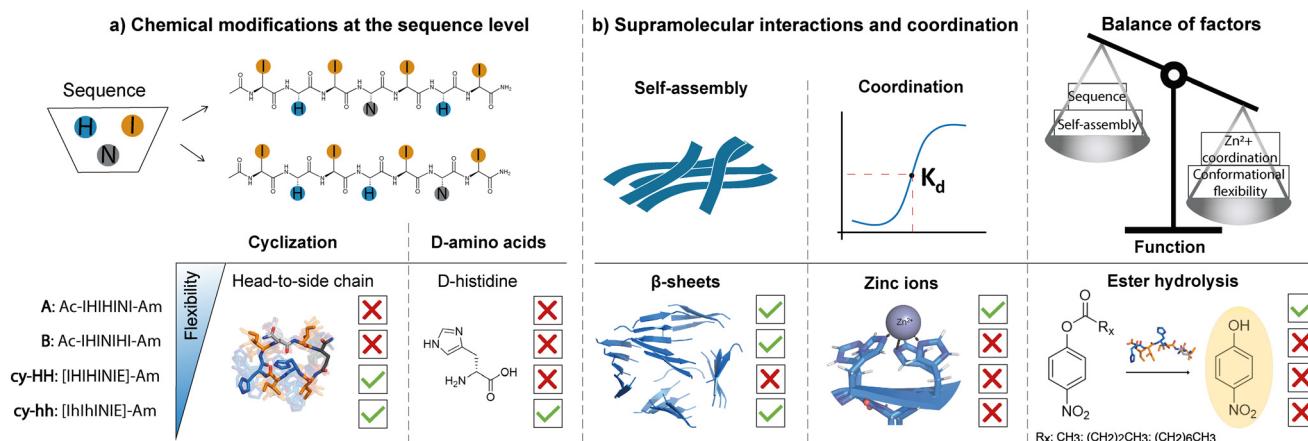
Fig. 1 Schematic representation of a) sequence-level modifications, including head-to-side chain cyclization and incorporation of D-histidines; and b) the consequent effects on self-assembly propensity, zinc ion coordination and catalytic activity in histidine-rich short peptides. We proposed two linear peptides (A and B) with different amino acid arrangements at the sequence level, where histidine residues, responsible for catalysis, were placed at different locations in the sequence. Both sequences self-assembled into β-sheets, however, only peptide A that efficiently coordinated zinc (K_d determined) showed catalytic activity. Modifications at the sequence level affecting peptide flexibility, through cyclization (cy-HH, cy-hh) and incorporation of D-histidines (cy-hh) in peptide A resulted in β-sheets for cy-hh and the absence of supramolecular structures for cy-HH, highlighting the influence of chirality on the self-assembly behavior of cyclic peptides. However, both modifications led to a lack of metal coordination resulting in a loss of esterase activity, showing that the interplay of various factors shapes the functionality of catalytic peptides.

IHIHINI-Am (Fig. S1†) and Ac-IHINIHI-Am (Fig. S2†), were N-terminal acetylated and C-terminal amidated to minimize the effect of terminal charges on catalytic efficiency.[34] For the same reason, the cyclic peptides, [IHIHINIE]-Am (Fig. S3†) and [IhIhINIE]-Am (Fig. S4†), were C-terminal amidated while the N-terminus was modified through cyclization. The E residue was added to the cyclic peptides to allow the head-to-side chain cyclization which was chosen to avoid the oligomerization that often arises with the backbone cyclization and to achieve higher purity by performing the cyclization on resin rather than in solution.[37] The aggregation behavior of the obtained peptides was assessed through the ThT assay, IR and AFM, which confirmed the propensity to form fibrillar β-sheet assemblies (Fig. 2). Furthermore, the secondary structure of the aggregates was determined using circular dichroism (CD) (Fig. 2) and modeled with molecular dynamics (MD) simulations (Fig. S13†), which confirmed their predominant β-sheet nature.

2.1 Impact of side chain length and amino acid disposition on the self-assembly propensity of linear peptides

The role of alternating hydrophilic and hydrophobic amino acids, particularly isoleucines and histidines, in the design of

promising catalytic peptide candidates has been well established in previous studies.[34–36] Histidine, being a common component of active sites in esterases, is frequently incorporated in the design of catalytic peptides.[38,39] Motivated by the Ac-IHIHIQI-Am sequence,[34] we made a specific amino acid modification by substituting glutamine with asparagine in Ac-IHIHINI-Am (peptide A). This substitution involves a minor difference of only one –CH₂ group in the side chain of the amino acid. Our hypothesis was that this slight alteration in the peptide sequence could potentially enhance self-assembly by promoting the formation of asparagine ladders.[40] These ladder-like structures feature repetitive patterns of asparagine residues that contribute to the stabilization of the supramolecular arrangement. Moreover, we examined the impact of the amino acid disposition within the sequence in Ac-IHINIHI-Am (peptide B). In this case, the asparagine residue was positioned at the center of the sequence, while maintaining the alternating pattern of hydrophobic and hydrophilic residues.

Circular dichroism (CD) and infrared (IR) spectroscopies were used to confirm the adoption of a supramolecular β-sheet conformation by peptides A and B. In the IR spectra (Fig. 2b), both peptides exhibited a distinct peak at 1628

Table 1 Overview of the proposed peptide sequences alongside their acronyms and modifications introduced at the sequence level (design strategies), followed by their aggregation propensity and activity

Sequence	Name	Cyclization	Sequence modification	Catalytic activity (p-NPA)	CAC (M)
Ac-IHIHINI-Am	A	—	Introduction of N	Yes	67
Ac-IHINIHI-Am	B	—	N to H position substitution	—	67
[IHIHINIE]-Am	cy-HH	Head-to-side chain	Addition of E for cyclization	—	—
[IhIhINIE]-Am	cy-hh	Head-to-side chain	Replacement of both H with h	—	54

This journal is © The Royal Society of Chemistry and IChemE 2023

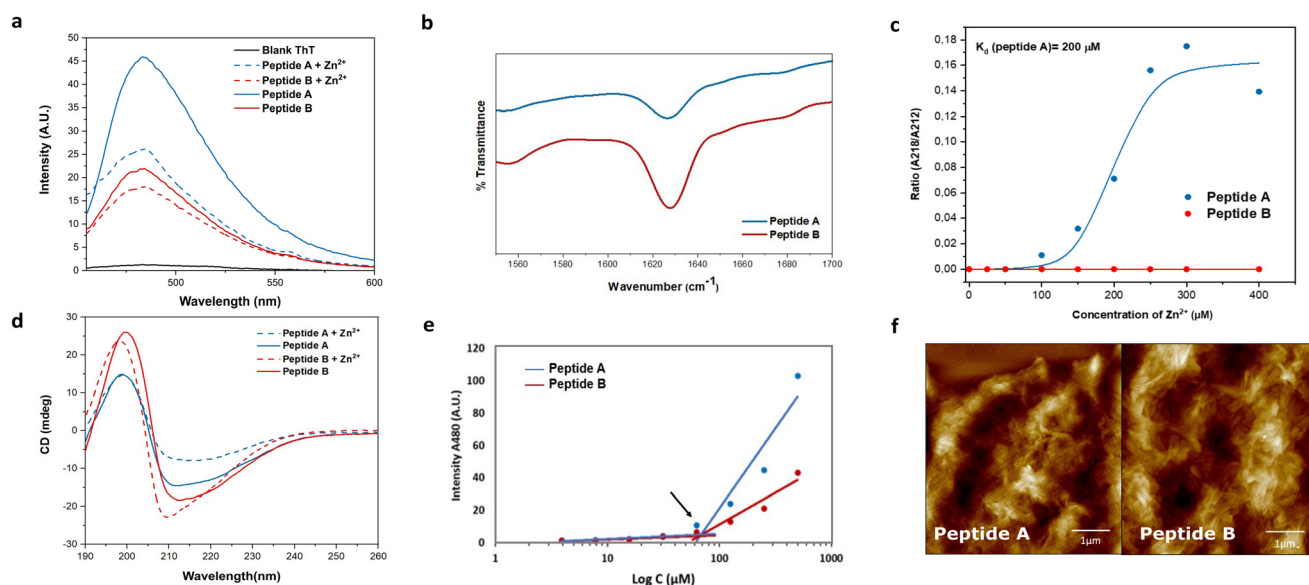*Mol. Syst. Des. Eng.*, 2023, **8**, 1371–1380 | **1373**

Fig. 2 Characterization of linear peptides: (a) ThT assay for peptides A (blue) and B (red) with Zn^{2+} (dashed line) and without Zn^{2+} (solid line) performed at 250 μM peptide concentration. (b) ATR-FTIR spectra of peptide A and peptide B showing a peak at 1623 cm^{-1} indicating the presence of β-sheets. (c) Zn^{2+} titration curve of peptide A (blue) and peptide B (red), demonstrating the differential affinity for the metal. Peptide A exhibits strong metal binding with a binding constant (K_d) of 200 μM, while peptide B shows no affinity. (d) CD spectra of peptide A (25 μM) and peptide B (25 μM) with and without Zn^{2+}, indicating the presence of β-sheet assemblies in both peptides. (e) CAC in MiliQ water, plotted for different concentrations of both peptides as a function of ThT fluorescence emission at 480 nm. (f) AFM images showing fibrillar morphologies for peptide A (left) and peptide B (right), recorded at a concentration of 250 μM (scale bar: 1 μm).

cm^{-1} attributed to the C=O stretching vibration of the amide bond, a characteristic feature of peptide self-assembly.[41] Under metal-free conditions, peptides A and B showed similar CD spectra, characterized by a minimum around 212 nm and a maximum at 197 nm, indicative of β-sheet-like assemblies (Fig. 2d). Upon the addition of Zn^{2+}, peptide A displayed a red shift of the minimum from 212 to 218 nm, indicating a more ordered cross-β configuration. In contrast, peptide B exhibited a blue shift in the minimum toward 210 nm, consistent with the formation of a less organized β-sheet-like arrangement, as previously reported.[34] These observations validate the hypothesis that substituting glutamine (Q) for asparagine (N) in peptide A improves the stability of its supramolecular β-sheet arrangement.

To explore the interaction between the peptides and the metal cofactor, a Zn^{2+} titration was conducted using CD, enabling the monitoring of structural changes as reflected by shifts in the minimum across a range of Zn^{2+} concentrations.[42] Peptide A exhibited a strong affinity for the metal cofactor with a binding constant (K_d) of 200 μM. On the contrary, peptide B showed a loss of affinity for Zn^{2+} (Fig. 2c) that could be due to different supramolecular arrangements for A and B. Peptide A is expected to assemble similarly to Ac-IHIHIQI-Am, with Ile residues constituting the central hydrophobic core and His residues projected outwards, facilitating metal ion coordination.[34,43] However, placement of Asn in the center of the peptide sequence (peptide B) could cause differential positioning of histidines within supramolecular assemblies or steric hindrance for efficient coordination, resulting in loss of binding affinity for

Zn^{2+} ions. At enzyme active sites, Zn^{2+} is typically coordinated in a trigonal bipyramidal or tetrahedral geometry[44] that might be difficult to achieve for peptides with increased distances between His residues (B). Furthermore, MD simulations provided insights into the conformational flexibility of peptide B, revealing significant fluctuations of its His residues over time, likely contributing to the lack of binding affinity to the metal cofactor (Fig. S12†).

Fibril formation was investigated using the thioflavin T (ThT) binding assay and atomic force microscopy (AFM). Peptide A demonstrated a higher enhancement in ThT fluorescence compared to peptide B, indicating a greater abundance of β-sheet-like assemblies (Fig. 2a). Interestingly, upon the addition of Zn^{2+}, the ThT signal was quenched, possibly due to coordination of Zn^{2+} with the ThT anilino group, leading to signal attenuation.[35] Importantly, the reduction in signal intensity was not uniform for both peptides, confirming distinct interactions with the metal. The critical aggregation concentration (CAC) of both peptides was determined at 67 μM, obtained by measuring the fluorescence intensity of ThT as a function of the peptide concentration (Fig. 2e). Furthermore, the AFM images provided visual evidence of bundles of fibers for both peptides (Fig. 2f).

To further confirm β-sheet formation, all-atom MD simulations were performed by simulating 24 instances of the same peptide molecule for each of the two linear peptides in 0.08 M Tris buffer. Both GROMACS simulations showed self-assembly in several shorter β-sheets (Fig. S13†), in contrast to the uniform β-sheet bilayer reported for the Ac-

MSDE

Paper

IHIHIQI-Am sequence.[34,36] The solvent accessible surface area (SASA) analysis of peptides A and B shows convergence to a stable surface in less than 50 ns for both molecules (Fig. S14†), with Ac-IHINIHI-Am having a slightly lower average SASA (150.25 nm^2) than Ac-IHIHINI-Am (140.13 nm^2). This indicates that both peptides exhibit rapid aggregation and self-assembly, forming stable nanostructures in solution.

2.2 Amino acid disposition within the sequence affects the functionality of linear peptides

The esterase activity of linear peptides was assessed using the widely employed p-NPA substrate. Peptide A demonstrated a moderate catalytic efficiency (k_{cat}/K_M) of 4.19 M^{-1} s^{-1} (Fig. 3a) at pH 7.4. To reflect the effect of the positional mutation of Q with N, the p-NPA assay was also performed at pH 8 and showed an improved catalytic performance for peptide A compared to the reported Ac-IHIHIQI-Am system,[34] yielding a k_{cat}/K_M value of 83.21 M^{-1} s^{-1} (Fig. S7†). On the contrary, peptide B showed a loss of activity in both the presence and absence of the metal cofactor. These results highlight the importance of selecting amino acids capable of coordinating zinc (Zn^{2+}) and arranging them appropriately within the peptide sequence to maintain catalytic activity. Our findings suggest that the self-assembly ability of histidine-rich peptides alone may not be sufficient to ensure the catalytic performance of Ac-IHIHINI-Am analogues, as opposed to the ability to control the catalytic efficiency in previously reported Ac-IHIHIQI-Am analogues where the β-sheet propensity could be correlated with catalytic activity.[34] To confirm the essential role of zinc for the catalytic function of peptide A, we performed a control experiment in which the catalytic activity of peptide A was assessed in the absence of zinc ions (Fig. S8†), resulting in lack of esterase activity. Furthermore, we evaluated the activity of peptide A on substrates with longer alkyl chains (Table 2). Our results showed improved activity for *para*-nitrophenyl butyrate (p-NPB) and reduced activity for *para*-nitrophenyl octanoate (p-NPO) (Fig. 3a and S9†). The enhanced activity for p-NPB indicates a higher affinity for the substrate, as reflected in the changes in K_M rather than k_{cat},

Table 2 Esterase activity of peptide A at pH 7.4 in the presence of 1 mM ZnCl$_2$ evaluated for p-NPA, p-NPB, p-NPO substrates

Substrate	k_{cat} (10^{-3} s^{-1})	K_M (10^{-3} M)	V_{max} (10^{-6} M s^{-1})	k_{cat}/K_m (M^{-1} s^{-1})
p-NPA	4.00 ± 0.01	0.98 ± 0.15	1.00 ± 0.01	4.19 ± 0.65
p-NPB	4.36 ± 0.36	0.55 ± 0.17	1.06 ± 0.09	7.83 ± 1.6
p-NPO	1.17 ± 0.17	12 ± 1.21	1.15 ± 0.041	0.41 ± 1.06

which may be attributed to the hydrophobic interactions between the Ile residues in the peptide and the alkyl chain of the substrate.

To better understand the relationship between peptide concentration and the corresponding catalytic activity, we performed p-NPA assays using varying concentrations of peptide A. The activity exhibited a positive correlation with the increase in peptide concentration, indicating that self-assembly contributes to the enhancement of catalytic activity. In particular, our findings showed first-order kinetics within the concentration range of 12.5–50 μM, below the CAC (Fig. 3b), indicating that the rate of the catalytic reaction is directly proportional to the peptide concentration. However, when the concentration exceeded the CAC (100 μM), a slight saturation of the curve was observed. This suggests that the system approached maximum velocity, reaching a point where the catalytic activity became independent of the peptide concentration, following zero-order kinetics. Changes in behavior can be attributed to various factors, including changes in surface area, confinement effects, and the accessibility of active sites within assemblies. Additionally, to satisfy the requirements of the Michaelis–Menten kinetics, the concentration of the substrate needs to be at least one order of magnitude higher than the concentration of the peptide catalyst. When the concentration of peptide A is above its CAC (100 μM), it approaches the substrate concentration limited by the poor solubility of p-NPA. Therefore, the observed activity at peptide concentrations above CAC might follow different kinetics. Although the esterase activity of peptide B was too low to accurately determine the parameters for the Michaelis–Menten
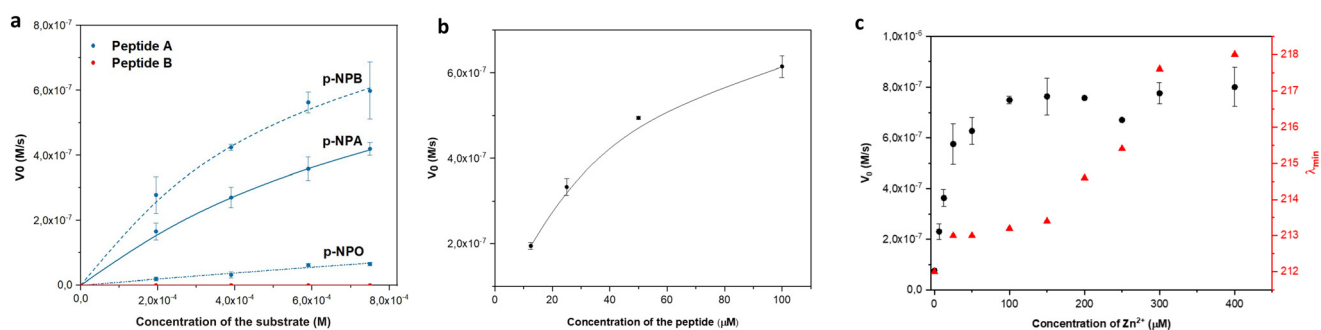

Fig. 3 Catalytic activity of linear peptides: (a) Michaelis–Menten plot showing the catalytic activity of peptides A (blue) and B (red) towards p-NPA, p-NPB, p-NPO. (b) Dependence of the p-NPA hydrolysis rate on the concentration of peptide A. (c) The activity of peptide A (black) and the shift in the minima (red) in CD as a function of Zn^{2+} concentration.

kinetics, we observed a linear increase in activity with increasing concentrations of the peptide (Fig. S6†).

We performed zinc titrations to explore the influence of metal concentration on the catalytic activity of peptide A and to establish a correlation with conformational changes, as determined by CD spectroscopy. Our findings showed that the peak activity coincided with the transition of the assemblies towards a more ordered structure (Fig. 3c). This indicates that a minimum of 4 eq of zinc is necessary to attain a catalytically competent species, which aligns with the initiation of the formation of an ordered supramolecular structure.

2.3 The effect of cyclization and chirality on catalytic activity and self-assembly propensity of peptide A derivatives

Cyclic peptides offer several advantages over linear ones, such as increased stability against proteases due to the constrained conformation provided by their cyclic structure, which leads to longer half-lives and improved bioavailability.[29] Additionally, cyclization can result in enhanced binding affinity and specificity for target molecules.[45,46] However, our understanding of cyclic catalytic peptides capable of coordinating metal atoms is limited. In this study, we aim to address this gap by proposing a cyclic analogue of the catalytically active peptide A (cy-HH). To achieve this, we incorporated a glutamic acid residue into the peptide sequence, which served as a linker and formed an amide bond with the N-terminus. The cyclization neutralized the side chain, eliminating any charge interference with the catalytic reaction. The cyclic analogue exhibited improved solubility compared to its linear counterpart, which

presented challenges in determining the critical aggregation concentration (CAC). Furthermore, analysis using ATR-FTIR, ThT binding, and CD (Fig. 4a–c) did not provide any evidence of β-sheet formation.

A more subtle way of controlling conformational constrains is through alternating the chirality of amino acid residues, which can influence the packing arrangements in self-assembled cyclic peptides. Alternating D- and L-amino acids promotes the formation of assemblies due to a growing number of intermolecular interactions.[12] By incorporating D-histidines into the cyclic peptide sequence (cy-hh), we restored a self-assembly pattern similar to that of its linear counterpart. Cy-hh exhibited an increase in ThT fluorescence intensity, indicating β-sheet formation (Fig. 4a) and displayed a CAC of 54 µM (Fig. S5†), comparable to linear sequences (67 µM). The fibrillar morphology of the nanostructures was confirmed by AFM (Fig. 4d). The self-assembly of cy-hh into β-sheets was further validated by the presence of a band at 1630 cm^{-1} in the IR spectrum and characteristic CD spectral features, including a minimum at 220 nm and a maximum at 197 nm (Fig. 4b and c). In contrast to linear peptides where zinc affects the arrangement of the supramolecular assemblies, cyclic peptides do not sense the addition of Zn^{2+} ions as no shifts in the minimum are observed in the CD spectra, suggesting a lack of interaction with the cofactor, which consequently results in the absence of catalytic function (Fig. 4c).

To investigate the potential relationship between conformational rigidity and coordination deficiency, we conducted MD simulations. RMSD measurements revealed reduced backbone fluctuations (Fig. S11†) for the cyclic peptides, and cluster analysis showed a decreased number of clusters (Fig. S10†), indicating their greater rigidity compared to their linear counterparts (Table 3).

3 Conclusions

In conclusion, our study highlights the crucial role of amino acid disposition within the sequence of linear peptides for their esterase activity. We demonstrated that selecting amino acids capable of coordinating Zn^{2+} and arranging them appropriately within the peptide sequence is essential for maintaining catalytic activity. Cyclization of linear peptides can impair their catalytic function by increasing rigidity, which hinders the coordination of metal ions. This rigidity limits the necessary sequence adjustments to optimize the conformation required for effective Zn^{2+} coordination. This conformational optimization process is more feasible in flexible and conformationally heterogeneous linear peptides. Furthermore, these results suggest that chirality can play a crucial role in the self-assembly propensity of cyclic peptides. Therefore, the design and optimization of cyclic peptides with improved catalytic activity and self-assembly properties require careful consideration of various factors, including rigidity, chirality, and coordination chemistry. Further structural modifications are necessary to restore catalytic
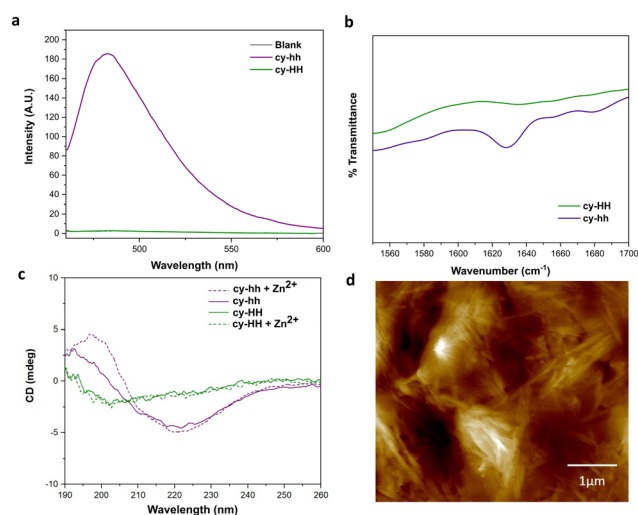

Fig. 4 Characterization of cyclic cy-HH (green) and cy-hh (purple) peptides: (a) ThT assay performed at 250 µM of peptide in presence (dashed line) and absence (solid line) of Zn^{2+}. (b) IR spectra showing a peak at 1630 cm^{-1} indicating β-sheets only for cy-hh. (c) CD spectra of cy-HH (25 µM) and cy-hh (25 µM) in presence and absence of Zn^{2+} showing β-sheets only for cy-hh. (d) AFM image showing elongated fibrils of cy-hh (250 µM).

1376 | *Mol. Syst. Des. Eng.*, 2023, **8**, 1371–1380

This journal is © The Royal Society of Chemistry and IChemE 2023

Table 3 MD-based cluster analysis of linear and cyclic peptides showing that the average RMSD values and His-His average distances are higher in peptides A and B compared to those of the cyclic ones. Cluster analysis shows a higher number of clusters and a lower percentage distribution of structures in the first three clusters for linear peptides

Peptide	Average RMSD (Å)	N clusters	1st cluster (%)	2nd cluster (%)	3rd cluster (%)	His-His avg distance (Å)
A	4.71	296	1.33%	0.66%	0.66%	11.03
B	4.62	295	1.00%	1.00%	0.66%	13.61
cy-HH	2.28	76	18.60%	14.95%	5.32%	9.42
cy-hh	1.75	30	52.16%	10.93%	7.95%	9.51

activity in the cyclic analogues cy-HH and cy-hh. These findings offer new prospects for the development of metal-dependent peptide-based catalysts in which the amino acids and their disposition within the sequence need to be carefully selected. We envision that the extension of this study to different cyclization strategies and other amino acid permutations will lead to the optimization of the geometry of the active residues and the discovery of next-generation histidine-rich peptide catalysts. With the application of this knowledge, we hope in the future to develop more efficient and selective peptide-based catalysts for ester hydrolysis.

4 Experimental

4.1 Materials

Lyophilized linear peptides (95.0%), N-terminal acetylated and C-terminal amidated, were custom synthesized by Genecust (Boynes, France). All p-nitrophenyl esters (95.0%), including p-nitrophenyl acetate (p-NPA), p-nitrophenyl butyrate (p-NPB) and p-nitrophenyl octanoate (p-NPO), Fmoc-amino acids, Novabiochem® resin (Rink Amide AM), ThT, DIPEA, HBTU, TIS, TFA and piperidine (99.0%) were purchased from Sigma-Aldrich (St. Louis, Missouri, SAD). $ZnCl_2$ was purchased from Gram mol (Zagreb, Croatia). All other chemicals and reagents are analytical grade and are available from commercial sources.

4.2 Peptide synthesis

Cyclic peptides were synthesized by fluorenylmethyloxycarbonyl (Fmoc) solid-phase peptide synthesis on the Novabiochem Rink Amide AM resin (100–200 mesh) (loading of 0.78 mmol g^{-1}) using L- and D-amino acids. The resin was swollen for 30 min in DMF. The removal of Fmoc was performed with 20% piperidine in DMF. Chain growth was carried out using a three-fold excess of amino acids over the resin in DMF, using N,N-diisopropylethylamine (DIPEA) and N,N,N',N'-tetramethyl-O-(1H-benzotriazol-1-yl) uronium hexafluorophosphate (HBTU) as coupling and activating agents in a 2:1 ratio relative to amino acids, respectively. The coupling and deprotection steps were separated by DMF (3 × 30 s) and DCM washes (3 × 30 s). Intramolecular (amide bond) cyclization was performed between the side chain of the C-terminal Glu (E) and the N-terminus. The Glu residue involved in intramolecular cyclization was protected with the 2-phenylisopropyl (O-2-PhiPr) group. After complete elongation of the peptide chain,

the resin was treated with 1% (v/v) trifluoroacetic acid (TFA) in DCM (4 × 10 min) for selective removal of O-2-PhiPr, followed by neutralization with 5% DIPEA in DCM (4 × 5 min). Cyclization was performed on resin with PyBOP/Hobt/DiPEA (5, 5 and 10 equiv) in DMF for 3 h. Mini-cleavage with ~5 mg resin was performed to check product yield after cyclization. The cleavage of the cyclic peptide from the resin was achieved using TFA : triisopropylsilane (TIS) : H_2O = 95 : 2.5 : 2.5. The crude peptide was precipitated and washed in cold diethyl ether, centrifuged (3 × 10 min) at 4 °C, dissolved in 20% acetonitrile (ACN) in MiliQ water, and lyophilized.

4.3 Peptide analysis and purification

The crude peptides were analyzed by HPLC-MS on the XSELECT CSH C18 column (4.6 × 150 mm, 3.5 μm, Waters, Milford, MA, USA) with an Agilent 1260 series HPLC chromatograph coupled to an Agilent 6460 triple quadrupole mass spectrometer system (Agilent Technologies, Santa Clara, CA, USA). The elution was carried out with linear gradients of solvent B (0.1% v/v TFA in ACN) into A (0.1% v/v TFA in H_2O) over 20 min. The peptides were purified by preparative HPLC on the Aeris PEPTIDE XB-C18 column (10 × 250 mm, 5 μm, Phenomenex) with an Agilent Infinity 1260 semipreparative HPLC instrument using a flow rate of 5 ml min^{-1} and linear gradients of solvent B (0.1% v/v TFA in ACN) in A (0.1% v/v TFA in H_2O) for 30 min with detection at 214 nm on a DAD detector. The purity of the collected fractions was analyzed and those with satisfactory purity (>90%) were merged and lyophilized. The purity of the final products was analyzed by HPLC-MS on the XSELECT CSH C18 column (4.6 × 150 mm, 3.5 μm, Waters, Milford, MA, USA) in an Agilent 1260 series HPLC chromatograph coupled to an Agilent 6460 triple quadrupole mass spectrometer system (Agilent Technologies, Santa Clara, CA, USA) eluting with linear gradients of solvent B (0.1% v/v TFA in ACN) into A (0.1% v/v TFA in H_2O) for 20 min at 1 mL min^{-1} flow rate.

4.4 Preparation of peptide solutions

The 1.1 mM stock solution of purified lyophilized peptides was prepared by dissolving the peptides in 10 mM HCl. The working solution at pH 7.4 was prepared by mixing 200 μL of the stock solution with 1.8 ml of buffer solution (25 mM Tris, 1 mM $ZnCl_2$).

4.5 Catalytic activity assessment

The catalytic activity assay was performed on a Hidex Sense microplate reader to monitor the absorbance of the product (*p*-nitrophenol) for 30 minutes (22 °C) in 96-well plates at 405 nm. Stock solutions of 0.1 M of *p*-nitrophenyl esters (*p*-nitrophenyl acetate, *p*-nitrophenyl butyrate, *p*-nitrophenyl octanoate) (Sigma-Aldrich, United States) were used to prepare substrate solutions in 25 mM Tris (pH 7.4), 1 mM $ZnCl_2$. 150 µL of freshly prepared substrate solutions (to the final substrate concentration of 0.195–0.75 mM) were added to 50 L of buffered (25 mM Tris, 1 mM $ZnCl_2$) peptide solutions at pH 7.4 (to a final peptide concentration of 25 µM). The calibration curve was experimentally obtained from a standard 4-nitrophenol (*p*-NP) solution (Sigma-Aldrich, United States) in the concentration range of 0–100 µM. The reported results correspond to the average of at least two independent measurements. Kinetic parameters were obtained by fitting the data to the Michaelis–Menten equation $V_0 = k_{cat} \cdot [E]_0 \cdot [S]_0 / (K_M + [S]_0)$ using Origin 2018 software.

4.6 Circular dichroism

The far-UV CD spectra (190–300 nm) were acquired with a Jasco J-815 spectropolarimeter with a Peltier temperature control system at 20 °C, in a 1 mm quartz cuvette under nitrogen flow and 2 nm bandwidth. Each spectrum represents an average of three scans. The peptide concentrations were maintained at 25 µM and the measurements were performed in 5 mM Tris (pH 7.4) or 5 mM Tris (pH 7.4) containing 0.5 mM $ZnCl_2$.

4.7 Zn^{2+} titrations

For the *p*-NPA assay analysis, 11 different samples were prepared on a 96-well plate. Each sample consisted of 50 µL of the peptide working solution, 100 µL of 25 mM pH 7.4 Tris buffer with various concentrations of $ZnCl_2$ (0, 6.25, 12.5, 25, 50, 100, 150, 200, 250, 300, 400 µM). Subsequently, 50 µL of *p*-NPA solution in 25 mM pH 7.4 Tris buffer (without additional zinc chloride) was added to each well, resulting in a final substrate concentration of 750 µM. For the CD measurements, nine different samples were prepared in Eppendorf tubes. Each sample contained 12.5 µL of the peptide stock solution, 500 µL of 5 mM pH 7.4 Tris buffer with various concentrations of $ZnCl_2$ (0, 25, 50, 100, 150, 200, 250, 300, 400 µM). Dissociation constants K_D (µM) were determined in OriginPro9 by fitting the data to the Hill equation $\delta_d = [Peptide_{free}]^n / (K_D^n + [Peptide_{free}])$ where K_D is the dissociation constant and n is the Hill coefficient that describes peptide cooperativity.

4.8 Thioflavin-T (ThT) binding assay and critical aggregation concentration (CAC) determination

Fluorescence measurements were performed using an Agilent Cary Eclipse fluorescence spectrophotometer. ThT binding assay was performed using a range of buffered (25 mM Tris, pH 7.4) peptide concentrations (0.0039–0.500 mM) with and without 1 mM $ZnCl_2$, incubated with ThT stock solution prepared in methanol to a final concentration of 25 µM for 15 minutes. The samples were excited at 450 nm and the emission spectra were recorded in the range of 460–600 nm on the spectrophotometer. The excitation and emission bandwidths were both set to 5 nm. The CAC was obtained by plotting the intensity of the emission peak at 480 nm against the peptide concentration.

4.9 Fourier-transform infrared spectroscopy (FTIR)

Hydrogen bonding patterns characteristic for peptide self-assembly were investigated using attenuated total reflectance Fourier transform infrared spectroscopy (ATR-FTIR). ATR-FTIR spectra were recorded for the peptide solutions in D_2O (Sigma-Aldrich, United States), using an Agilent Technologies Cary 630 FTIR in the range 650–4000 cm^{-1} with a resolution of 16 cm^{-1}.

4.10 Atomic force microscopy (AFM)

The surface topology scans of the analyzed samples are obtained by using the Bruker Dimension Icon atomic force microscope in tapping and ScanAsyst modes. Tapping mode was used to obtain a high resolution scan of surface detail by using a Bruker SNL-10 type D (low stiffness) silicon nitride cantilever with a silicon tip of 2 nm tip radius and ScanAsyst silicon nitride cantilevers. The dynamic properties of the cantilever such as natural frequency and normal stiffness are obtained using the thermal tuning method, where the thermal noise spectra of the cantilever were measured and fitted to a Lorentzian harmonic oscillator model in air which corresponded to 22 kHz for SNL10-D and 75 kHz for the ScanAsyst cantilever. The calibration obtained allows the use of a minimal contact force for the measurement that has minimal impact on the surface, so the average force used was 2 pN ± 5%. The scans were performed with scan sizes of 5 and 10 μm^2 selected from a large 90 μm^2 sweep scan with 512 scan lines each with 512 data points acquired per line. The obtained data was consequently processed in order to provide tilt and bow corrections using the proprietary Bruker Nanoscope Analysis software.

4.11 Molecular dynamics simulations

Molecular dynamics simulations were performed for linear (Ac-IHIHINI-Am, Ac-IHINIHI-Am) and head-to-side chain cyclized ([IHIHINIE]-Am, [IhIhINIE]-Am) peptides using the GROMACS simulation package (version 2023.00-TunePME) and the CHARMM36m force field.[47] Peptide molecules were built in Pymol[48] using the "fab" command and modified in the Avogadro software[49] to introduce head-to-side-chain cyclization and D-oriented histidines when needed. The Avogadro-generated MOL2 files were then uploaded to CHARMM-GUI's ligand reader and modeler (**https://www.**

1378 | *Mol. Syst. Des. Eng.*, 2023, **8**, 1371–1380

This journal is © The Royal Society of Chemistry and IChemE 2023

charmm-gui.org/?doc=input/ligandrm)[50,51] to create topologies and parameter files for such modified molecules. First, single peptide molecules were simulated to assess their flexibility, predominant conformation, and histidine distances. For this purpose, the peptides were modeled to have histidines with protonated ε-nitrogen atoms. Each solution box contained 0.08 M Tris buffer, which was also generated using ligand reader and modeler for the tris(hydroxymethyl)aminomethane molecule. The generated files were placed into the CHARMM-GUI's multicomponent assembler, prior to simulations in GROMACS. All simulations were performed using the TIP3P water model, using a temperature of 298.15 K, in a square water box 45 Å in side length. Energy minimization was limited to 50 000 steps with a convergence cutoff of 100.0 kJ mol^{-1} nm^{-1} using a steepest descent algorithm, which always ended before the step limitation was reached. The system was then equilibrated during 200 ps in an NPT ensemble using a Nose–Hoover thermostat. The simulations were run through cluster analysis using the GROMOS clustering system[52,53] in GROMACS. Whole peptide molecules (including the side chain and hydrogen atoms) were used for clustering, with a 0.1 nm RMSD cutoff.

To assess the aggregation propensity of linear peptides, and to estimate their aggregation time, multipeptide simulations were set up using the CHARMM-GUI's PDB reader and modeler[54,55] in building topology and parameter files for the multicomponent assembler. Ac-IHIHINI-Am and Ac-IHINIHI-Am were used to make two separate systems containing 24 instances of the same peptide, dissolved in a 60 Å water box and 0.025 M Tris buffer. The peptides were modeled to have histidines with protonated ε nitrogen in His at position 2 and protonated δ nitrogen in His at position 4. These systems were simulated for 500 ns. The same minimization and equilibration processes were used as with the first set of peptide simulations. A solvent accessible surface area (SASA) analysis[56] was performed on these multipeptide systems to evaluate their aggregation time.

All the simulations were run on Bura supercomputer, on 5 nodes for each individual simulation. The nodes contain 2 Xeon E5 processors with 64 GB memory, and the system runs on a Red Hat Enterprise Linux 7 and Slurm Workload Manager operating system.

Author contributions

Patrizia Janković: conceptualization, methodology, investigation, writing – original draft preparation. Marko Babić: methodology, formal analysis, writing – original draft preparation. Marko Perčić: methodology, visualization. Ana S. Pina: methodology, visualization. Daniela Kalafatovic: conceptualization, investigation, supervision, writing – reviewing and editing, funding acquisition. All authors approved the final version of the manuscript.

Conflicts of interest

There are no conflicts to declare.

Acknowledgements

Notes and references

1 X. Ren, D. Chen, Y. Wang, H. Li, Y. Zhang, H. Chen, X. Li and M. Huo, *J. Nanobiotechnol.*, 2022, **20**, 92.

2 R. Mandal, A. Ghosh, N. K. Rout, M. Prasad, B. Hazra, S. Sar, S. Das, A. Datta and P. K. Tarafdar, *Org. Biomol. Chem.*, 2023, **21**, 4473–4481.

3 A. Shamsabadi, T. Haghighi, S. Carvalho, L. C. Frenette and M. M. Stevens, *Adv. Mater.*, 2023, 2300184.

4 J. Yi, Q. Deng, Z. Liu, H. Wang, X. Liu, J. Ren and X. Qu, *Small*, 2023, 2301096.

5 P. Makam, S. S. Yamijala, V. S. Bhadram, L. J. Shimon, B. M. Wong and E. Gazit, *Nat. Commun.*, 2022, **13**, 1505.

6 H. Wei and E. Wang, *Chem. Soc. Rev.*, 2013, **42**, 6060–6093.

7 A. Chatterjee, A. Reja, S. Pal and D. Das, *Chem. Soc. Rev.*, 2022, **51**, 3047–3070.

8 T. Schnitzer, J. W. Rackl and H. Wennemers, *Chem. Sci.*, 2022, **13**, 8963–8967.

9 A. S. Pina, L. Morgado, K. L. Duncan, S. Carvalho, H. F. Carvalho, A. J. Barbosa, B. D. P. Mariz, I. P. Moreira, D. Kalafatovic and B. M. M. Faustino, *et al.*, *Chem. Sci.*, 2022, **13**, 210–217.

10 X. Liu, R. Waters, H. E. Gilbert, G. T. Barroso, K. M. Boyle and L. S. Witus, *RSC Adv.*, 2021, **11**, 23714–23718.

11 M. A. Beasley, A. D. Dunkelberger, M. D. Thum, E. S. Ryland, K. P. Fears, A. B. Grafton, J. C. Owrutsky, J. G. Lundin and C. R. So, *J. Mater. Chem. B*, 2022, **10**, 9400–9412.

12 S. Studer, D. A. Hansen, Z. L. Pianowski, P. R. Mittl, A. Debon, S. L. Guffy, B. S. Der, B. Kuhlman and D. Hilvert, *Science*, 2018, **362**, 1285–1288.

13 M. Frenkel-Pinter, M. Samanta, G. Ashkenasy and L. J. Leman, *Chem. Rev.*, 2020, **120**, 4707–4765.

14 V. Alva and A. N. Lupas, *Curr. Opin. Struct. Biol.*, 2018, **48**, 103–109.

15 J. Han, H. Gong, X. Ren and X. Yan, *Nano Today*, 2021, **41**, 101295.

16 Y. Lou, B. Zhang, X. Ye and Z.-G. Wang, *Mater. Today Nano*, 2023, 100302.

17 P. Dowari, M. K. Baroi, T. Das, B. K. Das, S. Das, S. Chowdhuri, A. Garg, A. Debnath and D. Das, *J. Colloid Interface Sci.*, 2022, **618**, 98–110.

18 L. Wang, N. Wang, W. Zhang, X. Cheng, Z. Yan, G. Shao, X. Wang, R. Wang and C. Fu, *Signal Transduction Targeted Ther.*, 2022, **7**, 48.

This journal is © The Royal Society of Chemistry and IChemE 2023

Mol. Syst. Des. Eng., 2023, **8**, 1371–1380 | **1379**

19 A. Levin, T. A. Hakala, L. Schnaider, G. J. Bernardes, E. Gazit and T. P. Knowles, *Nat. Rev. Chem.*, 2020, **4**, 615–634.

20 O. Zozulia, M. Dolan and I. Korendovych, *Chem. Soc. Rev.*, 2018, **47**, 3621–3639.

21 S. Carvalho, D. Q. Peralta Reis, S. V. Pereira, D. Kalafatovic and A. S. Pina, *Isr. J. Chem.*, 2022, **62**, e202200029.

22 A. Lampel, R. Ulijn and T. Tuttle, *Chem. Soc. Rev.*, 2018, **47**, 3737–3758.

23 P. Janković, I. Šantek, A. S. Pina and D. Kalafatovic, *Front. Chem.*, 2021, **9**, 723473.

24 Z. Li, S. Y. Joshi, Y. Wang, S. A. Deshmukh and J. B. Matson, *Angew. Chem., Int. Ed.*, 2023, e202303755.

25 R. Ree, S. Varland and T. Arnesen, *Exp. Mol. Med.*, 2018, **50**, 1–13.

26 Y. Marciano, N. Nayeem, D. Dave, R. V. Ulijn and M. Contel, *ACS Biomater. Sci. Eng.*, 2023, **9**, 3379–3389.

27 T. A. Hill, N. E. Shepherd, F. Diness and D. P. Fairlie, *Angew. Chem., Int. Ed.*, 2014, **53**, 13020–13041.

28 R. Jwad, D. Weissberger and L. Hunter, *Chem. Rev.*, 2020, **120**, 9743–9789.

29 H. Zhang and S. Chen, *RSC Chem. Biol.*, 2022, **3**, 18–31.

30 Y. Maeda, O. V. Makhlynets, H. Matsui and I. V. Korendovych, *Annu. Rev. Biomed. Eng.*, 2016, **18**, 311–328.

31 K. L. Duncan and R. V. Ulijn, *Biocatalysis*, 2015, **1**, 67–81.

32 P. Janković, E. Otović, G. Mauša and D. Kalafatovic, *Data Brief*, 2023, 109290.

33 S. Lai, D. Yang, Y. Wang, X. Ju, W. Liu, H. Li, D. Wang, Y. Zhao, J. Wang and H. Xu, *Colloids Surf., A*, 2023, **665**, 131257.

34 C. M. Rufo, Y. S. Moroz, O. V. Moroz, J. Stohr, T. A. Smith, X. Hu, W. F. DeGrado and I. V. Korendovych, *Nat. Chem.*, 2014, **6**, 303–309.

35 Z. Al-Garawi, B. McIntosh, D. Neill-Hall, A. Hatimy, S. Sweet, M. Bagley and L. Serpell, *Nanoscale*, 2017, **9**, 10773–10783.

36 R. Song, X. Wu, B. Xue, Y. Yang, W. Huang, G. Zeng, J. Wang, W. Li, Y. Cao and W. Wang, *et al.*, *J. Am. Chem. Soc.*, 2018, **141**, 223–231.

37 L. Gentilucci, R. De Marco and L. Cerisoli, *Curr. Pharm. Des.*, 2010, **16**, 3185–3203.

38 M. Babić, P. Janković, S. Marchesan, G. Mauša and D. Kalafatovic, *J. Chem. Inf. Model.*, 2022, **62**, 6398–6410.

39 M. Belieres, N. Chouini-Lalanne and C. Dejugnat, *RSC Adv.*, 2015, **5**, 35830–35842.

40 T. D. Do, N. E. De Almeida, N. E. LaPointe, A. Chamas, S. C. Feinstein and M. T. Bowers, *Anal. Chem.*, 2016, **88**, 868–876.

41 P. I. Haris and D. Chapman, *Biopolymers*, 1995, **37**, 251–263.

42 A. Rodger and M. A. Ismail, *Spectrophotometry and Spectrofluorimetry: A Practical Approach*, Oxford University Press, 2000.

43 M. Lee, T. Wang, O. V. Makhlynets, Y. Wu, N. F. Polizzi, H. Wu, P. M. Gosavi, J. Stohr, I. V. Korendovych and W. F. DeGrado, *et al.*, *Proc. Natl. Acad. Sci. U. S. A.*, 2017, **114**, 6191–6196.

44 K. A. McCall, C. Chin Huang and C. A. Fierke, *J. Nutr.*, 2000, **130**, 1437S–1446S.

45 K. Patel, L. J. Walport, J. L. Walshe, P. D. Solomon, J. K. Low, D. H. Tran, K. S. Mouradian, A. P. Silva, L. Wilkinson-White and A. Norman, *et al.*, *Proc. Natl. Acad. Sci. U. S. A.*, 2020, **117**, 26728–26738.

46 S. H. Joo, *Biomol. Ther.*, 2012, **20**, 19.

47 J. Huang, S. Rauscher, G. Nawrocki, T. Ran, M. Feig, B. L. de Groot, H. Grubmuller and A. D. MacKerell, *Nat. Methods*, 2017, **14**, 71–73.

48 L. Schrodinger and W. DeLano, *PyMOL*, **http://www.pymol.org/pymol**.

49 M. D. Hanwell, D. E. Curtis, D. C. Lonie, T. Vandermeersch, E. Zurek and G. R. Hutchison, *J. Cheminf.*, 2012, **4**, 17.

50 S. Jo, T. Kim, V. G. Iyer and W. Im, *J. Comput. Chem.*, 2008, **29**, 1859–1865.

51 S. Kim, J. Lee, S. Jo, C. L. Brooks III, H. S. Lee and W. Im, *J. Comput. Chem.*, 2017, **38**, 1879–1886.

52 X. Daura, K. Gademann, B. Jaun, D. Seebach, W. F. van Gunsteren and A. E. Mark, *Angew. Chem., Int. Ed.*, 1999, **38**, 236–240.

53 H. Berendsen, D. van der Spoel and R. van Drunen, *Comput. Phys. Commun.*, 1995, **91**, 43–56.

54 S. Jo, X. Cheng, S. M. Islam, L. Huang, H. Rui, A. Zhu, H. S. Lee, Y. Qi, W. Han, K. Vanommeslaeghe, A. D. MacKerell, B. Roux and W. Im, *Biomolecular Modelling and Simulations*, Academic Press, 2014, vol. 96, pp. 235–265.

55 S.-J. Park, N. Kern, T. Brown, J. Lee and W. Im, *J. Mol. Biol.*, 2023, 167995.

56 F. Eisenhaber, P. Lijnzaad, P. Argos, C. Sander and M. Scharf, *J. Comput. Chem.*, 1995, **16**, 273–284.

Electronic supplementary information (ESI)

Factors influencing the catalytic activity of metal-dependent histidine-rich peptides: sequence, conformation, stereochemistry, self-assembly or their interplay?

Patrizia Janković,[a] Marko Babić,[a] Marko Perčić,[b,c,d], Ana S. Pina,[e] and Daniela Kalafatovic,[*a,d]

[a] University of Rijeka, Department of Biotechnology, Radmile Matejčić 2, 51000 Rijeka, Croatia.
[b] University of Rijeka, Faculty of Engineering, Vukovarska 58, 51000 Rijeka, Croatia.
[c] University of Rijeka, Centre for Micro- and Nanosciences and Technologies, 51000 Rijeka, Croatia.
[d] University of Rijeka, Center for Artificial Intelligence and Cybersecurity, 51000 Rijeka, Croatia.
[e] Instituto de Tecnologia Química e Biológica António Xavier (ITQB), Universidade Nova de Lisboa, Av. da República, 2780-157, Oeiras, Portugal.

* Correspondence: daniela.kalafatovic@uniri.hr
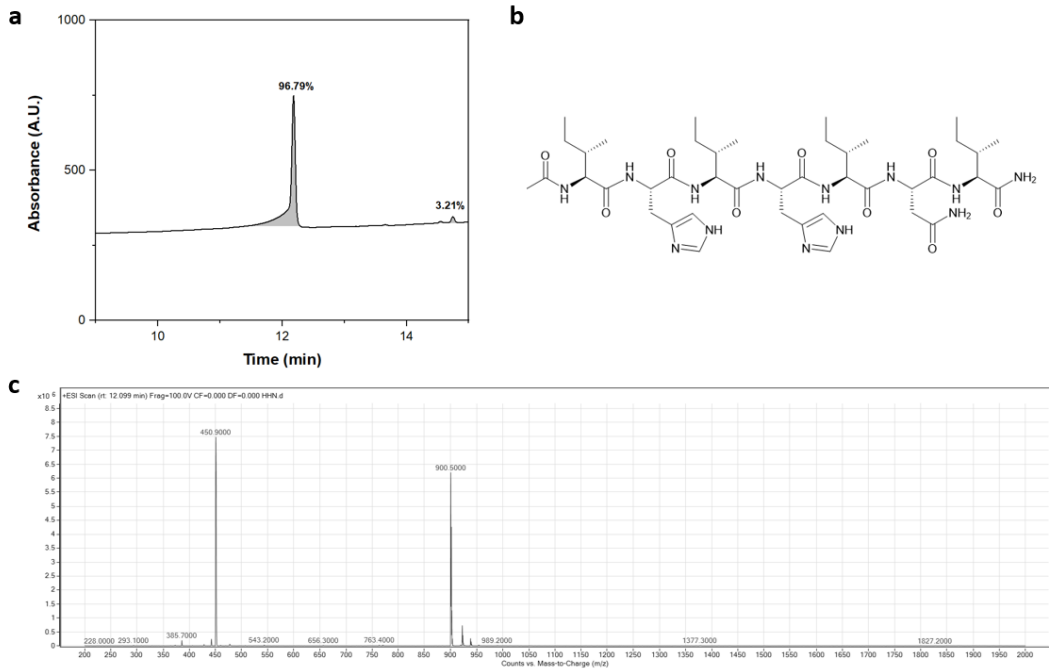
Figure S1: **a**) LC chromatogram at 220 nm (purity of 96.79%), **b**) chemical structure and (**c**) the MS trace for Ac-IHIHINI-Am (peptide A) (m/z 900.5) .
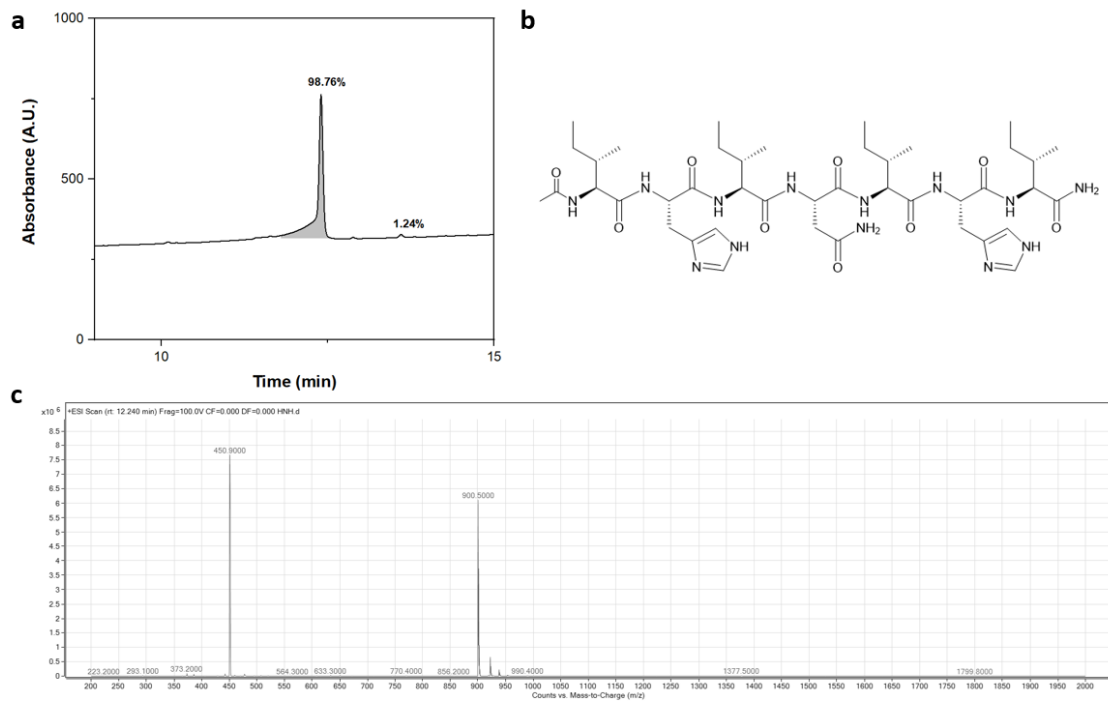
Figure S2: **a**) LC chromatogram at 220 nm (purity of 98.76%), **b**) chemical structure and (**c**) the MS trace for Ac-IHINIHI-Am (peptide B) (m/z 900.5) .
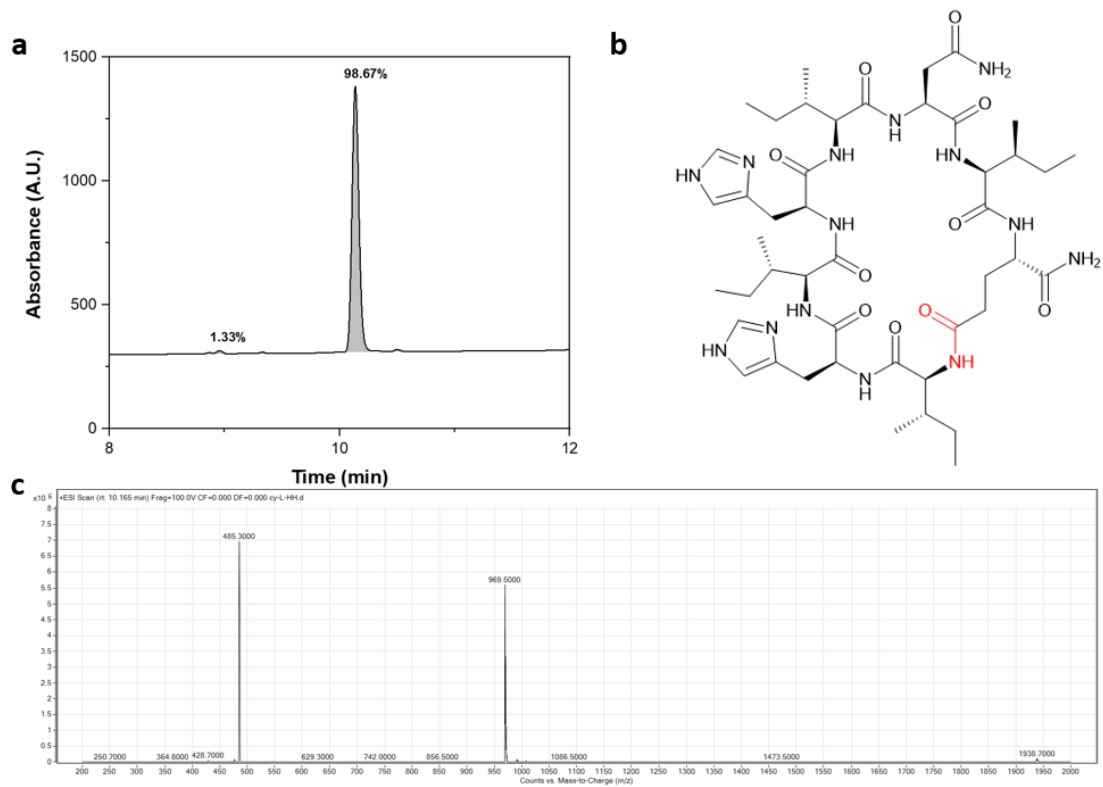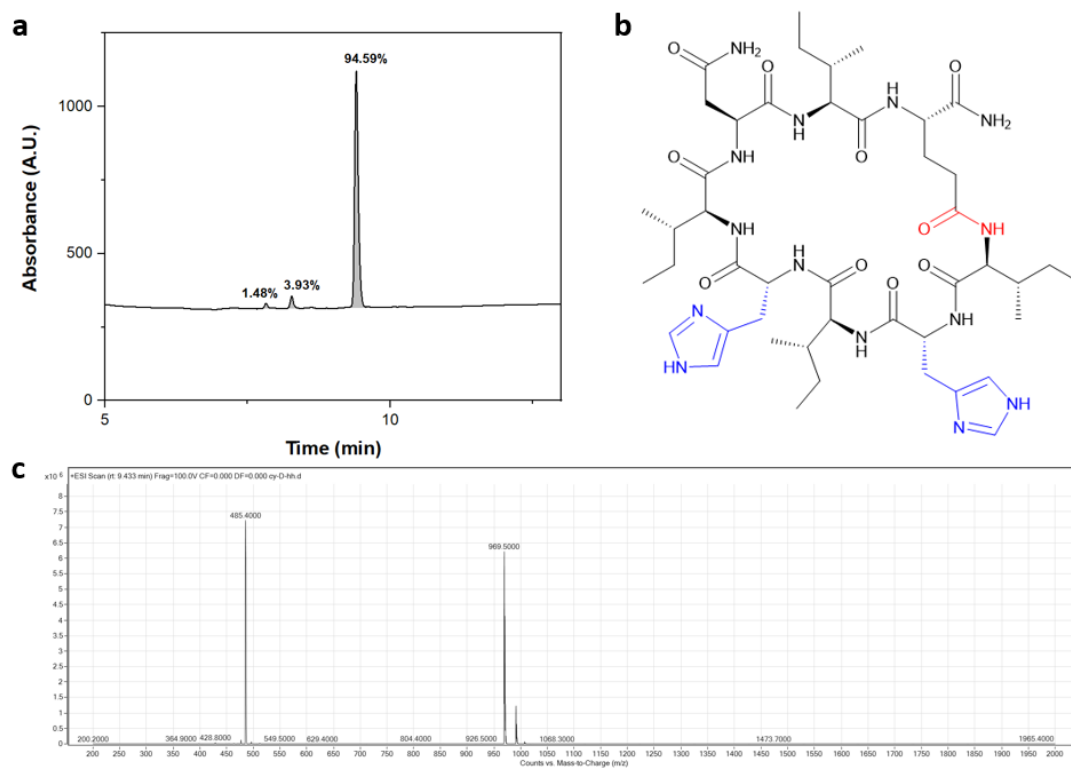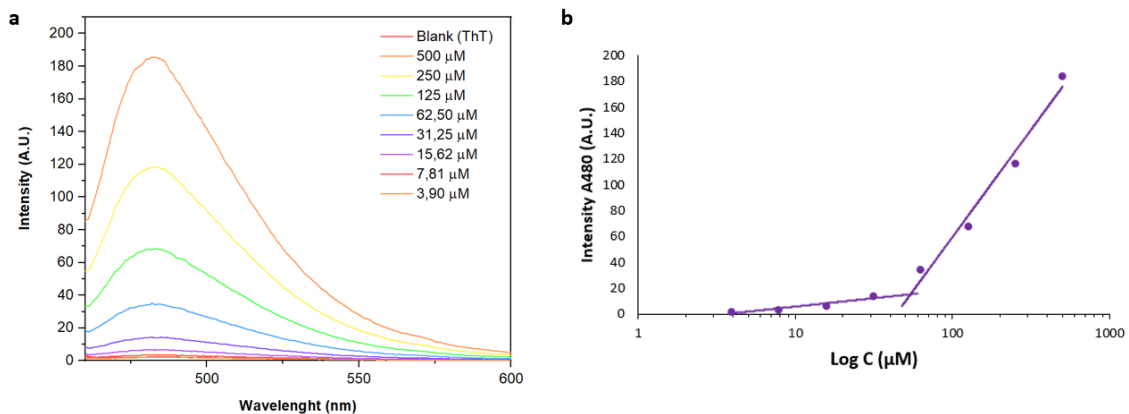
Figure S3: **a**) LC chromatogram at 220 nm (purity of 98.67%), **b**) chemical structure and (**c**) the MS trace for [IHIHINI]-Am (cy-HH) (m/z 969.5) .

Figure S4: **a**) LC chromatogram at 220 nm (purity of 94.59%), **b**) chemical structure and (**c**) the MS trace for [IhIhINI]-Am (cy-hh) (m/z 969.5) .

Figure S5: **a**) Fluorescence intensities of ThT at different concentrations of cy-hh, **b**) CAC in MiliQ water, plotted as a function of ThT fluorescence emission at 480 nm.
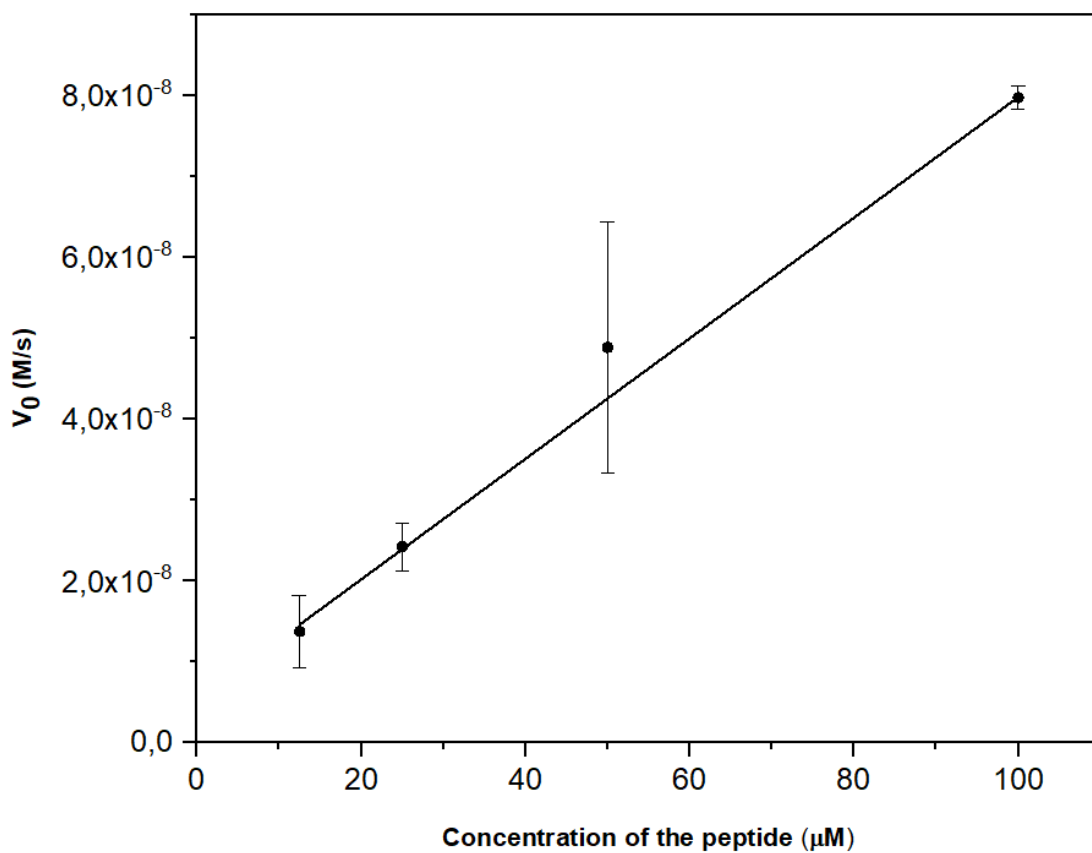

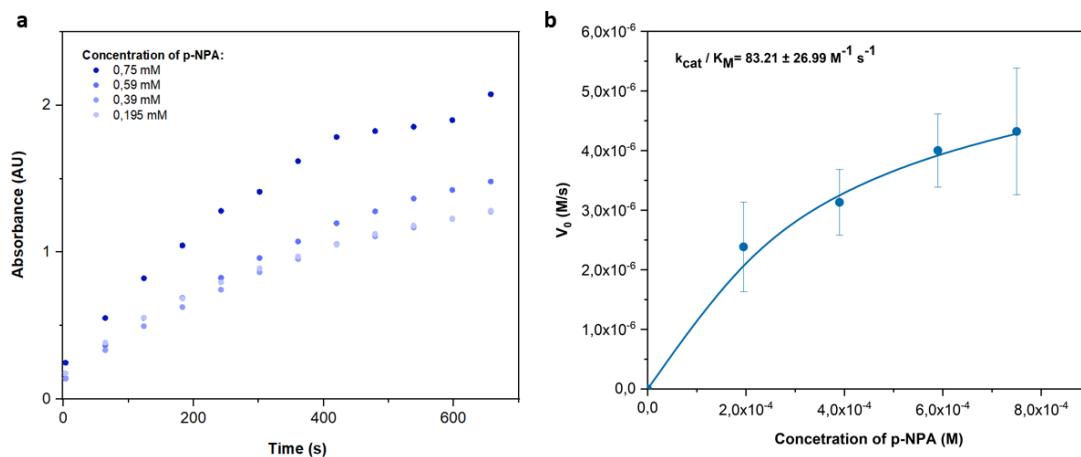Figure S6: Dependence of p-NPA hydrolysis rate on the concentration of the peptide B.

Figure S7: (a) Kinetic plot and (b) Michaelis-Menten graph for peptide A in 25 mM TRIS, 1 mM $ZnCl_2$ at pH 8 was employed for the determination of a k_{cat}/K_M value of 83.21 ± 26.99 M^{-1} s^{-1}.
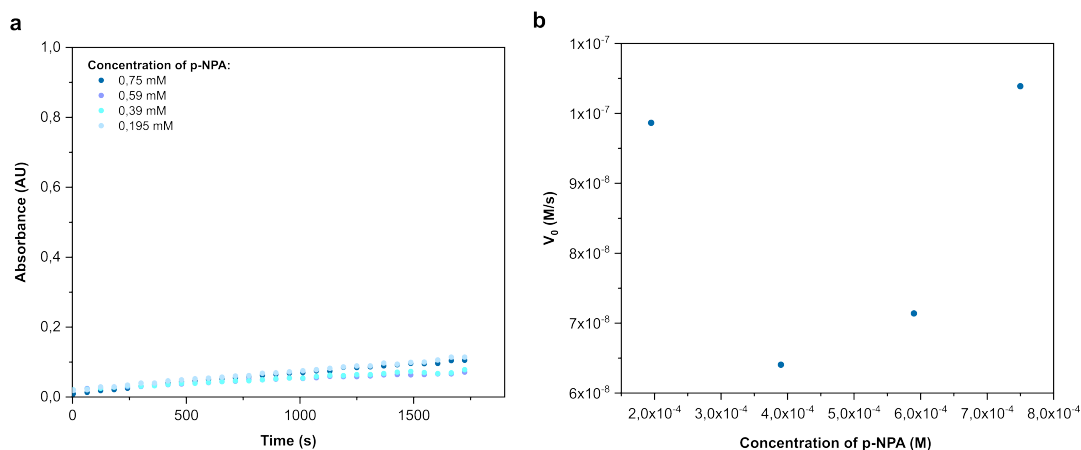

Figure S8: (a) Kinetic plot and (b) Michaelis-Menten graph for Peptide A in 25 mM TRIS Buffer at pH 7.4 without $ZnCl_2$, demonstrating minimal catalytic activity resulting in the inability to calculate kinetic parameters.
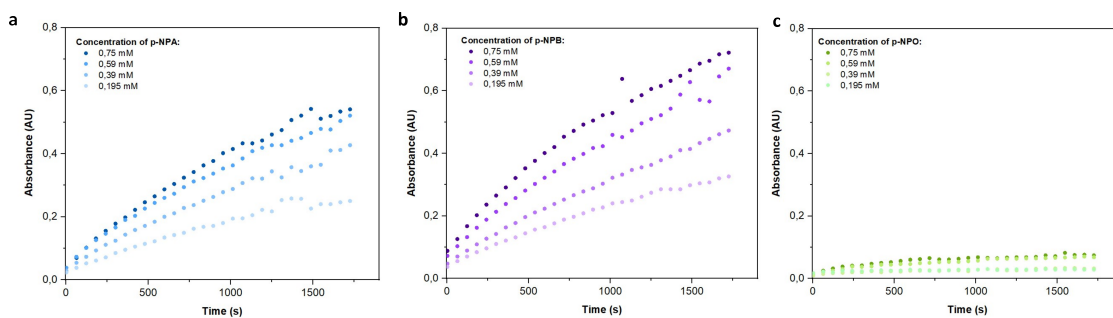

Figure S9: Kinetic plots of a) p-NPA, b) p-NPB, and c) p-NPO assayed for Peptide A at pH 7.4 in 25 mM TRIS Buffer with 1 mM $ZnCl_2$.
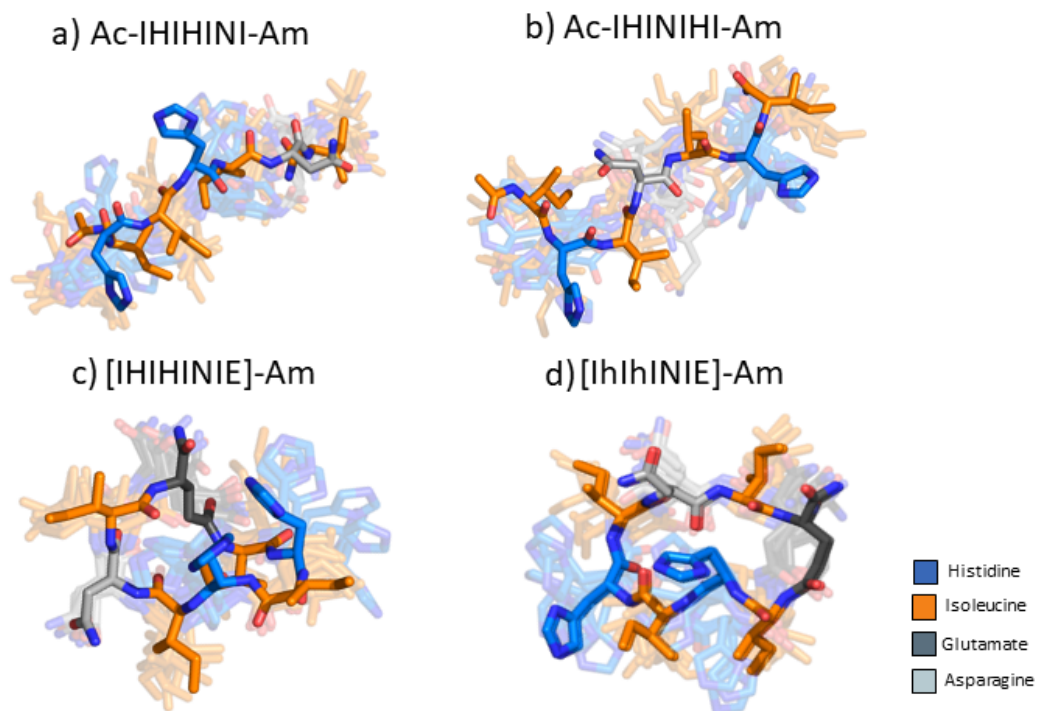
Figure S10: Cluster analysis of (**a**) Ac-IHIHINI-Am; (**b**) Ac-IHINIHI-Am; (**c**) [IHIHINIE]-Am; (**d**) [IhIhINIE]-Am. Clusters 1 to 10 are overlapped, the most dominant cluster is opaque, the remaining 9 are transparent.
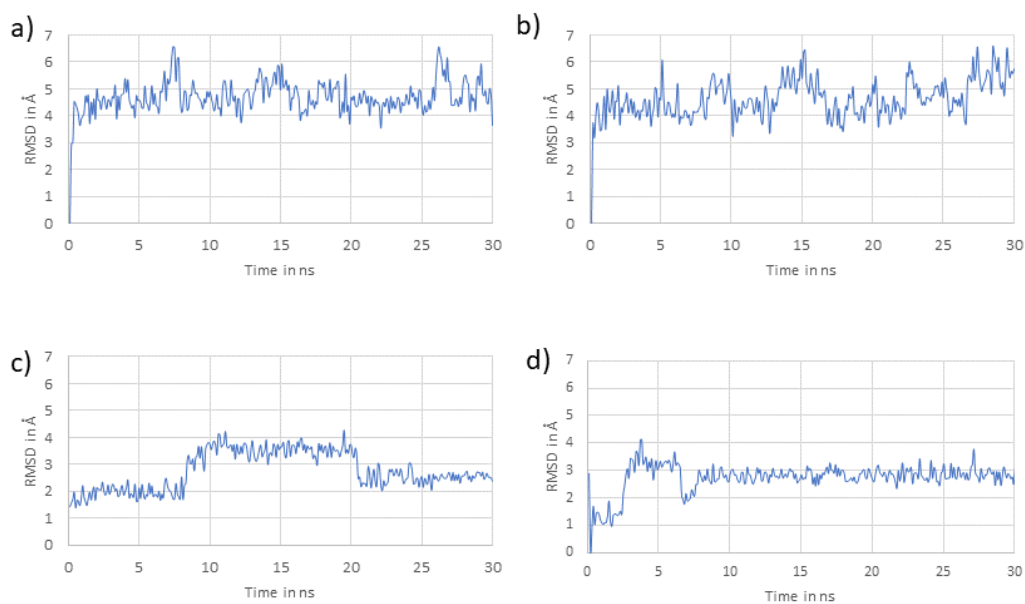

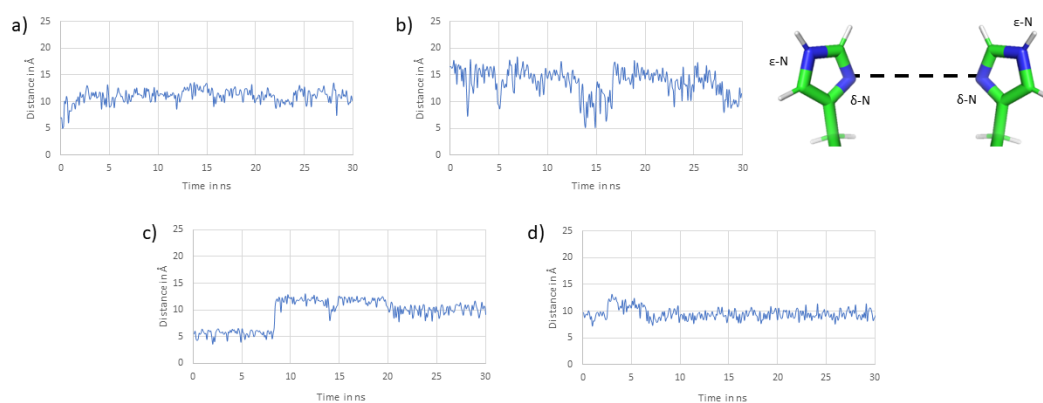Figure S11: RMSD plots for (**a**) Ac-IHIHINI-Am; (**b**) Ac-IHINIHI-Am; (**c**) [IHIHINIE]-Am; (**d**) [IhIhINIE]-Am.

Figure S12: N-δ-His to N-δ-His average distance plots (reported in Table 3) for (**a**) Ac-IHIHINI-Am; (**b**) Ac-IHINIHI-Am; (**c**) [IHIHINIE]-Am; (**d**) [IhIhINIE]-Am.
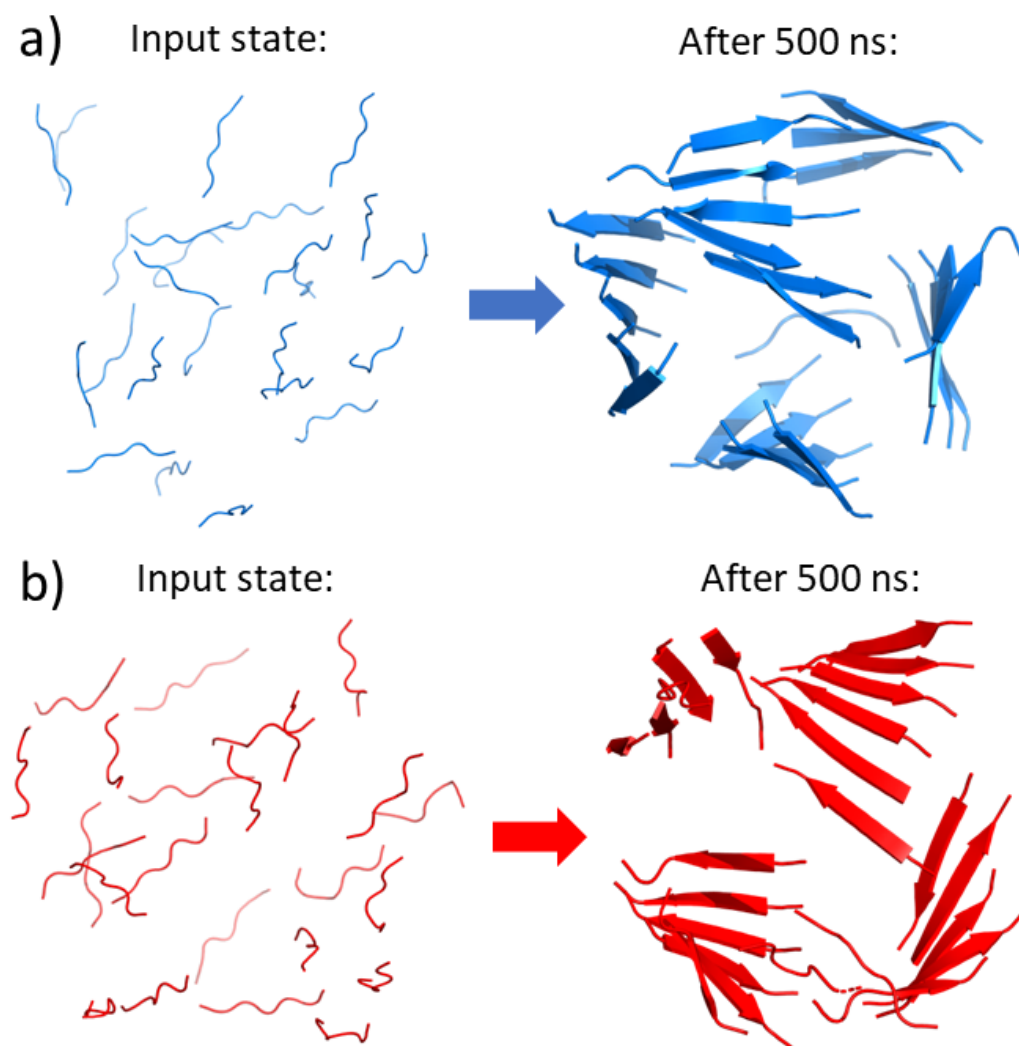

Figure S13: MD simulations of linear peptides (**a**) Ac-IHIHINI-Am; (**b**) Ac-IHINIHI-Am. The images show the initial Monte-Carlo placement of 24 peptides in solution and their aggregation into β-sheet structures after 500 ns.
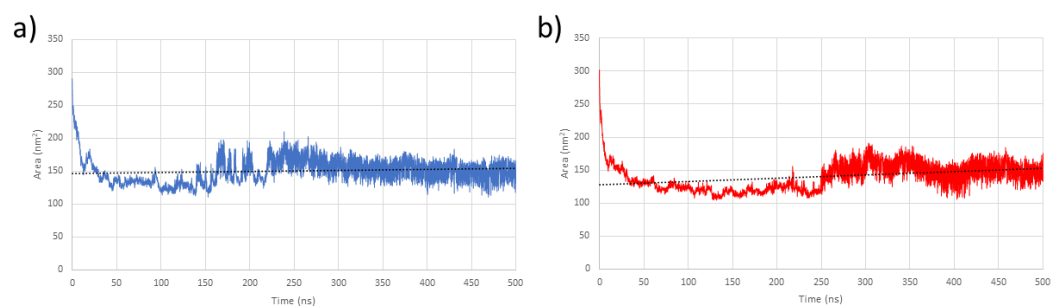
Figure S14: SASA analysis of (**a**) Ac-IHIHINI-Am; (**b**) Ac-IHINIHI-Am simulations in water and 0.08 M Tris buffer

Short catalytic peptides with tunable activity: Cys confers functionality and adaptability

Patrizia Janković[1] and **Daniela Kalafatović**[1,✉]

[1]University of Rijeka, Faculty of Biotechnology and Drug Development, Radmile Matejčić 2, 51000 Rijeka, Croatia

This study explores the catalytic potential of short peptides containing Cys, a potent nucleophile, able to hydrolyze a variety of ester substrates, including *p*-NPP and ATP, while enabling control and direction of catalytic activity through thiol oxidation. We identified Ac-CTLGLGSHCGG-Am (CG11), as a potential tunable catalyst capable of hydrolyzing ester and phosphoester substrates. We synthesized multiple analogues with varying sequence compositions and lengths and determined the effect of these changes on the catalytic efficiency. We showed that cyclization through disulfide bridge formation offered tunability and reversibility, while head-to-side chain cyclization conferred excellent resistance to proteases. Additionally, we demonstrated the ability of inactive cy-CG11 to undergo reduction and ring opening to its linear functional form in a physiological setting, specifically in the presence of elevated glutathione levels. These findings provide valuable insights for fine-tuning the characteristics of peptide-based catalysts and pave the way to their potential applicability in a biological context such as targeting glutathione disbalance and providing phosphatase activity.

Introduction

Catalytic peptides play an important role in facilitating various biochemical reactions and find applications in electrochemical sensing, environmental remediation and industrial production (1–5). Comprised of short amino acid sequences, peptides with their innate biocompatibility (6) became promising catalysts that have the ability to mimic enzyme functions with improved versatility and selectivity compared to inorganic designs (7–9). However, the development of effective peptide catalysis presents challenges due to structural flexibility and conformational heterogeneity of short peptides compared to well-defined 3D enzyme structures. To this end, peptide self-assembly in ordered supramolecular nanostructures or compartmentalization into coacervates, formed through intermolecular forces, emerged as a way to improve catalytic performance (10–12). Existing peptide-based design strategies include scaffolds in which catalytic triad or His residues are inserted, and in combination with metal cofactors promote catalytic activity (12–14). The most common triad used in catalytic peptides is Ser, His and Asp/Glu as nucleophile, base and acid, respectively (15, 16). However, little attention has been paid to Cys as a nucleophile in the design of catalytic peptides (17).

Cysteine (Cys), a versatile sulfur-containing amino acid, plays a fundamental role in biological processes (18). The thiol group of Cys, characterized by its tunable reactivity and ability to regenerate, serves a critical role in redox sensitization, essential for cellular signaling and antioxidant defense mechanisms, in addition to its involvement in catalysis (19).

In proteins, Cys is highly conserved only if needed for a specific function such as nucleophilicity, high affinity metal binding, and/or structural stabilization through disulfide bridges, whereby the distance between cysteine residues is also strictly conserved determined by their requirement to either maintain a reduced state or engage in disulfide bridge formation (20). Cys can often be found in organisms that live in harsh environments, such as thermofiles, where disulfide bonds serve as structural stabilizers. However, its low abundance at protein surfaces might be an evolutionary adaptation as a consequence of its high reactivity at physiological pH. The Ser-to-Cys mutation in the active site of engineered lipases can improve their activity and even lead to a change in the catalytic mechanism (21). However, in protein engineering, such reactivity can pose challenges, and sulfur chemistry is often suppressed by substituting Cys with Ser, that shows a similar chemical structure but lower reactivity (22). In peptide design, we can leverage and control the reactivity of Cys through the environment, exploiting it as an advantageous feature for tunable functionality.

In this paper, we set out to determine whether we could design tunable short peptide catalysts able to sense the redox environment. This dual function of catalysis and sensing would be conferred by fine-tuning the number of Cys residues, and consequently the corresponding number of thiol groups in the peptide sequence, which would adjust its redox state depending on the environment. Taking inspiration from protein-glutamate methylesterases (CheD), a bacterial enzyme involved in the chemotaxis signaling pathway (23, 24) that uses Cys as nucleophile for its catalytic mechanism, we designed the Ac-TLGLGSHCGG-Am (CG10) decapeptide. Interestingly, in CheD's active site, the catalytic triad residues were not only proximal in spatial configuration but also closely located at the sequence level. As shown in Figure 1, we selected residues important for catalysis (Thr, His and Cys) (25) referred to as functional and connected them through a structural moiety (LGLGS) and added a GG linker at the C-terminus for easier synthesis. Through a series of mutations at the sequence level, we identified that Ac-CTLGLGSHCGG-Am (CG11) has esterase and phosphoesterase activity that can be switched off (cyclic) and on (linear) with redox changes.
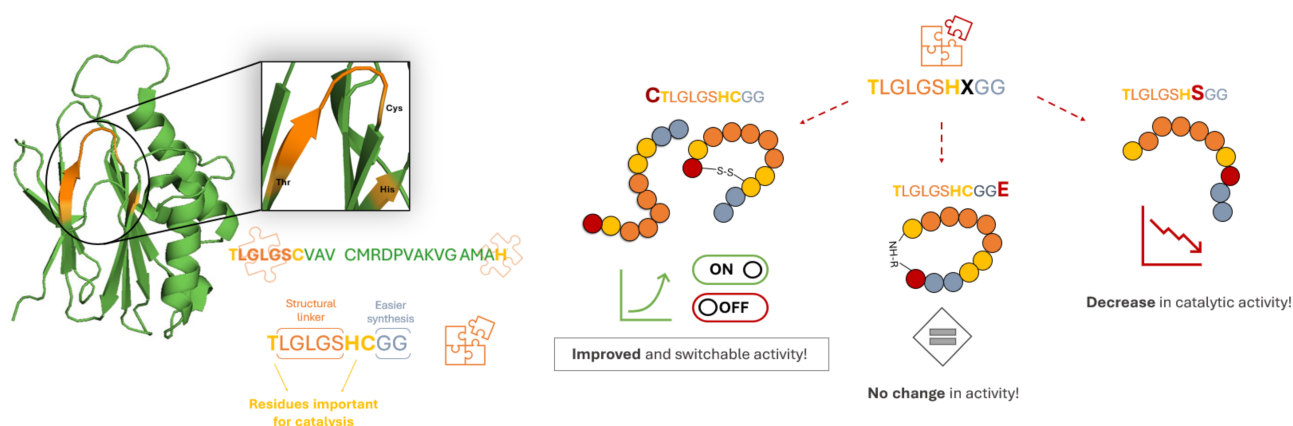
Fig. 1. Taking inspiration from protein-glutamate methylesterases (CheD) belonging to the class of carboxylic-ester hydrolases (EC3.1.1), we designed the Ac-TLGLGSHCGG-Am (CG10) peptide by selecting residues important for catalysis (Thr, His and Cys) referred to as functional and connecting them through a structural moiety (LGLGS) with the addition of GG linker for easier synthesis to avoid Cys racemization. Through modifications of the CG110 sequence, aimed at regulating the number of free thiol groups, including the addition of Cys at the N-terminus (CG11), cyclization of CG11 through disulfide bridge formation (cy-CG11), addition of Glu at the C-terminus for head-to-side chain cyclization (cy-TE10), and a Cys to Ser nucleophile mutation (TSH10), we correlated catalytic efficiency with the number of free thiol groups. We identified Ac-CTLGLGSHCGG-Am (CG11) as the best catalyst that offers dual esterase and phosphoesterase activity that can be switched off (cyclic) and on (linear) with changes in the redox environment.

Results

We propose short catalytic peptides containing one or more Cys residues and show how modifications at the sequence level, including spontaneous and synthetically controlled cyclization, can affect their catalytic activity (Table 1). This was confirmed on the model reaction for ester hydrolysis using *p*-NPA assay, where the catalytic efficiency could be correlated with the number of free thiol groups in the sequence. Furthermore, the CG11 peptide also showed phosphatase activity when tested on more complex substrates such as *p*-NPP and the biologically relevant ATP.

Number of free thiol groups determines the catalytic efficiency of short peptides. Inspired by the active site of protein-glutamate methylesterase (CheD), belonging to the class of carboxylic-ester hydrolases (EC3.1.1), the Ac-TLGLGSHCGG-Am (CG10) sequence was adapted to contain Thr, His and Cys triad residues separated by the LGLGS structural spacer and the GG moiety at the C-terminus to avoid racemization of Cys during solid phase peptide synthesis (SPPS). All proposed sequences were acetylated at the N-terminus and amidated at the C-terminus to minimize the effect of terminal charges on catalytic efficiency (26). The main modifications of the original CG10 sequence introduced with the intention to control the number of free thiol groups, are as follows:

- Addition of Cys at the N-terminus (CG11)

- Cyclization of CG11 through disulfide bridge formation (cy-CG11)

- Addition of the Glu at the C-terminus and head-to-side chain cyclization (cy-TE10)

- Cys to Ser nucleophile mutation (TSH10)

Two of these modifications led to cyclic analogues, with the aim of assessing the effect of rigidity on catalytic activity in addition to the sequence composition. Cyclization of peptides is advantageous because it leads to enhanced structural rigidity, improved serum stability, higher binding affinity for receptors, and better cell membrane permeability (27, 28), characteristics that are important for biomedical applications. We have previously shown that head-to-side chain cyclization of histidine-rich peptide catalysts led to a loss of catalytic activity because the rigidity of the cyclic peptide affected zinc coordination efficiency, important for catalysis (11). We have also shown that an interplay of sequence composition, self-assembly propensity and metal coordination efficiency dictated the catalytic activity. However, the triad-based peptide analogues presented in this paper are not cofactor-mediated, and therefore they offer an opportunity to directly evaluate the effect of cyclization on the catalytic efficiency of short linear and cyclic versions.

For this purpose, CG10 was modified by adding a Cys residue to its N-terminus (CG11) with two intentions: i) to determine the impact of an additional thiol group on *p*-NPA hydrolysis of CG11 in its linear form and ii) to allow the cyclization through disulfide bridge formation (cy-CG11) and evaluate the *p*-NPA hydrolysis by its cyclic form. Alternatively, Glu was added at the C-terminus of CG10 to allow the head-to-side chain cyclization by forming an amide bond between the N-terminus and the Glu side chain (cy-TE10), after selective deprotection of the 2-phenylisopropyl (O-2-PhiPr) group. In this way, the cyclization did not affect the nucleophile as in the cy-CG11 analogue, allowing the comparison of the linear (CG10) and cyclic (cy-TE10) versions with one free Cys residue.

The linear CG10 peptide exhibited a catalytic efficiency (k_{cat}/K_M) of 5.22 $M^{-1}s^{-1}$ in the hydrolysis of *p*-NPA, a performance comparable to that of previously described catalytic systems that utilize residues from the catalytic triad

Sequence	Acronym	Sequence feature / modification	k_{cat} $\times 10^{-2}$ (s^{-1})	K_M $\times 10^{-3}$ (M)
Ac-**TLGLGSHC**GG-Am	CG10	Residues important for catalysis (Thr, His, Cys)	0,7	1,36
Ac-**C**TLGLGSH**C**GG-Am	CG11	Introduction of Cys at N-terminus	1,0	1,36
[**TLGLGSHC**GGE]-Am	cy-TE10	Introduction of Glu at C-terminus & cyclization	0,5	0,91
[**C**TLGLGSH**C**GG]-Am	cy-CG11	Cyclization through S-S bond	2,0	48,0
Ac-**TLGLGSHS**GG-Am	TSH10	Cys to Ser nucleophile mutation	0,1	1,76

(13). However, to our knowledge, CG10 represents the first instance of a short peptide-based system achieving such catalytic activity without the need for self-assembly. Upon the addition of N-terminal Cys (CG11), the activity improved to a k_{cat}/K_M of 7.37 $M^{-1}s^{-1}$, exceeding the catalytic efficiencies of many systems utilizing the catalytic triad reported to date (13).

Next, addressing the challenge posed by the inherent flexibility of linear peptides leading to lower catalytic efficiencies compared to enzymes, we evaluated the catalytic activity of cyclic analogues obtained by two different cyclization methods: one with no free thiol groups (cy-CG11) and the one that preserves the free thiol group (cy-TE10). The cy-CG11 analogue was obtained by performing intramolecular thiol oxidation between the side chains of two Cys residues. Cyclization was performed under controlled conditions with low concentrations of peptides to avoid dimerization and oligomerization, yielding a cyclic counterpart (cy-CG11). Although it retained other components of the catalytic triad such as Thr and His, cy-CG11 exhibited unexpectedly low efficiency, with a k_{cat}/K_M of 0.42 $M^{-1}s^{-1}$ (Fig. 2). On the other hand, the cyclic analogue with one free thiol, cy-TE10 was synthesized by introducing a glutamic acid at the C-terminus of CG10 to allow head-to-side chain cyclization while maintaining the free Cys nucleophile within the sequence. Cy-TE10 showed catalytic activity comparable to that of its linear analogue CG10, with a k_{cat}/K_M of 5.21 $M^{-1}s^{-1}$. These results indicate that in the absence of the thiol nucleophile other residues are unable to take on its role, resulting in loss of activity. However, when the catalytic efficiencies of the linear analogues CG10 and CG11, which differ by one Cys, are compared, the observed increase in efficiency is not directly proportional to the number of free thiol groups in the sequence, suggesting that the interplay of multiple factors at the sequence level, possibly including other components of the catalytic triad, determine the overall catalytic efficiency.

Furthermore, we aimed to determine whether the activity strictly relies on the presence of free thiols or other amino acids commonly found to be part of the catalytic triad could take over the catalytic function. CG10 was modified by replacing Cys (containing a thiol group) with Ser (containing a hydroxyl group) (TSH10). This mutation led to a 9-fold lower catalytic efficiency of TSH10 (k_{cat}/K_M of 0.57 $M^{-1}s^{-1}$) compared to CG10 (Fig. 1), indicating that the reaction of p-NPA hydrolysis is specifically susceptible to the presence of Cys and its free thiol groups.

In summary, CG11 showed improved catalytic activity compared to CG10, but this enhanced activity was compromised by thiol oxidation, leading to cyclization (cy-CG11), underscoring the indispensability of Cys for catalysis. On the other hand, head-to-side chain cyclization (cy-TE10) preserved the catalytic activity, as it did not affect the indispensable free thiol group in the sequence. Moreover, the substitution of Cys with Ser (TSH10) resulted in a decrease in activity, highlighting the superior role of Cys as nucleophile.
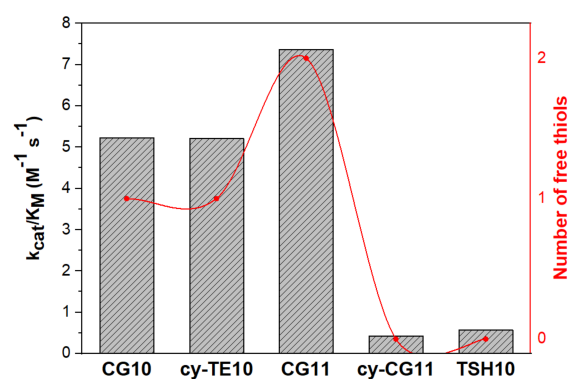

Fig. 2. Effect of thiol groups and sequence length on catalytic activity. Histogram of catalytic efficiency of peptides with two free thiol groups (CG11), one free thiol group (cy-TE10, CG10) and whitout free thiols (TSH10, cy-CG11) showing that cysteins are crucial for the catalytic activity towards p-NPA.

For comparison with CG10-based sequences, derived from the active site of the CheD enzyme, that rely on the presence of Cys, we identified a potential peptide catalyst inspired by a different enyzme, 1-alkyl-2-acetylglycerophosphocholine esterase, which naturally contains Ser as part of the catalytic triad. The proposed sequence, Ac-SGNYDYLHGE-Am (SE10), in addition to the nucleophile, incorporates Asp and His as catalytic acid and base, respectively. Gly and Asn are incorporated as residues that form the oxyanion hole, while two Tyr residues and one Leu are included to surround the catalytic acid and base, replicating their arrangement within the enzyme active site. Additionally, we included a Glu at the C-terminus for cyclization through the previously described head-to-side chain method. The obtained SE10 peptide demonstrated a k_{cat}/K_M of 1.19 $M^{-1}s^{-1}$ for the hydrolysis of p-NPA, that remained unchanged upon cyclization into cy-SE10 (Fig. S12). However, this represents a 4-fold decrease in activity compared to CG10. These findings underscore the significance of opting for Cys over Ser as a nucleophile in short catalytic peptides for ester hydrolysis and pave the way for catalytic control through dynamic covalent chemistry by managing thiol oxidation.

Reversible oxidation of CG11 can be controlled by the environment. It is well known that systems with mul-
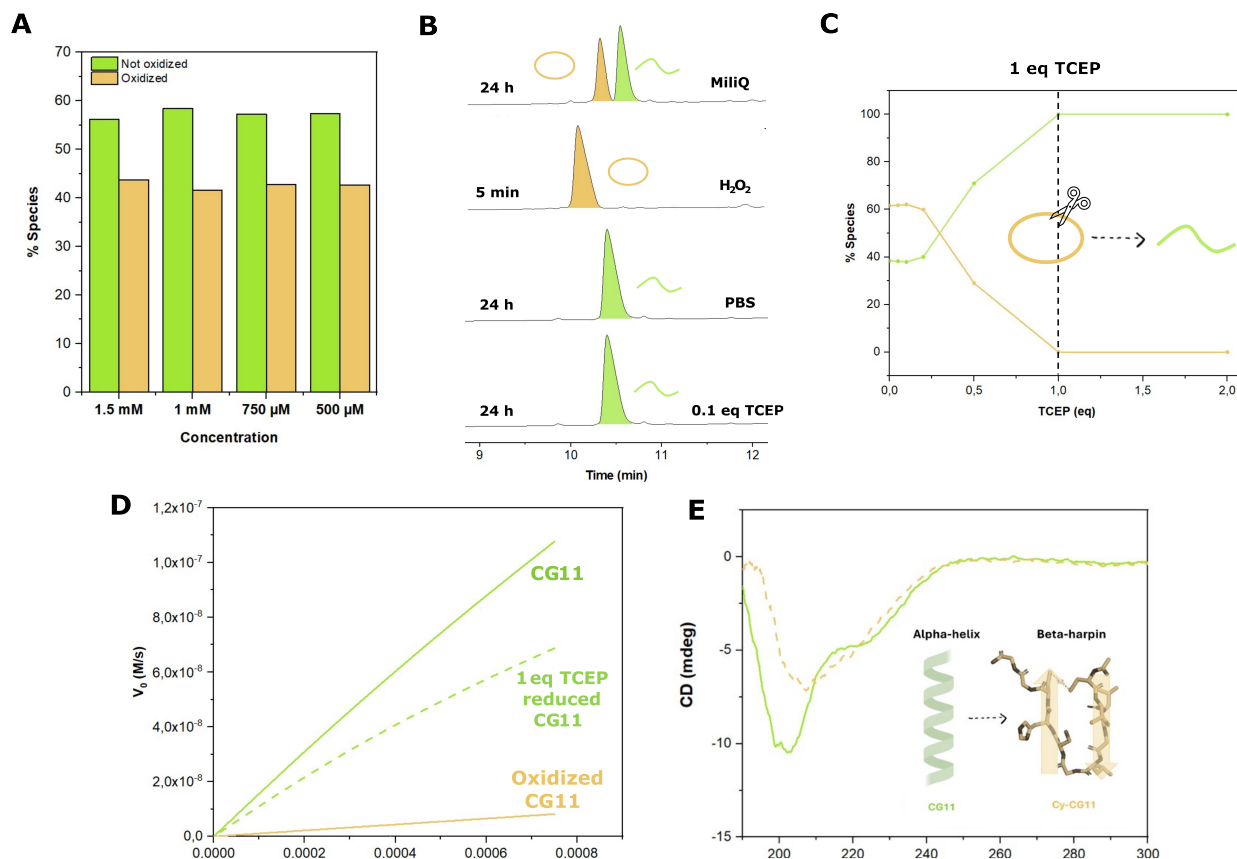
Fig. 3. Controlling thiol oxidation for tunable catalytic activity: A) Histogram illustrating the consistent conversion rate of CG11 (green) to cy-CG11 (yellow), unaffected by the concentration of CG11. B) Environmental factors influence CG11 oxidation, with the cyclic form observed in MiliQ (for 24 h) or rapidly induced with H_2O_2 (in 5 minutes), while the linear, reduced form is maintained in PBS buffer or with the addition of 0.1 eq of TCEP. C) Reverting the cyclic peptide to its linear form requires 100 times more TCEP (1 eq) for complete conversion. D) Dynamic modulation of the redox state allows for the on-and-off switching of catalytic activity in CG11, with cy-CG11 exhibiting significant activity restoration upon the addition of 1 eq TCEP. E) Oxidation induces a structural shift, with cy-CG11 (yellow) adopting a β-hairpin conformation and CG11 exhibiting a helical structure.

tiple thiol groups are prone to oligomerization and have the ability to transition between various states, forming trimers, tetramers, etc., until they reach thermodynamic equilibrium and stabilize in a particular structure (29). The occurrence of intermolecular disulfide bridges in peptides can lead to the formation of dimers or oligomers, depending on the number of available thiol groups. Alternatively, intramolecular bonding can lead to cyclization through the formation of a disulfide bridge. Dimerization is often controlled by concentration, and experimental conditions generally require very low concentrations of Cys-containtig peptides to favor intramolecular thiol oxidation (19, 30). Consequently, we followed a specific protocol that used peptide concentrations of 10^{-5} M to perform a controlled cyclization of CG11 into cy-CG11 through the formation of a disulfide bridge.

To better understand the behavior of our peptide at higher concentrations, we wanted to identify the critical concentration at which intermolecular dimer formation is preferred over intramolecular cyclization. Additionally, we aimed to deepen our understanding of the kinetics of spontaneous oxidation of CG11 and to determine which form represents the thermodynamic minimum. For this purpose, we dissolved varying concentrations of CG11 in MiliQ water and moni-

tored the spontaneous oxidation process over 24 hours using LC-MS. The peptide consistently exhibited a preference for intramolecular disulfide bond formation, always leading to the cyclic form, rather than engaging in the formation of dimers, trimers, or larger oligomers (Fig. 3 A). Furthermore, CG11 was subjected to different redox environments to investigate the controllability of oxidation kinetics. Upon the addition of hydrogen peroxide, the peptide exhibited rapid oxidation, while when placed in PBS buffer or supplemented with a reducing agent such as TCEP, it maintained its monomeric linear form over 24 hours (Fig. 3 B). The difference observed between the peptides behaviour in PBS buffer and MiliQ water could be due to the presence of metal traces in MiliQ water that serve as a catalyst for oxidation, wheres this effect is minimized with the addition of salts from the buffer that potentially bind and neutralize these metals (31).

Upon achieving control over the oxidation of the linear peptide, we investigated the potential to reduce the cyclic peptide to its linear form, utilizing the redox environment as a switch for functionality. Various concentrations of TCEP were tested to open the ring by reducing the already formed disulfide bridges in cy-CG11. Interestingly, a concentration of 1 equivalent (eq) of TCEP, which is 100 times higher than

the amount used to prevent disulfide bridge formation, proved necessary to break the bonds and revert the peptide to its linear configuration (Fig. 3 C).

These observations confirm the dynamic nature of the CG11's behavior and its responsiveness to external oxidative or reducing conditions.

Redox environment as a switch for catalytic activity. Cysteine, as part of short catalytic peptides, presents a unique opportunity for tunability. As shown in the previous section, thiol oxidation directly impacts catalytic activity of CG11, and manipulation of its oxidation kinetics in a redox environment is feasible. To explore the synergy of these characteristics and achieve a peptide with tunable activity, we analyzed the catalytic activity of CG11 obtained by cy-CG11 ring opening upon TCEP addition. We observed a recovery in activity with a k_{cat}/K_M of 4.29 $M^{-1}s^{-1}$, providing evidence of the peptide's tunable catalytic properties mediated by thiol oxidation (Fig. 3 D). When comparing the CG11 peptide obtained through TCEP mediated reduction of cy-CG11 and the linear CG11, we observed a variation in activity which might result from a subtle pH shift caused by TCEP, as this reducing agent decreases pH levels. This alteration in pH is known to affect the absorbance of p-NP at 405 nm, which is utilized to assess product formation, potentially resulting in a false impression of activity reduction (32).

Circular dichroism (CD) analysis revealed that oxidation not only affects the functionality of the peptides but also induces structural rearrangement. The linear analogue adopts a helical structure, which undergoes a transformation into a β-hairpin-like one upon cyclization. This structural reorganization may contribute to the decline in catalytic activity of the oxidized cy-CG11 variant (Fig. 3 E).

Demonstrating effective responsiveness to a deliberately induced harsh reducing environment using 1 eq of TCEP, we proceeded to assess the ability of cy-CG11 to undergo reduction and ring opening to its linear functional form, in a more physiological setting, specifically in the presence of elevated levels of glutathione (GSH). The ratio of GSH to its oxidized form, GSSG, helps to maintain redox balance in human cells. Perturbations in this balance are associated with various diseases, including tumors, where GSH concentrations can exceed those in the bloodstream by over 1000-fold (33). We subjected cy-CG11 to increasing concentrations of GSH (1 mM, 5 mM, and 10 mM) and observed the formation of its linear form (CG11) within 5 minutes, proportional to the amount of GSH added (Figure S13). This result indicates that cy-CG11 may function as a peptide with selective activity, being activated specifically in the presence of high GSH levels. The advantage of switchable activity allows for the precise targeting of only diseased tissue, ensuring it remains inactive in healthy cells and thereby reducing potential side effects. With this approach, the peptide-mediated hydrolysis could interfere with cell signaling pathways or cause the breakdown of crucial molecules specifically in tumor cells, leading to a targeted cell death. Furthermore, the reduction of cy-CG11 to its catalytically active linear form (CG11) leads
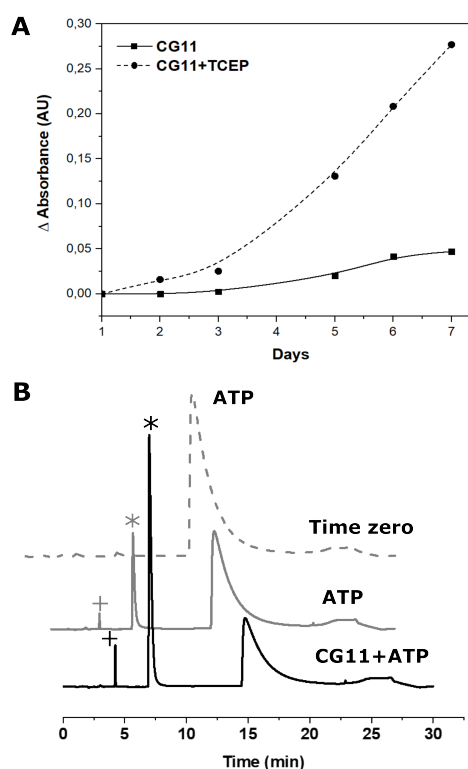

Fig. 4. CG11 is able to hydrolyze complex substrates: (A) CG11 showing best activity for the hydrolysis of p-NPP in the presence of 0.1 eq of TCEP; (B) ATP hydrolysis in the presence of CG11 with 0.1 eq TCEP shows a 30% increase in ADP (*) and AMP(+) production rate over 10 days.

to the oxidation of GSH into GSSG, lowering the concentration of GSH and suppressing its protective role against oxidative stress, which is crucial for the survival of tumor tissues (34).

CG11 is able to hydrolyze biologically relevant substrates. While p-NPA serves as a rapid screening tool for high-throughput analysis, its stability limits its applicability in complex biological environments. To assess the efficiency and adaptability of catalytic peptides to more intricate biological scenarios, we performed catalytic tests using two more complex substrates: p-Nitrophenyl Phosphate (p-NPP) and adenosine triphosphate (ATP). p-NPP is a widely used substrate in enzymatic assays to study the catalytic activity of phosphatases and related enzymes. Similarly to p-NPA, this colorimetric substrate releases p-nitrophenol upon hydrolysis, and its activity can be monitored at 405 nm, (8, 35).

ATP hydrolysis represents a fundamental cellular process critical for maintaining energy homeostasis and supporting various biological functions (36). ATP acts as the primary energy source in cells, facilitating the storage and transfer of energy for essential cellular activities. Hydrolysis of ATP involves the cleavage of a phosphate group, leading to the release of energy and the formation of adenosine diphosphate (ADP) and inorganic phosphate (Pi).

The hydrolysis of p-NPP exhibits a slower reaction compared to p-NPA, and this involves incubating the peptide with the substrate for a 7-day period with daily monitoring of reaction

progress. As demonstrated, cys-rich peptides are prone to spontaneous oxidation over time, significantly affecting their catalytic activity. Therefore, selecting an appropriate reducing agent becomes critical to preserve their functionality. Our results demonstrate that CG11 effectively hydrolyzes *p*-NPP, with TCEP as the reducing agent, whereas the hydrolysis is less effective when TCEP is not added, underscoring the importance of thiol groups in preserving the phosphatase activity, similarly to their role in esterase activity (Fig. 4 A).

Next, we evaluated the catalytic activity of CG11 using a more complex substrate, ATP, with TCEP as reducing agent. We monitored the hydrolysis of ATP into adenosine diphosphate (ADP) and inorganic phosphate (Pi) over a 10-day period. The results revealed a 30% increase in ADP production, showcasing the peptide's ability to hydrolyze a biologically relevant substrate such as ATP (Fig. 4 B). These findings have significant implications for potential drug development, indicating the versatility and applicability of our peptide for targeting complex biological molecules.
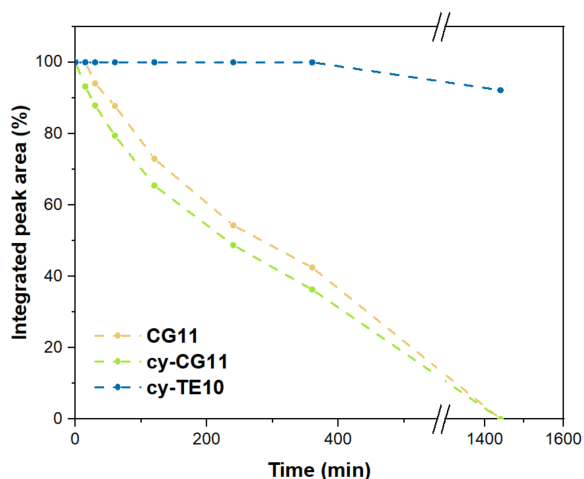

Fig. 5. Serum stability of peptides over 24 h: CG11 (green), cy-CG11 (yellow) show similar stability with a half-life of 3.5 h, while cy-TE10 (blue) shows almost no degradation over 24 h.

Serum stability is improved through unnatural cyclization. The potency of peptides in biological applications is based on their ability to evade proteases in the human body. Strategies commonly employed to enhance serum stability and remove protease-recognized motifs include modifications at the sequence level, such as the introduction of D-amino acids (37), cyclization (38, 39), and capping of the N-terminus (40, 41).

We evaluated the serum stability of linear CG11 along with cyclic cy-CG11 and cy-TE10 analogues obtained through different cyclization methods to confirm the potential improvement in stability conferred by cyclization. The linear peptide was designed with N-terminus acetylation, a strategy known to enhance catalytic activity by eliminating terminal charges and improving stability. The linear CG11 demonstrated a half-life ($t_{1/2}$) of 3.5 hours, undergoing complete degradation over 24 h 5. The stability of cy-CG11, obtained through

the disulfide bridge formation, exibited a similar half life to that of the linear counterpart ($t_{1/2}$= 3.25 h). This suggests that proteases recognize the spontaneously formed disulfide bridge in cy-CG11 similarly to the linear structure. However, employing head-to-side chain cyclization (in cy-TE10) led to a notable enhancement in stability, showing no signs of degradation during the 24-hour observation period, indicating a significant advantage of this cyclization approach for peptide stability.

In summary, we demonstrate that cyclization via disulfide bridges does not improve serum stability, yet it plays a crucial role in the tunability of catalytic activity, as this form of cyclization can be reversed, converting the inactive cyclic peptide back to its linear, catalytically active counterpart. Conversely, head-to-side chain cyclization, a method not occurring in nature, yields a catalytically active peptide with exceptional serum stability. This highlights the specific benefits of different cyclization strategies in influencing peptide stability and catalytic activity, which must be carefully considered in the design of cyclic peptides. The selection of a cyclization method should be tailored based on the required properties for the intended application, ensuring optimal performance and stability.

In our case, the tunable activity of cy-CG11 stands out as a determining advantage of this design strategy. Therefore, we plan to explore additional techniques to improve serum stability, including the integration of D-amino acids, while being careful not to disrupt the essential tunable activity driven by thiol oxidation. With this approach we aim to create a stable cyclic peptide that converts to its active linear form at the site of action, carries out its function, and is subsequently cleared from the body.

Effect of spacer length on catalytic activity and spontaneous cyclization. Analogues of the most promising catalytic peptide, CG11 featuring triad residues (Cys, His, Thr) and an additional N-terminal Cys, separated by a structural spacer composed of repeating Gly and Leu residues (LGLG) and a Ser were synthesized to explore the impact of varying spacer lengths on its functionality and capacity for self-driven cyclization (Table 2). Initially, we altered the original LGLGS spacer, simplifying it to a shorter motif, and synthesized two variants featuring 2 amino acid shorter sequences containing LG (CG9a) or GL(CG9b) between the triad Thr and His. Subsequently, we created a variant containing only Leu as the spacer (CG8), hypothesizing that its side chain could contribute to interactions with other amino acids, potentially influencing the peptide's functionality and cyclization propensity. This assumption was based on the fact that Gly is typically employed to extend the distance between amino acids, offering limited functional contributions beyond spatial separation. Finally, we synthesized an analogue that completely lacked the LGLG spacer (CG7).

All synthesized analogues displayed activity comparable to the original CG11 sequence (Figure S14 A). This observation suggests that the length of the spacer minimally affects the hydrolysis of *p*-NPA (Table 2). Further analyses are necessary to investigate whether these shorter peptides adopt any

secondary structure and to assess their effectiveness in hydrolyzing complex substrates, such as *p*-NPP and ATP.

Table 2. Overview of the proposed peptide sequences with varying spacer (LGLG) lenghts with their oxidation to the cyclic form and catalytic efficiency

Sequence	Acronym	Oxidation	k_{cat}/K_M $(\mathrm{M^{-1}\,s^{-1}})$
Ac-CTLGSHCGG-Am	CG9a	Yes	7,37
Ac-CTGLSHCGG-Am	CG9b	Yes	7,63
Ac-CTLSHCGG-Am	CG8	Yes	5,43
Ac-CTSHCGG-Am	CG7	No	7,28

Furthermore, we aimed to investigate whether sequence length impacts spontaneous cyclization, to determine if adaptability could be maintained even in shorter sequences. The intramolecular disulfide bridge formation process occurs only when the sequence can adopt a conformation in which the two Cys are close in space at a distance shorter than 2 Å (42) facilitating the formation of a covalent bond between two thiol groups. Conducting a 24-hour LC-MS analysis, we demonstrate that a minimum distance of 4 amino acids is required between two thiol groups to facilitate the formation of an intramolecular disulfide bridge. In particular, the Ac-CTSHCGG-Am (CG7) sequence, with only three amino acids between the two cysteines, did not cyclize nor dimerize under these conditions (Figure S14 B). However, the lack of dimerization or oligomerization could be attributed to the micromolar concentration range used in this experiment.

Conclusions

In this study, we introduce the concept of incorporating a potent nucleophile, Cys, capable of hydrolyzing various substrates, including p-NPA, *p*-NPP, and ATP, while enabling control and direction of its activity through thiol oxidation. This introduces the possibility for these peptides to serve as both sensors of the redox environment and agents with controllable, site-specific actions in the body. Our exploration of two cyclization methods revealed that disulfide bridge formation offers tunability and reversibility, while head-to-side chain exhibited excellent resistance to proteases. Biological applications of catalytic peptides have received limited attention, with existing designs relying on metal cofactors and self-assembly, which presents challenges in orchestrating activity within complex environments such as the human body. Our findings provide valuable insights into the optimization of the characteristics of catalytic peptides, paving the way for innovative research in creating adaptable catalysts for biomedical use. This advancement opens up potential for applications such as developing precise drug delivery systems and novel therapeutic approaches, facilitating the use of catalytic peptides in healthcare.

Bibliography

1. Wenqi Wang, Rui Han, Kai Tang, Shuju Zhao, Caifeng Ding, and Xiliang Luo. Biocompatible peptide hydrogels with excellent antibacterial and catalytic properties for electrochemical sensing application. *Analytica Chimica Acta*, 1154:338295, 2021.
2. Biplab Mondal, Dipayan Bairagi, Nibedita Nandi, Biswanath Hansda, Krishna Sundar Das, Charlotte JC Edwards-Gayle, Valeria Castelletto, Ian W Hamley, and Arindam Banerjee. Peptide-based gel in environmental remediation: removal of toxic organic dyes and hazardous pb2+ and cd2+ ions from wastewater and oil spill recovery. *Langmuir*, 36(43): 12942–12953, 2020.
3. Annette F Dexter and Anton PJ Middelberg. Peptides as functional surfactants. *Industrial & Engineering Chemistry Research*, 47(17):6391–6398, 2008.
4. Tobias Schnitzer, Jonas W Rackl, and Helma Wennemers. Stereoselective peptide catalysis in complex environments–from river water to cell lysates. *Chemical Science*, 13(31):8963–8967, 2022.
5. Xinyu Liu, Riley Waters, Hannah E Gilbert, Gage T Barroso, Kelsey M Boyle, and Leah S Witus. The role of β-hairpin conformation in ester hydrolysis peptide catalysts based on a trpzip scaffold. *RSC advances*, 11(38):23714–23718, 2021.
6. Lei Wang, Nanxi Wang, Wenping Zhang, Xurui Cheng, Zhibin Yan, Gang Shao, Xi Wang, Rui Wang, and Caiyun Fu. Therapeutic peptides: Current applications and future directions. *Signal Transduction and Targeted Therapy*, 7(1):48, 2022.
7. Jingjing Han, Haoning Gong, Xiaokang Ren, and Xuehai Yan. Supramolecular nanozymes based on peptide self-assembly for biomimetic catalysis. *Nano Today*, 41:101295, 2021.
8. Ana S Pina, Leonor Morgado, Krystyna L Duncan, Sara Carvalho, Henrique F Carvalho, Arménio JM Barbosa, Beatriz de P Mariz, Inês P Moreira, Daniela Kalafatovic, Bruno M Morais Faustino, et al. Discovery of phosphotyrosine-binding oligopeptides with supramolecular target selectivity. *Chemical science*, 13(1):210–217, 2022.
9. Ayan Chatterjee, Antara Reja, Sumit Pal, and Dibyendu Das. Systems chemistry of peptide-assemblies for biochemical transformations. *Chemical Society Reviews*, 2022.
10. Patrizia Janković, Iva Šantek, Ana Sofia Pina, and Daniela Kalafatovic. Exploiting peptide self-assembly for the development of minimalistic viral mimetics. *Frontiers in Chemistry*, 9: 723473, 2021.
11. Patrizia Janković, Marko Babić, Marko Perčić, Ana S Pina, and Daniela Kalafatovic. Factors influencing the catalytic activity of metal-dependent histidine-rich peptides: sequence, conformation, stereochemistry, self-assembly or their interplay? *Molecular Systems Design & Engineering*, 8(11):1371–1380, 2023.
12. O Zozulia, MA Dolan, and IV Korendovych. Catalytic peptide assemblies. *Chemical Society Reviews*, 47(10):3621–3639, 2018.
13. Patrizia Janković, Erik Otović, Goran Mauša, and Daniela Kalafatovic. Manually curated dataset of catalytic peptides for ester hydrolysis. *Data in Brief*, page 109290, 2023.
14. Sara Carvalho, David Q Peralta Reis, Sara V Pereira, Daniela Kalafatovic, and Ana Sofia Pina. Catalytic peptides: The challenge between simplicity and functionality. *Israel Journal of Chemistry*, 62(9-10):e202200029, 2022.
15. Avigail Baruch-Leshem, Corinne Chevallard, Frédéric Gobeaux, Patrick Guenoun, Jean Daillant, Philippe Fontaine, Michel Goldmann, Ariel Kushmaro, and Hanna Rapaport. Catalytically active peptides affected by self-assembly and residues order. *Colloids and Surfaces B: Biointerfaces*, 203:111751, 2021.
16. Chunqiu Zhang, Xiangdong Xue, Quan Luo, Yiwei Li, Keni Yang, Xiaoxi Zhuang, Yonggang Jiang, Jinchao Zhang, Junqiu Liu, Guozhang Zou, et al. Self-assembled peptide nanofibers designed as biological enzymes for catalyzing ester hydrolysis. *Acs Nano*, 8(11):11715–11723, 2014.
17. Tsukasa Takahashi, Michelle Cheung, Thomas Butterweck, Steve Schankweiler, and Michael J Heller. Quest for a turnover mechanism in peptide-based enzyme mimics. *Catalysis Communications*, 59:206–210, 2015.
18. David Barford. The role of cysteine residues as redox-sensitive regulatory switches. *Current opinion in structural biology*, 14(6):679–686, 2004.
19. Leslie B Poole. The basics of thiols and cysteines in redox biology and chemistry. *Free Radical Biology and Medicine*, 80:148–157, 2015.
20. Stefano M Marino and Vadim N Gladyshev. Cysteine function governs its conservation and degeneration and restricts its utilization on protein surfaces. *Journal of molecular biology*, 404(5):902–916, 2010.
21. Yixin Cen, Warispreet Singh, Mamatjan Arkin, Thomas S Moody, Meilan Huang, Jiahai Zhou, Qi Wu, and Manfred T Reetz. Artificial cysteine-lipases with high activity and altered catalytic mechanism created by laboratory evolution. *Nature communications*, 10(1):3198, 2019.
22. Luis Moroder. Isosteric replacement of sulfur with other chalcogens in peptides and proteins. *Journal of peptide science: an official publication of the European Peptide Society*, 11(4): 187–214, 2005.
23. Christopher J Kristich and George W Ordal. Bacillus subtilis ched is a chemoreceptor modification enzyme required for chemotaxis. *Journal of biological chemistry*, 277(28):25356–25362, 2002.
24. George D Glekas, Matthew J Plutz, Hanna E Walukiewicz, George M Allen, Christopher V Rao, and George W Ordal. Elucidation of the multiple roles of ched in b acillus subtilis chemotaxis. *Molecular microbiology*, 86(3):743–756, 2012.
25. Xingjuan Chao, Travis J Muff, Sang-Youn Park, Sheng Zhang, Abiola M Pollard, George W Ordal, Alexandrine M Bilwes, and Brian R Crane. A receptor-modifying deamidase in complex with a signaling phosphatase reveals reciprocal regulation. *Cell*, 124(3):561–571, 2006.
26. Caroline M Rufo, Yurii S Moroz, Olesia V Moroz, Jan Stöhr, Tyler A Smith, Xiaozhen Hu, William F DeGrado, and Ivan V Korendovych. Short peptides self-assemble to produce catalytic amyloids. *Nature chemistry*, 6(4):303–309, 2014.
27. Karishma Patel, Louise J Walport, James L Walshe, Paul D Solomon, Jason KK Low, Daniel H Tran, Kevork S Mouradian, Ana PG Silva, Lorna Wilkinson-White, Alexander Norman, et al. Cyclic peptides can engage a single binding pocket through highly divergent modes. *Proceedings of the National Academy of Sciences*, 117(43):26728–26738, 2020.
28. Elena Schartmann, Sarah Schemmert, Tamar Ziehm, Leonie HE Leithold, Nan Jiang, Markus Tusche, N Joni Shah, Karl-Josef Langen, Janine Kutzsche, Dieter Willbold, et al.

Comparison of blood-brain barrier penetration efficiencies between linear and cyclic all-d-enantiomeric peptides developed for the treatment of alzheimer's disease. *European journal of pharmaceutical sciences*, 114:93–102, 2018.

29. Bin Liu, Juntian Wu, Marc Geerts, Omer Markovitch, Charalampos G Pappas, Kai Liu, and Sijbren Otto. Out-of-equilibrium self-replication allows selection for dynamic kinetic stability in a system of competing replicators. *Angewandte Chemie International Edition*, 61(18): e202117605, 2022.

30. Masayuki Kirihara, Yasutaka Asai, Shiho Ogawa, Takuya Noguchi, Akihiko Hatano, and Yoshiro Hirai. A mild and environmentally benign oxidation of thiols to disulfides. *Synthesis*, pages 3286–3289, 2007.

31. GA Bagiyan, IK Koroleva, NV Soroka, and AV Ufimtsev. Oxidation of thiol compounds by molecular oxygen in aqueous solutions. *Russian chemical bulletin*, 52:1135–1141, 2003.

32. Patrizia Janković and Daniela Kalafatovic. Determining the esterase activity of peptides and peptide assemblies. 2024.

33. Yang Gao, Yun Li, Hongmei Cao, Haixue Jia, Dianyu Wang, Chunhua Ren, Zhongyan Wang, Cuihong Yang, and Jianfeng Liu. Hypertoxic self-assembled peptide with dual functions of glutathione depletion and biosynthesis inhibition for selective tumor ferroptosis and pyroptosis. *Journal of Nanobiotechnology*, 20(1):1–14, 2022.

34. Luke Kennedy, Jagdeep K Sandhu, Mary-Ellen Harper, and Miroslava Cuperlovic-Culf. Role of glutathione in cancer: From mechanisms to therapies. *Biomolecules*, 10(10):1429, 2020.

35. Jacqueline Montalibet, Kathryn I Skorey, and Brian P Kennedy. Protein tyrosine phosphatase: enzymatic assays. *Methods*, 35(1):2–8, 2005.

36. Jingwen Zhou, Liming Liu, Zhongping Shi, Guocheng Du, and Jian Chen. Atp in current biotechnology: regulation, applications and perspectives. *Biotechnology advances*, 27(1): 94–101, 2009.

37. Maria C Lucana, Yolanda Arruga, Emilia Petrachi, Albert Roig, Roberta Lucchi, and Benjamí Oller-Salvia. Protease-resistant peptides for targeting and intracellular delivery of therapeutics. *Pharmaceutics*, 13(12):2065, 2021.

38. Timothy A Hill, Nicholas E Shepherd, Frederik Diness, and David P Fairlie. Constraining cyclic peptides to mimic protein structure motifs. *Angewandte Chemie International Edition*, 53(48):13020–13041, 2014.

39. Rasha Jwad, Daniel Weissberger, and Luke Hunter. Strategies for fine-tuning the conformations of cyclic peptides. *Chemical Reviews*, 120(17):9743–9789, 2020.

40. Rasmus Ree, Sylvia Varland, and Thomas Arnesen. Spotlight on protein n-terminal acetylation. *Experimental & molecular medicine*, 50(7):1–13, 2018.

41. Yaron Marciano, Nazia Nayeem, Dhwanit Dave, Rein V Ulijn, and Maria Contel. N-acetylation of biodegradable supramolecular peptide nanofilaments selectively enhances their proteolytic stability for targeted delivery of gold-based anticancer agents. *ACS Biomaterials Science & Engineering*, 9(6):3379–3389, 2023.

42. Ming-an Sun, Yejun Wang, Qing Zhang, Yiji Xia, Wei Ge, and Dianjing Guo. Prediction of reversible disulfide based on features from local structural signatures. *BMC genomics*, 18: 1–10, 2017.

Supplementary Note 1: Materials and methods

Materials. All *p*-nitrophenyl esters (95.0%), including *p*-nitrophenyl acetate (*p*-NPA) and *p*-nitrophenyl phosphate (p-NPP), ATP, Fmoc-amino acids, Novabiochem® resin (Rink Amide AM) human serum, PBS, HEPES, GSH, GSSG, DIPEA, HBTU, TIS, TFA, guanidine hydrochloride and piperidine (99.0%) were purchased from Sigma-Aldrich (St. Louis, Missouri, SAD). All other chemicals and reagents are analytical grade and are available from commercial sources.

Peptide synthesis. The linear peptides were synthesized using standard fluorenylmethyloxycarbonyl (Fmoc) solid phase peptide synthesis on Rink (Novabiochem) Amide AM resin (100–200 mesh) with a loading of 0.78 mmol g^1). The resin was swollen for 30 min in DMF. The removal of Fmoc was performed with 20% piperidine in DMF. Chain growth was carried out using a three fold excess of L-amino acids over the resin in DMF, using N,N-diisopropylethylamine (DIPEA) and N,N,N′,N′-tetramethyl-O-(1H-benzotriazol-1-yl)uronium hexafluorophosphate (HBTU) as coupling and activating agents in a 2:1 ratio relative to amino acids, respectively. The coupling and deprotection steps were separated by DMF (3 × 30 s) and DCM washes (3 × 30 s).

Head-to-side chain cyclization. Intramolecular cyclization was performed on the resin through amide bond between the side chain of the C-terminal Glu (E) and the N-terminus, as previously reported (11). Briefly, after complete elongation of the peptide chain, the 2-phenylisopropyl (O-2-PhiPr) protecting group was selectively removed from the Glu residue using 1% (v/v) trifluoroacetic acid (TFA) in DCM (4 × 10 min), which was followed by neutralization with 5% DIPEA in DCM (4 × 5 min). On resin cyclization was performed with PyBOP/Hobt/DiPEA (5, 5 and 10 equiv) in DMF for 3 h. The cyclic peptide was cleaved from the resin using TFA:triisopropylsilane (TIS):H2O = 95:2.5:2.5. The crude peptide was precipitated and washed in cold diethyl ether, centrifuged (3 × 10 min) at 4 °C, dissolved in 20% acetonitrile (ACN) in MiliQ water, and lyophilized.

Disulfide bridge formation. The linear peptide was dissolved in 0.1 M NH$_4$OAc and 1 M CH$_6$ClN$_3$, pH 8.5 under a N$_2$ atmosphere. This dissolution took place in the presence of 1 M guanidine hydrochloride and a combination of reduced and oxidized glutathione, resulting in a desired peptide:GSH:GSSG ratio of 1:100:10. Following a gentle stirring period of 24 hours at 25°C, analysis by liquid chromatography coupled to mass spectrometry confirmed the completion of the oxidation process. Subsequently, the reaction mixture was quenched by the addition of acetic acid until reaching a pH of 3. The desalting process involved solid-phase extraction, employing a C18 column. Elution was carried out using a mixture of MiliQ water and ACN, with 0.1% TFA.

Peptide analysis and purification. The crude peptides were analyzed by HPLC-MS on the XSELECT CSH C18 column (4.6 × 150 mm, 3.5 μm, Waters, Milford, MA, USA) with an Agilent 1260 series HPLC chromatograph coupled to an Agilent 6460 triple quadrupole mass spectrometer system (Agilent Technologies, Santa Clara, CA, USA). The elution was carried out with linear gradients of solvent B (0.1% v/v TFA in ACN) into A (0.1% v/v TFA in H$_2$O) over 20 min. Peptides were purified by preparative HPLC on the Aeris PEPTIDE XB-C18 column (10 × 250 mm, 5 µm, Phenomenex) with an Agilent Infinity 1260 semi-preparative HPLC instrument using a flow rate of 5 ml / min and linear gradients of solvent B (0.1% v/v TFA in ACN) in A (0.1% v/v TFA in H$_2$O) for 30 min with detection at 214 nm on a DAD detector. The purity of the collected fractions was analyzed and those with satisfactory purity (> 90%) were merged and lyophilized. The purity of the final products was analyzed by HPLC-MS on the XSELECT CSH C18 column (4.6 × 150 mm, 3.5 μm, Waters, Milford, MA, USA) in an Agilent 1260 series HPLC chromatograph coupled to an Agilent 6460 triple quadrupole mass spectrometer system (Agilent Technologies, Santa Clara, CA, USA) eluting with linear gradients of solvent B (0.1% v/v TFA in ACN) in A (0.1% v/v TFA in H$_2$O) for 20 min at 1 mL/min flow rate.

Catalytic activity assessment. The catalytic activity assay was performed on a Hidex Sense microplate reader to monitor the absorbance of the product (*p*-nitrophenol) for 30 minutes (22°C) in 96-well plates at 405 nm. Stock solutions of 0.1 M of *p*-Nitrophenyl esters (*p*-Nitrophenyl acetate, *p*-Nitrophenyl phosphate)(Sigma-Aldrich, United States) and ATP were used to prepare substrate solutions in PBS (pH 7.4). 150 µL of freshly prepared substrate solutions (to the final substrate concentration of 0.195 - 2.5 mM) were added to 50 µL of buffered (PBS) peptide solutions at pH 7.4 (to a final peptide concentration of 25 µM). The calibration curve was experimentally obtained from a standard 4-nitrophenol (*p*-NP) solution (Sigma-Aldrich, United States) in the concentration range of 0-100 μM. The reported results correspond to the average of at least two independent measurements. The kinetic parameters were obtained by fitting the data to the Michaelis-Menten equation $V_0 = k_{cat} \cdot [E]_0 \cdot [S]_0 / (K_M + [S]_0)$ using the Origin 2018 software.

Serum stability. Peptides were dissolved at 1 mM in HEPES buffer (10 mM, pH 7). Next, 600 µL of peptide solution were mixed (1:1 v/v) with 600 µL of human serum, to a 0.5 mM final concentration. The mixture was incubated at 37 °C and, at various time points, 50 µL were taken and precipitated with 200 µL cold methanol. The samples were centrifuged at 13,000 rpm for 10 min. Afterwards, 50 µL of each supernatant were injected on the XSELECT CSH C18 column (4.6 × 150 mm, 3.5 μm, Waters, Milford, MA, USA) on an Agilent 1260 series HPLC chromatograph coupled to an Agilent 6460 triple quadrupole

mass spectrometer system (Agilent Technologies, Santa Clara, CA, USA) and analysed using a 0–45% linear gradient of MeCN into 0.1% TFA in MiliQ over 20 min with 1 mL/min flow rate. PDA detection at 214 nm was used. Controls included blank serum (25 µL each of 1:1 v/v serum + HEPES buffer, then precipitation with 200 µL cold methanol), untreated peptide (25 µL of 0.1 mM stock in HEPES buffer + 25 µL HEPES buffer, then precipitation with 200 µL cold methanol), and a zero-time sample (200 µL cold methanol + 25 µL serum + 25 µL 1 mM peptide stock); the peptide was added last to avoid any contact with protease. The controls were analyzed by LC-MS as described above. Three independent replicates were performed.

Circular Dichroism. The far-UV CD spectra (190-300 nm) were acquired with a Jasco J-815 spectropolarimeter with a Peltier temperature control system at 20 °C, in a 1 mm quartz cuvette under nitrogen flow and 2 nm bandwidth. Each spectrum represents an average of three scans. Peptide concentrations were maintained at 25 μM and measurements were made in PBS.

Supplementary Note 2: Additional data

A

B

C
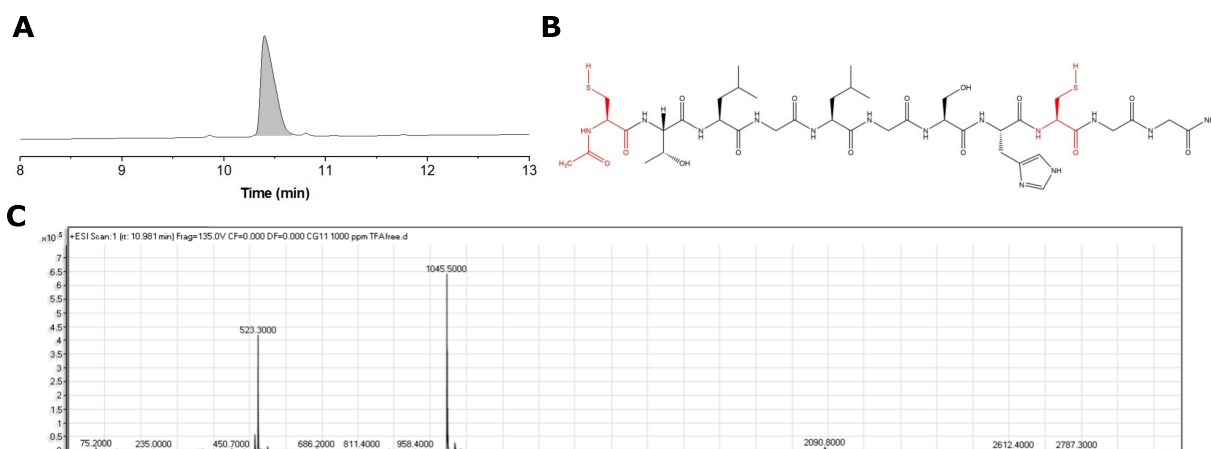
Supplementary Figure S1: a) LC chromatogram at 220 nm (purity of 97%), b) chemical structure and (c) the MS trace for Ac-CTLGLGSHCGG-Am (CG11) (m/z 1044.4)

A

B

C
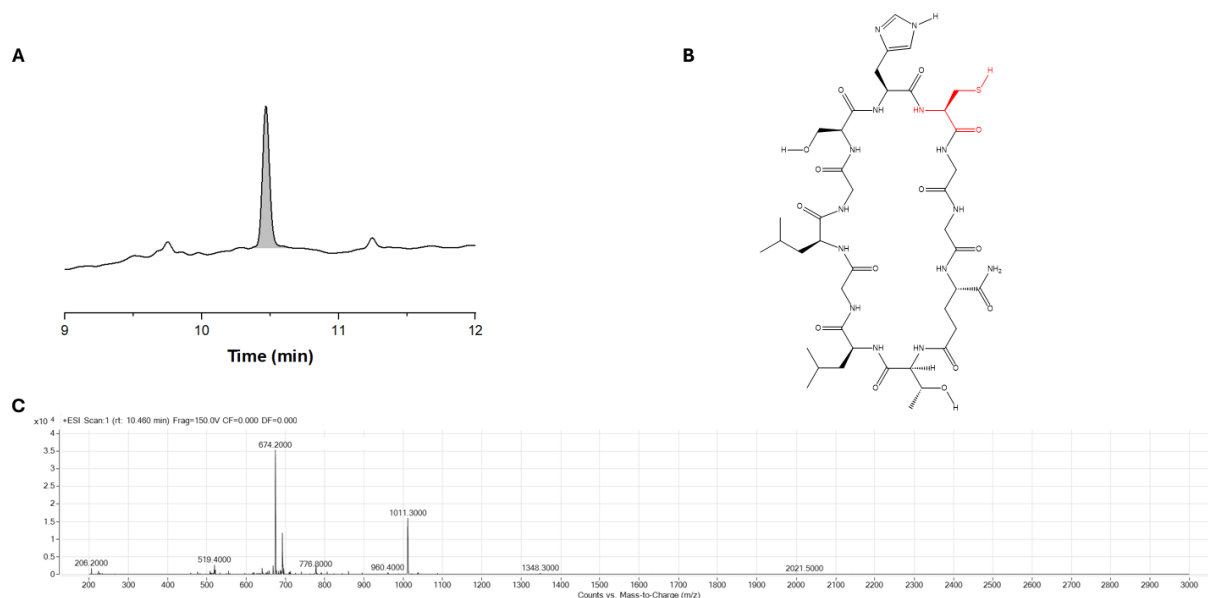
Supplementary Figure S2: a) LC chromatogram at 220 nm (purity of 91%), b) chemical structure and (c) the MS trace for Ac-[TLGLGSHCGGE]-Am (cy-TE10) (m/z 1010.1)
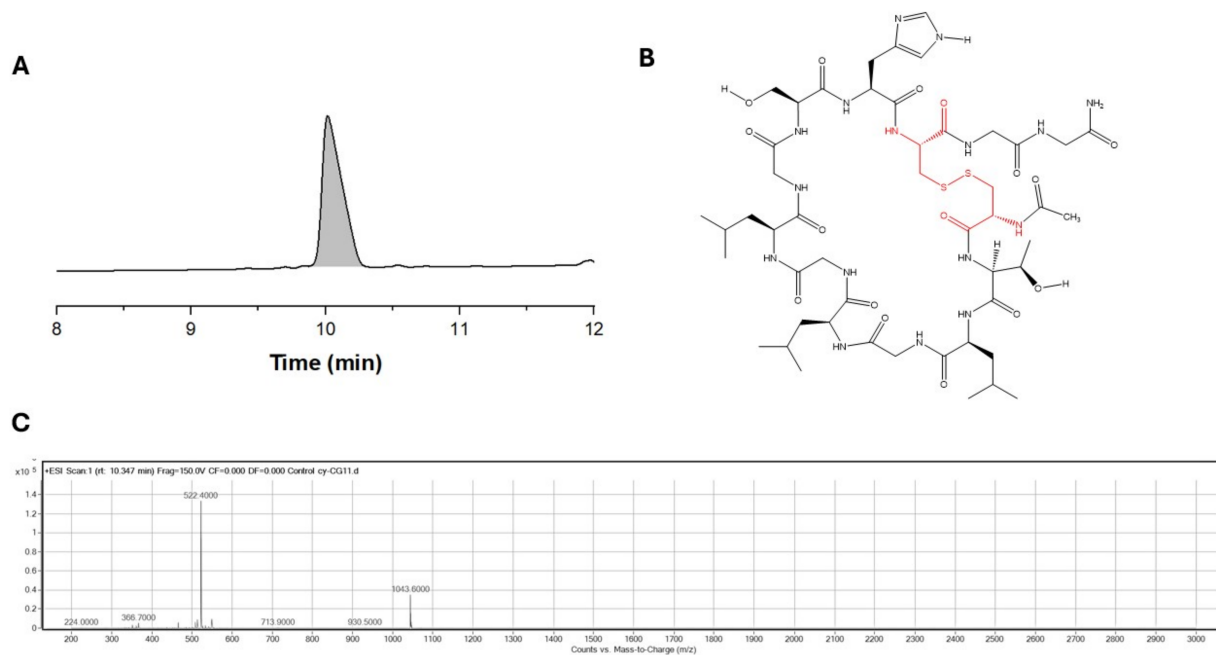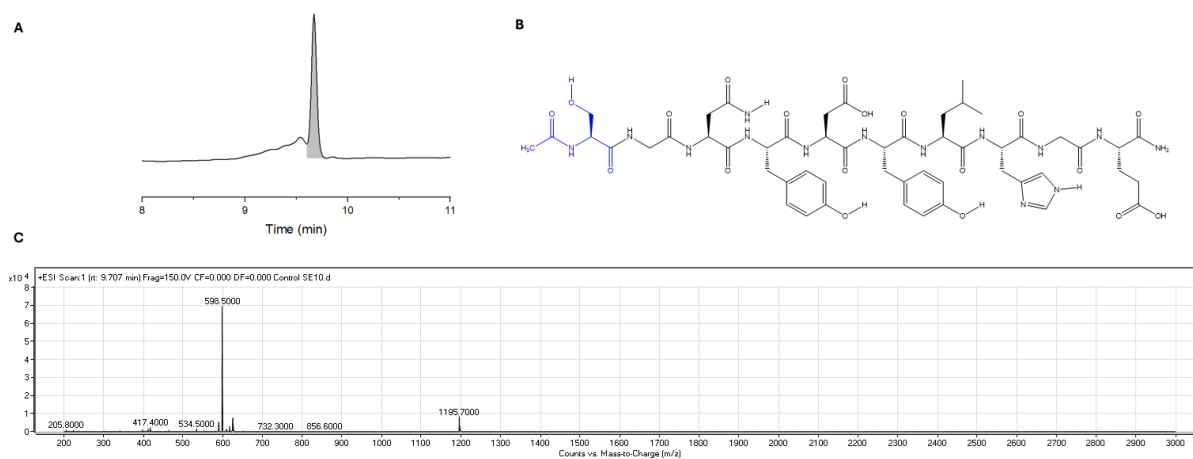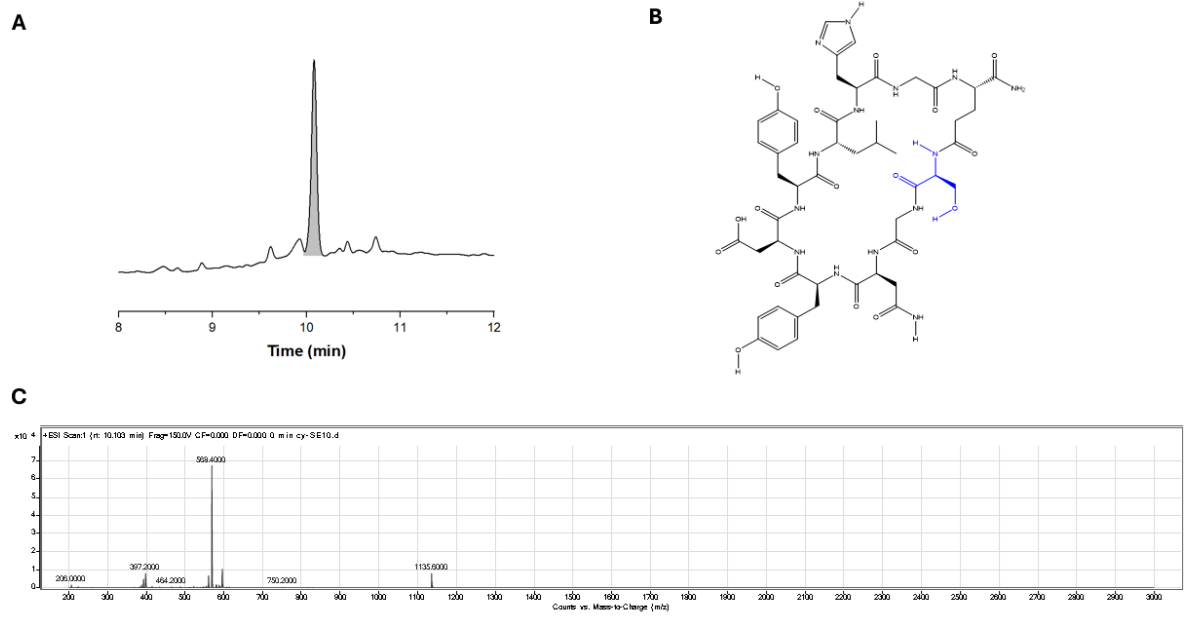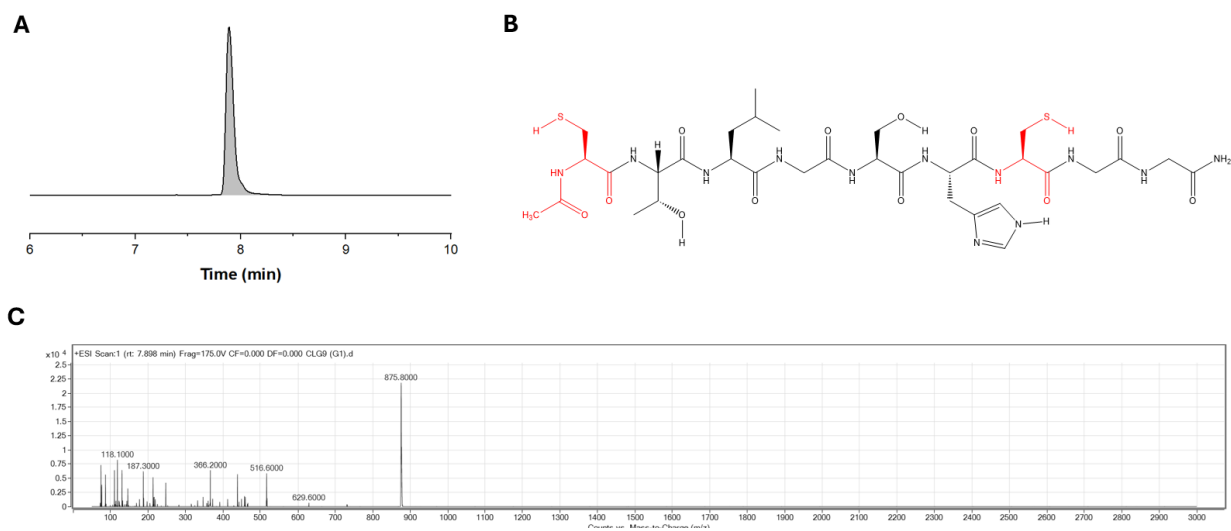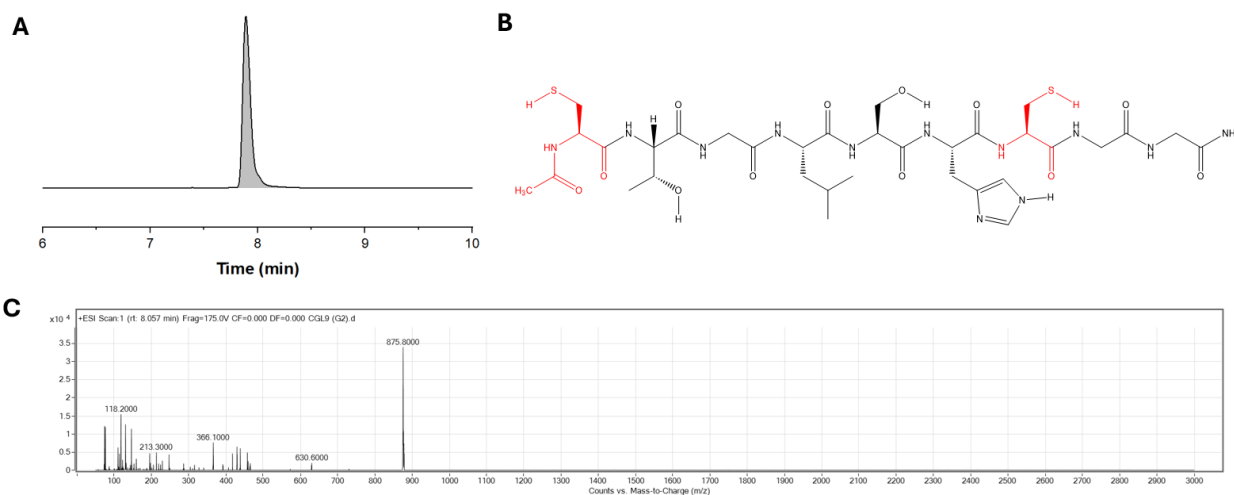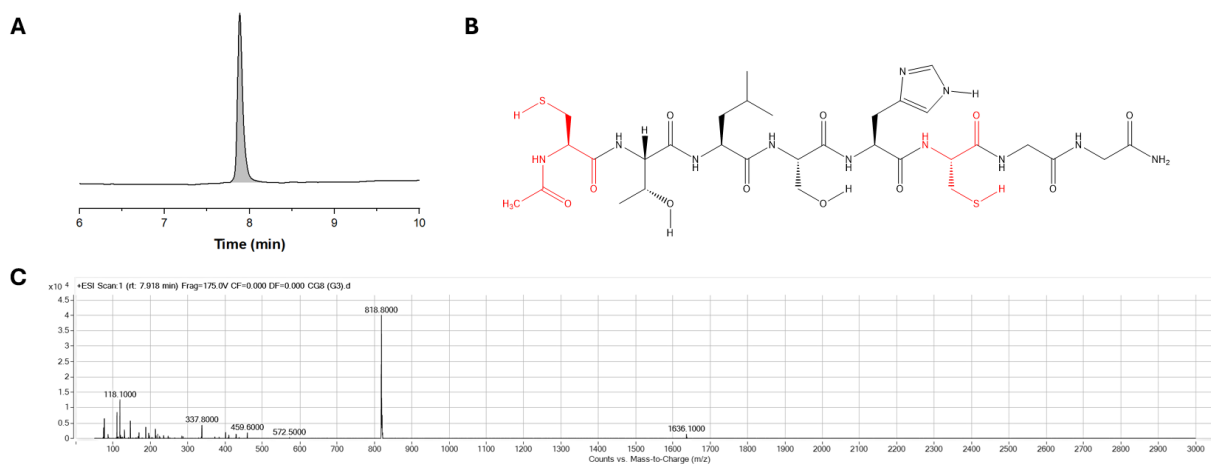
Supplementary Figure S3: a) LC chromatogram at 220 nm (purity of 99%), b) chemical structure and (c) the MS trace for Ac-[CTLGLGSHCGG]-Am (cy-CG11) (m/z 1042.1)
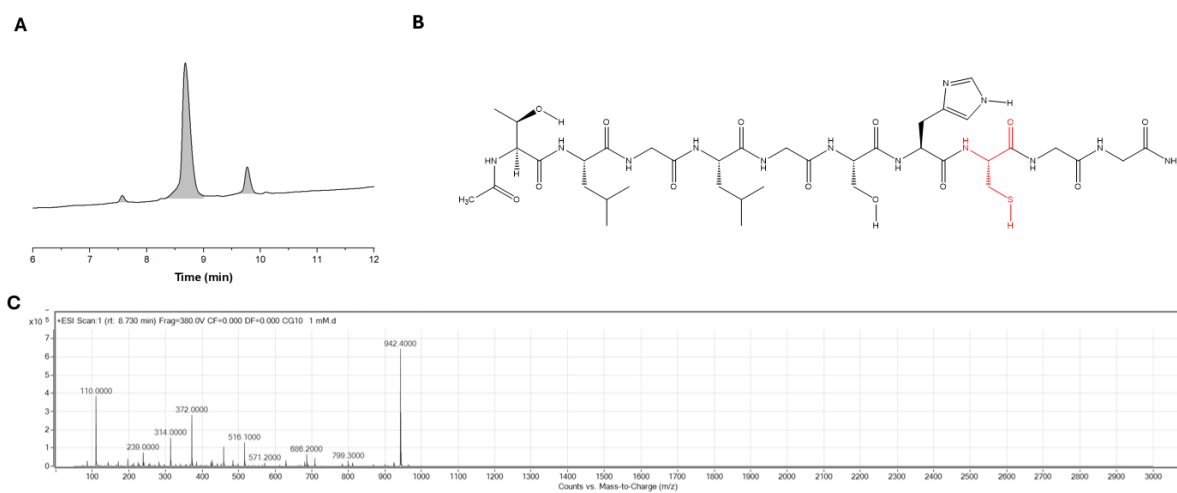
Supplementary Figure S4: a) LC chromatogram at 220 nm (purity of 89%), b) chemical structure and (c) the MS trace for Ac-TLGLGSHCGG-Am (CG10) (m/z 941.4)
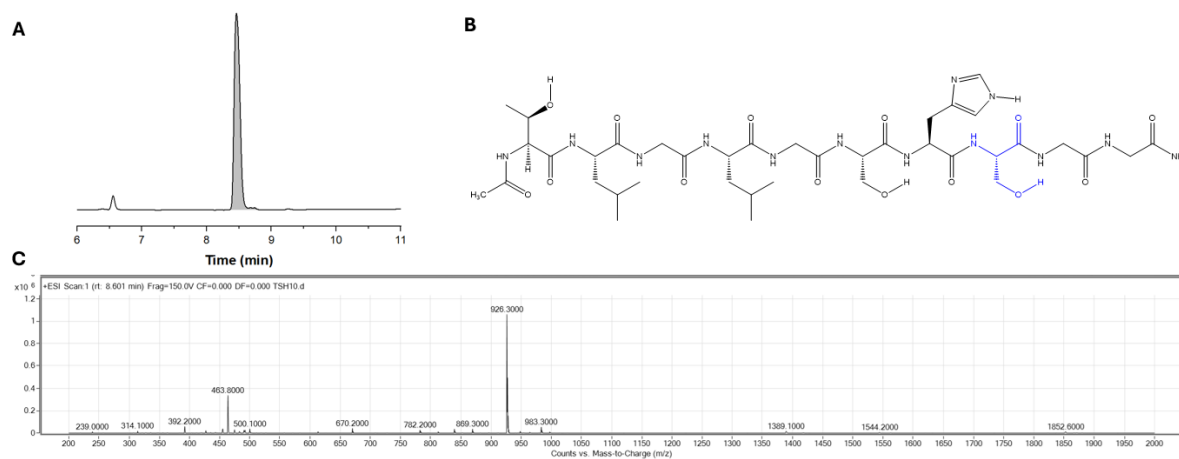
Supplementary Figure S5: a) LC chromatogram at 220 nm (purity of 94%), b) chemical structure and (c) the MS trace for Ac-TLGLGSHSGG-Am (TSH10) (m/z 925.4)

Supplementary Figure S6: a) LC chromatogram at 220 nm (purity of 85%), b) chemical structure and (c) the MS trace for Ac-SGNYDYLHGE-Am (SE10) (m/z 1094.4)
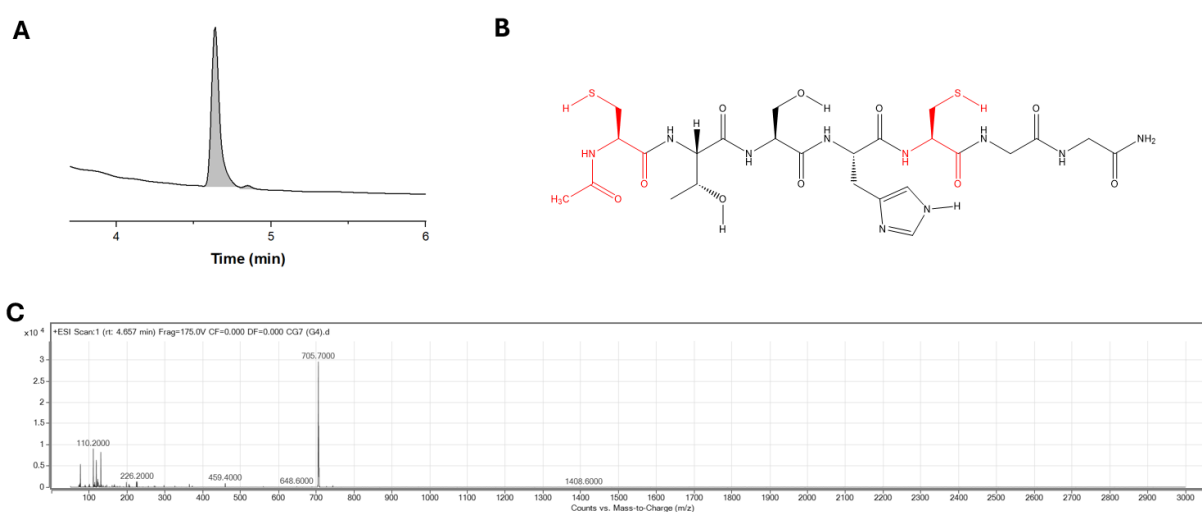
Supplementary Figure S7: a) LC chromatogram at 220 nm (purity of 80%), b) chemical structure and (c) the MS trace for [SGNYDYLHGE]-Am (SE10) (m/z 1034.4)

Supplementary Figure S8: a) LC chromatogram at 220 nm (purity of 100%), b) chemical structure and (c) the MS trace for Ac-CTLGSHCGG-Am (CG9a) (m/z 874.3)

A

B

C

Supplementary Figure S9: a) LC chromatogram at 220 nm (purity of 100%), b) chemical structure and (c) the MS trace for Ac-CTGLSHCGG-Am (CG9b) (m/z 874.3)

A

B

C

Supplementary Figure S10: a) LC chromatogram at 220 nm (purity of 100%), b) chemical structure and (c) the MS trace for Ac-CTLSHCGG-Am (CG8) (m/z 817.3)

A

B

C

Supplementary Figure S11: A) LC chromatogram at 220 nm (purity of 99%), B) chemical structure and (C) the MS trace for Ac-CTSHCGG-Am (CG7) (m/z 704.2)
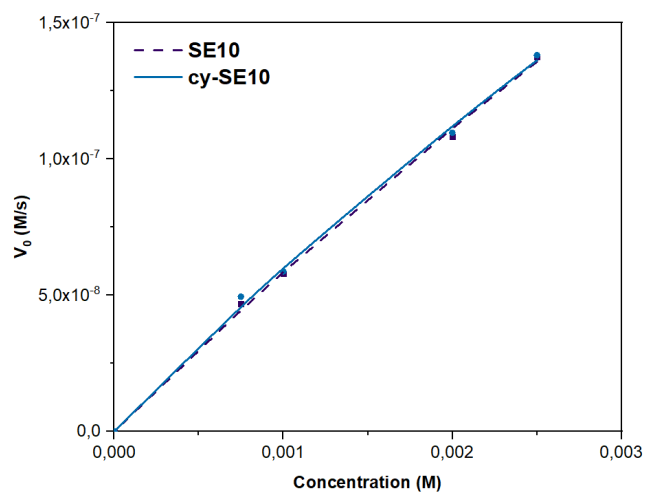
Supplementary Figure S12: SE10 and cy-SE10 display identical catalytic activities for the hydrolysis of the *p*-NPA substrate
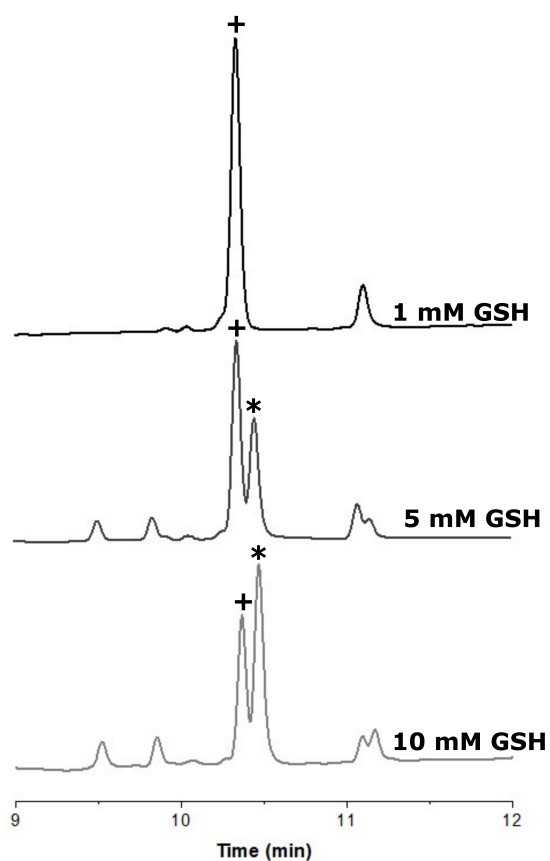
Supplementary Figure S13: The addition of increasing GSH concentrations (1 mM, 5 mM, and 10 mM) to 1 mM of cy-CG11 (+) facilitated the conversion into its linear variant, CG11 (*) with the conversion rate being directly proportional to GSH concentration. Addition of 10 mM GSH resulted in more than 50% conversion rate into the linear variant.
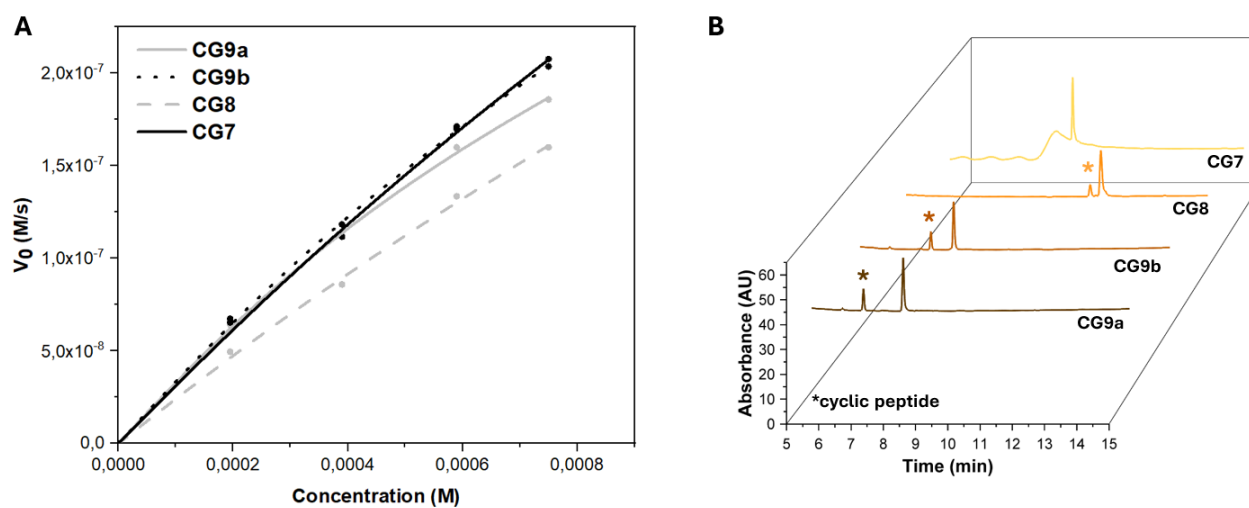
Supplementary Figure S14: A) Comparison of shorter versions of the original sequence (CG11) on the catalytic efficiency showing that sequence lenght has no impact on the hydrolysis of *p*-NPA. B) Shorter analogues, lacking portions of the GLGL spacer, exhibit similar oxidation kinetics; only the complete GLGL spacer removal (CG7) allows the peptide to remain in its linear form for 24 hours.

Determining the esterase activity of peptides and peptide assemblies

Patrizia Janković and Daniela Kalafatovic[*]
Faculty of Biotechnology and Drug Development, University of Rijeka, Rijeka, Croatia
*Corresponding author. e-mail address: daniela.kalafatovic@uniri.hr

Contents

Abstract

Catalytic peptides are gaining attention as alternatives to enzymes, especially in industrial applications. Recent advances in peptide design have improved their catalytic efficiency with approaches such as self-assembly and metal ion complexation. However, the fundamental principles governing peptide catalysis at the sequence level are still being explored. Ester hydrolysis, a well-studied reaction, serves as a widely employed method to evaluate the catalytic potential of peptides. The standard colorimetric reaction involving *para*-nitrophenyl acetate hydrolysis acts as a benchmark assay, providing a straightforward and efficient screening method for rapidly identifying potential catalysts. However, maintaining standardized conditions is crucial for reproducible results, given that factors such as pH, temperature, and substrate concentration can introduce unwanted variability. This necessity becomes particularly pronounced when working with peptides, which often exhibit slower reaction rates compared to enzymes, making even minor variations significantly influential on the final outcome. In this context, we present a refined protocol for assessing the catalytic activity of peptides and peptide assemblies, addressing critical considerations for reproducibility and accuracy.
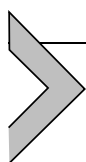
1. Introduction

Catalytic peptides are short biomolecules capable of catalyzing chemical reactions, including ester hydrolysis (Carvalho et al., 2022; Chatterjee et al., 2022; Pina et al., 2022). They offer several advantages compared to enzymes, such as ease of synthesis and use, cost effectiveness, high tunability and modularity, pH and heat stability, and compatibility with organic solvents (Schnitzer et al., 2022; Zozulia et al., 2018). These characteristics make peptides a promising alternative to enzymes, particularly in industrial applications.

Several peptide design strategies have been proposed in the last decade often inspired by active sites found in enzymes, including amino acids relevant for the catalytic reaction such as Ser, His and Asp (Takahashi et al., 2015; Zhang et al., 2014). In the analysis of active sites within esterases featuring unique catalytic mechanisms based on the catalytic triad, it was discovered that while the triad is highly conserved, the constituent residues are initially spaced apart in the sequence (Babić et al., 2022). However, upon adopting the enzyme's active 3D structure, these residues are brought into close proximity, enabling the catalytic reaction. In short peptides, essential catalytic residues are frequently situated in close proximity to each other. Because of their limited length, these peptides often lack specific conformations. Due to this conformational flexibility, peptides alone are not sufficient to obtain the desired catalytic efficiency. Multiple strategies have been developed to improve the catalytic potential of peptides by expoiting self-assembly (Carlomagno et al., 2020; Levin et al., 2020; Liu et al., 2021; Song et al., 2018). These approaches involve designing polyproline helices with precise placement of specific residues within the helix or integrating peptide self-assembly with the complexation of Zn^{2+} ions, offering more effective alternatives to the use of peptide monomers (Huang et al., 2017; Rufo et al., 2014). However, little is known about the principles that govern the catalytic activity of short peptides at the sequence level. From previous studies, it is evident that the residues that make up the sequence and their disposition within the sequence are crucial (Baruch-Leshem et al., 2021; Janković et al., 2023).

One of the most extensively studied reactions involving catalytic peptides is ester hydrolysis (Anderson et al., 1994). To assess the catalytic activity of enzymes and peptides, researchers commonly employ the *para*-nitrophenyl acetate (*p*-NPA) assay (Fig. 1) (Díaz-Caballero et al., 2020; Friedmann et al., 2015; Zhang et al., 2017). In this colorimetric assay, enzymatic measurements are carried out using *para*-nitrophenol (*p*-NP)
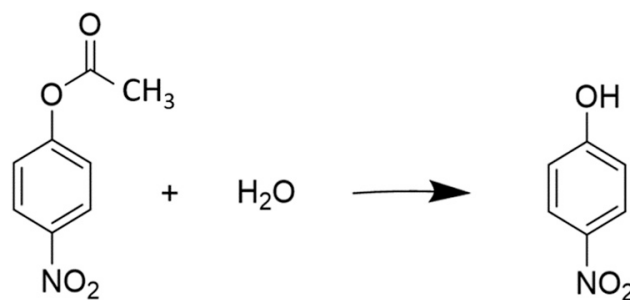
Fig. 1 *p*-NPA hydrolysis reaction and indication of yellow *p*-NP product formation having absorbance at 405 nm upon hydrolysis.

derivatives such as *p*–NPA, *para*–nitrophenyl butirate (*p*–NPB), *para*–nitrophenyl octanoate (*p*–NPO), specifically esters, which are susceptible to hydrolysis by enzymes or peptides, resulting in the release of *p*–NP as a product. The formation of this product can be monitored using Ultraviolet–Visible spectroscopy. This assay is widely applied for its simplicity and cost–effectiveness, making it suitable for high–throughput screening and the simultaneous analyses of multiple peptides or enzymes. It provides a means to standardize reaction conditions and enables the creation of comprehensive and uniform data sets that allow for the comparison of various catalytic systems (Janković et al., 2023).

However, to ensure that the results are reproducible and comparable, it is imperative to standardize the conditions under which the assay is performed. Notably, when peptides are used, the reaction often proceeds at a slower rate than when analyzing enzymes. As a result, factors such as pH, temperature, and substrate concentration can exert a significant influence on the assay outcome and must be carefully taken into account.

Herein, we will describe the evaluation of the catalytic activity of peptides and peptide assemblies using the *p*–NPA assay. We will specifically explore how various environmental factors can influence the reproducibility of the results.
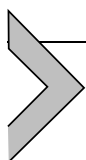
## 2. Kinetic assay protocol

Materials:
1. Microplate(s) or cuvettes
2. Spectrophotometer capable of measuring absorbance at 405 nm
3. *p*–NPA substrate
4. Peptide sample
5. Buffer solution (e.g., phosphate buffer) at appropriate pH

6. Control sample without the peptide catalyst

7. Standards (*p*-NP) with known concentrations for calibration

Procedure:

1. Prepare the *p*-NPA substrate solution:
   - Weigh the appropriate amount of *p*-NPA substrate and dissolve it in acetonitrile or methanol and then dillute it with a buffer solution to a desired concentration (typically 0.5–1 mM). Use a chemical hood when handling *p*-NPA, as it can release noxious fumes.
   - Ensure that the pH of the substrate solution matches the desired assay conditions (typically around pH 7.0–8.0).

2. In separate tubes or wells, set up the following reaction mixtures:
   - Sample reaction mixture containing the peptide-based catalyst together with the *p*-NPA substrate solution and buffer solution to maintain the desired pH
   - Negative control mixture containing the buffer solution and *p*-NPA substrate solution
   - Standard solution (*p*-NP standards with known concentrations of *p*-NP, buffer solution)

3. Incubation and measurement of *p*-NP formation:
   - Incubate all reaction mixtures at an appropriate temperature (typically 25 °C–37 °C) for a defined period (e.g., 10–30 min).
   - The incubation time may vary depending on the peptide being tested.
   - Measure the absorbance of each reaction mixture at 405 nm using a spectrophotometer. Ensure that the spectrophotometer is properly calibrated.
   - Generate a calibration curve by recording the absorbance spectra of predetermined concentrations of *p*-nitrophenol (*p*-NP)

4. Data analysis:
   - Calculate the rate of *p*-NP formation or the change in absorbance over time for each reaction.
   - Subtract the absorbance of the negative control, corresponding to the autohydrolysis of *p*-NPA
   - Determine the catalytic activity through Michaelis-Menten Kinetics.
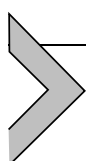
3. Michaelis-Menten kinetics

Enzyme kinetics is a specialized field within biochemistry that focuses on quantitatively measuring the rates of reactions that are catalyzed by

enzymes and studying the factors that influence these rates, and can also be extended to the analysis of catalytic peptides (Berg et al., 2013).

The concept of reaction rate refers to the rate at which reactants are converted into products and can be categorized into different orders based on their dependence on the reactant concentrations. In a zero–order kinetics, the reaction rate remains constant and is unaffected by changes in the concentration of the reactants. On the other hand, reactions in which the rate is directly proportional to the concentration of a single reactant are known as first–order reactions. Many common chemical reactions (e.g. nucleophilic substitution), referred to as bimolecular reactions, involve the interaction of two reactants, and fall under the category of second–order kinetics. However, there are instances where second–order reactions may exhibit characteristics of first–order reactions. For example, when one reactant, let us say, B, is present in a substantial excess compared to another reactant, A, which has a low initial concentration, the reaction appears to be first–order with respect to A. In this case, the reaction rate is determined primarily by the concentration of A and is relatively insensitive to the presence of excess B. Such reactions are often described as pseudo–first–order reactions.

The simplest way to investigate the rate of a reaction is by measuring the concentration of products over time. For this purpose, the formation of the product is measured for a series of different substrate concentrations over time (Fig. 2A). The concentration of the product increases over time until it reaches a point where there is no further net change in the concentrations of the substrate and product. In this case, the catalysts are still actively converting the substrate into a product and vice versa, but equilibrium has been reached.

In the early twentieth century, biochemists Leonor Michaelis and Maud Menten proposed a simple model that explains the observed kinetic properties. The core of their concept lies in the creation of a distinct
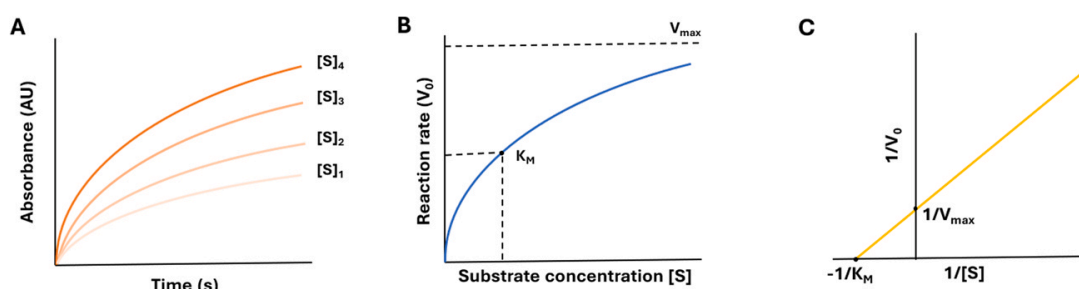

Fig. 2 Schematic representation of: (A) kinetic plots for different substrate concentrations, (B) Michaelis-Menten plot, and (C) Lineweaver-Burk plot.

enzyme-substrate complex, which serves as a crucial intermediate state in catalysis, and the corresponding kinetics is defined by the Michaelis-Menten graph and equation. The Michaelis-Menten graph, that typically takes the form of a hyperbolic curve, presents a visual representation of the relationship between reaction velocity and substrate concentration (Fig. 2B). The Michaelis-Menten equation provides a mathematical framework for quantifying the rates of these enzymatic reactions.

$$V_0 = \frac{V_{max}[S]}{K_M + [S]} \tag{1}$$

In this equation, K_M represents the substrate concentration at which the reaction rate reaches half of its maximum, while V_{max} is the highest achievable rate when all enzyme active sites are fully engaged. These entities offer valuable insights on concepts such as substrate saturation, enzyme efficiency, and substrate affinity (as characterized by K_M). Notably, this equation is derived through a sequence of substitutions, assuming a pseudo-first-order reaction. This assumption implies that the substrate concentration is at least one order of magnitude greater than that of the catalysts, resulting in negligible influence on the reaction rate by the substrate concentration. Before the era of non-linear curve fitting, the Lineweaver-Burk plot served as a valuable method for determining the values of K_M and V_{max} (Fig. 2C) where V_{max} can be derived from the intercept with the y axis, while K_M is determined from the slope.

$$\frac{1}{V_0} = \frac{K_M}{V_{max}} \frac{1}{[S]} + \frac{1}{V_{max}} \tag{2}$$
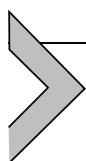
4. Catalytic activity of peptide assemblies

Catalytic peptides often exhibit lower catalytic efficiencies because they lack well-defined three-dimensional structures, which are characteristic of enzymes. To address this issue, researchers have turned to peptide self-assembly, a strategy in which peptides can organize themselves into nanostructures with a higher degree of order, leading to improved catalytic efficiency. However, achieving self-assembly often requires high molar concentrations of peptides, which can pose challenges when aiming to adhere to the Michaelis-Menten principle, which recommends maintaining a catalyst concentration difference of one order of magnitude

compared to that of the substrate. Often, this is due to the poor solubility of the substrate in buffers used for catalytic activity assessment. One compound frequently used in experimental assays to study catalytic peptides is *p*-NPA. This chemical has limited solubility in water (0.53 mg/mL) due to its inherent hydrophobic nature. In experimental setups, a common approach involves the preparation of a highly concentrated stock solution of *p*-NPA in organic solvents such as acetonitrile or methanol. This concentrated solution is then carefully diluted into a buffer solution, while ensuring that the substrate remains completely dissolved, thereby preventing any undesirable precipitation. It is important to note that *p*-NPA has demonstrated a propensity to precipitate at concentrations exceeding 1 mM. Therefore, when designing experiments involving peptide assemblies, this substrate limitation should be taken into account.
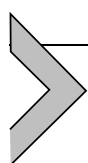
5. Impact of pH and temperature on the *p*-NPA assay

Factors such as pH and temperature play critical roles in the hydrolysis of *p*-NPA. pH affects the ionization state of reactants and catalysts, while temperature affects the kinetic energy of molecules. Typically, hydrolysis reactions occur faster around the optimal pH for the specific enzyme or peptide-based catalyst involved. For many esterases, the optimal pH is often in the neutral to slightly alkaline range, around pH 7–8. In addition to considering the ionization state, it is crucial to take into account the protonation state of the product, *p*-NP, during the detection step using UV/Vis spectroscopy. At pH levels below the pKa of *p*-NP, it predominantly exists in a protonated form, appearing colorless and displaying an absorption peak at 320 nm. This means that, even though the hydrolysis of *p*-NPA occurs under these conditions, the resulting product is not easily observable. However, when the pH exceeds 7.15, *p*-NP undergoes deprotonation, leading to the creation of a yellow-colored deprotonated form, which can be detected at 405 nm. Furthermore, as the pH increases further above 7.15, the intensity of the yellow color becomes more pronounced, making it increasingly visible and quantifiable (Fig. 3).

Consequently, when conducting experiments involving the hydrolysis of *p*-NPA and the detection of *p*-NP, researchers typically choose a pH above 7.15 to ensure that the reaction product is easily visible. This pH threshold ensures that the color change associated with the hydrolysis reaction is observable, facilitating the accurate determination of the
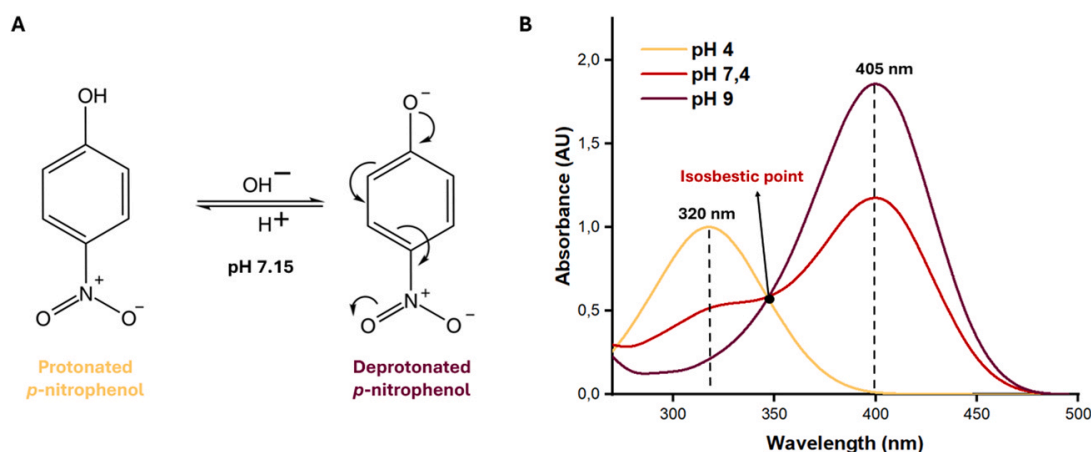
Fig. 3 Differential UV/Vis absorption of *p*-nitrophenol (*p*-NP) influenced by pH. (A) Molecular structures depicting the protonated and deprotonated forms of *p*-NP. (B) UV/Vis absorption spectra for *p*-NP at three different pH levels: 4 (protonated) with maximum absorption at 320 nm, 7.4 (partially protonated), and 9 (deprotonated) with maximum absorption at 405 nm. The intersection of absorbance spectra at different pH values is identified as the isosbestic point.

enzymatic activity or reaction kinetics. Moreover, it is important to consider the stability of the substrate that decreases with increasing pH. This is evident in the pronounced increase in the substrate's autohydrolysis rate under basic conditions.

To address these challenges, measurements can be conducted at a specific wavelength known as the isosbestic point. This feature is of substantial significance in analytical techniques, particularly in cases involving complex mixtures of chemical compounds, when there is a need to monitor concentration changes during a reaction or process. In UV/Vis spectroscopy, the isosbestic point corresponds to a specific wavelength at which two or more chemical species within a mixture exhibit identical absorbance values. Visually, it is the point on a graph plotting the absorbance against the wavelength where the absorption curves of different species intersect or cross each other. This characteristic makes it a valuable tool for quantitative analysis, especially in scenarios where isolating or quantifying individual components in the mixture proves challenging.

Additionally, like many chemical reactions, the hydrolysis of *p*–NPA is influenced by the temperature, with higher temperatures generally leading to an acceleration of the reaction rate. Furthermore, as the temperature increases, the product can also undergo autohydrolysis more rapidly, with this difference being more prominent in a phosphate–based buffer (PBS) (Fig. 4).
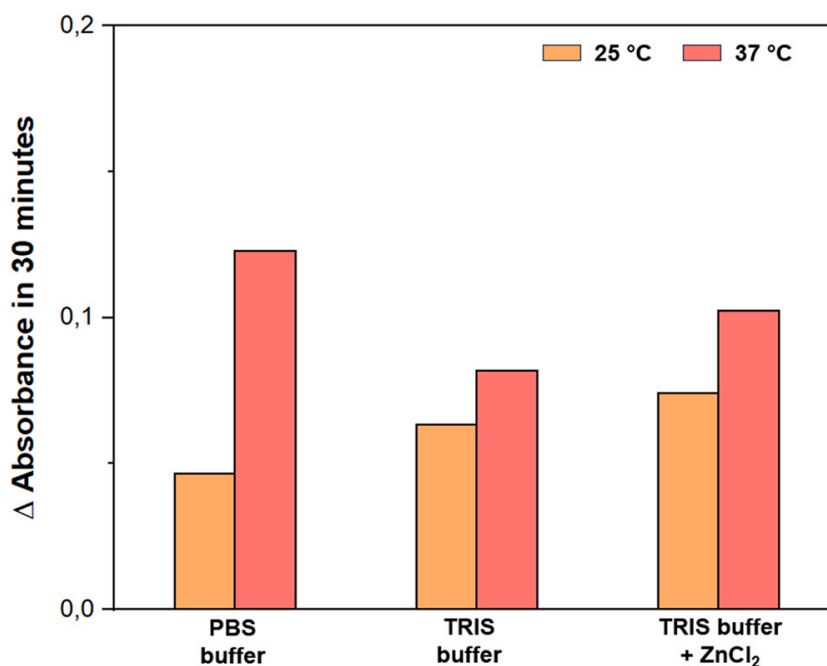
Fig. 4 The conversion of p-NPA to p-NP is illustrated by the variation in absorbance at 405 nm over a 30 min period under 25 °C (orange) and 37 °C (red) and different buffer conditions (PBS, TRIS, and TRIS-ZnCl$_2$), revealing an elevated autohydrolysis rate at 37 °C in PBS.

With all this in mind, it becomes evident that we should carefully take into account and fine-tune both the pH and the temperature to ensure consistent and reproducible results.

6. Conclusion

In this chapter, we described a method for evaluating the catalytic activity of peptides and peptide assemblies. Our chosen approach involved the use of the widely accepted colorimetric p-NPA assay, a commonly employed technique in the field of enzyme kinetics.

Unlike enzymes, peptides exhibit greater resilience to environmental factors such as pH and temperature, maintaining their activity. This raises the question whether the p-NPA assay is the first choice method for evaluating their catalytic efficacy. Although the p-NPA assay proved to be valuable for the initial screening of catalytic peptides and peptide assemblies, it is crucial to recognize its limitations and should not be considered as the only standard. The susceptibility of the p-NPA substrate to environmental variables, including temperature and pH, introduces the potential for non-reproducible results. Therefore, despite its apparent simplicity, precise execution is imperative to ensure reliable and consistent results.

Furthermore, to advance our understanding and application of catalytic peptides, there is a need to transition toward the use of more stable and biologically relevant substrates such as *p*-nitrophenyl phosphate (*p*-NPP), adenosine triphosphate (ATP), etc. This shift would provide a more accurate representation of the peptides' catalytic capabilities under conditions that closely mimic biological environments, ultimately paving the way for their broader utilization in diverse scientific and industrial contexts.

Acknowledgements

References

Anderson, J., Byrne, T., Woelfel, K., Meany, J., Spyridis, G., & Pocker, Y. (1994). The hydrolysis of p-nitrophenyl acetate: A versatile reaction to study enzyme kinetics. *Journal of Chemical Education, 71*(8), 715.

Babić, M., Janković, P., Marchesan, S., Mauša, G., & Kalafatovic, D. (2022). Esterase sequence composition patterns for the identification of catalytic triad microenvironment motifs. *Journal of Chemical Information and Modeling, 62*(24), 6398–6410.

Baruch-Leshem, A., Chevallard, C., Gobeaux, F., Guenoun, P., Daillant, J., Fontaine, P., ... Kushmaro, A., Rapaport, H. (2021). Catalytically active peptides affected by self-assembly and residues order. *Colloids and Surfaces B: Biointerfaces, 203*, 111751.

Berg, J. M., Tymoczko, J. L., & Stryer, L. (2013). Biokemija. *Školska knjiga, Zagreb, 1026*.

Carlomagno, T., Cringoli, M. C., Kralj, S., Kurbasic, M., Fornasiero, P., Pengo, P., & Marchesan, S. (2020). Biocatalysis of d, l-peptide nanofibrillar hydrogel. *Molecules, 25*(13), 2995.

Carvalho, S., Peralta Reis, D. Q., Pereira, S. V., Kalafatovic, D., & Pina, A. S. (2022). Catalytic peptides: The challenge between simplicity and functionality. *Israel Journal of Chemistry, 62*(9–10), e202200029.

Chatterjee, A., Reja, A., Pal, S., & Das, D. (2022). Systems chemistry of peptide-assemblies for biochemical transformations. *Chemical Society Reviews, 51*, 3047–3070.

Díaz-Caballero, M., Navarro, S., Nuez-Martínez, M., Peccati, F., Rodríguez-Santiago, L., Sodupe, M., ... Ventura, S. (2020). ph-responsive self-assembly of amyloid fibrils for dual hydrolase-oxidase reactions. *ACS Catalysis, 11*(2), 595–607.

Friedmann, M. P., Torbeev, V., Zelenay, V., Sobol, A., Greenwald, J., & Riek, R. (2015). Towards prebiotic catalytic amyloids using high throughput screening. *PloS One, 10*(12), e0143948.

Huang, J., Rauscher, S., Nawrocki, G., Ran, T., Feig, M., de Groot, B. L., ... MacKerell, A. D. (2017). Charmm36m: An improved force field for folded and intrinsically disordered proteins. *Nature Methods, 14*(1), 71–73.

Janković, P., Babić, M., Perčić, M., Pina, A. S., & Kalafatovic, D. (2023). Factors influencing the catalytic activity of metal-dependent histidine-rich peptides: Sequence, conformation, stereochemistry, self-assembly or their interplay? *Molecular Systems Design & Engineering, 8*(11), 1371–1380.

Janković, P., Otović, E., Mauša, G., & Kalafatovic, D. (2023). Manually curated dataset of catalytic peptides for ester hydrolysis. *Data in Brief*, 109290.

Levin, A., Hakala, T. A., Schnaider, L., Bernardes, G. J., Gazit, E., & Knowles, T. P. (2020). Biomimetic peptide self-assembly for functional materials. *Nature Reviews Chemistry, 4*(11), 615–634.

Liu, X., Waters, R., Gilbert, H. E., Barroso, G. T., Boyle, K. M., & Witus, L. S. (2021). The role of β-hairpin conformation in ester hydrolysis peptide catalysts based on a trpzip scaffold. *RSC Advances, 11*(38), 23714–23718.

Pina, A. S., Morgado, L., Duncan, K. L., Carvalho, S., Carvalho, H. F., Barbosa, A. J., Mariz, B.d. P., Moreira, I. P., Kalafatovic, D., Faustino, B. M. M., et al. (2022). Discovery of phosphotyrosine-binding oligopeptides with supramolecular target selectivity. *Chemical Science, 13*(1), 210–217.

Rufo, C. M., Moroz, Y. S., Moroz, O. V., Stöhr, J., Smith, T. A., Hu, X., ... Korendovych, I. V. (2014). Short peptides self-assemble to produce catalytic amyloids. *Nature Chemistry, 6*(4), 303–309.

Schnitzer, T., Rackl, J. W., & Wennemers, H. (2022). Stereoselective peptide catalysis in complex environments-from river water to cell lysates. *Chemical Science, 13*(31), 8963–8967.

Song, R., Wu, X., Xue, B., Yang, Y., Huang, W., Zeng, G., Wang, J., Li, W., Cao, Y., Wang, W., et al. (2018). Principles governing catalytic activity of self-assembled short peptides. *Journal of the American Chemical Society, 141*(1), 223–231.

Takahashi, T., Cheung, M., Butterweck, T., Schankweiler, S., & Heller, M. J. (2015). Quest for a turnover mechanism in peptide-based enzyme mimics. *Catalysis Communications, 59*, 206–210.

Zhang, C., Shafi, R., Lampel, A., MacPherson, D., Pappas, C. G., Narang, V., ... Ulijn, R. V. (2017). Switchable hydrolase based on reversible formation of supramolecular catalytic site using a self-assembling peptide. *Angewandte Chemie International Edition, 56*(46), 14511–14515.

Zhang, C., Xue, X., Luo, Q., Li, Y., Yang, K., Zhuang, X., Jiang, Y., Zhang, J., Liu, J., Zou, G., et al. (2014). Self-assembled peptide nanofibers designed as biological enzymes for catalyzing ester hydrolysis. *Acs Nano, 8*(11), 11715–11723.

Zozulia, O., Dolan, M., & Korendovych, I. (2018). Catalytic peptide assemblies. *Chemical Society Reviews, 47*(10), 3621–3639.